Article:
Edelman, Nathaniel, Frandsen, Paul, Miyagi, Michael et al. (26 more authors) (2019) Genomic architecture and introgression shape a butterfly radiation. Science. pp. 594-599. ISSN 0036-8075

https://doi.org/10.1126/science.aaw2090

Title: Genomic architecture and introgression shape a butterfly radiation

Authors: Nathaniel B. Edelman[1*], Paul B. Frandsen[2,3], Michael Miyagi[1], Bernardo Clavijo[4], John Davey[5], Rebecca Dikow[3], Gonzalo García-Accinelli[4], Steven M. Van Belleghem[6], Nick Patterson[7,8], Daniel E. Neafsey[8,9], Richard Challis[10], Sujai Kumar[11], Gilson R. P. Moreira[12], Camilo Salazar[13], Mathieu Chouteau[14], Brian A. Counterman[15], Riccardo Papa[6,16], Mark Blaxter[10], Robert D. Reed[17], Kanchon K. Dasmahapatra[5], Marcus Kronforst[18], Mathieu Joron[19], Chris D. Jiggins[20], W. Owen McMillan[21], Federica Di Palma[4], Andrew J. Blumberg[22], John Wakeley[1], David Jaffe[8,23], James Mallet[1*]

Affiliations:

[1]Department of Organismic and Evolutionary Biology, Harvard University, Cambridge, MA, 02138, USA

[2]Department of Plant and Wildlife Sciences, Brigham Young University, Provo, UT, 84602, USA

[3]Data Science Lab, Office of the Chief Information Officer, Smithsonian Institution, Washington, D.C., 20560, USA

[4]Earlham Institute, Norwich Research Park, NR4 7UZ, UK

[5]Department of Biology, University of York, YO10 5DD, UK

[6]Department of Biology, University of Puerto Rico, Río Piedras Campus, San Juan, Puerto Rico

[7]Department of Human Evolutionary Biology, Harvard University, Cambridge, MA, 02138, USA

[8]Broad Institute of MIT and Harvard, Cambridge, MA, 02142, USA

[9]Harvard TH Chan School of Public Health, Boston, MA, 02115, USA

[10]Wellcome Sanger Institute, Wellcome Genome Campus, Cambridge, CB10 1SA

[11]Institute of Evolutionary Biology, University of Edinburgh, Edinburgh, EH9 3JT, UK

[12]Departamento de Zoologia, Universidade Federal do Rio Grande do Sul, Porto Alegre, Brasil

[13]Biology Program, Faculty of Natural Sciences and Mathematics, Universidad del Rosario, Carrera 24, No. 63C-69, Bogotá, D.C. 111221, Colombia

[14]Laboratoire Ecologie, Evolution, Interactions des Systèmes Amazoniens (LEEISA), USR 3456, Université De Guyane, CNRS Guyane, 275 Route de Montabo, 97334 Cayenne, French Guiana.

[15]Department of Biological Sciences, Mississippi State University, Starkville, Mississippi 39762, USA

[16]Molecular Sciences and Research Center, University of Puerto Rico, San Juan, Puerto Rico

[17]Department of Ecology and Evolutionary Biology, Cornell University, Ithaca, NY 14853, USA

[18]Department of Ecology and Evolution, University of Chicago, Chicago, IL 60637, USA

[19]CEFE, CNRS, Université de Montpellier, Université Paul Valéry Montpellier 3, EPHE, IRD, Montpellier, France

[20]Department of Zoology, University of Cambridge, Cambridge CB2 3EJ, UK

[21]Smithsonian Tropical Research Institute, Apartado 0843-03092, Panamá, Panama

[22]Department of Mathematics, University of Texas, Austin, TX, 78712, USA

[23]10x Genomics, Pleasanton, California 94566, USA

*Correspondence to: nedelman@g.harvard.edu; jmallet@oeb.harvard.edu

Abstract:

We use twenty *de novo* genome assemblies to probe the speciation history and architecture of gene flow in rapidly radiating *Heliconius* butterflies. Our tests to distinguish incomplete lineage sorting from introgression indicate that gene flow has obscured several ancient phylogenetic relationships in this group over large swathes of the genome. Introgressed loci are underrepresented in low recombination and gene-rich regions, consistent with the purging of foreign alleles more tightly linked to incompatibility loci. We identify a hitherto unknown inversion that traps a color pattern switch locus. We infer that this inversion was transferred between lineages via introgression and is convergent with a similar rearrangement in another part of the genus. These multiple *de novo* genome sequences enable improved understanding of the importance of introgression and selective processes in adaptive radiation.

One Sentence Summary: Introgression has been a major contributor of genealogical discordance throughout *Heliconius* evolution, varying across the genome with local recombination rate, gene density, and genome architecture.

Main Text: Adaptive radiations play a fundamental role in generating biodiversity. Initiated by key innovations and ecological opportunity, radiation is fueled by niche competition that promotes rapid diversification of species (*1*). Reticulate evolution may enhance radiation by introducing genetic variation, enabling rapidly emerging populations to take advantage of novel ecological opportunities (*2*, *3*). Diverging from its sister genus *Eueides* ~12 My ago, *Heliconius* radiated in a burst of speciation in the last ~5 My (*4*). Introgression is well known in *Heliconius*, with widespread reticulate evolution across the genus (*5*), though this has been disputed (*6*). Nonetheless, how introgression varies across the genome is known only in one pair of sister lineages (*7*, *8*). Here, we use multiple *de novo* whole genome assemblies to improve the resolution of introgression, incomplete lineage sorting (ILS), and genome architecture in deeper branches of the *Heliconius* phylogeny.

Phylogenetic analysis

We generated 20 *de novo* genome assemblies for species in both major *Heliconius* sub-clades and three additional genera of Heliconiini. Here we align the sixteen highest quality Heliconiini assemblies to two *Heliconius* reference genomes and seven other Lepidoptera genomes, resulting in an alignment of 25 taxa (*9*). *De novo* assembly provides superior sequence information for low complexity regions, allows for discovery of structural rearrangements, and improves alignment of evolutionarily distant clades (*10*). Other studies in *Heliconius* have shown a high level of phylogenetic discordance, arguably a result of rampant introgression (*4*, *5*). We attempted to reconstruct a bifurcating species tree by estimating relationships using protein-coding genes, conserved coding regions, and conserved non-coding regions. We generated phylogenies with coalescent-based and concatenation approaches, using both the full Lepidoptera alignment and a restricted, Heliconiini-only sub-alignment. These topologies were largely congruent among analytical approaches, but weakly supported nodes were resolved inconsistently. These approaches therefore failed to resolve the phylogeny of *Heliconius* as a simple bifurcating tree (Fig. 1A, Fig. S20).

To determine whether hybridization was a cause of the species tree uncertainty, we calculated Patterson's *D*-statistics (*11*) for every triplet of the 13 *Heliconius* species, using a member of the sister genus, *Eueides tales,* as outgroup. In 201 of 286 triplets, we observed values significantly different from zero based on block-jackknifing, demonstrating strong evidence for introgression (Fig. S53). However, these tests alone yield little quantitative information about admixture. We therefore used phyloNet (*12*) to infer reticulate phylogenetic networks of these species on the basis of random samples of one hundred 10 kb windows across the alignment. For each sample, we co-estimated all 100 regional gene trees and the overall species network in parallel (*12*). To improve alignments, we analyzed the *melpomene*-silvaniform group with respect to the *H. melpomene* Hmel2.5 assembly (*13*) and the *erato-sara* group with respect to the *H. erato demophoon* v1 assembly (*9*, *14*). Most species exhibited an admixture event at some point in their history using this method; we confirmed extensive reticulation among silvaniform species and discovered major gene flow events in the *erato-sara* clade. Based on these results, we propose the reticulate phylogenies in Fig. 1B-C.

Correlation of local ancestry with genome architecture

We next analyzed the distribution of tree topologies across the genome, again treating each major clade separately and using its respective reference genome. The *melpomene*-silvaniform group lacked topological consensus, unsurprisingly since introgression, especially of key mimicry loci, is well known from this clade (*15*). The most common tree topology was found in only 4.3% of windows, with an additional 14 topologies appearing in 1.0-3.4% of windows (Fig. S19-Fig. S21). By contrast, we here focus on the *erato-sara* group, where two topologies dominate (Fig. 2). One (Tree 2, Fig. 2B) matched our bifurcating consensus topology (Fig. 1A) and a recently published tree (*4*), while the other (Tree 1) differs in that it places *H. hecalesia* and *H. telesiphe* as sisters.

Regions with local topologies discordant from the species tree may have arisen through introgression or ILS. In order to make within-topology locus-by-locus inferences, we developed a statistical test to distinguish between ILS and introgression based on the distribution of internal branch lengths among windows for a given three-taxon subtree, conditional on its topology. We call this method Quantifying Introgression via Branch Lengths (QuIBL). In the absence of introgression, we expect internal branch lengths of triplet topologies discordant with the species tree (due to ILS) to be exponentially distributed. However, if introgression has occurred, their distribution should have that same exponential component, but also include an additional component with a non-zero mode corresponding to the time between the introgression event and the most recent common ancestor of all three species (*9*). Like other tree-based methods, QuIBL is potentially sensitive to the assumption that each tree is inferred from loci with limited internal recombination (Fig. S75). We therefore chose small (5 kb) windows to reduce the probability of intra-locus recombination breakpoints.

For every triplet in the *erato-sara* clade, we calculate the likelihood that the distribution of internal branch lengths is consistent with introgression or with ILS only. We formally distinguish between these two models using a BIC test with a strict cutoff of $\Delta BIC > 10$. Consistent with our results from *D*-statistics, we find that 13 of 20 triplets have evidence for introgression (Table S13). For example, using QuIBL on the triplet *H. erato-H. hecalesia-H. telesiphe,* we infer that 76% of discordant loci, or 38% of all loci genome-wide, are introgressed. Averaging over all

triplets, we infer that 71% (67% with BIC filtering) of loci with discordant gene trees have a history of introgression, or 20% (19% with BIC filtering) of all triplet loci, indicating a broad signal of introgression throughout the clade (Equation 7.7, Table S13; see (*9*) for additional discussion).

In hybrid populations, individuals have genomic regions that originate from different species and may be incompatible with the recipient genome or with their environment (*16*). Linked selection causes harmless or even beneficial introgressed loci to be removed along with these deleterious loci if they are tightly linked; this effect depends on the strength of selection and the local recombination rate (*17*, *18*). We therefore expect introgressed loci to be enriched in regions where selection is likely to be weak, such as gene deserts, or in regions of high recombination, where harmless introgressed loci more readily recombine away from linked incompatibility loci.

In *Heliconius*, even distant species like *H. erato* and *H. melpomene* have the same number of broadly collinear chromosomes (*13*), facilitating direct comparisons among species. Furthermore, each chromosome in *Heliconius* has approximately one crossover per chromosome per meiosis in males (there is no crossing over in female *Heliconius*) (*14*, *19*). Chromosomes vary in length, and chromosome size is inversely proportional to recombination rate per base pair (*8*, *13*). We found a strong correlation between the fraction of windows in each chromosome that show a given topology and physical chromosome length (Fig. 3A). Such relationships exist for all 8 trees in Fig. 2B (*9*), but we focus here on the two most common trees: Tree 1 has a strongly negative correlation with chromosome size (r^2=0.883, t= 11.7, 18 *d.f.*, p<0.0001) while Tree 2 (concordant with our inferred species tree) has a positive correlation (r^2=0.726, t=6.9, 18 *d.f.*, p<0.0001). Results from QuIBL indicate that 94% of windows that recover a Tree 1 triplet topology are consistent with introgression (Fig. S70, Table S13). The Z (sex) chromosome 21, is strongly enriched for Tree 2, suggesting it may harbor more incompatibility loci than autosomes. Interspecific hybrid females in *Heliconius* are often sterile, conforming to Haldane's Rule, and sex chromosomes have been implicated as particularly important in generating incompatibilities (*8*, *20-24*).

To test whether the pattern we observe among chromosomes is related to differences in recombination, we investigated the relationship between recombination rate and tree topology within chromosomes. Recombination rate declines at the ends of chromosomes (Fig. S85), and the species tree (Tree 2) is more abundant in those regions (Fig. 3B). In addition, when windows are grouped by local recombination rate calculated from population genetic data (*9*, *14*), we observe a strong relationship with the recovered topology (Fig. 3C). Finally, we observe a minor enrichment of Tree 1 in regions of very low gene density, but this effect is weak (Fig. 3D) compared to that of recombination. Taken together, these results show that tighter linkage on longer chromosomes, and in lower recombination regions within chromosomes leads to removal of more introgressed variation in those regions. This very strong correlation is consistent with a highly polygenic architecture of incompatibilities between species.

Introgression of a convergent inversion

The topology block size distribution in the *erato* clade generally decayed exponentially (Fig. 2C), but two unusually long blocks contained minor topologies: one on chromosome 2 (Tree 3, composed of three sub-blocks) and the other on chromosome 15 (Tree 4). Our study of the ~3

Mb topology block on chromosome 2 confirms an earlier finding of an inversion in *H. erato* (*13*), and we show here that its rare topology is most likely explained by ILS including a long period of ancestral polymorphism (Fig. S95).

The topology block on chromosome 15 is of particular interest, as it spans *cortex*, a genetic hotspot of wing color pattern diversity in Lepidoptera (*25*, *26*). We hypothesized that this block could be an inversion, as in *H. numata*, where the P_1 'supergene' inversion polymorphism around *cortex* controls color pattern switching among mimicry morphs (*27*). This block recovers *H. telesiphe* and *H. hecalesia* as a monophyletic subclade, which together are sister to the *sara* clade (Fig. 2B, Tree 4). We searched our *de novo* assemblies for contigs that mapped across topology transitions. Taking *H. melpomene* as the standard arrangement, we find clear inversion breakpoints in *H. telesiphe, H. hecalesia, H. sara,* and *H. demeter*. Conversely, *H. erato, H. himera,* and *E. tales* all contain contigs that map in their entirety across the breakpoints (Fig. 4A), implying that they have the ancestral *H. melpomene* arrangement.

This chromosome 15 inversion covers almost exactly the same region as the 400 kb P_1 inversion in *H. numata* (*25*, *27*, *28*). However, *de novo* contigs from our *H. numata* assembly show that the breakpoints of P_1 are close to but not identical to those of the inversion in the *erato* clade (Fig. 4A). Furthermore, in topologies for *H. numata, H. telesiphe, H. erato,* and *E. tales* across chromosome 15, not a single window recovered *H. numata* and *H. telesiphe* as a monophyletic subclade, as would be expected if the *erato* group inversion was homologous to P_1 in *H. numata*.

We used QuIBL with the triplet (*H. erato* +*H. telesiphe* + *H. sara*) to elucidate the evolutionary history of this inversion. A small internal branch would suggest ILS while a large internal branch would be more consistent with introgression (Fig. 4B). The average internal branch length in the inversion was much longer than the genome-wide average, corresponding to a 79% probability of introgression (Fig. 4C). If the inversion was polymorphic in the ancestral population for some time, we could also recover a similarly long internal branch (Fig. 4B, center). We distinguish between this longer-term polymorphic scenario and introgression by comparing the genetic distance (D_{XY}) between *H. telesiphe* and *H. sara,* represented by T_3 in Fig. 4B. Normalized D_{XY} (as in Fig. S95) within the inversion is ~25% less than in the rest of the genome. Given that this is a large genomic block, introgression is therefore the most parsimonious explanation for the evolutionary history of the inversion (Fig. 4D) (*29*).

Discussion

Species involved in rapid radiations are prone to hybridization due to frequent geographical overlap with closely related taxa. In both *melpomene* and *erato* clades of *Heliconius*, introgression has overwritten the original bifurcation history of several species across large swathes of the genome, a pattern also observed in *Anopheles* mosquitos (*30*). This observation is also consistent with genomic analysis of other rapid radiations characterized by widespread hybridization and introgression, including Darwin's finches (*2*) and African cichlids (*31*). In other radiations, the role of introgression is less clear: in *Tamias* chipmunks, widespread introgression of mitochondrial DNA was identified, in contrast to an absence of evidence for nuclear gene flow (*32*). With few genomic comparisons available to date, it is perhaps too early to say whether introgression is a major feature of adaptive radiations in general, but evidence thus far suggests this to be the case.

Our results raise the question of why some genomic regions cross species boundaries while others do not. In the *erato* clade, we find a strong correlation between recombination rate and introgression probability. Similar associations with topology also exist between sister species in the *melpomene* clade (7). Associations between recombination and introgression in actively hybridizing populations of sword-tail fish (*Xiphophorus*) and monkey flowers (*Mimulus*) support the role of linked selection on a highly polygenic landscape of interspecific incompatibilities (*18*, *33*, *34*). Our results establish that this relationship persists and may indeed be strengthened with time since introgression. While hybridization is ongoing, many introgressed blocks are constantly reintroduced into the population. If linked to weakly deleterious alleles, introgressed loci will be finally purged by linked selection only long after introgression ceases.

Recombination rate alone cannot account for differential introgression, so we must delve into specific regions to elucidate their function and relevance to speciation. It is critical, therefore, to have tools that can confidently identify introgressed loci, and much effort has gone into developing such methods (*11*, *35*). Our test using internal branch lengths in triplet gene trees is based in coalescent theory and takes advantage of the discriminatory power of a property of gene trees not explicitly accounted for by other methods. QuIBL allows us to assess probability of introgression for each locus in each species triplet (*8*). Here, we employ this method to identify the evolutionary origin of a convergent inversion that has undergone multiple independent introgression events, and to show that genomic regions with discordant topologies arose mostly through hybridization. Just as sex aids adaptation within species, occasional introgression and recombination among species can have major long-term effects on the genome, contributing variation that could fuel rapid adaptive divergence and radiation.

References and Notes

1. D. Schluter, *The Ecology of Adaptive Radiation* (OUP Oxford, 2000).

2. S. Lamichhaney, J. Berglund, M. S. Almén, K. Maqbool, M. Grabherr, A. Martinez-Barrio, M. Promerová, C.-J. Rubin, C. Wang, N. Zamani, B. R. Grant, P. R. Grant, M. T. Webster, L. Andersson, Evolution of Darwin's finches and their beaks revealed by genome sequencing. *Nature* **518**, 371–375 (2015).

3. J. B. Pease, D. C. Haak, M. W. Hahn, L. C. Moyle, Phylogenomics reveals three sources of adaptive variation during a rapid radiation. *PLoS Biol.* **14**, e1002379 (2016).

4. K. M. Kozak, N. Wahlberg, A. F. E. Neild, K. K. Dasmahapatra, J. Mallet, C. D. Jiggins, Multilocus species trees show the recent adaptive radiation of the mimetic *Heliconius* butterflies. *Syst. Biol.* **64**, 505–524 (2015).

5. K. M. Kozak, O. McMillan, M. Joron, C. D. Jiggins, Genome-wide admixture is common across the *Heliconius* radiation. *bioRxiv*, 414201 (2018).

6. A. V. Z. Brower, I. J. G. Orduña, Missing data, clade support and "reticulation": the molecular systematics of *Heliconius* and related genera (Lepidoptera: Nymphalidae) re-examined. *Cladistics* **34**, 151–166 (2018).

7. S. H. Martin, K. K. Dasmahapatra, N. J. Nadeau, C. Salazar, J. R. Walters, F. Simpson, M. Blaxter, A. Manica, J. Mallet, C. D. Jiggins, Genome-wide evidence for speciation with gene flow in Heliconius butterflies. *Genome Research* **23**, 1817–1828 (2013).

8. S. H. Martin, J. W. Davey, C. Salazar, C. D. Jiggins, Recombination rate variation shapes barriers to introgression across butterfly genomes. *PLoS Biol.* **17**, e2006288 (2019).

9. Materials and methods are available as supplementary materials.

10. *Drosophila* 12 Genomes Consortium, Evolution of genes and genomes on the *Drosophila* phylogeny. *Nature* **450**, 203–218 (2007).

11. N. Patterson, P. Moorjani, Y. Luo, S. Mallick, N. Rohland, Y. Zhan, T. Genschoreck, T. Webster, D. Reich, Ancient admixture in human history. *Genetics* **192**, 1065–1093 (2012).

12. D. Wen, L. Nakhleh, Co-estimating reticulate phylogenies and gene trees from multi-locus sequence data. *Syst. Biol.* **61**, 170–457 (2017).

13. J. W. Davey, S. L. Barker, P. M. Rastas, A. Pinharanda, S. H. Martin, R. Durbin, W. O. McMillan, R. M. Merrill, C. D. Jiggins, No evidence for maintenance of a sympatric *Heliconius* species barrier by chromosomal inversions. *Evolution Letters* **1**, 138–154 (2017).

14. S. M. Van Belleghem, P. Rastas, A. Papanicolaou, S. H. Martin, C. F. Arias, M. A. Supple, J. J. Hanly, J. Mallet, J. J. Lewis, H. M. Hines, M. Ruiz, C. Salazar, M. Linares,

G. R. P. Moreira, C. D. Jiggins, B. A. Counterman, W. O. McMillan, R. Papa, Complex modular architecture around a simple toolkit of wing pattern genes. *Nat. Ecol. Evol.* **1**, 52 (2017).

15. C. D. Jiggins, *The Ecology and Evolution of Heliconius Butterflies* (Oxford University Press, 2017).

16. J. A. Coyne, H. A. Orr, *Speciation* (Sinauer Associates Incorporated, 2004).

17. D. J. Begun, C. F. Aquadro, Levels of naturally occurring DNA polymorphism correlate with recombination rates in *D. melanogaster*. *Nature* **356**, 519–520 (1992).

18. M. Schumer, C. Xu, D. L. Powell, A. Durvasula, L. Skov, C. Holland, J. C. Blazier, S. Sankararaman, P. Andolfatto, G. G. Rosenthal, M. Przeworski, Natural selection interacts with recombination to shape the evolution of hybrid genomes. *Science* **360**, 656–660 (2018).

19. J. W. Davey, M. Chouteau, S. L. Barker, L. Maroja, S. W. Baxter, F. Simpson, M. Joron, J. Mallet, K. K. Dasmahapatra, C. D. Jiggins, Major improvements to the *Heliconius melpomene* genome assembly used to confirm 10 chromosome fusion events in 6 million years of butterfly evolution. *G3: Genes|Genomes|Genetics* **6**, 695–708 (2016).

20. T. Dobzhansky, *Genetics and the Origin of Species* (Columbia University Press, 1937).

21. H. A. Orr, M. Turelli, Dominance and Haldane's rule. *Genetics* **143**, 613–616 (1996).

22. C. D. Jiggins, M. Linares, R. E. Naisbit, C. Salazar, Z. H. Yang, J. Mallet, Sex-linked hybrid sterility in a butterfly. *Evolution* **55**, 1631–1638 (2001).

23. R. E. Naisbit, C. D. Jiggins, M. Linares, C. Salazar, J. Mallet, Hybrid sterility, Haldane's rule and speciation in *Heliconius cydno* and *H. melpomene*. *Genetics* **161**, 1517–1526 (2002).

24. S. M. Van Belleghem, M. Baquero, R. Papa, C. Salazar, W. O. McMillan, B. A. Counterman, C. D. Jiggins, S. H. Martin, Patterns of Z chromosome divergence among *Heliconius* species highlight the importance of historical demography. *Mol. Ecol.* **27**, 3852–3872 (2018).

25. M. Joron, R. Papa, M. Beltrán, N. Chamberlain, J. Mavárez, S. Baxter, M. Abanto, E. Bermingham, S. J. Humphray, J. Rogers, H. Beasley, K. Barlow, R. H. ffrench-Constant, J. Mallet, W. O. McMillan, C. D. Jiggins, A conserved supergene locus controls colour pattern diversity in *Heliconius* butterflies. *PLoS Biol.* **4**, e303–10 (2006).

26. N. J. Nadeau, C. Pardo-Diaz, A. Whibley, M. A. Supple, S. V. Saenko, R. W. R. Wallbank, G. C. Wu, L. Maroja, L. Ferguson, J. J. Hanly, H. Hines, C. Salazar, R. M. Merrill, A. J. Dowling, R. H. ffrench-Constant, V. Llaurens, M. Joron, W. O. McMillan, C. D. Jiggins, The gene *cortex* controls mimicry and crypsis in butterflies and moths. *Nature* **534**, 106–110 (2016).

27. P. Jay, A. Whibley, L. Frezal, M. Á. Rodríguez de Cara, R. W. Nowell, J. Mallet, K. K. Dasmahapatra, M. Joron, Supergene evolution triggered by the introgression of a chromosomal inversion. *Curr. Biol.* **28**, 1839–1845.e3 (2018).

28. M. Joron, L. Frezal, R. T. Jones, N. L. Chamberlain, S. F. Lee, C. R. Haag, A. Whibley, M. Becuwe, S. W. Baxter, L. Ferguson, P. A. Wilkinson, C. Salazar, C. Davidson, R. Clark, M. A. Quail, H. Beasley, R. Glithero, C. Lloyd, S. Sims, M. C. Jones, J. Rogers, C. D. Jiggins, R. H. ffrench-Constant, Chromosomal rearrangements maintain a polymorphic supergene controlling butterfly mimicry. *Nature* **477**, 203–206 (2011).

29. F. Roda, F. K. Mendes, M. W. Hahn, R. Hopkins, Genomic evidence of gene flow during reinforcement in Texas *Phlox*. *Mol. Ecol.* **26**, 2317–2330 (2017).

30. M. C. Fontaine, J. B. Pease, A. Steele, R. M. Waterhouse, D. E. Neafsey, I. V. Sharakhov, X. Jiang, A. B. Hall, F. Catteruccia, E. Kakani, S. N. Mitchell, Y.-C. Wu, H. A. Smith, R. R. Love, M. K. Lawniczak, M. A. Slotman, S. J. Emrich, M. W. Hahn, N. J. Besansky, Extensive introgression in a malaria vector species complex revealed by phylogenomics. *Science* **347**, 1258524–1258524 (2015).

31. J. I. Meier, D. A. Marques, S. Mwaiko, C. E. Wagner, L. Excoffier, O. Seehausen, Ancient hybridization fuels rapid cichlid fish adaptive radiations. *Nat. Commun.* **8**, 14363–11 (2017).

32. J. M. Good, D. Vanderpool, S. Keeble, K. Bi, Negligible nuclear introgression despite complete mitochondrial capture between two species of chipmunks. *Evolution* **69**, 1961–1972 (2015).

33. Y. Brandvain, A. M. Kenney, L. Flagel, G. Coop, A. L. Sweigart, Speciation and introgression between *Mimulus nasutus* and *Mimulus guttatus*. *PLoS Genet.* **10**, e1004410 (2014).

34. H. F. Gante, M. Matschiner, M. Malmstrøm, K. S. Jakobsen, S. Jentoft, W. Salzburger, Genomics of speciation and introgression in Princess cichlid fishes from Lake Tanganyika. *Mol. Ecol.* **25**, 6143–6161 (2016).

35. S. H. Martin, J. W. Davey, C. D. Jiggins, Evaluating the use of ABBA-BABA statistics to locate introgressed loci. *Mol. Biol. Evol.* **32**, 244–257 (2015).

36. The *Heliconius* Genome Consortium, Butterfly genome reveals promiscuous exchange of mimicry adaptations among species. *Nature* **487**, 94–98 (2012).

37. Broad Institute, DISCOVAR: Assemble genomes, find variants. *https://www.broadinstitute.org/software/discovar/blog* (2015).

38. D. Mapleson, G. Garcia Accinelli, G. Kettleborough, J. Wright, B. J. Clavijo, B. Berger, KAT: a K-mer analysis toolkit to quality control NGS datasets and genome assemblies. *Bioinformatics* **33**, 574–576 (2017).

39. R. Luo, B. Liu, Y. Xie, Z. Li, W. Huang, J. Yuan, G. He, Y. Chen, Q. Pan, Y. Liu, J. Tang, G. Wu, H. Zhang, Y. Shi, Y. Liu, C. Yu, B. Wang, Y. Lu, C. Han, D. W. Cheung, S.-M. Yiu, S. Peng, Z. Xiaoqian, G. Liu, X. Liao, Y. Li, H. Yang, J. Wang, T.-W. Lam, J. Wang, SOAPdenovo2: an empirically improved memory-efficient short-read de novo assembler. *GigaScience* **1**, 18 (2012).

40. G. W. Vurture, F. J. Sedlazeck, M. Nattestad, C. J. Underwood, H. Fang, J. Gurtowski, M. C. Schatz, GenomeScope: fast reference-free genome profiling from short reads. *Bioinformatics* **33**, 2202–2204 (2017).

41. G. Marçais, C. Kingsford, A fast, lock-free approach for efficient parallel counting of occurrences of k-mers. *Bioinformatics* **27**, 764–770 (2011).

42. A. Smit, R. Hubley, P. Green, RepeatMasker Open-4.0. *www.repeatmasker.org* (2013).

43. F. A. Simão, R. M. Waterhouse, P. Ioannidis, E. V. Kriventseva, E. M. Zdobnov, BUSCO: assessing genome assembly and annotation completeness with single-copy orthologs. *Bioinformatics* **31**, 3210–3212 (2015).

44. B. Paten, D. Earl, N. Nguyen, M. Diekhans, D. Zerbino, D. Haussler, Cactus: Algorithms for genome multiple sequence alignment. *Genome Research* **21**, 1512–1528 (2011).

45. G. Hickey, B. Paten, D. Earl, D. Zerbino, D. Haussler, HAL: a hierarchical format for storing and analyzing multiple genome alignments. *Bioinformatics* **29**, 1341–1342 (2013).

46. M. J. Hubisz, K. S. Pollard, A. Siepel, PHAST and RPHAST: phylogenetic analysis with space/time models. *Brief. Bioinformatics* **12**, 41–51 (2011).

47. W. J. Kent, C. W. Sugnet, T. S. Furey, K. M. Roskin, T. H. Pringle, A. M. Zahler, D. Haussler, The human genome browser at UCSC. *Genome Research* **12**, 996–1006 (2002).

48. B. Misof, K. Misof, A Monte Carlo approach successfully identifies randomness in multiple sequence alignments: a more objective means of data exclusion. *Syst. Biol.* **58**, 21–34 (2009).

49. P. Kück, ALICUT: a Perlscript which cuts ALISCORE identified RSS. *Department of Bioinformatics, Zoologisches Forschungsmuseum A. Koenig (ZFMK), Bonn, Germany, version* **2** (2009).

50. S. Kalyaanamoorthy, B. Q. Minh, T. K. F. Wong, A. von Haeseler, L. S. Jermiin, ModelFinder: fast model selection for accurate phylogenetic estimates. *Nat. Methods* **14**, 587–589 (2017).

51. L.-T. Nguyen, H. A. Schmidt, A. von Haeseler, B. Q. Minh, IQ-TREE: a fast and effective stochastic algorithm for estimating maximum-likelihood phylogenies. *Mol. Biol. Evol.* **32**, 268–274 (2015).

52. D. T. Hoang, O. Chernomor, A. von Haeseler, B. Q. Minh, L. S. Vinh, UFBoot2: Improving the ultrafast bootstrap approximation. *Mol. Biol. Evol.* **35**, 518–522 (2018).

53. S. Mirarab, R. Reaz, M. S. Bayzid, T. Zimmermann, M. S. Swenson, T. Warnow, ASTRAL: genome-scale coalescent-based species tree estimation. *Bioinformatics* **30**, i541–8 (2014).

54. P. Kück, K. Meusemann, FASconCAT: Convenient handling of data matrices. *Mol. Phylogenetics Evol* **56**, 1115–1118 (2010).

55. A. R. Quinlan, BEDTools: The Swiss-army tool for genome feature analysis. *Curr. Protoc. Bioinformatics* **47**, 11.12.1–34 (2014).

56. E. Paradis, K. Schliep, ape 5.0: an environment for modern phylogenetics and evolutionary analyses in R. *Bioinformatics* **9**, 532. (2018).

57. A. J. Page, B. Taylor, A. J. Delaney, J. Soares, T. Seemann, J. A. Keane, S. R. Harris, SNP-sites: rapid efficient extraction of SNPs from multi-FASTA alignments. *Microb. Genom.* **2**, e000056 (2016).

58. B. Gel, E. Serra, karyoploteR: an R/Bioconductor package to plot customizable genomes displaying arbitrary data. *Bioinformatics* **33**, 3088–3090 (2017).

59. A. H. Chan, P. A. Jenkins, Y. S. Song, Genome-wide fine-scale recombination rate variation in *Drosophila melanogaster*. *PLoS Genet.* **8**, e1003090 (2012).

60. G. A. Van der Auwera, M. O. Carneiro, C. Hartl, R. Poplin, G. del Angel, A. L. Moonshine, T. Jordan, K. Shakir, D. Roazen, J. Thibault, E. Banks, K. V. Garimella, D. Altshuler, S. Gabriel, M. A. DePristo, From FastQ data to high-confidence variant calls: the genome analysis toolkit best practices pipeline. *Curr. Protoc. Bioinformatics* **43**, 11.10.1–11.10.33 (2013).

61. B. L. Browning, S. R. Browning, Genotype imputation with millions of reference samples. *Am. J. Hum. Genet.* **98**, 116–126 (2016).

62. R. R. Hudson, 2002, Generating samples under a Wright–Fisher neutral model of genetic variation. *Genome Biol. Evol.* **18**, 337–338 (2002).

63. J. Kelleher, A. M. Etheridge, G. McVean, Efficient coalescent simulation and genealogical analysis for large sample sizes. *PLoS Comput. Biol.* **12**, e1004842 (2016).

64. A. Rambaut, N. C. Grassly, Seq-Gen: an application for the Monte Carlo simulation of DNA sequence evolution along phylogenetic trees. *Comput. Appl. Biosci.* **13**, 235–238 (1997).

65. S. Guindon, J.-F. Dufayard, V. Lefort, M. Anisimova, W. Hordijk, O. Gascuel, New algorithms and methods to estimate maximum-likelihood phylogenies: assessing the performance of PhyML 3.0. *Syst. Biol.* **59**, 307–321 (2010).

66. H. Thorvaldsdottir, J. T. Robinson, J. P. Mesirov, Integrative genomics viewer (IGV): high-performance genomics data visualization and exploration. *Brief. Bioinformatics* **14**, 178–192 (2013).

67. N. I. Weisenfeld, S. Yin, T. Sharpe, B. Lau, R. Hegarty, L. Holmes, B. Sogoloff, D. Tabbaa, L. Williams, C. Russ, C. Nusbaum, E. S. Lander, Broad Institute, D. B. Jaffe, Comprehensive variation discovery in single human genomes. *Nat. Genet.* **46**, 1350–1355 (2014).

68. R. R. Love, N. I. Weisenfeld, D. B. Jaffe, N. J. Besansky, D. E. Neafsey, Evaluation of DISCOVAR de novo using a mosquito sample for cost-effective short-read genome assembly. *BMC Genomics* **17**, 187–10 (2016).

69. B. Clavijo, G. Garcia Accinelli, J. Wright, D. Heavens, K. Barr, L. Yanes, F. Di Palma, W2RAP: a pipeline for high quality, robust assemblies of large complex genomes from short read data. *bioRxiv*, 110999 (2017).

70. A. V. Zimin, D. Puiu, R. Hall, S. Kingan, B. J. Clavijo, S. L. Salzberg, The first near-complete assembly of the hexaploid bread wheat genome, *Triticum aestivum*. *GigaScience* **6**, 705 (2017).

71. P. Paajanen, G. Kettleborough, E. López-Girona, M. Giolai, D. Heavens, D. Baker, A. Lister, F. Cugliandolo, G. Wilde, I. Hein, I. Macaulay, G. J. Bryan, M. D. Clark, A critical comparison of technologies for a plant genome sequencing project. *GigaScience* (2019), doi:10.1093/gigascience/giy163.

72. S. Goodwin, J. D. McPherson, W. R. McCombie, Coming of age: ten years of next-generation sequencing technologies. *Nature Reviews Genetics* **17**, 333–351 (2016).

73. D. A. Ray, J. R. Grimshaw, M. K. Halsey, J. M. Korstian, A. B. Osmanski, K. A. M. Sullivan, K. A. Wolf, H. Reddy, N. Foley, R. D. Stevens, B. Knisbacher, O. Levy, B. Counterman, N. B. Edelman, J. Mallet, Simultaneous TE analysis of 19 Heliconiine butterflies yields novel insights into rapid TE-based genome diversification and multiple SINE births and deaths. *Genome Biol. Evol.* (2019).

74. V. Ahola, R. Lehtonen, P. Somervuo, L. Salmela, P. Koskinen, P. Rastas, N. Välimäki, L. Paulin, J. Kvist, N. Wahlberg, J. Tanskanen, E. A. Hornett, L. C. Ferguson, S. Luo, Z. Cao, M. A. de Jong, A. Duplouy, O.-P. Smolander, H. Vogel, R. C. McCoy, K. Qian, W. S. Chong, Q. Zhang, F. Ahmad, J. K. Haukka, A. Joshi, J. Salojärvi, C. W. Wheat, E. Grosse-Wilde, D. Hughes, R. Katainen, E. Pitkänen, J. Ylinen, R. M. Waterhouse, M. Turunen, A. Vähärautio, S. P. Ojanen, A. H. Schulman, M. Taipale, D. Lawson, E. Ukkonen, V. Mäkinen, M. R. Goldsmith, L. Holm, P. Auvinen, M. J. Frilander, I. Hanski, The Glanville fritillary genome retains an ancient karyotype and reveals selective chromosomal fusions in Lepidoptera. *Nat. Commun.* **5**, 4737 (2014).

75. R. W. Nowell, B. Elsworth, V. Oostra, B. J. Zwaan, C. W. Wheat, M. Saastamoinen, I. J. Saccheri, A. E. Van't Hof, B. R. Wasik, H. Connahs, M. L. Aslam, S. Kumar, R. J.

Challis, A. Monteiro, P. M. Brakefield, M. Blaxter, A high-coverage draft genome of the mycalesine butterfly *Bicyclus anynana*. *GigaScience* **6**, 1–7 (2017).

76. S. Zhan, W. Zhang, K. Niitepõld, J. Hsu, J. F. Haeger, M. P. Zalucki, S. Altizer, J. C. de Roode, S. M. Reppert, M. R. Kronforst, The genetics of monarch butterfly migration and warning colouration. *Nature* **514**, 317–321 (2014).

77. H. Nishikawa, T. Iijima, R. Kajitani, J. Yamaguchi, T. Ando, Y. Suzuki, S. Sugano, A. Fujiyama, S. Kosugi, H. Hirakawa, S. Tabata, K. Ozaki, H. Morimoto, K. Ihara, M. Obara, H. Hori, T. Itoh, H. Fujiwara, A genetic mechanism for female-limited Batesian mimicry in *Papilio* butterfly. *Nat. Genet.* **47**, 405–409 (2015).

78. Q. Cong, D. Borek, Z. Otwinowski, N. V. Grishin, Skipper genome sheds light on unique phenotypic traits and phylogeny. *BMC Genomics* **16**, 639 (2015).

79. The International Silkworm Genome Consortium, The genome of a lepidopteran model insect, the silkworm *Bombyx mori*. *Insect Biochem. Mol. Biol.* **38**, 1036–1045 (2008).

80. M. You, Z. Yue, W. He, X. Yang, G. Yang, M. Xie, D. Zhan, S. W. Baxter, L. Vasseur, G. M. Gurr, C. J. Douglas, J. Bai, P. Wang, K. Cui, S. Huang, X. Li, Q. Zhou, Z. Wu, Q. Chen, C. Liu, B. Wang, X. Li, X. Xu, C. Lu, M. Hu, J. W. Davey, S. M. Smith, M. Chen, X. Xia, W. Tang, F. Ke, D. Zheng, Y. Hu, F. Song, Y. You, X. Ma, L. Peng, Y. Zheng, Y. Liang, Y. Chen, L. Yu, Y. Zhang, Y. Liu, G. Li, L. Fang, J. Li, X. Zhou, Y. Luo, C. Gou, J. Wang, J. Wang, H. Yang, J. Wang, A heterozygous moth genome provides insights into herbivory and detoxification. *Nat. Genet.* **45**, 220–225 (2013).

81. T. C. Bruen, H. Philippe, D. Bryant, A simple and robust statistical test for detecting the presence of recombination. *Genetics* **172**, 2665–2681 (2006).

82. B. M. Peter, Admixture, population structure, and F-statistics. *Genetics* **202**, 1485–1501 (2016).

83. S. Zairis, H. Khiabanian, A. J. Blumberg, R. Rabadan, Genomic data analysis in tree spaces. *arxiv.org* (2016).

84. S. H. Martin, M. Möst, W. J. Palmer, C. Salazar, W. O. McMillan, F. M. Jiggins, C. D. Jiggins, Natural selection and genetic diversity in the butterfly *Heliconius melpomene*. *Genetics* **203**, 525–541 (2016).

85. J. Wakeley, *Coalescent Theory* (Roberts and Co, 2008).

86. F. de Mendiburu, *Una herramienta de análisis estadístico para la investigación agrícola* (Universidad Nacional de Ingeniería, Lima, 2009).

87. A. Pinharanda, S. H. Martin, S. L. Barker, J. W. Davey, C. D. Jiggins, The comparative landscape of duplications in *Heliconius melpomene* and *Heliconius cydno*. *Heredity* **118**, 78–87 (2017).

88. L. Nakhleh, A metric on the space of reduced phylogenetic networks. *IEEE/ACM Trans Comput Biol Bioinform* **7**, 218–222 (2010).

Acknowledgments: We thank the Harvard FAS Research Computing team and the Smithsonian Institution for their support. Conversations with S. Martin were instrumental in developing our thinking around recombination rate. We also thank J. Edelman for assistance with the Scaffolding With DISCOVAR pipeline and J. Zhu and L. Nakhleh for their guidance with the PhyloNet toolkit. We thank E. Harney for assistance with qpGraph, as well as N. Rosser, F. Seixas, T. Xiong, P. Muralidhar and C. Veller for illuminating discussions. **Funding:** This project was funded by a SPARC Grant from the Broad Institute of Harvard and MIT and startup and studentship funds from Harvard University for JM and NBE. Additional funding through NSF grant DGE1745303 to MM; BBSRC, Core Strategic Programme Grant BB/CSP17270/1 at the Earlham Institute for BC, GGA, and FDP; a Herchel Smith Postdoctoral Research Fellowship and a Smithsonian Tropical Research Institute Fellowship for JWD; NSF grant OIA 1736026 to BC and RP; Brazilian National Council for Scientific and Technological Development" (CNPq) grant 309853/2014-1 to GRPM; Fondos Concursables Universidad del Rosario 2016-PIN-2017-001 to CS; Marie Sklodowska-Curie fellowship (FITINV, N 655857) and NSERC fellowship for MC; NERC award UKSBS PR18037 to MB; NSF grant IOS-1656514 to RDR; NSF grant IOS-1656389 to RP; NERC NE/K012886/1 to KKD; NSF grant IOS-1452648 and NIH grant GM108626 to MK; MJ is supported by French National Research Agency: ANR-12-JSV7-0005-HybEvol and ANR-18-CE02-0019-Supergene. AB was supported by NIH grants 5U54CA193313 and GG010211-R01-HIV, and AFOSR grant FA9550-18-1-0415. DEN was supported in part by Federal funds from the National Institute of Allergy and Infectious Diseases, National Institutes of Health, Department of Health and Human Services, under Grant Number U19AI110818 to the Broad Institute. DBJ's work on *DISCOVAR de novo* was funded in part with federal funds from the National Human Genome Research Institute, US National Institutes of Health, US Department of Health and Human Services, under grants R01HG003474 and U54HG003067. LepBase development was supported by BBSRC grants BB/K020161/1 and BB/R015325/1. **Author contributions:** NBE, NP, DEN, RC, SK, MB, RDR, KKD, MK, MJ, CDJ, WOM, DJ, and JM conceived the project; NBE, PBF, MM, BC, DJ, and JM designed experiments; JD, GM, CS, MC, BAC, RDR, KKD, MJ, CDJ, WOM, and JM supplied specimens and extracted DNA; DJ, BC, GGA, and FDP assembled genomes, PBF inferred species trees; NBE performed reference gap filling, phylogenetic network, local gene tree, recombination rate, and genome structure analyses; JD and SVB generated linkage maps, MM, JW, and AB developed the branch length test; NBE and JM wrote and edited the manuscript with input from all authors. **Competing interests:** Authors declare no competing interests. **Data and materials availability:** Reads generated are available in the SRA, BioProject PRJNA531399. Genome assemblies are available on LepBase (http://lepbase.org). The full multi-species, whole genome alignment, as well as sub-alignments for windows and their respective inferred phylogenies are available on Dryad, DOI 10.5061/dryad.b7bj832. Also on Dryad are configuration files for progressiveCactus, the inferred LD recombination map for *H.* erato, loci used for phyloNet, and repeatMasker output for all assemblies. All code used to analyze data is available on Zenodo repositories, DOIs 10.5281/zenodo.3286366 and 10.5281/zenodo.2653677.

Supplementary Materials:
Materials and Methods
Fig.s S1- S95
Tables S1- S14
References (36-88)

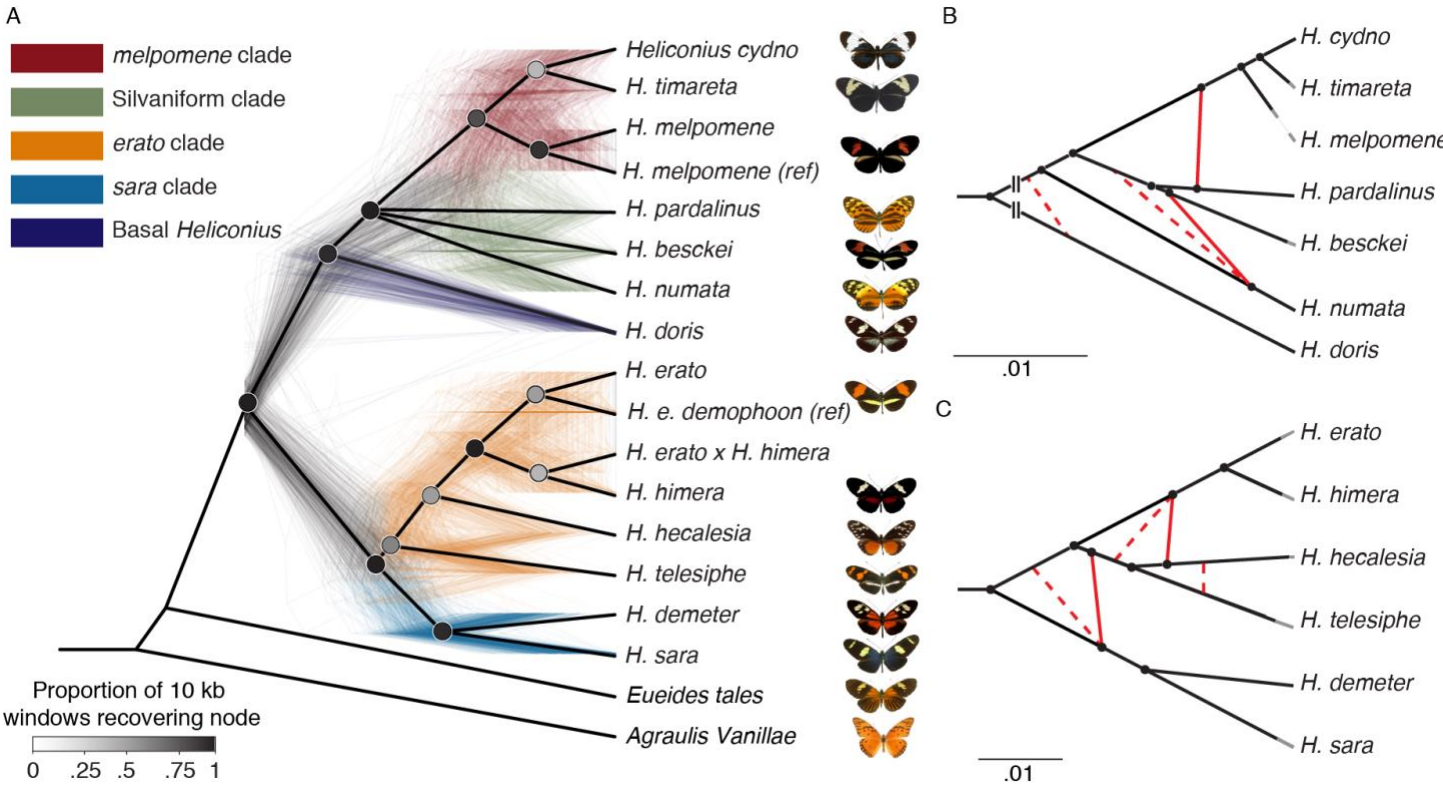

Fig. 1: Phylogeny and phylogenetic networks of *Heliconius* show lack of support for bifurcating tree.
A. All nodes resolved in a majority of species trees are shown in this cladogram (heavy black lines), while the poorly resolved silvaniform clade is collapsed as a polytomy (Fig. S20). The 500 colored trees were sampled from 10 kb non-overlapping windows and constructed with maximum likelihood. **B, C.** High-confidence tree structure (black) and introgression events (red) are shown as solid lines. Dashed red lines indicate weakly supported introgression events. Grey branch ends are cosmetic. The *melpomene*-silvaniform clade is shown in **B**, the *erato-sara* clade in **C.** Euclidean lengths of solid black lines are proportional to genetic distance along the branches. Scale bars in units of substitutions per site. Breaks at the base in **B** indicate that the branch leading to *H. doris* has been shortened for display.

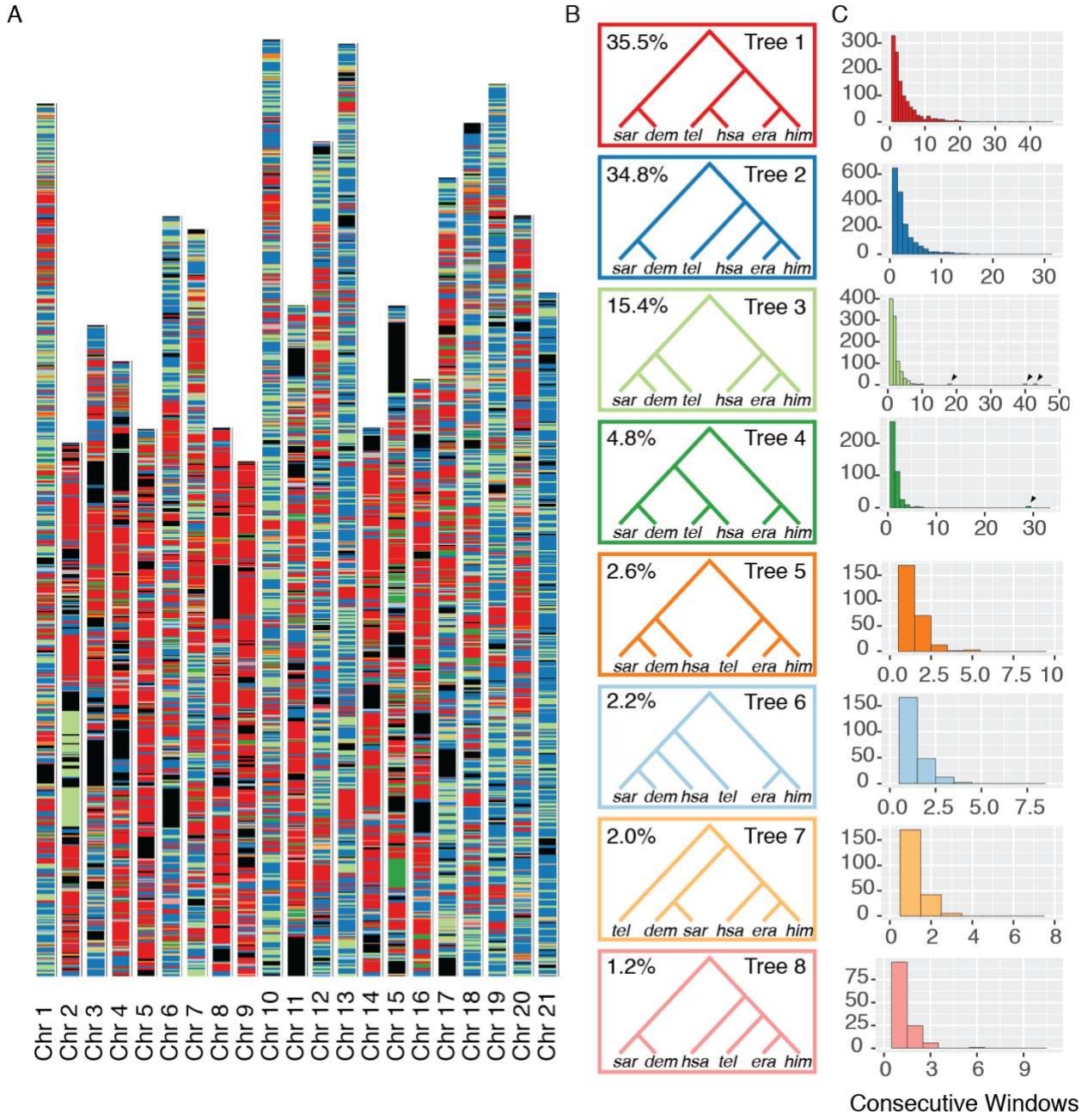

Fig. 2: Local evolutionary history in the *erato-sara* clade is heterogeneous across the genome. **A.** Each bar represents a chromosome, in terms of the *H. erato* reference (*14*). Colored bands represent tree topologies of each 50 kb window; colors correspond to the topologies in **B**, with black regions showing missing data. **B.** The eight most common trees are shown. The value in the top left corner is the percentage of all 50 kb windows that recover that topology. **C.** Each histogram corresponds to the topology of the same color in **B**, and shows the distribution of the number of consecutive 50 kb windows with that topology. Arrows indicate long blocks in inversions.

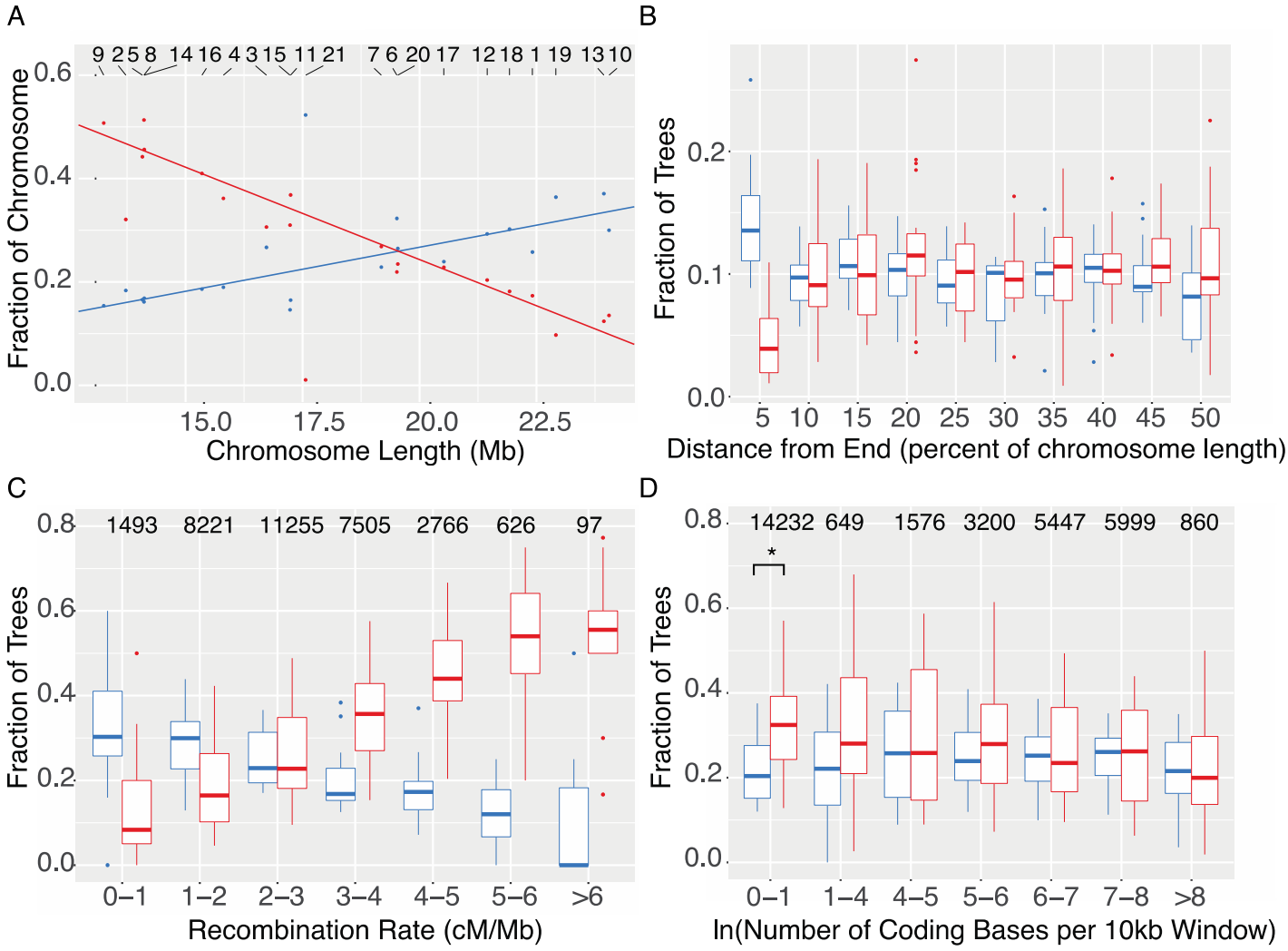

Fig. 3: Chromosomal architecture is strongly correlated with local topology.
Tree 1 is shown in red, and Tree 2 is shown in blue, as in Fig. 2. **A.** Tree 1 shows a negative relationship with chromosome size, while Tree 2 shows a positive relationship. Lines are linear regressions with chromosome 21 excluded. Numbers along top indicate chromosome number. **B.** Each chromosome was divided into 10 equally sized bins, and the occupancy of each topology in each bin was calculated as the number of windows that recovered the topology in the bin divided by the number of windows that recovered the topology in the chromosome. **C.** Windows are binned by recombination rate, and boxes show the fraction of each tree in each bin for each chromosome separately. Numbers above boxes are the number of windows in each bin. **D.** Boxes show the relationship of tree topology with coding density. Asterisk denotes significance at 5% level (paired t-test, $p<0.025$). In all boxplots, central line is median, box edges are first and third quartile, and whiskers extend to the largest value no further than 1.5*(inter-quartile range).

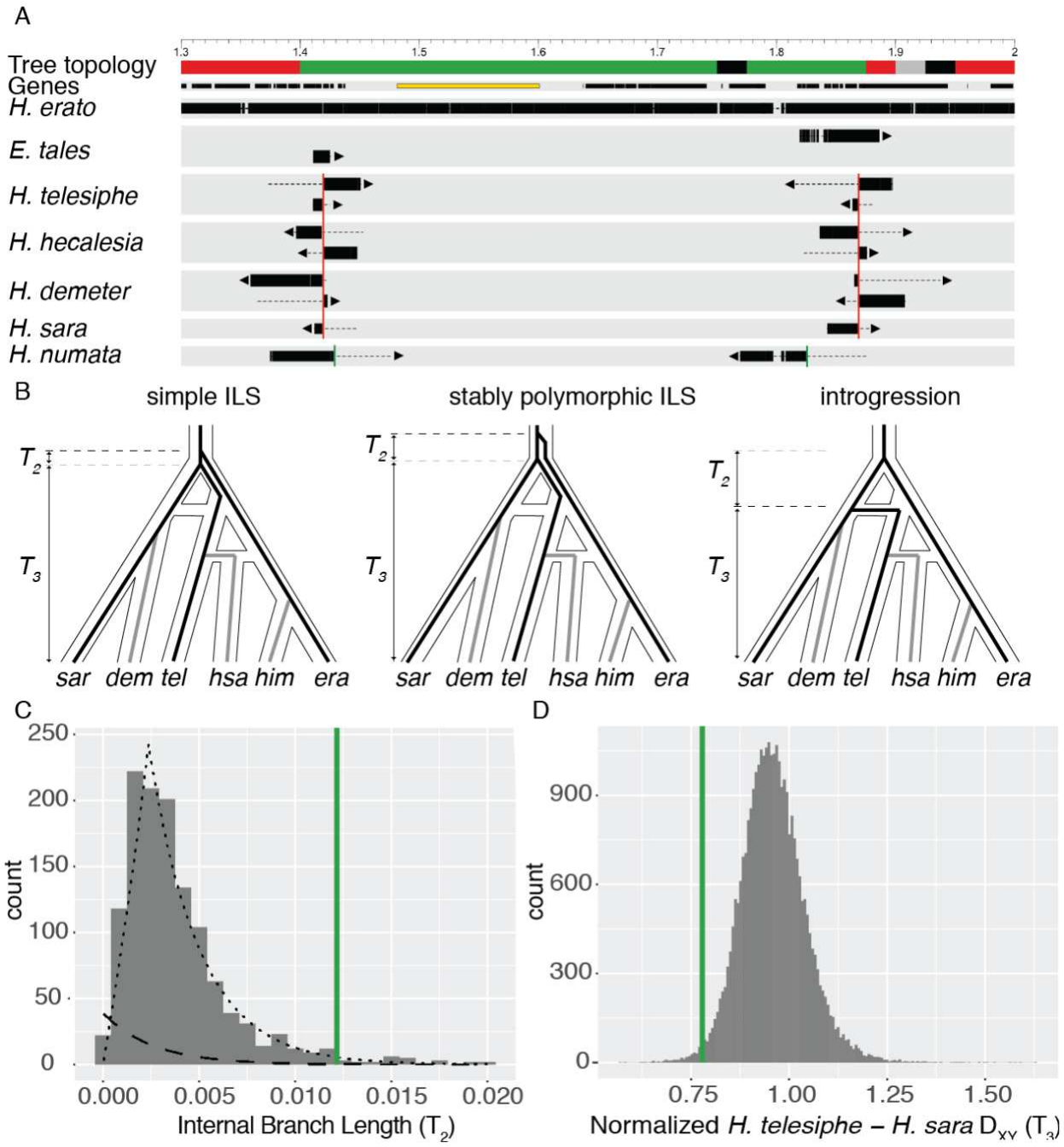

Fig. 4: Parallel evolution of a major inversion at the *cortex* supergene locus.
A. Map of 1.7 Mb region on chromosome 15. Coordinates are in terms of Hmel 2.5, and ticks are in Mb. Tree topology colors correspond to those in Fig. 2. Genes are shown as black rectangles; *cortex* is highlighted in yellow. Each line shows the mapping of a single contig. Aligned sections of each contig are shown as thick bars, while unaligned sections are shown as dotted lines. Arrows indicate the strand of the alignment. The *H. erato* group breakpoints are shown with red vertical lines, while the *H. numata* breakpoints are shown with green vertical lines. **B.** Evolutionary hypotheses consistent with the topology observed in this inversion in the context of the previously estimated phylogenetic network. The three species used in the triplet gene tree method – *H. erato, H. telesiphe,* and *H. sara* – are shown as black lines, while lineages not included are shown as grey lines. **C.** Histogram of internal branch lengths (T_2) in windows with the topology *H. erato, (H. telesiphe, H. sara)*. The inferred ILS distribution is shown as a

dashed line, and the inferred introgression distribution is shown as a dotted line. The average internal branch length in the inversion is shown as a green vertical line. **D.** Histogram of normalized D_{XY} (T_3) between *H. telesiphe* and *H. sara.* Mean normalized D_{XY} in the inversion is shown as a green vertical line

Science
AAAS

Supplementary Materials for

Genomic architecture and introgression shape a butterfly radiation

Nathaniel B. Edelman, Paul B. Frandsen, Michael Miyagi, Bernardo Clavijo, John Davey, Rebecca Dikow, Gonzalo García-Accinelli, Steven van Belleghem, Nick Patterson, Daniel E. Neafsey, Richard Challis, Sujai Kumar, Gilson Moreira, Camilo Salazar, Mathieu Chouteau, Brian Counterman, Riccardo Papa, Mark Blaxter, Robert D. Reed, Kanchon Dasmahapatra, Marcus Kronforst, Mathieu Joron, Chris D. Jiggins, W. Owen McMillan, Federica Di Palma, Andrew J. Blumberg, John Wakeley, David Jaffe, James Mallet

Correspondence to: nedelman@g.harvard.edu; jmallet@oeb.harvard.edu

This PDF file includes:
Materials and Methods
Figs. S1- S95
Tables S1- S14
References (36-88)

Table of Contents

Materials and methods

Samples

Individuals for sequencing were collected mainly in the wild, while others were from partially inbred stocks (Table S1). For *Heliconius melpomene*, we used a sibling of the strain of the original reference individual for the Hmel1 and Hmel2.5 assemblies (*36*). We also sequenced parents of a cross between *H. erato* and *H. himera*, and one of their F1 hybrid offspring – the *H. erato* mother was a sibling from the inbred strain used in the *H. erato demophoon* v1 genome (*14*).

Genome assembly with *DISCOVAR de novo* and w2rap

DNA was extracted from each specimen (Table S1). DNA samples were fragmented to ~450 bp and sequenced to at least 60x coverage using paired-end, 250 bp reads on the Illumina Hi-Seq 2500 according to the *DISCOVAR de novo* protocol (*37*). The w2rap-contigger was then used to assemble contigs (Table S2). Heterozygous genomes such as these yield complex assembly graphs where loci fail to collapse into a single representation and instead are often expanded into two alternative alleles (Fig. S1, left side). To overcome this problem, we filtered initial contigs to create a collapsed mosaic of haplotypes where each locus is represented by only one of the alternative alleles, ignoring phase, using the following procedure:

1) Homozygous content was selected using frequency of kmer spectra (*38*); this is content shared by both haplotypes and in a mosaic collapsed scenario should be included only once in the solution.

2) Initial contigs were sorted by size and filtered one at a time starting from the longest.

3) A tally was kept for all included content and resulting contigs were filtered by comparing the content that they had from the selected unique set and not already included in the final set. If a contig contained mostly kmers already included in the final set this contig was marked as complementary and saved in a separate file.

This method will for the most part result in inclusion of only one alternative allele at each locus in the final set of contigs. This filtered set of contigs with a putative single representation for each locus was then further scaffolded, using the same paired-end sequence data, with SOAPdenovo2 scaffolder (*39*) (Fig. S1, right side)

Assembly quality assessment

We used a custom python script (genomeStats.py) employing standard formulae to extract the number of contigs, their lengths, and N50 scores. In order to estimate heterozygosity, we used the k-mer based method GenomeScope (*40*). This online tool uses the output of jellyfish (*41*), which we ran with the commands

jellyfish count -m 15 -o <count output> -s 2000M -t 16 -F 2 -C <(zcat <readSfastq>) <(zcat <reads2.fastq>)
jellyfish histo -t 16 <count output> > <hist output>

We characterized the repeat content with RepeatMasker v4.05 (*42*). For each genome, we used the command

RepeatMasker -pa 4 -species hexapoda -xsmall -nocut <genome.fa> .

We include full results on Dryad.

We used BUSCO_v2 (*43*) with the arthropoda_odb9 database to compute the percentage of complete, partial, duplicated, and missing genes in our genome assemblies. Specifically, we used the command:

BUSCO.py -i <genome fasta> -c 32 -m geno -l arthropoda_odb9 -sp heliconius_melpomene1 -o <output file> -r

We summarized the data with BUSCO_plot.py, using R to display the results.

Alignment

w2rap Genomes with fewer than 50,000 scaffolds were aligned with previously published, representative genomes from across the lepidopteran phylogeny using progressiveCactus (*44*). This tool generates pairwise alignments in cactus graph format between each pair of sister species, generating inferred ancestral sequences. It iteratively continues this process for each node of an input phylogeny, generating blocks of aligned homologous sequence among all input genomes. This process allows alignment blocks to be projected onto the coordinates of any genome assembly and produces little bias towards segments highly similar to any one reference genome. All configuration files are available on Dryad, and additional information can be found in Supplementary Information Section 3.

Phylogeny

Species tree construction

We extracted nine different datasets to compute species phylogenies, consisting of two main types of data. First are "fully-aligned blocks". These were divided into coding and non-coding, as well as full Lepidoptera and Heliconiini, but all were filtered in the same way. Specifically we used the tool hal2maf from the haltools suite (*45*) to convert the hal-format multi-genome alignment into Multiple Alignment Format (MAF), with *H. melpomene* Hmel2.5 as the reference. This MAF file contains a separate "alignment block" for each homologous segment in the multi-species alignment. We filtered these alignment blocks for unambiguously aligned regions using phast tools (*46*) and a custom python script (getSingleCopy.py). We retained any alignment block in which all species of interest were represented by a single sequence. If either of these two criteria were not met, the entire alignment block was rejected. Genomic coordinates in BED format were intersected with coding sequence entries in the Hmel2.5 annotation file to separate coding from non-coding blocks. Finally, each filtered alignment was converted to fasta using msa_view from the phast suite. Before estimating gene trees, we further filtered our alignments for those with at least 10 phylogenetically informative sites.

The second set of data are gene alignments. We first extracted gene models from the Hmel2.5 annotation file with UCSC Kent binaries (*47*), then used the resulting gene model bed file to extract hal alignments to MAF. Next, we applied the unambiguous alignment filter detailed above, and further filtered the dataset so that included only loci that included all species, were 150 base pairs or longer, and had 10 or greater parsimony informative sites. This filtered set of alignments were then masked using Aliscore (*48*) and then trimmed using AliCUT (*49*)

For each of the nine datasets, we first estimated individual locus maximum likelihood trees (for gene-based trees, each locus consisted of all coding sequence within each gene, while the block trees were single contiguous stretches of fully-aligned sequence). We selected the best model for each locus using ModelFinder as implemented into IQtree (*50*, *51*). Following model selection, we estimated the best ML tree and 1000 ultra-fast bootstraps using IQtree (*52*). Since it is well known that, due to ILS, individual gene trees can be discordant with the species tree, we used a coalescent based method, ASTRAL (*53*), which accounts for discordance among gene trees, to generate species trees. ASTRAL takes individual gene trees as input and generates a species tree estimate by searching for the species tree that is most congruent with quartets garnered from the input gene trees. Using the resulting best ML trees from each locus as input, we generated species trees in ASTRAL (*53*). For each dataset, we also generated concatenated supermatrices using FASconCAT v.1 (*54*). We selected models for each supermatrix, first by searching for the best partitioning scheme using the relaxed clustering algorithm implemented in IQtree, using the individual loci as the starting data blocks, and second, by estimating substitution models for each partitioning scheme subset using ModelFinder. We then used the best fit model partitioning scheme to estimate maximum likelihood trees on the supermatrix. For each data set we performed 10 ML searches, five with parsimony starting trees and five with random starting trees in IQtree and chose the topology with the best maximum likelihood score.

DensiTree construction

We defined 10 kb non-overlapping windows on the *H. melpomene* (*13*) chromosomal scale using the *makewindows* tool in bedtools v2.1 (*55*). We then translated the chromosomal coordinates to scaffold coordinates using *bedtools intersect,* and extracted alignments from each window using *hal2maf* from the haltools suite (*45*). We filtered the MAF alignments for alignment blocks that were present as a single copy with a custom python script (getSingleCopy.py). We converted the MAF files to fasta with *msa_view*, and reconstructed phylogenetic trees with IQTree, using the GTR model and with 1000 bootstrap replicates. After obtaining a single best tree for each window, we filtered for windows with a final alignment length of >= 2000 bp, mean bootstrap support for the tree >= 80, and fewer than 25% total missing sites. We then sampled 500 trees and visualized them with ape v5.1 (*56*) in R. Summary statistics were calculated using code modified from https://github.com/mmatschiner/tutorials/blob/master/analysis_of_introgression_with_chromosome_length_alignments

Introgression analysis

ADMIXTOOLS

We first extracted MAF alignments of each scaffold from the HAL-formatted whole genome alignment using the hal2maf command from the haltools suite (*45*), with the *H. melpomene* Hmel2 genome as reference. We then converted from MAF to FASTA using the msa_view tool from the PHAST toolkit (*46*) FASTA to VCF using snp-sites (*57*), and finally VCF to

EIGENSTRAT using the vcf2eigenstrat tool from the gdc suite. Scaffold positions were converted to chromosomal positions using a custom python script (scafNamesToNums.py). Sites were included if they were present in all species (i.e. no missing data or gaps) as a single copy, bi-allelic SNPs. This resulted in a set of 6,671,421 SNPs.

We computed all possible *D*-statistics using the qpDstat command with default parameters, and considered all triplets of the 13 *Heliconius* species, holding *E. tales* constant as the outgroup. We assessed significance through a block-jackknifing approach as implemented in Admixtools (*11*), and applied a Bonferroni correction to assign significance at the 95% confidence level to a p-value of 1.37×10^{-4}, which corresponds to a Z-score of 3.81.

Sliding window tree building
Trees were inferred as described in "*DensiTree construction*", except that windows were 50 kb in length with start sites 25 kb apart on the *H. erato demophoon* v1 (*14*) chromosomal scale. In addition, a minimum of 5 kb of fully-aligned sites was required in order for a window to be used. After obtaining a single best tree for each qualifying window, we categorized them by topology with a custom python script (findCommonTrees.py) and visualized the results in R using the package *karyoploteR* (*58*).

PhyloNet
Due to computational limits, we were unable to analyze the whole *Heliconius* data set at once. We therefore divided our analysis into the *erato* and *melpomene* clades. When analyzing the *erato* clade, we used the *H. erato demophoon* genome v1 (*14*) as our reference, and when analyzing the *H. melpomene* clade, we used Hmel2 as our reference (*19*). We defined 10 kb windows, spaced 50 kb apart using the *makewindows* tool in bedtools v2.1. This was done to yield approximately independent of 10 kb windows; linkage disequilibrium blocks in *H.melpomene* are about 10 kb long, with virtually all disequilibrium lost by 100 kb (*36*).We then extracted MAF alignments of each region from the whole-genome alignment using the tool *hal2maf***.** We considered only single-copy regions, and filtered for windows with at least 1000 bp aligned among all species. This resulted in 5445 usable *erato* clade windows and 3208 *melpomene* clade windows. Because of computational constraints, we were only able to include a subset of the alignments in a single run of the PhyloNet v3.6.7 program MCMC_Seq. We therefore ran 100 iterations of the program for the *melpomene* clade and 150 for the *erato* clade, each time sampling 100 random loci without replacement. We ran a 10,000,000-iteration chain with a 2,000,000-iteration burn-in, sampling every 5,000 iterations. We also included two hot-chains of scale 2.0 and 3.0, and specified the maximum number of reticulations as 6. We generated consensus networks from these results in a method fully outlined in Supplementary Information Section 6.

Topology distribution
Trees were inferred as described in "*DensiTree construction*". To determine the fraction of each tree topology on each chromosome, we divided the number of windows that recovered the given topology by the total number of windows that successfully resolved any topology on that chromosome. For the distance to end of chromosome, we used the center of each window as the reference point and calculated the number of base pairs between that reference and the nearest edge. We then divided each chromosome into 10 equally-sized bins and calculated the fraction of each bin that recovered each topology in each chromosome independently. We assigned each of our 10 kb windows a local recombination rate (*14*) by intersecting the window positions with the

recombination map using bedtools (*55*). We then split the windows into bins based on their local recombination rate, and calculated the fraction of each bin that recovered each topology, again evaluating each chromosome separately. Finally, we used the gene annotations from *H. erato demophoon* v1 (*14*) to determine the number of coding bases in each 10 kb window. We found that the number of coding bases per window was distributed approximately exponentially, so we log-transformed the data before dividing it into bins. We then determined the topology distributions per bin per chromosome as above.

Recombination rate estimates

We estimated fine-scale variation in recombination rate along the *H. erato demophoon* chromosomes from linkage disequilibrium in population genetic data using LDhelmet v1.7 (*59*). Genotypes were called from whole genome resequencing data of ten *H. erato demophoon* individuals from Panama obtained from Van Belleghem et al. 2017 (*14*) using the Genome Analysis Tool Kit Haplotypecaller (*60*) with default parameters. Individuals' genotypes were subsequently phased along each *H. erato demophoon* reference genome scaffold using Beagle v4.1 (*61*) with default parameters. For further analysis, phased genotypes were retained only if they had a minimum depth (DP) ≥ 10, maximum depth (DP) ≤ 100 (to avoid false SNPs due to mapping in repetitive regions), and for variant calls, a minimum genotype quality (GQ) ≥ 30. Next, from the phased genotypes, fasta sequences were generated for 50 kb windows. These 50 kb windows were transformed to haplotype configuration files with the recommended window size of 50 SNPs used by LDhelmet to estimate composite likelihoods of the recombination rate. From the haplotype configuration files, lookup tables for two-locus pairwise recombination likelihoods and Padé coefficients were generated within the recommended value range. Transition matrices were calculated for each chromosome separately by comparing genotypes obtained from *H. erato demophoon* to the outgroup species *H. ricini*, *H. sara*, *H. telesiphe*, *H. clysonymous*, *H. hortense*, *H. hermathena* and *H. charithonia*. The likelihood lookup tables, Padé coefficients and transition matrices were used in the rjMCMC procedure of LDhelmet to estimate the recombination map. In this latter step, 1,000,000 Markov chain iterations were run with a burn-in of 100,000 iterations, a window size of 50 SNPs and block penalty of 50. For convenience, recombination rate estimates (ρ) were converted to cM/Mb by scaling values for each chromosome according to the map length of each chromosome as obtained from pedigree data.

Triplet Gene Tree Test

We first calculated "gene trees" for 5 kb abutting loci (windows). In order to mitigate linkage between loci, we sampled rougly 10% of the loci for our analysis. We then split each full gene tree into its component triplet topologies, determined the outgroup for each triplet, and calculated the internal branch length. We next grouped each set of branch lengths by triplet and by outgroup, and for each subset determined the likelihood that the branch lengths were best described by a simple exponential distribution as expected under ILS or a mixture of ILS and either introgression or speciation processes. The full method is detailed in Supplementary Information Section 7.

Simulations

Simulations were performed in ms (*62*) and msPrime (*63*). For each simulation, 1000 independent loci were generated using the parameters detailed in Supplementary Information

Section 7. From the tree outputs, sequences were generated for each locus using seq-gen (*64*). D and f_d statistics, as well as maximum likelihood trees (*65*) were then calculated from the sequence data using scripts from https://github.com/simonhmartin/genomics_general. Confidence intervals were generated by calculating means from random samples of 500 loci with replacement 100 times. We report the maximum and minimum values from those bootstrap samples. Similarly, QuIBL confidence intervals were generated by randomly sampling trees from 500 loci, using those as inputs to QuIBL, and reporting the maximum and minimum introgression fraction.

Mapping inversions

We first identified regions of interest (ROI) based on the coordinates of the first and last windows that displayed the altered tree topology. We then used the command *halLiftover* from the haltools suite to identify the contigs of each species that mapped to the ROI. We used a custom python script (pslToBed.py) to extract the relative positions of each alignment block on each contig and filtered for those that had segments aligned in both directions in the region of interest. We inspected these candidate contigs manually with IGV (*66*) and identified those in which the beginning of the contig mapped in one direction to one side of the ROI, and the end mapped in the opposite direction to the other side of the ROI. We used the coordinates where the contig alignments terminated as candidate breakpoints, and manually inspected all contig alignments for those that mapped across the breakpoints in a single direction.

Supplementary Text

Section 1. *DISCOVAR de novo*/w2rap Assembly and Quality

As stated in the main text, our initial assemblies contained many uncollapsed haplotypes, so that single-copy genomic loci actually appeared multiple times in k-mer plots (Fig. S1, left side). We used the protocol detailed in the main text methods to collapse those haplotypes in the final assembly (Fig. S1, right side).

We assessed the quality of our *de novo* assembled genomes by calculating standard metrics including N50, number of contigs, repeat content, and gene content. These values can be found in Table S2. N50 values reported here are relatively low compared to published *Heliconius* genomes due to the fact that they were assembled solely using short-read Illumina sequencing, and the number of contigs is relatively large for the same reason. Both of these metrics were quite variable, with N50 values ranging from 21,413 to 106,325 and number of contigs ranging from 17,678 to 62,414. We investigated whether the variation in contiguity could be explained by repeat content by evaluating each *de novo* genome with RepeatMasker (*42*). The distribution of repeat content appeared bimodal, with most *melpomene* clade species containing roughly 15% masked bases and most *erato* clade species containing 18-22% masked bases. However, there was no correlation between repeat content and N50 (Fig. S2).

Another possible factor contributing to variation in contiguity is heterozygosity. Heterozygosity may have been especially important, as *Heliconius* species generally have 1-5% heterozygous sites, and most of our specimens were wild-caught rather than inbred. We estimated heterozygosity using the k-mer based GenomeScope method (*40*), but found no correlation between heterozygosity and N50 value (Fig. S3). The only variable we tested that was correlated with N50 was contig number which, if genome sizes are comparable, is as expected (Fig. S4).

We further assessed the quality of the genome assemblies by aligning the *H. melpomene* and *H. erato* w2rap genomes to their respective reference assemblies (14, 19). We examined the coverage of the w2rap assembly on the previously published reference and vice versa and found that on average the w2rap assemblies covered 94 percent of the reference genomes, while the reference genomes covered 91 percent of the w2rap genomes (Table S3). The discrepancy is likely due in large part to a difference in total assembly size. The *H. melpomene* w2rap assembly is 14 Mb (5.2%) larger than Hmel2, and the *H. erato* w2rap assembly is 58 Mb (15%) larger than the *H. erato demophoon* reference. This difference cannot be explained purely by overrepresentation of repetitive elements, as the overall proportion of the genome identified by RepeatMasker as repeats is almost identical between the conspecific assemblies (*42*). It is more likely that the larger w2rap genome sizes are caused by uncollapsed haplotypes due to stringent thresholds employed in w2rap for collapsing heterozygous regions. This hypothesis is further supported by the observation that the F1 interspecific hybrid individual (*H. erato/H. himera* hybrid) has by far the largest total assembly size among *Heliconius* species and by BUSCO analysis showing slight increases in duplicated genes relative to high quality lepidopteran assemblies, as well as to other w2rap assemblies (Fig. S5) (*43*).

Apart from genomic coverage, we also queried whether w2rap contigs contained assembly errors by mapping all scaffolds greater than 1000 bp of the *H. melpomene w2rap* genome onto its

conspecific reference Hmel2. In order to assess alignment quality, we scored each contig according to the following scale. Colors in parentheses correspond to those in Fig. S6-Fig. S8:

Unique Map (dark green): The entire w2rap contig maps as a block to a single location in the genome.
All Inside (light green): The alignment of the contig may be broken into multiple blocks, but more than 95% of the contig maps to a single location defined by projecting the ends of the contig out from its highest quality alignment block.
>75% inside (yellow): More than 75%, but less than 95% of the contig maps to a single location as defined above.
>50% inside (orange): More than 50%, but less than 75% of the contig maps to a single location as defined above.
>50% Scaffold (pink): Fewer than 50% of the contig maps to a single location, but more than 50% of the contig maps to a single scaffold.
<50% Scaffold (red): There is no scaffold in which more than 50% of the contig maps.
2X Duplicated (sky blue): entire contig maps to exactly 2 locations in genome.
<=5X Duplicated (blue): entire contig maps to 3-5 locations in genome.
>5x Duplicated (dark blue): entire contig maps to at least 5 locations in genome.

We expect that each contig should map to a unique location in the reference, and we find that to be the case for 4,540 contigs (38% of contigs, 45% of genome size). We find that an additional 4,827 contigs (41% of contigs, 49% of genome size) map primarily to a single contig but not a single location (Fig. S6-Fig. S8). These cases could indicate that the w2rap contigs contain repetitive elements, are chimeric in content, or were able to bridge a gap in the reference assembly. We developed a method to identify regions that were likely in the latter case and successfully used the w2rap assembly to patch gaps in the Hmel2 reference (Supplement Section 2). A similar successful approach had also been adopted using our first pass *DISCOVAR de novo H. erato* assembly by the team assembling the *H. erato demophoon* reference genome (*14*).

Conclusion: comparison of DISCOVAR/w2rap with other assembly methods

This 20 genomes project was designed in 2013, testing how a then-novel, low-cost, short-read-only genome sequencing and assembly methodology (DISCOVAR *de novo*), might aid comparative genomics in non-model organisms such as *Heliconius*. The DISCOVAR assembler was originally designed as a variant caller for the human genome (*67*), but was later extended and upgraded to allow whole genome assembly for large genomes, under the name DISCOVAR *de novo* (*37*). More recently, DISCOVAR *de novo* (*68*) and a successor assembly method, w2rap (*69*), have been used to aid assembly of complex polyploid plant genomes, such as hexaploid wheat (*70*, *71*). These methods attempt to push low cost, short read sequencing to assemble very high quality contigs, by taking advantage of low cost, high sequence read accuracy, and relative computational simplicity of a single PCR-free library type with relatively long Illumina reads (2 x 250bp paired end).

As can be seen from the results above, w2rap used on the basic DISCOVAR protocol sequence data for Heliconiini was successful in assembling contigs of up to N50 lengths of ~ 20-100 kb (Table S2), but presumably due to the presence of perfect repeats longer than ~ 500 bp, failed to obtain greater contiguity. Nonetheless as we show below (Section 2), w2rap contigs can successfully be used to patch a substantial fraction of gaps found in traditional mixed library projects (e.g. Illumina, mate pair, and PacBio). In our case, these were the reference assemblies, *Heliconius erato* (*14*) and *Heliconius melpomene* where 30% of gaps could be patched (Section S2 below). We demonstrate below that this is because higher fidelity sequencing of imperfect repeats or low complexity regions by DISCOVAR complements the longer scaffolds obtainable by mixed library methods. We believe that this may be because higher levels of base-call errors from platforms like PacBio are very difficult for assembly methods to distinguish from imperfect repeats, at least without the added cost of very high PacBio or other long-read coverage. PCR-free Illumina-based sequencing protocols such as in DISCOVAR thus have the potential to provide low cost supplements to these more conventional mixed library projects, especially in complex genomes with many imperfect repeats (see also (*71*)).

Today, the Illumina HiSeq 2500 platform capable of sequencing 2x250bp reads upon which DISCOVAR was originally built is obsolete, and the purpose specific library construction pipeline at The Broad Institute is no longer supported. But PCR-free libraries of similar characteristics have become the current standard, and the 2x250bp reads in Illumina platforms have returned with the Illumina Novaseq, due to their sustained use in both small structural variant detection and assembly. Assembly of short read sequence data is often aided these days by longer range technologies: long-reads such as PacBio and Oxford nanopore, linked reads (e.g. 10X), or Hi-C (*72*), but short-read data remains a feature of most sequencing projects for its higher consensus accuracy. With PCR-free libraries now commonplace, and 2x250bp reads re-introduced with an even lower cost in the new Illumina platforms, we expect these analysis methods to co-exist with longer-range technologies for the time being.

Section 2: Scaffolding With *DISCOVAR*

The assemblies in this study were generated with high coverage, PCR-free sequencing. One advantage of this strategy is that slightly imperfect repeats can be distinguished more readily than in traditional assemblies that must account for PCR errors and base call uncertainty. Generally, contigs tend to "break" when they encounter repetitive elements, and if w2rap is more efficient at assembling these areas, we should be able to link contigs within scaffolds with the *de novo* assemblies. In fact, we may be able to correct ordering and orientation errors as well, but here we focus minimally on gap-filling between contigs. We developed a pipeline "Scaffolding With *DISCOVAR*" (SWD) for this purpose, though it can be used with any pair of assemblies and is not limited to *DISCOVAR/w2rap*. Code is available at www.github.com/nbedelman/ScaffoldingWithDiscovar . SWD was designed with the assumption that one assembly has high-confidence scaffolding but some gaps ("reference genome"), and the other has high-confidence base-call quality but is not well scaffolded ("filler genome"). The flow chart for this process is shown in Fig. S9 and is composed of 4 major steps. Below we give an explanation of the process assuming one is attempting to fill gaps between contigs within scaffolds. The tool will also be useful for ordering and orienting scaffolds, but these functionalities are still under development as of this writing. The commands below can be altered to fill gaps between scaffolds within chromosomes by simply replacing "chromosome" for "scaffold" and "scaffold" for "contig".

Step 1: Preparing the data
SWD takes:
1) a reference genome fasta with a sequence for every scaffold and containing a string of Ns between each contig,
2) a reference genome fasta with a sequence for every contig,
3) a map in bed format indicating the location of each contig on its respective scaffold, and
4) a filler genome.

If a user has (1), the scripts "*makeGenomeMap.py*" (SWD script) and *bedtools getfasta* (from the bedtools suite) will convert such reference genome FASTA files into (2) and (3). *makeGenomeMap.py* is capable of dividing a genome either at regions of *at least* a given number of N's (default) or a specific number of Ns (flag "exact").

Step 2: Aligning the filler genome to the reference genome
This pipeline was developed using LAST, but any aligner can be used so long as the output is in MAF format (*45*). The SWD package has wrapper scripts for building a genome index and running the LAST aligner *(SWD.py genomeBuild* and *SWD.py lastAlign*), which are optional but hopefully useful. After the genome has been aligned, the pipeline follows the chain and net protocol developed by UCSC, which can be read in more detail here (*46*). This ensures that we are examining the location of best alignment for each filler genome contig on the reference genome.

Step 3: Filtering for contigs that may be useful in gap-filling
We convert the resulting MAF alignments into specially-formatted BED files. Specifically, each BED file is comprised of the alignment location of a single filler genome contig and contains information as to which part of the contig aligns to which reference region, and provides a score based on how contiguous the full contig alignment is. The scoring strategy begins by projecting

the location of the end points of the contig out from the longest sub-alignment. For example, if a *DISCOVAR* contig is 10 kb in length, and its longest sub-alignment begins at contig position 2000 and ends at contig position 5000, and maps to a reference scaffold from positions 102000 to 105000, the projected position would be from reference scaffold 100000 to 110000 (Fig. S10-S11). The contig would then be scored as follows:

10: The contig maps as a single alignment to a single location in the reference genome
9: The contig maps as multiple sub-alignments, but at least 95% maps within the projected region
8: At least 75% of the contig maps within the projected region
7: At least 50% of the contig maps within the projected region
6: At least 50% of the contig maps to the same scaffold as the longest sub-alignment
5: Less than 50% of the contig maps to the same scaffold as the longest sub-alignment
4: The entirety of the contig maps to exactly two locations in the reference genome
3: The entirety of the contig maps to 3-5 locations in the reference genome
2: The entirety of the contig maps to more than 5 locations in the reference genome

Contigs whose score ranges from 6 to 8 are retained for the next step.

Step 4: Gap Filling
This step takes as input the bed files of contigs that passed the filter in step 3, the fasta file of reference genome contigs, and the fasta file of the filler genome contigs. For gap filling, as was done here, the flag "consecutiveOnly" must be set to True. The procedure in this step is as follows:

First, we identify groups of reference contigs and filler contigs that are linked together. For example, if filler contig 1 overlaps with reference contigs A and B, and filler contig 2 overlaps with reference contigs B and C, reference contigs A, B, and C, and filler contigs 1 and 2 would form a group. Next, we consolidate sub-alignments that are collinear and neighbor one another on a single reference contig. Once the sub-alignments are consolidated, we form super-contigs by joining together all the reference contigs that can be linked by each filler contig. In order to approve a link, there must be at least 1000bp of aligned sites on each of the reference scaffolds, and the order and orientation must be correct. This means that for reference contigs A and B to be linked by filler contig 1, the beginning of filler contig 1 must overlap the end of reference contig A by at least 1000bp, and the end of filler contig 1 must overlap the beginning of reference contig B by at least 1000bp. Once the super-contigs are made with the information from each individual fill contig, the super-scaffolds within a group are linked together in a similar manner. In each case, the end of the reference contig being joined will be replaced by the filler contig that overlaps it. This ensures contiguity across the gap and reflects the heuristic that the per-base accuracy of the filler contig is more trustworthy in these areas than the reference contig (Fig. S11-S12, Table S4).

In this study, we filled gaps solely within reference scaffolds. Taking a conservative approach, in which we assumed that the published order of contigs was correct, we were able to fill 30% of gaps (899/2990 stretches of >= 100 Ns) and increased the contig N50 by 39%. The overall genome size was reduced by 97 kb, after a reduction of 248 kb of Ns (Table S5). A similar approach was previously employed to use DISCOVAR data to fill gaps in the *H. erato*

demophoon v1 reference genome (*14*), resulting in a 12x improvement in N50. We examined the regions of the w2rap contigs that were inserted into the reference genome and found that they were more than twice as rich in repetitive elements as the full genome. This elevation was driven primarily by retroelements (15.69% of inserted sequences, 1.52% of whole genome) and small RNAs (9.41% of inserted sequences, 0.02% of whole genome). Interestingly, the abundance of DNA transposons decreased in inserted regions, comprising just 4.72% as opposed to 10% in the whole genome (Table S6). In order to confirm that our scaffolding procedure was not collapsing tandem repeats into single elements, we calculated read coverage in 10 kb windows and compared the mean coverage of gap-filled regions to that of other genomic loci. We found that the distribution of coverage depth was similar between the two groups, consistent with valid contig joins (Fig. S13-Fig. S15). The transposon content of these genome assemblies has been studied in great detail; see Ray *et al* 2019 (*73*)

Section 3: progressiveCactus Alignment

We generated a multi-species whole genome alignment using progressiveCactus (*44*). In order to create a high-quality alignment with power to detect evolutionary change at the root of the *Heliconius* clade, we filtered *de novo Heliconius* assemblies for those with fewer than 50,000 scaffolds, and further filtered the resulting assemblies for scaffolds larger than 1000 base pairs. We included previously published Lepidoptera assemblies including three additional species in the family *Nymphalidae* (*Melitaea cinxia* v1.0 (*74*), *Bicyclus anynana* v1.2 (*75*) and *Danaus plexippus* v3 (*76*)), one additional butterfly (*Papilio polytes* v1.0 (*77*), one skipper (*Lerema accius* v1.1 (*78*)), and two moths, (*Bombyx mori* ASM15162v1 (*79*) and *Plutella xylostella* DBM_GJ_v1.1 (*80*)). Genome size filtering was performed with a custom python script (filterGenome.py).

In order to run progressiveCactus on the Harvard Odyssey compute cluster, modification of the program was carried out by Harvard Research Computing to integrate with the SLURM scheduler. The modified version we used can be found here: https://github.com/harvardinformatics/progressiveCactus .

The final alignment was run with the command

```
runProgressiveCactus.sh <sequence file> <work directory> <hal output file>
--batchSystem=slurm \
--slurm-partition=serial_requeue \
--slurm-jobname <job name> \
--slurm-scriptpath=<batch script path> \
--slurm-time=1440 --slurm-constraint='holyib' \
--defaultMemory=6000000000 --bigMemoryThreshold=5000000000 \
--retryCount=3 --bigBatchSystem=singleMachine \
--configFile=local_config.xml \
--maxThreads=32 \
--logLevel=DEBUG \
--stats
```

All config files are available on Dryad.

In order to assess the success of the progressiveCactus alignment, we calculated pairwise alignment coverage between all species and *H. melpomene* Hmel2.5 (*13*) (Fig. S16, Table S7). We also computed cumulative 'alignment depth' using *H. melpomene* and *B. mori* as reference sequences. The cumulative alignment depth is a measure, calculated for each number between 0 and the total species in the alignment, of the percent of the reference genome that is aligned among at least that number of species (Fig. S17, Fig. S18).

Section 4: Phylogeny

This data and the resulting alignment comprise a truly genome-wide dataset that we used to infer phylogenies on multiple subsets of the data. In general, we analyzed three different data sets: full genes, fully aligned sites (defined as sites that contain a nucleotide for each species in the alignment) that are coding, and fully aligned sites that are non-coding. For the block alignments, we generated the same data sets for only those taxa included in Heliconiini (*Heliconius* species plus *Agraulis* and *Eueides*) (Table S7), and we further partitioned these data into regions greater than or equal to 100 base pairs, and greater than or equal to 150 base pairs. For the gene set, we removed all genes that had missing taxa, were shorter than 150 base pairs, and had fewer than 10 parsimony informative sites. In order to identify sites from the alignment that could mislead phylogenetic analysis due to random signal, we used Aliscore (*48*). Aliscore performs Monte Carlo resampling within a sliding window across the alignment and identifies regions of the alignment that are indiscernible from randomly generated sequence. Those regions were then removed using AliCUT v2.31 (*49*).

For each data set, we generated single locus trees, ASTRAL "species" trees (using the single locus trees as input), and concatenated trees. For each single locus tree, we used IQtree v. 1.6.1 to estimate the model (using the ModelFinder function in IQtree), the tree, and 1000 ultrafast bootstraps (command: iqtree -s <alignment> -m MFP -bb 1000 -safe) (*50-52*). For each concatenated species tree, we used IQtree v1.6.5 to:

(1) select an optimal partitioning scheme using the relaxed clustering algorithm (command: iqtree -s <alignment> -spp <partition_definition> -m TESTMERGEONLY -rclusterf 5 -rcluster-max 5000 -mset GTR -nt 48),

(2) select optimal models for each subset in the partitioning scheme selected from the previous run using ModelFinder, followed by a ML tree search and 1000 ultrafast bootstrap (command: iqtree -s <alignment> -spp <partition_definition>.best_scheme.nex -m MFP -nt 24 -safe -bb 1000), and

(3) conduct 15 additional ML searches for each concatenated data set using the relaxed clustering + ModelFinder partitioning scheme generated in step 2 (command for each search: iqtree -s <alignment> -spp <partition_definition>.best_scheme.nex -nt 24 -bb 1000 -safe). For each set of trees, we selected the tree with the best maximuim likelihood value.

As mentioned in the main text, trees generated from all methods were largely congruent. However, there were some interesting differences between phylogenies inferred from each dataset. To aid interpretaion and allow for direct comparison of tree topologies, we have summarized the support for each node of the consensus phylogeny in graphical format, shown in Fig. S19 and Fig. S20. In addition, one region of the tree was so poorly resolved that we maintained it as a polytomy in Fig. 1A. Specifically, monophyly of the traditional silvaniform group is supported by both analyses using full genes, but only a small subset of analyses that used fully-aligned blocks. In contrast, the clade *H. pardalinus* + *H. melpomene* subgroup is supported by almost all analyses that rely on fully-aligned coding blocks, and a topology with *H. besckei* basal to the other silvaniforms + the *H. melpomene* group is supported in a set of fully-

aligned coding blocks using a coalescent approach (Fig. S20 B). In addition we display node support based on the number of non-overlapping windows that contain each node. We restrict this data to those alignments >= 2 kb and with >= 80% bootstrap support, as in the heat map on Fig. 1A. A DensiTree figure with branch length information discarded highlights the relative frequency of each type of topology observed (Fig. S21). We summarize these resulting datasets by calculating the alignment length (total sites in the alignment), number of fully-aligned sites (sites with a nucleotide present for each species), mean bootstrap support, number of phylogenetically informative sites, total percent missing data, and probability of internal recombination (*81*) (Fig. S22-Fig. S33)

All inferred species trees are shown individually in Fig. S34-Fig. S51.

Section 5: *D*-statistics

We calculated *D*-statistics for all 364 triplets of the selected 14 *Heliconius* species, holding *Eueides tales* constant as the outgroup (we excluded the two w2rap assemblies that were conspecific with a reference genome). For each triplet, we calculated the *D*-statistic for all three possible species topologies. The distribution of the lowest *D*-statistic score for each triplet are shown in Fig. S52, and the corresponding Z-scores are shown in Fig. S53. Excluding the hybrid, which is inappropriately included as a "species" in a test for gene flow, we had 286 triplets total; this value is therefore reported in the main text.

To ensure our analysis was not biased due to aligning the genomes with a guide tree, we calculated *D*-statistics for the same set of species using an alternative progressiveCactus alignment with a guide tree that reflects a different order of branching in the uncertain silvaniform clade (*42*). In addition, the two alignments differed in species composition. The "LepBase" alignment included all genome assemblies, including those of low quality (accessed from lepbase.org). The values for the two alignments within each clade were very highly correlated, indicating no strong effect of the input guide tree on these results (Fig. S54, green points). Across clades, the correlation was not perfect, particularly when the *H. doris* genome was one of the samples (Table S9-Table S11, Fig. S54, blue points). Anomalies over longer evolutionary distances are expected, as the *D*-statistic was developed to examine very similar populations and assumes only a single mutation per polymorphic site. In addition, this deviation from the main correlation did not affect our downstream analyses, as we focused only on within-clade alignments.

Consistent with our other analyses, the strongest *D*-statistic we observed in the *erato-sara* clade was using the topology (*E. tales,(H. telesiphe,(H. hecalesia, H. erato)))* (Table S9). Here, the statistic was strongly negative, implying introgression between *H. telesiphe* and *H. hecalesia.* This helps to explain the discrepancy between the consensus species tree, in which *H. hecalesia* groups with *H. himera* and *H. erato* as in earlier studies, and the PhyloNet base topology, in which *H. telesiphe* and *H. hecalesia* are sisters (Fig. 1C). In addition, we find evidence for an association between both *H. telesiphe* and *H. hecalesia* with *H. sara* and *H. demeter.* This is consistent with the introgression proposed for the chromosome 15 inversion, and with the deep introgression event inferred by PhyloNet (Fig. 1C).

In the *melpomene*-silvaniform clade, the strongest *D*-statistic implied gene flow between *H. melpomene* and *H. pardalinus* to the exclusion of *H. besckei* (Table S10). Again, this is consistent with the network proposed in Fig. 1B, where *H. pardalinus* is inferred to have introgressed with the ancestor of *H. melpomene* + *H. cydno* + *H. timareta*. When examining the three silvaniform species, none of the possible topological relationships yields a *D*-statistic below 0.11, or a *Z*-value below 31. These high values imply that there is not a truly tree-like relationship among these species, consistent with our inability to resolve the polytomy shown in Fig. 1A and expanded upon in Fig. S20.

Section 6: Phylogenetic Networks

As stated in the main text, we used the MCMC_Seq method of PhyloNet to generate phylogenetic networks for the *erato* and *melpomene* clades separately. The MCMC_Seq method takes sequence alignments as input, and simultaneously estimates each local gene tree and the species network through the course of its MCMC run. Using sequence alignments in this way incorporates more information than contained in independently inferred gene trees, and in theory requires fewer loci to accurately reconstruct the true species network(*12*). We started by running 100 iterations of the program using 100 randomly sampled loci each time. We considered all runs in which the final output network had greater than 50% posterior probability, and summarized the results by generating a correlation matrix of those networks based on Luay Nakhleh's metric of reduced phylogenetic network similarity (*43*). We calculated each pairwise similarity score, and then used the R heatmap function to group all trees by similarity (Fig. S55-Fig. S56). For the *melpomene* clade, there was a single region of tree-space that was strongly supported. However, there were still slight differences among the specific networks represented in that strongly-supported region. Therefore, the most common introgression events are represented as solid red lines in the main text (Fig. 1B), while the less-common events are represented as dashed lines. We feel that this representation captures the uncertainty inherent in this analysis (main text, Fig. 1C). However, the *erato* clade was less clear, and we therefore repeated the analysis using 150 loci per run and doubled the chain length. Still, several regions of tree space seemed equally supported. Upon close examination, many of the differences are simply in direction or timing of introgression events. The clearest structural difference (i.e. change to the backbone tree structure) was that roughly half of the networks infer a base tree that recovers *H. telesiphe* and *H. hecalesia* as a monophyletic clade that admixed with the ancestor of *H. erato* and *H. himera.* The other half recovers *H. hecalesia* as sister to *H. erato* and *H. himera*, and identifies an introgression event either from *H. telesiphe* into *H. hecalesia* or vice versa. The remainder of the uncertainty lies in the timing of the introgression event into the ancestor of *H. sara* and *H. demeter.* Various networks place it at all possible branches of the tree with the exceptions of the *H erato* and *H. himera* terminal branches. As in the *melpomene* clade, the most strongly supported introgression events are represented by solid lines while less well-supported events are indicated by dashed lines.

We next aimed to test the robustness of the network results by repeating our analysis with other inference methods. A major drawback of the MCMC_Seq method above is its limitation to small datasets, so we only used a subset of available data in each run, and were only able to combine them after running each set. We therefore used another PhyloNet method, Infer_Network_MPL, to corroborate the result. This method uses all loci, but uses inferred gene trees as input data as opposed to sequence alignments (*50*, *51*). The method estimates the network by maximizing pseudolikelihood scores based on those input trees. We inferred gene trees using PhyML (*52*, *65*) from the same set of loci used in the MCMC_Seq method. In both clades, the major introgression events identified by MCMC_Seq were also found by Infer_Network_MPL, though not always in the same direction (i.e. *H. besckei-H. numata* in the *melpomene*-silvaniform clade; *H. sara/H. demeter - H. telesiphe/H.hecalesia* in the *erato-sara* clade) (Fig. S57).

Finally, we used the biallelic SNP dataset generated for our *D*-statistic analysis to generate a phylogenetic network with qpGraph (*53*). We iteratively added taxa to a model according to the following algorithm:

1. Begin with 3 species that have a well-defined, bifurcating history.
2. Add one species ("test taxon") to the tree in its most likely location based on previously published phylogenies and D-statistic values.
3. Run qpGraph.
4. If all statistics are equal to 0, return to 2. If not, continue to 5.
5. If the test taxon can be moved to a different location without adding a reticulation node, continue to 6. If not, move to 8
6. Move the test taxon to a different location without adding a reticulation node. The position should be informed by the output of qpGraph.
7. Return to 3.
8. Add a reticulation node whose position is informed by the output of qpGraph.
9. Return to 3.

Continue until all species are included in the phylogenetic network.

This method was successful for the *erato* clade *(*Fig. S58), because sister species relationships between *H. erato* and *H. himera*, as well as *H. sara* and *H. demeter*, were generally stable. This allowed us to build a backbone tree and vary the placements and admixture events involving *H. hecalesia* and *H. telesiphe* until we had a reasonably well-supported tree. These admixture events included the previously supported events between *H. hecalesia* and *H. telesiphe*, and between *H. telesiphe* and *H. sara*+*H. demeter*. The backbone tree differs slightly from that inferred by either PhyloNet method, most notably by the placement of *H. hecalesia* as sister to *H. sara*+*H. demeter*. However, a significant amount of *H. hecalesia* genetic material is inferred to trace its ancestry to its more classical placement as sister to *H. erato*+*H. himera.* We were also able to infer small admixture events involving *H. demeter.* This differs from the PhyloNet methods, which inferred admixture events involving the ancestor of *H. sara* and *H. demeter.*

Unfortunately, we were not able to use the qpGraph method with the *melpomene* clade. No sister species relationships were stable, and the space of possible models proved too large to search manually.

Section 7. Quantifying Introgression via Branch Lengths (QuIBL)

7.1 Introduction

Identifying introgression through its genetic signatures is of interest due to its impact on adaptation and speciation. However, random features such as deep coalescence (also called incomplete lineage sorting, or ILS) can muddy the signal of introgression by generating gene trees which differ from the species tree without any interspecies gene flow. One robust genome-wide approach to detecting introgression is Patterson's D statistic, which looks at imbalances in the frequency of discordant gene tree topologies (*11*). This statistic and related F statistics can be motivated from a coalescent standpoint (*82*), and can provide genome-wide estimates of introgression. Our goal in this section is to explain new tests that can be used to obtain more localized information. Specifically, we describe a test that does not rely on topology imbalances, but instead use the additional information in gene tree branch lengths within topologies to locate introgressed loci or estimate the likelihood that a given region displays its gene tree topology due to introgression rather than ILS.

We present a statistical framework for assessing whether a given set of gene trees shows evidence for introgression events or could be generated by ILS alone, as well as for calculating the odds that a given discordant locus was generated by ILS or introgression. The required calculations are unwieldy on the full gene tree, so inspired by the approach of Zairis *et al.* (*83*), we study the statistics of the set of three-leaf gene subtrees for each gene genealogy in our sample. Rather than consider every relationship in our sample at a particular locus, we take all sets of three terminals in the original tree and examine these triplet trees independently of each other. In particular, we compare the internal branch length of a given triplet at a locus to the genome-wide distribution of branch lengths in that triplet to classify it as likely introgressed or not. We implement this procedure as 'Quantifying Introgression via Internal Branch Lengths,' or QuIBL (https://github.com/michaelmiyagi/QuIBL). We assess the accuracy of QuIBL via coalescent simulations of gene trees detailed in section 7.5.4, and find that it performs well at inferring both the timing and proportion of introgression from nonrecombining loci. In addition, we compare QuIBL to D We use the following notation in the remainder of the section.

N_e	Effective population size, assumed to be constant through time.
u	Per-site, per-generation mutation rate.
θ	$4N_eu$, the population mutation parameter.
$EXP(\lambda)$	Exponential distribution with scale parameter λ.
$TEXP(\lambda, C)$	Truncated exponential distribution with scale parameter λ and truncation point C.
S_i	Time interval during which the species tree has exactly i extant lineages, measured in units of $2N_e$ generations.
H	Time back from the present until a hybridization event, measured in units of $2N_e$ generations.

Definitions S7.1

7.2 Motivation and assumptions

The method detailed in this supplement represents both the use of an alternative type of evidence in the assessment of the likelihood of introgression throughout the genome, as well as a test for introgression in a locus-by-locus manner. A particular innovation of this framework is its assignment of probabilities of introgression for individual loci under the multispecies network coalescent by leveraging expectation maximization, as detailed in section 7.5.1. Methods such as ABBA-BABA use information about the genome-wide frequencies of different site patterns, which give robust results but cannot always resolve local patterns of introgression in the genome, and rely on gene tree asymmetries to infer introgression.

By using information about the branch length distributions detailed in section 7.4, QuIBL only uses the inferred gene tree topology for partitioning the data. This means that each topology of each triplet is tested independently, and consequently we use a different line of evidence than site pattern-based introgression metrics like f_d (*35*). Thus, our method can be used in a complementary fashion with these statistics to produce an even more robust picture of the gene flow history of a set of taxa.

The theoretical justification for our method requires the hypothesis that the data take the form of nonrecombining neutral loci; this is standard for multispecies network coalescent resolution methods such as PhyloNet (*12*). As part of our model, we also assume that population sizes are constant within each individual branch of the multispecies network, as arbitrary changes in population size can create selection-like distortions in the expected distribution of coalescence times.

Via coalescent simulations detailed in section 7.5.4, we demonstrate that when our assumptions about the loci are met, QuIBL is consistently conservative about introgression events, and that the noise added by mutation causes conservative estimation of introgression rates. Additional sequence simulations described in sections 7.5.5 and 7.5.7.1 show that QuIBL is conservative and accurate at recovering the observable introgression fraction under a variety of demographic scenarios and recombination rates both absolutely and relative to D and f_d.

7.3 Intuition

We model the distribution of the length of the internal branch of a gene tree as a mixture of distributions resulting from the coalescence of two lineages within a branch of the species tree which only they share (e.g. introgression or speciation) and coalescence within the common ancestral population (e.g. ILS). Consider the simple case of a rooted species tree with three terminals. We can use coalescent theory to derive the expected branch length distribution of gene trees generated by that species tree. ILS alone will generate all three topologies with equal frequency and expected branch lengths, since the three lineages are exchangeable once they have reached the ancestral population. In addition to this, the gene tree topology consistent with the species tree is realized when the two sister lineages coalesce within the internal branch of the species tree, and as a result this matching gene tree topology will be both enriched in frequency and contain longer internal branches (Fig. S59).

We condition on the gene tree topology, and focus on the information present in its internal branch. Gene trees generated by ILS will have an internal branch length that follows an exponential distribution with scale parameter equal to one when time is measured in units of $2N_e$ generations.

If there is no introgression, all discordant gene tree topologies are generated by ILS alone, and will have internal branches sampled from an $EXP(1)$ distribution. In contrast, the concordant gene tree topology will have internal branches pulled from the distribution $EXP(1) + S_2 - TEXP(1, S_2)$, as shown in Fig. S60. Further, as shown in Fig. S61, if introgression has occurred at a locus, we can take the corresponding set of paths in the species network and obtain another distribution of the form $EXP(1) + C - TEXP(1, C)$.

The full branch length distribution for a given gene tree topology will be a mixture generated by multiple of these phenomena. Our goal is to use the observed branch length distributions to infer the mixture proportions of gene trees coming from each possible source.

7.4 The mixture distribution of internal branches of triplets

So far we have described the internal branch length of a triplet gene tree as $EXP(1) + C - TEXP(1, C)$ in coalescent units. In reality, branch lengths must be inferred from genetic data, in units proportional to mutations rather than N_e. We assume that they are measured in units of substitutions per site. If we take mutations to be Poisson distributed along the branches of the genealogy we require a scaling factor of $\lambda = \theta/2$. This gives us the following:

$$f(x; C, \lambda) = \begin{cases} \frac{1}{2\lambda}(1 + e^C)e^{-x/\lambda} & C\lambda \leq x \\ \frac{e^{-x/\lambda} - e^{x/\lambda}}{2\lambda(1-e^c)} & C\lambda > x \\ 0 & x < 0 \end{cases}$$

Equation S7.1: The branch length distribution.

Notably, this is non-differentiable at $C\lambda$, where it achieves its maximum, and reduces to an exponential distribution when $C = 0$, corresponding to the lineages being sampled from a single population. For any given gene tree triplet topology, the internal branch length distribution will be a mixture of distributions of this type (Fig. S62). There will always be some ILS component that has $C = 0$, with a possible additional distribution with C corresponding to the amount of time during which the two sister gene lineages are isolated. In reality, the mixture proportions between these distributions will be determined by the effective population sizes and lengths of each branch in the species tree. However, our implementation of expectation maximization to infer these parameters treats them as independent for computational simplicity, as it allows us to estimate the mixture proportions and parameters of each distribution iteratively (explained in greater detail in section 7.5.1). We find that our method still performs well despite this relaxation (see sections 7.5.4 and 7.5.5).

7.5 Inference

Since we need to estimate both the assignment of each locus to a distribution as well as the parameters of the distributions themselves, we use an iterative inference algorithm called expectation maximization (EM), which we describe using notation from definitions S7.2. Given K distributions to fit, EM works by alternating between two problems. First is the E-step, where we calculate the relative probability that a given branch length could be sampled from either of the distributions given values for the parameters $\{C_k\lambda\}$, λ, and$\{\pi_k\}$ (the peak locations, scaling, and mixing proportions respectively). Next is the M-step, where we fix the probabilities calculated in the E-step and search for the values of $\{C_k\}$, λ, and $\{\pi_k\}$ that maximize the log-likelihood.

X	The data, in the form of internal branch lengths in units of substitutions per site, represented as a vector with length n.
x_i	The i^{th} branch length in X.
K	The total number of contributing distributions in the observed triplet branch length mixture distribution, either 1 or 2 in our implementation.
λ	Scaling factor for converting the distributions in coalescent units to the observed branch lengths ($2N_e\mu$).
C_k	Interval parameter C of the k^{th} distribution.
π_k	Mixing proportion of the k^{th} distribution.
$q_{C\lambda}(x_i)$	$\pi_i f(x; C, \lambda)/\Sigma_k^K \pi_k f(x; C, \lambda)$, the soft assignment of the value x_i to either of the two K in $\{0, 1\}$.
$\log(L(\{x_i\}, \{C_k\}, \lambda))$	The log-likelihood, $\log \prod_{x_i \in X} \sum_{C_k} \pi_k f(x_i; C, \lambda)$.

Definitions S7.2

As we need a fixed K, we will define two competing models for each gene tree triplet topology, one with initial parameters $K = 1, C_1 = 0$ (a pure ILS model) and another with $K = 2, C_1 = 0, C_2 = 1$ (a model with a non-ILS component, whether due to speciation and/or introgression).

7.5.1 Expectation Maximization

We use EM to infer the parameters of the mixture models (see algorithm, Fig. S63). For the initial values, we take the mixture proportion of the k^{th} distribution, π_k to be $1/K$, $C_0 = 0$, and $C_1 = 1$. Given $\{C_k\}$, the optimal assignments of data to the k^{th} distribution is the ratio $\pi_k f(x; C, \lambda)/\Sigma_k^K \pi_k f(x; C, \lambda)$, which we denote $q_{C_k\lambda}(x_i)$. We update this value in the E-step and split the M-step into two parts, updating first the the peak of the k^{th} distribution ($C_k\lambda$) followed by the scalar λ conditioned on $C_k\lambda$. This repeats until the change in log-likelihood is below an input precision threshold, or a user-specified number of iterations have passed.

7.5.1.1 Picking $C\lambda$

In the M-step we want to maximize the log-likelihood by solving the following for each k:

$$C_k\lambda = \text{argmax}_{C,\lambda} \Sigma_{i=1}^n q_{C_k}(x_i) ln(f(x; C, \lambda))$$

However, since f is not differentiable at $C\lambda$ we need to consider points on either side of each $C\lambda$ separately. We rewrite $\Sigma_{i=1}^n q_{C_k}(x_i) \log(f(x; C, \lambda))$ in terms of the data above and below $C\lambda$:

$$\begin{aligned}
\text{E}[\log(L)] &= \sum_{x_i<C\lambda} q_C(x_i) \log\left(\frac{-e^{\frac{x_i}{\lambda}} + e^{\frac{x_i}{\lambda}}}{2\lambda(-1+e^C)}\right) + \sum_{x_i \geq C\lambda} q_C(x_i)\Big(-\log(2) + \log\left(\frac{e^{\frac{-x_i}{\lambda}}(1+e^C)}{2\lambda}\right)\Big) \\
&= \sum_{x_i<C\lambda} q_C(x_i)(\log(\sinh(x_i/\lambda))) - \sum_{x_i>C\lambda} q_C \log(e^{\frac{-x_i}{\lambda}/2\lambda}) + \sum_{x_i>C\lambda} q_C(-\log(2)) \\
&+ \sum_{x_i>C\lambda} q_C(x_i)(\log(1+e^C)) - \sum_{x_i<C\lambda} q_C(x_i)(\log(e^C - 1))
\end{aligned}$$

Equation S7.2: The expectation of the log-likelihood.

Conditioned on a particular value of λ, only the two terms on the last line differ between values of $C\lambda$ equal to sequential elements of the data. Furthermore, they are both convex, and consequently the whole sum is convex for values of $C\lambda$ between adjacent values in X. As a result, the expected likelihood is maximized by $C\lambda$ taking on a value realized by the branch lengths in the data. We need only search these finite possible values for our optimal $C\lambda$ and return it.

7.5.1.2 Finding the conditional λ using gradient ascent

To find λ given $C_k\lambda$, we calculate the λ-derivative of $\log(L)$ at the given value for λ and change λ by an amount proportional to this quantity. In the space of mixture models we are considering, we only need this derivative for $k = 2$, as when $k = 1, C_1 = 0$ we only have an exponential and the maximum likelihood estimate of λ is $\bar{x_i}$. For the former case, we still take $C_1 = 0$ as the exponential ILS component. This gives us the following for $k = 2$:

$$
\begin{aligned}
\log(L) &= \log \prod_{x_i \in X} \sum_{C_k} \pi_k * f(x_i; C_k, \lambda) \\
\frac{\partial \log(L)}{\partial \lambda} &= \partial\lambda \sum_{x_i \in X} \log \sum_{C_k} \pi_k * f(x_i; C_k, \lambda) \\
&= \sum_{x_i \in X} \partial\lambda \log(\pi_1 * f(x_i; C_1, \lambda) + \pi_2 * f(x_i; C_2, \lambda)) \\
&= \begin{cases}
\frac{-C_2\lambda - \lambda + \frac{C_2\lambda(2-\pi_2)}{\pi_2 e^{C_2\lambda} + 2 - \pi_2} + x}{\lambda^2} & C_2\lambda \leq x \\
\frac{\frac{C_2\lambda}{e^{C_2\lambda}-1} - \lambda - \frac{C_2\lambda(2-\pi_2) + \pi_2(2x - C_2\lambda)e^{\frac{2x}{\lambda}}}{2(1-\pi_2)\left(e^{C_2\lambda}-1\right) + \pi_2\left(e^{\frac{2x}{\lambda}}-1\right)} + x}{\lambda^2} & C_2\lambda > x
\end{cases}
\end{aligned}
$$

Equation S7.3: The derivative of the log likelihood with respect to λ.

We note that this can be extended to $K > 2$, but we do not observe distributions with more than two modes in our dataset. For completeness, we include the $k = 3$ case below. We use the following symbols for simplicity: $C_2\lambda = \beta$, $C_3\lambda = \gamma$, $\pi_2 = p$, and $\pi_3 = q$.

$$
\begin{cases}
\frac{x\cosh\left(\frac{x}{\lambda}\right)\left(-\frac{p}{e^{\beta/\lambda}-1} - \frac{q}{e^{\gamma/\lambda}-1}\right) + \sinh\left(\frac{x}{\lambda}\right)\left(\frac{p\left(e^{\beta/\lambda}(\beta-\lambda)+\lambda\right)}{\left(e^{\beta/\lambda}-1\right)^2} - \frac{\lambda q}{e^{\gamma/\lambda}-1} + \frac{1}{4}\gamma q \operatorname{csch}^2\left(\frac{\gamma}{2\lambda}\right)\right) + (p+q-1)\left(-e^{-\frac{x}{\lambda}}\right)(x-\lambda)}{\lambda^2\left(\sinh\left(\frac{x}{\lambda}\right)\left(\frac{p}{e^{\beta/\lambda}-1} + \frac{q}{e^{\gamma/\lambda}-1}\right) - (p+q-1)e^{-\frac{x}{\lambda}}\right)} & x_i < \beta, \gamma \\
\frac{\frac{px\left(e^{\beta/\lambda}+1\right)e^{-\frac{x}{\lambda}}}{2\lambda^3} - \frac{\beta p e^{\frac{\beta}{\lambda}-\frac{x}{\lambda}}}{2\lambda^3} - \frac{p\left(e^{\beta/\lambda}+1\right)e^{-\frac{x}{\lambda}}}{2\lambda^2} + \frac{x(-p-q+1)e^{-\frac{x}{\lambda}}}{\lambda^3} - \frac{(-p-q+1)e^{-\frac{x}{\lambda}}}{\lambda^2} + \frac{\gamma q e^{\gamma/\lambda}\sinh\left(\frac{x}{\lambda}\right)}{\lambda^3\left(e^{\gamma/\lambda}-1\right)^2} - \frac{qx\cosh\left(\frac{x}{\lambda}\right)}{\lambda^3\left(e^{\gamma/\lambda}-1\right)} - \frac{q\sinh\left(\frac{x}{\lambda}\right)}{\lambda^2\left(e^{\gamma/\lambda}-1\right)}}{\frac{p\left(e^{\beta/\lambda}+1\right)e^{-\frac{x}{\lambda}}}{2\lambda} + \frac{(-p-q+1)e^{-\frac{x}{\lambda}}}{\lambda} + \frac{q\sinh\left(\frac{x}{\lambda}\right)}{\lambda\left(e^{\gamma/\lambda}-1\right)}} & \beta \leq x_i < \gamma \\
-\frac{\gamma + \lambda + \frac{p(\beta-\gamma)e^{\beta/\lambda} + \gamma(p+q-2)}{p\left(e^{\beta/\lambda}-1\right) + q\left(e^{\gamma/\lambda}-1\right) + 2} - x}{\lambda^2} & \beta, \gamma \leq x_i
\end{cases}
$$

Equation S7.4: The derivative evaluated for the general three distribution mixture case.

We then add a value proportional to the derivative by a factor s to the current value of λ and check the likelihood. If it increases, we keep the new value and repeat until convergence. If at any point the proposed step decreases the likelihood, we decrease s by half and retry until we find the appropriate step size.

We note that given external knowledge about the value of $\lambda = \theta/2$, we recommend inputting this value directly, which our implementation supports. This both speeds up the procedure and increases power for inferring C and π.

7.5.2 Discrete case

If there is sufficient recombination or insufficient mutation such that the average locus contains $O(1)$ SNPs, treating the branch lengths as continuous may be misleading. Instead, one could use the discrete distribution of the counts of mutations on branches in the same way as the branch lengths, which we have included for completeness. We derive the probability mass function by treating mutations as a Poisson process with parameter a random variable distributed as the true coalescent branch length. Given our branch length distribution $f(l; C, \lambda)$, and taking $\Gamma(a, b)$ as the upper incomplete gamma function, we can write this as the following:

$$
\begin{aligned}
P(X=n) =& E[P(X=n|l)] = \int_0^\infty \left(e^{-\theta l/2} \frac{(\theta l/2)^n}{n!} \right) f(l; C, \lambda) dl \\
P(X=n) =& \theta^n \Bigg(((\theta^2-4)^{-2n-1}((\theta^2-4)^n((\theta-2)^{n+1}(\Gamma(n+1, \frac{1}{2}C(\theta+2)) - n\Gamma(n)) \\
&+ (\theta+2)^{n+1}\Gamma(n+1)) - (\theta+2)((\theta-2)(\theta+2)^2)^n\Gamma(n+1, \frac{1}{2}C(\theta-2))))/((e^C-1)n!) \\
&+ \frac{(e^C+1)(\theta+2)^{-n-1}\Gamma(n+1, \frac{1}{2}C(\theta+2))}{\Gamma(n+1)} \Bigg)
\end{aligned}
$$

Equation S7.5: The PMF for the SNP counts on internal branches.

Notice that we have reparameterized from λ to θ, the population mutation rate. For computational efficiency, we'll still use the inferred branch lengths as the search space for C. As a result, the algorithm remains unchanged, except that our likelihood is now composed of the above probability mass function. We include this for completeness, but do not use this formulation in our analysis, as it is significantly slower and our windows have many more than $O(1)$ SNPs on average.

7.5.3 Model selection

EM requires that we input a specified value for K, the number of distributions. As a result, we can test each triplet for K equal to 2 (an introgression model) and K=1 (an ILS-only model) as described in the opening of section 7.5. The introgression proportion estimates from the $K = 2$ test can be taken directly, or a filter can be applied to take only introgression events which significantly improve the likelihood fit of our model over an ILS-only model. To discriminate between these, we use the Bayesian Information Criterion test (BIC) in order to penalize models based on their number of parameters. We calculate the BIC value of the model using the following equation, where N is the number of datapoints in a topology, and $\hat{L}$ is the likelihood of the model with parameters we estimate via EM:

$$BIC = \log(N) * (2 * K - 1) - 2\log(\hat{L})$$

Equation S7.6: The Bayesian Information Criterion test.

The first term is meant to capture the number of parameters in a given model, with each distribution indexed by k having a value for C_k and a mixture proportion p_k, the latter of which must sum to 1. The model with the lower BIC value is then preferred, with a significance threshold for ΔBIC of > 10, which was selected prior to analysis per the standard set by Kass and Raftery. If the $K = 2$ introgression model is not significantly supported, we say that the introgression proportion fit to the data does not sigificantly improve the fit over an ILS-only model. We report these inferred introgression values in addition to the raw values as an additional, conservative, estimator.

7.5.4 Coalescent simulation tests

To verify the behavior of the procedure given knowledge of the true gene genealogies, we simulated coalescent trees using msprime (*63*) and observed the error in the parameter estimates (Fig. S64). Trees were generated with a fixed λ such that the reported branch lengths are in units of $2N$ generations, with N fixed at 10^6 to approximate *Heliconius* (*84*). We performed ten replicates of 650 trees for each combination of the parameter values for π_1 and C detailed in Table S12.

As we see only error in the form of false negatives (Fig. S64 B), and only at low mixing proportions (Fig. S64 C), these plots combined demonstrate that the error arises almost entirely as a result of the

non-exponential introgression distribution being mixed in at low frequencies (< 60 trees). In addition, we find in larger tests that this threshold is a result of the number of points rather than the proportion itself.

We find that the additional noise generated by only observing the sequence data on non-recombining blocks rather than the true coalescent branch lengths does not strongly change our inference. For this test, we first generated the genealogies for 1000 loci of length 1kb using msprime, under a three species model with demographic parameters detailed in Fig. S65. Then, we performed 100 replicates of the conversion of these trees to sequences using Seq-Gen *(64)* with a GTR mutation model with $\mu = 3 * 10^{-9}$, and lastly used PhyML *(65)* to infer trees for the generated loci. For these tests we used $N_e = 10^6$ to match our expectations for *Heliconius*, and generated the underlying gene genealogies when $C = 3N_e$ and the observable proportion of introgressed loci that do not experience ILS was 0.783, as we want to diagnose error due to sequence simulation and not ambiguity in the coalescent trees (the whole process of generating the 1000 true coalescent histories, then converting them to sequence data and model fitting 100 independent times apiece was replicated a total of 5 times, with one representative replicate shown in Fig. S66).

From these, the effect of sequence noise appears to be conservative as well, inflating the reported C value slightly (Fig. S66 A), which naturally decreases the estimated introgression probability (Fig. S66 B). This result is in line with the simulations conducted in section 7.5.5, and may reflect a slight conservative bias endowed by the depletion of zero-length branches due to our tree inference step.

7.5.5 Effects of demography

So far, we have assumed that population sizes are constant throughout the tree. To see if this assumption is fundamentally limiting, We tested whether our method is stable in inferring the observable introgression fraction, or the set of loci which migrate backwards in time but then do not go on to experience ILS. This quantity can be obtained from the backwards-in-time migration rate by multiplying the migration rate by the coalescence probability in the branch during the interval C *(85)*. We simulated a number of alternate demographic histories, generated sequence data, inferred trees, and estimated introgression fraction as we would with real data. In general, we find our method is robust to such tests, and is consistently conservative, as detailed below.

Our demographic tests were modeled on those of Martin *et al*, 2016 (*84*). The null demography used is presented in Fig. S65. We identify three relevant branches: the source of introgression, the recipient of introgression, and the common ancestor. We then chose one of these branches to alter in each test. For the source and recipient populations, we allowed the size to either double or halve at the time in which they split into their own lineage. For the ancestor, the size either doubles or halves partway up the branch, 8E6 generations from the present. We report the results for base population sizes of 250,000, 500,000, 1 million, and 2 million based on (*84*) (Fig. S67). Each simulation was run in msprime, with the sequences generated using Seq-Gen under the default GTR model, and trees inferred using PhyML. For completeness, we also report the expected introgression fraction as either simulated migration rate or observable introgression fraction (Fig. S68, S69) (again, this latter value is the probability that an allele is introgressed and does not experience ILS).

7.5.6 Effects of data filtering

In addition to these simulations, we tested the output when different filterings of the input data were used. In order to test the effect of recombination within our 5 kb blocks, we removed any windows that had significant support for an internal recombination breakpoint as measured by the phi test (*77*). Here, we find support for introgression in 68% of discordant topologies. We also used a highly filtered set, where we removed any windows with $< 80\%$ mean bootstrap support, < 50 phylogenetically informative sites, and $> 25\%$ missing data. Here, we recover overall more topologies concordant with the species tree (76% instead of 71%), but those with discordant topologies have a much higher probability of introgression: 94%. A similar result was found when we used the more distant *Eueides tales* as our outgroup, where we recovered 90.3% introgression amongst discordant topologies. These latter two filters select for conserved regions. Because gene trees inferred from loci experiencing ILS will have short internal branches, they may receive low bootstrap support. Filtering such loci out could therefore mask the exponential component of

our branch length distributions, biasing QuIBL's inference towards a higher introgression proportion. We therefore choose the more conservative approach of minimal filtering.

7.5.7 Output interpretation

Full results for the *erato-sara* clade of *Heliconius* can be found in Table S13. For each triplet topology in our two distribution model, C_2 corresponds to an estimate of the time in units of $2N_e$ generations that the two sister lineages were isolated from the third species. π_2 is an estimate of what fraction of the gene trees in the input that were not generated via ILS. λ corresponds to the single best estimate of $\theta/2$ for the branch in the species tree where the two sister lineages coalesced, averaging over both the ILS and non-ILS gene trees. One difficulty in interpreting model support for introgression is that hidden recombination events can bias the branch length estimates to be longer than the true coalescent history, increasing our inferred introgression probability. However, we mitigated this by selecting small windows which are less likely to contain a recombination breakpoint, and checked for the ILS modes this would generate as detailed above.

We show an example of the output from the method in Fig. S70. Distributions inferred using unlinked loci were used to calculate ILS and non-ILS probabilities for all windows in the genome. The triplet considered here is *H. erato + H. hecalesia + H. telesiphe*, and it was chosen because it illuminates the major introgression event between *H. hecalesia and H. telesiphe* discussed in the main text. According to the species tree, both previously published and inferred here, *H. telesiphe* should be the outgroup. The topology where *H. erato* is the outgroup is consistent with introgression between *H. telesiphe* and *H. hecalesia*, though it could also represent ILS. We do not infer large scale introgression between *H. telesiphe* and *H. erato* (Table S13), so we expect that many of the topologies with *H. hecalesia* as the outgroup correspond to ILS. The raw internal branch lengths are shown in Fig. S70 A-B, and it is clear that the topology corresponding to ILS has a significantly shorter internal branch than either of the other two topologies. This difference is borne out in the non-ILS proportion (Fig. S70 C), which reaches a relatively small maximum value of π_2 as compared to the other two topologies and plateaus, as shown in Fig. S70 D.

7.5.7.1 Output summary and f_d comparison

We compare this output to that of f_d using the same window alignments. We find that when examining the introgression topology (*H. erato* as outgroup), internal branch length is strongly, positively correlated with f_d (Fig. S71 A). When considering the inferred non-ILS probability, this correlation still exists, but the non-ILS probability is significantly higher than f_d, and has much of its mass at the maximum value (Fig. S71 B). The difference in absolute value is due to the fact that f_d loses power as time since introgression increases (*35*). We were interested in testing whether the plateau of introgression probabilities was biologically meaningful, or whether we may be losing power by not discriminating amongst trees with branch lengths above the threshold C_2. As explained in the main text, we expect introgressed regions to be more common in regions of high recombination, and this expectation should hold when conditioning on the topology and testing for introgression probability. We therefore used only those windows that recovered the introgression topology, and compared the correlation between QuIBL introgression probability, f_d, or raw internal branch length with chromosome size and local recombination rate. In the chromosome size comparison, all metrics are significantly correlated, with QuIBL being strongest (p=3.7 x 10^{-7}, r^2=.758, Fig. S71C) followed by f_d (p=2 x 10^{-4}, r^2=.543, Fig. S71D) and raw internal branch length (p=5.9 x 10^{-4}, r^2=.490). When comparing the introgression metrics to recombination rate, only QuIBL (p=3.7 x 10^{-7}, r^2=.758, Fig. S71E) and f_d (p=2 x 10^{-4}, r^2=.543, Fig. S71F) show a significant correlation, and not raw internal branch length (p=0.8, r^2=2.8 x 10^{-6}) These results are consistent with a biologically meaningful interpretation of the plateau in introgression probability.

Given the results of the independent triplet analyses, we can synthesize them by looking at the output for all tree topologies in all triplets. Fig. S72 A shows the distribution of C_2 values inferred from all triplets of the 13 Heliconius species in this study, while Fig. S72 B displays the corresponding π_2 non-ILS proportions. Among topologies with a considerable number of representative trees, non-ILS proportion increases with increase branch length, C_2, as expected (Fig. S72 C). Also as expected, topologies concordant with the species tree mostly show high values for π_2. There are some exceptions, most notably in triplets of the form *(H. demeter or H. sara) + H. telesiphe + (H. erato or H. himera)* (blue dots, π_2 <=.5, Fig. S72 C-D).

Such triplets correspond to branch 7-8 in Fig. S19 and are briefly discussed in Section 8 below. The low π_2 values are consistent with uncertainty as to the placement of *H. telesiphe* and with an extremely short internal branch leading from *H. telesiphe* to the ancestor of *H. sara* + *H. demeter*, such that most trees, even with the "species tree" topology arose via ILS. Those topologies with very few representative trees can often recover spurious values of C_2 and π_2, but as a percentage of ancestry in the genome, they are not impactful (Fig. S72 D). Based on these values in Fig. S72 D, we define a metric to assess the whole-genome triplet-by-triplet support for introgression. Let τ be the set of triplet topologies derived from the full taxon list, and τ_D the subset of these which are inconsistent with the species tree. Then we can represent the total proportion of introgressed triplet tests among discordant trees as the following:

$$E_{intro} = \frac{\sum_{\tau_D} \pi_2 * n}{\sum_{\tau_D} n}$$

Equation S7.7: Our estimate of introgression, equal to the sum of the introgression proportions for all discordant triplet gene trees over the total number of discordant triplet gene trees.

Where π_2 and n take values estimated for the triplet in τ_D we are considering. In order to compute the total proportion of triplet gene trees derived through introgression, we simply change the denominator in Equation S7.7 to the total number of inferred trees, both discordant and concordant. We note that this value is averaged over all triplet gene trees, and as a result is closely related but not equal to the proportion of loci in the genome that have introgression anywhere in their history.

In order to facilitate a direct comparison with our π_2 value for each topology, we calculated mean values for D and f_d for each of the 13 *Heliconius* species triplets, holding *E. tales* as the outgroup. π for a given "outgroup" in our method corresponds to the D or f_d statistic when that taxon is in the P1 position. This notation follows Patterson (*11*), where the topology is specified as (((P1,P2),P3),P4). f_d explicitly tests for introgression between P2 and P3. For example, consider the triplet *H. erato* + *H. hecalesia* + *H. telesiphe*, as above. When investigating possible introgression between *H. hecalesia* and *H. telesiphe*, those two species would be in the P2 and P3 position, respectively. In our method, we observe introgression between those two species when *H. erato* is the outgroup. Because the behavior of D and f_d with mis-specified trees is unclear, we only calculated comparisons in which the topologies were concordant with the species tree.

Results for these topologies are shown in Fig. S73. With respect to f_d, our non-ILS proportions are correlated but consistently higher for topologies with appreciable numbers of trees. We believe that this is due to the loss of power to detect introgression using f_d with increased time since the introgression event (*35*, additional discussion below). D is more strongly correlated with QuIBL's estimates, but also tends to be lower than QuIBL. This is unexpected given the results from our simulations above and below, in which QuIBL is consistently conservative relative to D. One explanation for this is that there may have been introgression between both pairs of species: P1-P3 and P2-P3. D values represent the difference of discordant site patterns, and would therefore underreport introgression if it occurred between both pairs of species. In contrast, QuIBL treats each putative introgression event independently.

In D and related tests, only biallelic sites are considered, and each such site is assigned a pattern in which the ancestral allele is denoted A, derived allele B, and the order is P1, P2, P3, O in the topology structure detailed above. In the case of a single haplotype per population, f_d for a given window becomes

$$f_d = \frac{\sum C_{ABBA}(i) - C_{BABA}(i)}{\sum C_{ABBA}(i) + C_{AABA}(i) + C_{ABAA}(i)}$$

Equation S7.8: f_d, an introgression estimator from Martin *et al.*

Where $C_{Pattern}(i)$ is the count of either 1 or 0, depending on whether or not the specified pattern is observed at site i in the window (modified from (*35*)). Here, it can be seen that the denominator includes sites private to P2 and P3. Therefore, as time since introgression increases, the number of $AABA$ and $ABAA$ sites increase as well, yielding lower estimates for f_d.The D statistic does not have this same property, and does show a correlation with our data, but it was designed for very closely related species and assumes that all $ABBA$ or $BABA$ sites arise due to either ILS or introgression (*11*). With additional

divergence time, this assumption is more likely to be violated due to convergent or multiple mutations at a single site, yielding more noise. To confirm this pattern, we simulated a number of different scenarios in which the backbone tree is held constant, but the time of introgression is varied. In Fig. S74 and S75, we use the same backbone tree as above, and vary window size, migration time, and population size. In every case, QuIBL non-ILS proportion remains constant, while f_d decreases with time since introgression. D appears to estimate the introgression fraction quite well with no recombination. In cases that include recombination (Fig. S76), D overestimates introgression, f_d consistently underestimates introgression, and QuIBL is robust until recombination greatly exceeds mutation rate. Even in this case, however, QuIBL is closer to the simulated migration rate than D or f_d.

Section 8: Topology distribution

We calculated regional topologies in sliding windows across the genome in a number of different configurations. Interestingly, although we have a single multi-genome alignment, the fraction of windows that recovered each topology varied depending on whether the *H. erato demophoon* v1 or Hmel2.5 coordinates were used as reference. This may be due to weaker alignability between the *erato-sara* clade genomes and the Hmel2.5 assembly relative to *H. erato demophoon*, or may be due to the fact that the *H. erato demophoon* genome is approximately 100 Mb (33%) larger than the Hmel2.5 genome. The genome topology map using the Hmel2.5 coordinates is shown in Fig. S77A, and the most common topologies, their relative fractions, and block length distributions are shown in Fig. S77B,C. We also used 10 kb non-overlapping windows instead of 50 kb when mapping onto the *H. erato* genome. The chromosomal map constructed from these data are shown in Fig. S78, while basic alignment and phylogeny statistics including alignment length, number of phylogenetically informative sites, bootstrap support, missing data, and probability of recombination within a window are shown in Fig. S79 and Fig. S80. Those windows with at least 2 kb of aligned sites and mean bootstrap value >= 80 were used for all subsequent analyses of topology distributions. To ensure that variation in topology distribution along the genome was not driven by factors aside from recombination *per se*, we calculated the above general statistics for windows recovering each tree topology, as well as windows binned into recombination quintiles. We compared groups using the Kruskal-Wallace test, followed by the post-hoc Fisher's least significant difference (LSD) test with a Bonferroni correction, as implemented in the agricolae package (v1.3-0) in R (*86*). In all figures using this method, groups that are not significantly different from each other are labelled with the same letter. When applicable, we subset each category of data so that we compare equally-sized groups. We found no significant differences between the two major trees in any statistic aside from intra-window recombination (Fig. S81). Among recombination quintiles, there was a trend in which the higher recombination regions contained more phylogenetically informative sites. However, this trend did was not carried over into tree confidence as measured by bootstrap support. As expected, the recombination quintiles as calculated by LDHelmet correlated with probability of recombination within each window (Fig. S82).

With these data, we aimed to elucidate structural genomic features associated with regional evolutionary histories, and therefore first characterized the ways in which those structural features vary and co-vary across the genome. Recombination rate is higher in regions of low gene density (Fig. S83, Fig. S84), and is lower at the edge of chromosomes (Fig. S85). However, gene density is constant across chromosomal position (Fig. S86). There is an unexpected, slightly positive relationship between chromosome size and gene density (Fig. S87), and a strongly negative relationship between chromosome size and average recombination rate (Fig. S88), though this correlation is weaker than in *H. melpomene* (*8*, *87*), though the sample size for *H. erato* is much lower than that for *H. melpomene.*

As stated in the main text, the fraction of a given topology recovered in each chromosome was strongly correlated with that chromosome's total size in base pairs, and relationships for all 8 of the most common topologies are shown in Fig. S89, and their correlation coefficients are listed in Table S14. The Z chromosome was excluded when computing correlation coefficients, as the values recovered from it are clear outliers, almost certainly because the Z chromosome is often

involved in F1 hybrid female sterility, in accordance with Haldane's Rule (*22*, *23*). Values from the chromosomes that contain inversions (chromosome 2 and chromosome 15) are also outliers, but as they form a minority of each chromosome, we included their chromosomes in this analysis; thus reported values are conservative estimates. Tree labels in Table S14 correspond to those in the main text Fig. 2B. All 8 most common topologies had significant associations with chromosome size ($p<.05$), with correlation coefficients (r^2) ranging from 0.197 to 0.883. We also examined the correlation between topology and binned position along the chromosome – Fig. S90 reflects the per-bin breakdown (all topologies within a bin sum to 1), while Fig. S91 reflects the per-tree breakdown (all measures of each tree type sum to 1). Regardless of how we split the data, we find an increase in "species tree" topology in the low-recombination regions at the edges of chromosomes. We then binned windows by their recombination rate as determined by linkage disequilibrium (*14*), and again saw a very strong negative correlation between species tree topology and recombination rate Fig. S92. Finally, we also predicted that topology would be associated with the density of coding sequence per window if incompatibility alleles were more likely to be in coding sequence. That relationship is much weaker, but we detect a minor decrease in species tree topologies in regions with very low coding sequence density (Fig. S93).

Interestingly, some triplets we examined show a reversal of the prevailing correlation with chromosome size. When examining the topology restricted to the triplet *H. demeter – H. telesiphe – H. erato*, windows with the "species tree topology", (*H. demeter, (H. telesiphe, H. erato*)) are slightly negatively correlated with chromosome size, while windows with the "introgression topology" (*H. erato, (H. demeter, H. telesiphe*)) show a slight positive correlation (Fig. S94). A small subset of our ASTRAL species trees also support this topology, but the relationships are weak.

Section 9: Chromosome 2 Inversion
return to top

As mentioned in the main text, a large region on chromosome 2 displayed a topology discordant with the most common species relationships in the *H. erato* group. This region corresponds to a previously described inversion between *H. erato* and *H. melpomene.* We confirmed that this was in fact that inverted region by mapping all *erato* clade contigs onto Hmel2 (Fig. S74). We found clear evidence of an inversion in the *H. erato demophooon* reference genome, as well as the *H. hecalesia de novo* assembly. We also found contigs in *H. sara* and *H. demeter* that mapped across one of the inversion breakpoints, indicating that they are in the same orientation as *H. melpomene.* However, the breakpoints of this inversion are flanked by repetitive sequence that was difficult to align among all species, especially the left-hand breakpoint. Therefore, we infer the orientation of the inversion in *H. himera* and *H. telesiphe* based on the local topology (Fig. S95 A; Topology is Tree 3 in main text Fig. 2B). As was done for the chromosome 15 inversion in the main text, we used the branch length method in combination with D_{XY} to evaluate whether the discordant history seen in this region was due to ILS, inversion, or some other process. Again, we used the *H. sara, H. telesiphe, H. erato* triplet, and again we found that the internal branch length in the inversion was much larger than expected under simple ILS (Fig. S95 E). However, in contrast to the chromosome 15 inversion, normalized D_{XY} between *H. sara* and *H. telesiphe* was very close to the genome-wide average (Fig. S95 F). Normalized D_{XY} (T_3) is calculated as D_{XY} between *H. telesiphe* and *H. sara* divided by the mean pairwise D_{XY} among all species in each region. This combination of statistics supports a history in which the inversion originated in the ancestor of the *erato-sara* clade and remained polymorphic for some time before speciation of the taxa we sampled.

In addition to ancestral polymorpism, the homologous region shows strong F_{ST} peaks between *H. erato* subspecies (*14*), so it is possible that this inversion remains polymorphic among some extant lineages. No ecological or other functional role has been implicated for this inversion, but such a large ancestrally polymorphic inversion that remains polymorphic to this day almost certainly indicates some sort of balancing selection.

Supplementary Figures

DAS_09-93 - *Heliconius burneyi*

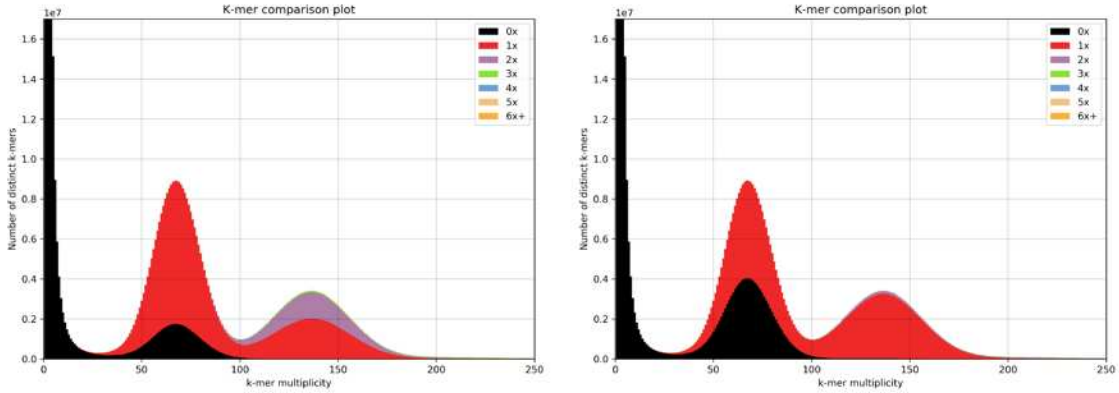

DAS_09-132 - *Eueides tales*

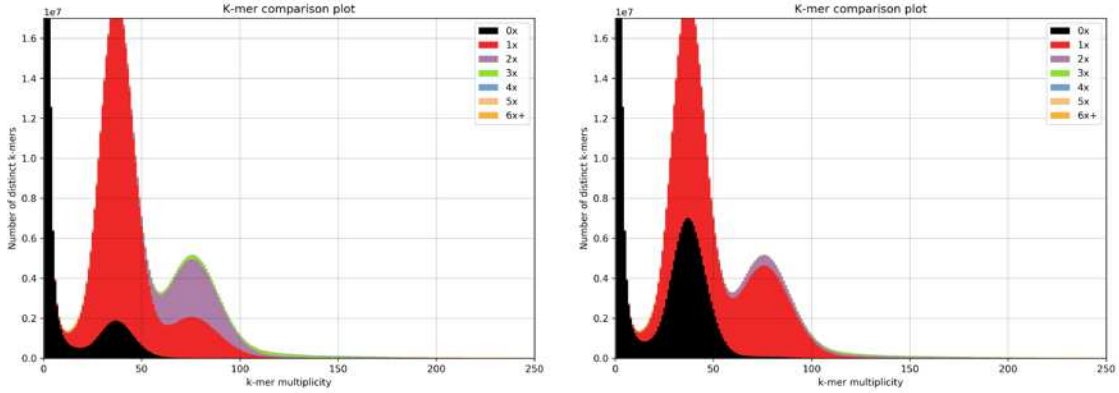

DAS_09-229 - *Heliconius telesiphe* (contaminated)

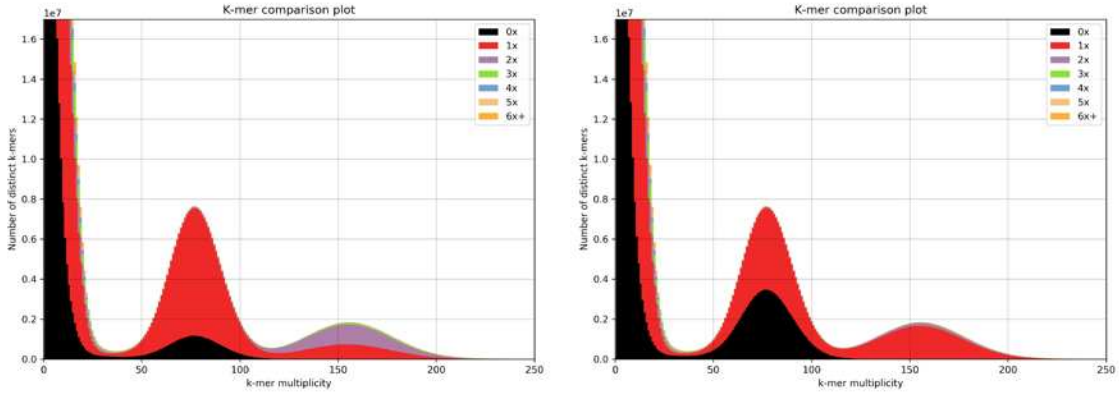

DAS_11-919 - *Heliconius telesiphe*

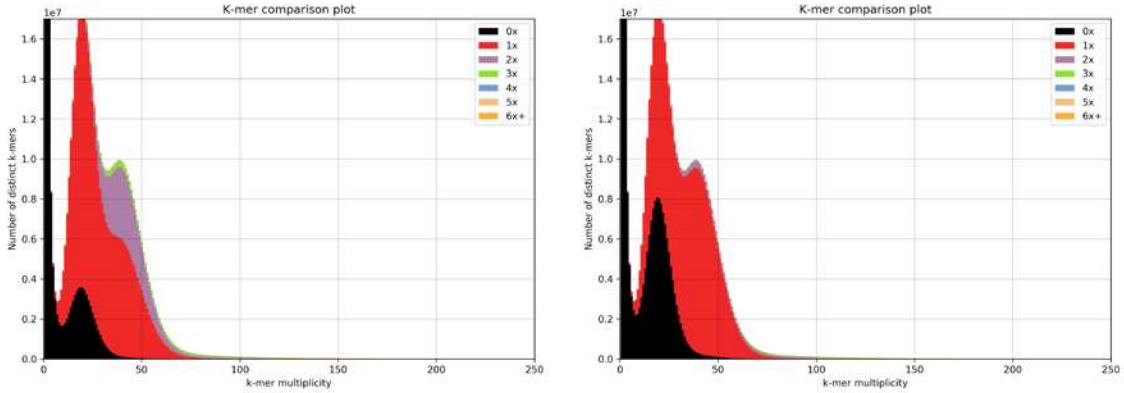

CAM-008802 - *Heliconius sara*

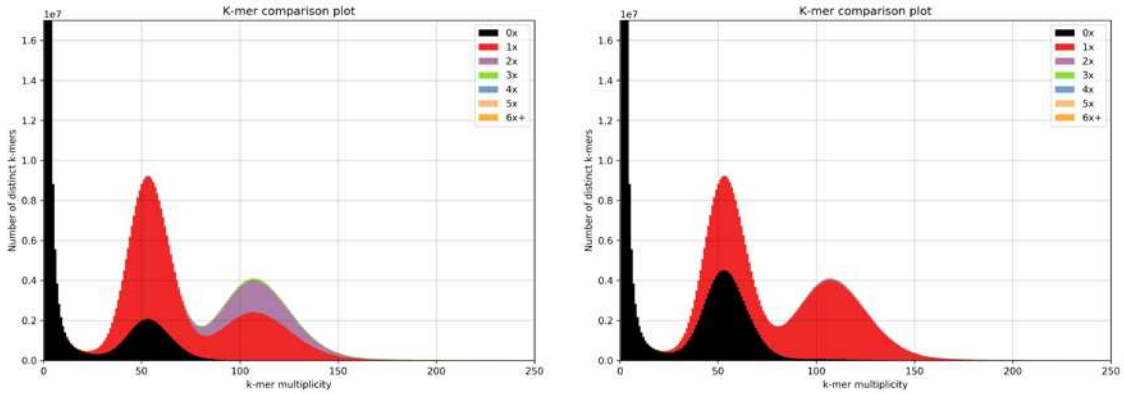

DAV_3 - *Heliconius hecale* (replaced)

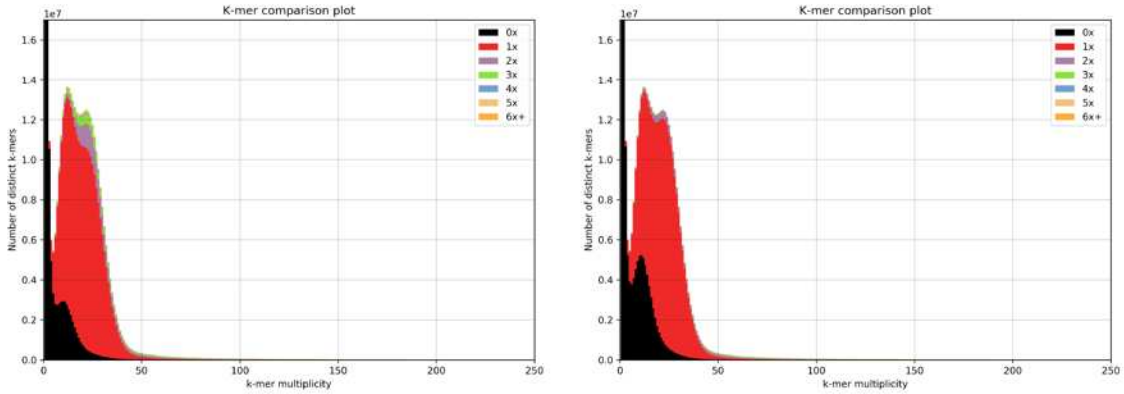

MCM_6897 - *Heliconius doris*

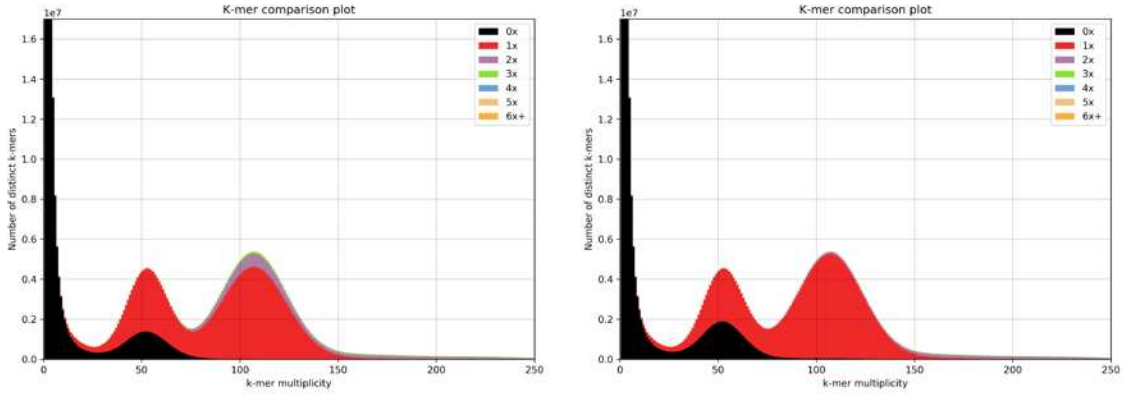

CAM-002492 - *Heliconius hecalesia*

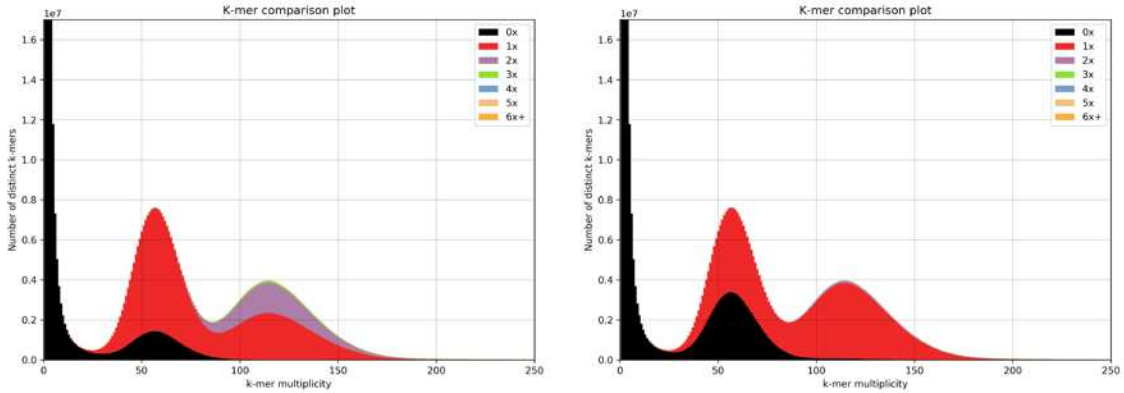

DAS_11-759 *Dryas iulia*

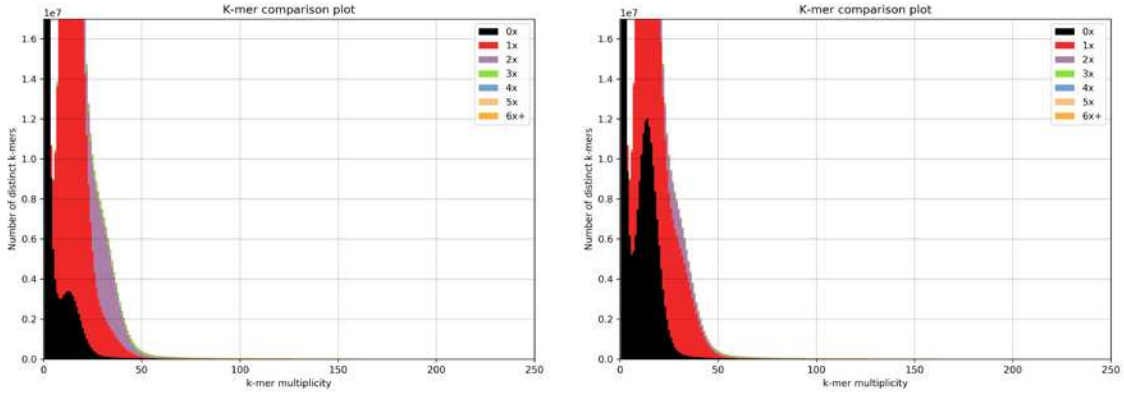

MCM_6900 - *Heliconius himera*

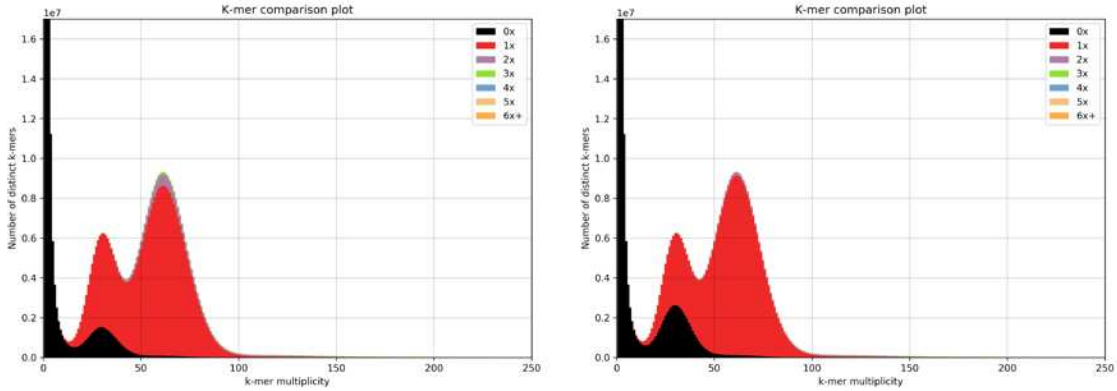

MCM_7203 - *Heliconius hecale*

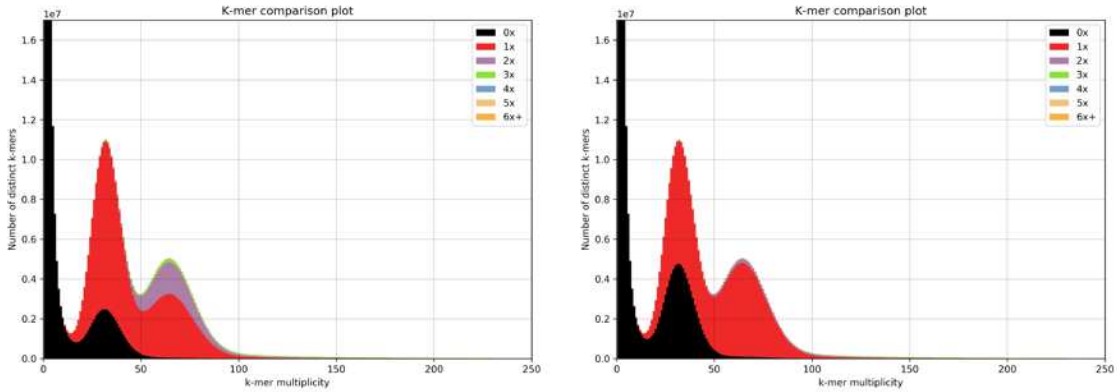

MCM_6700 - *Heliconius erato* x *himera* F1

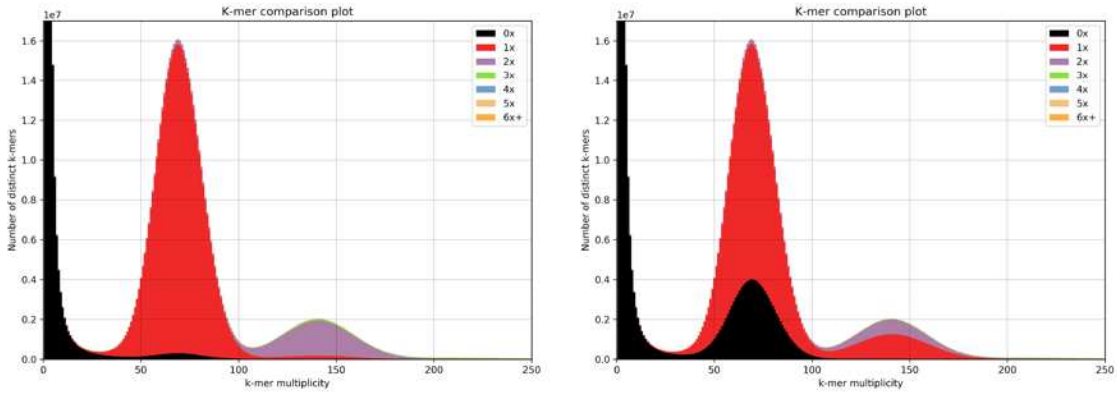

REE *Agraulis vanillae*

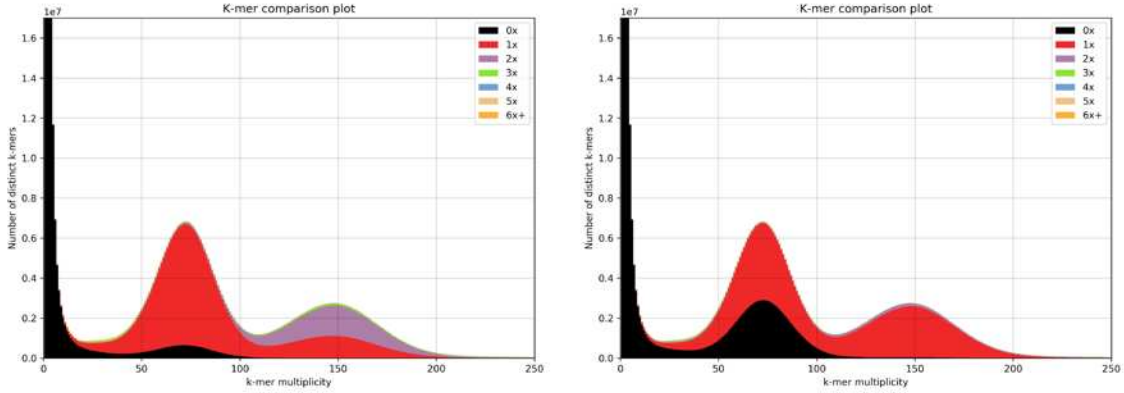

MCM_6394 - *Heliconius erato* mother

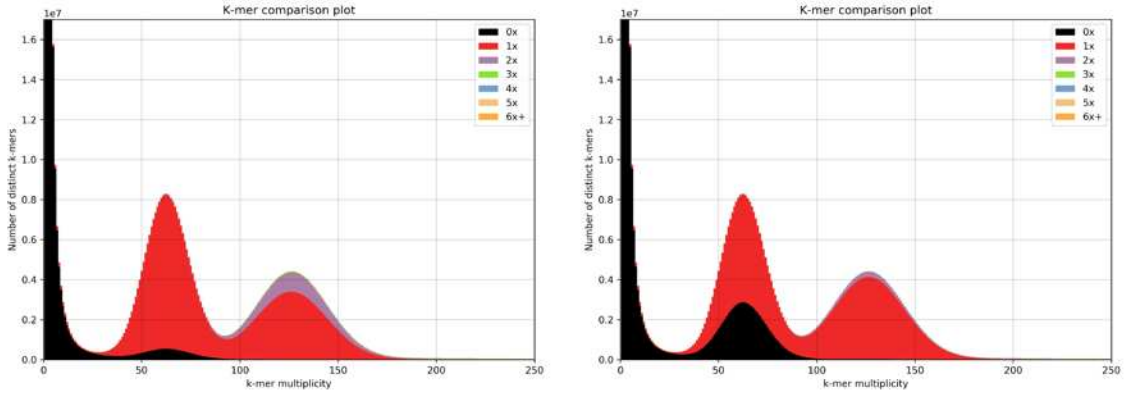

MCM_6363 - *Heliconius himera* father

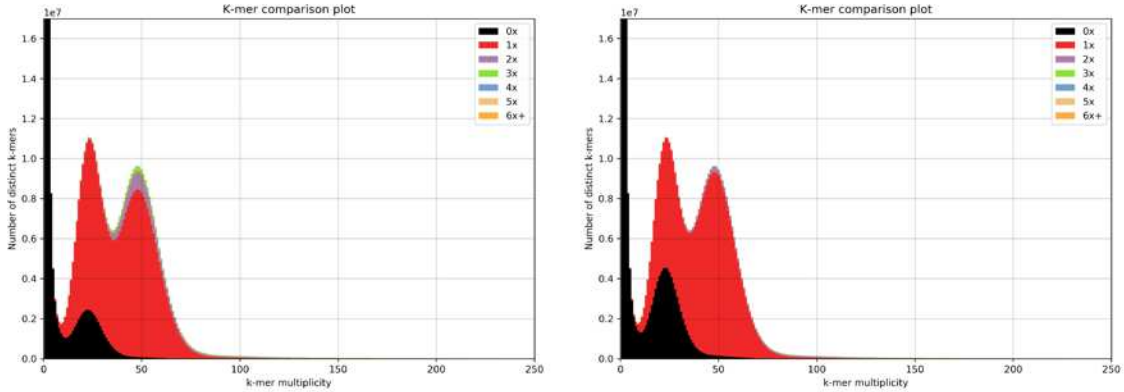

DAV_2 - *Heliconius cydno*

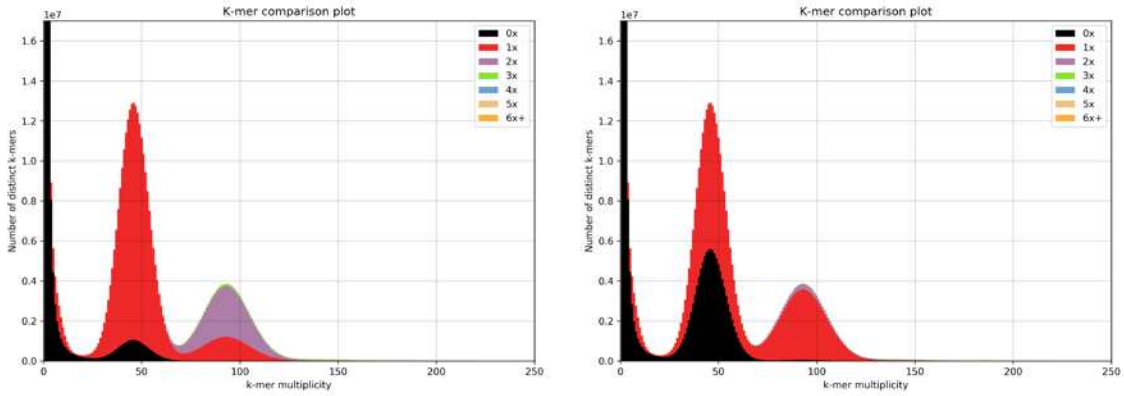

DAV_4 - *Heliconius numata*

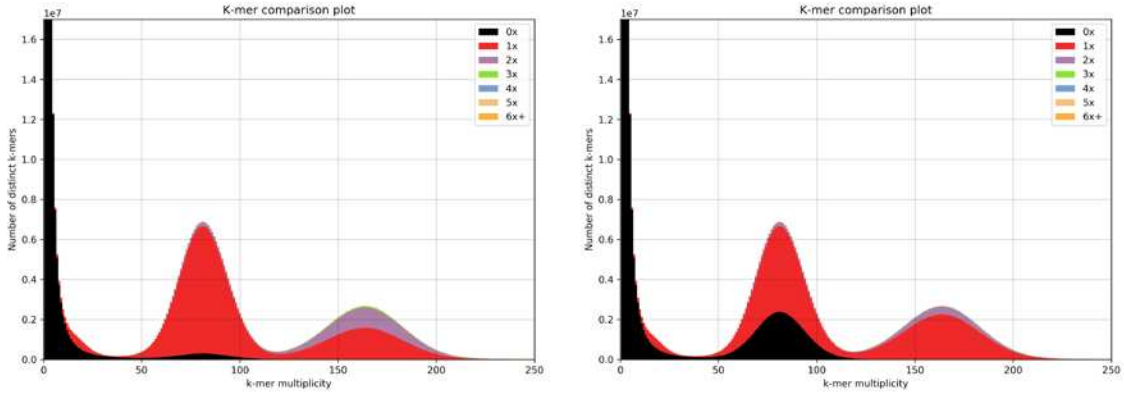

DAV_5 - *Heliconius melpomene*

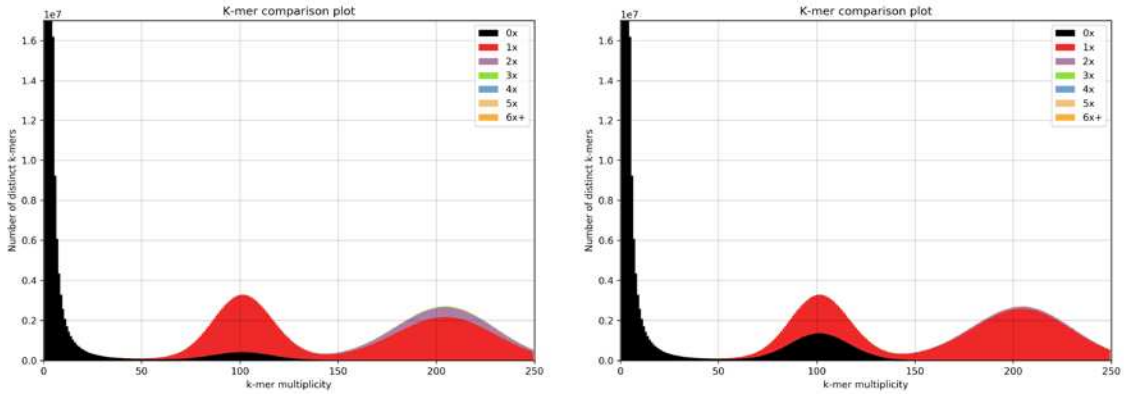

DAS_GELE - *Heliconius elevatus*

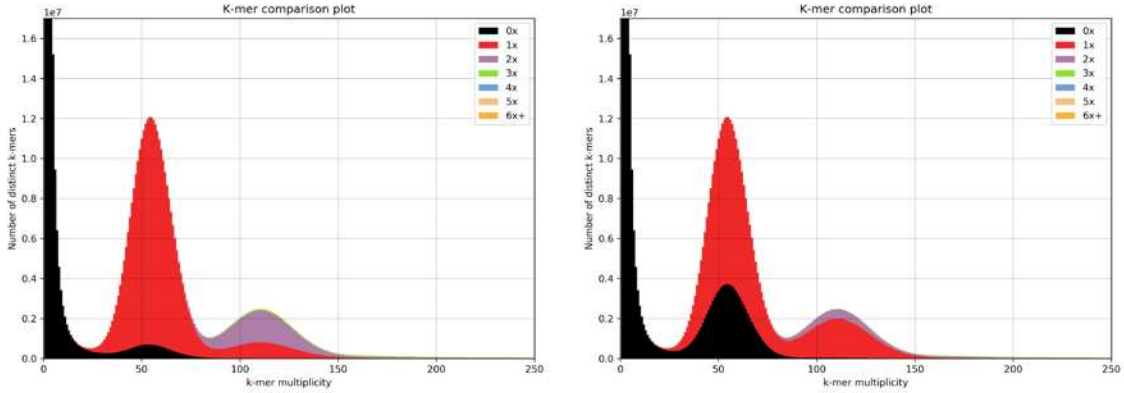

DAS_REL13_139 - *Heliconius pardalinus*

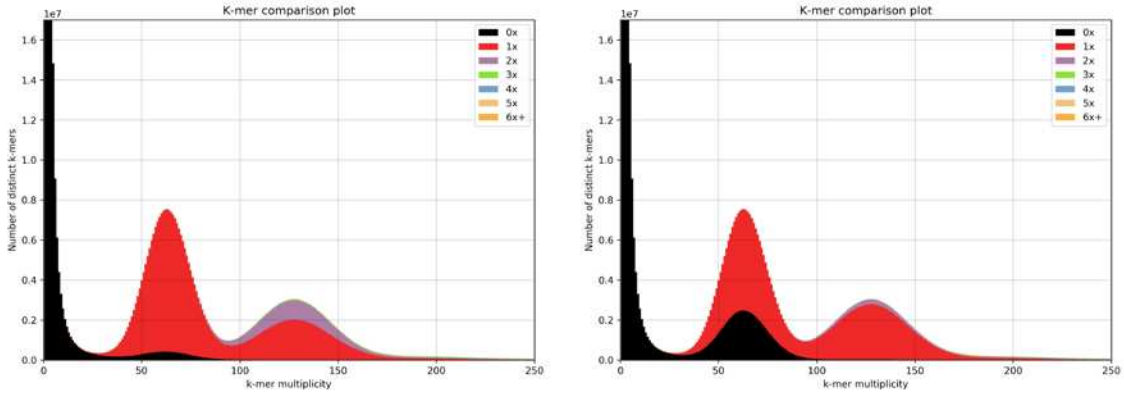

DAV_1 - *Heliconius timareta*

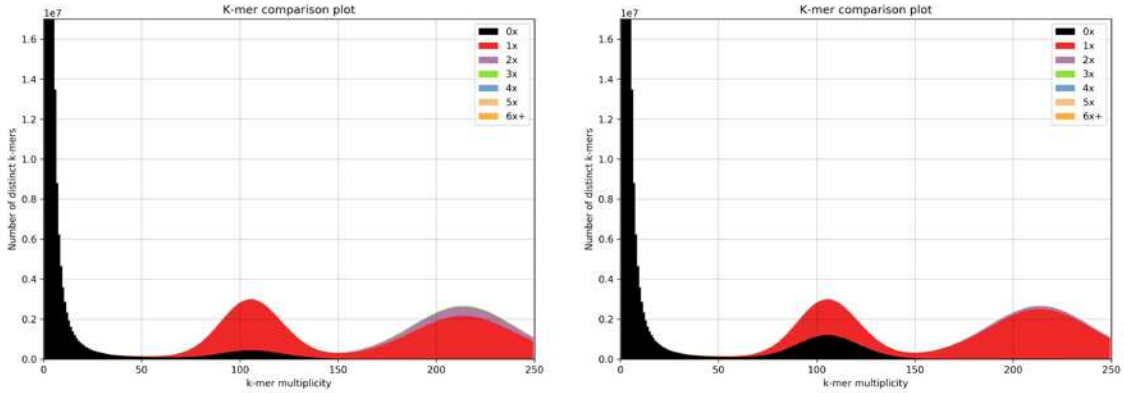

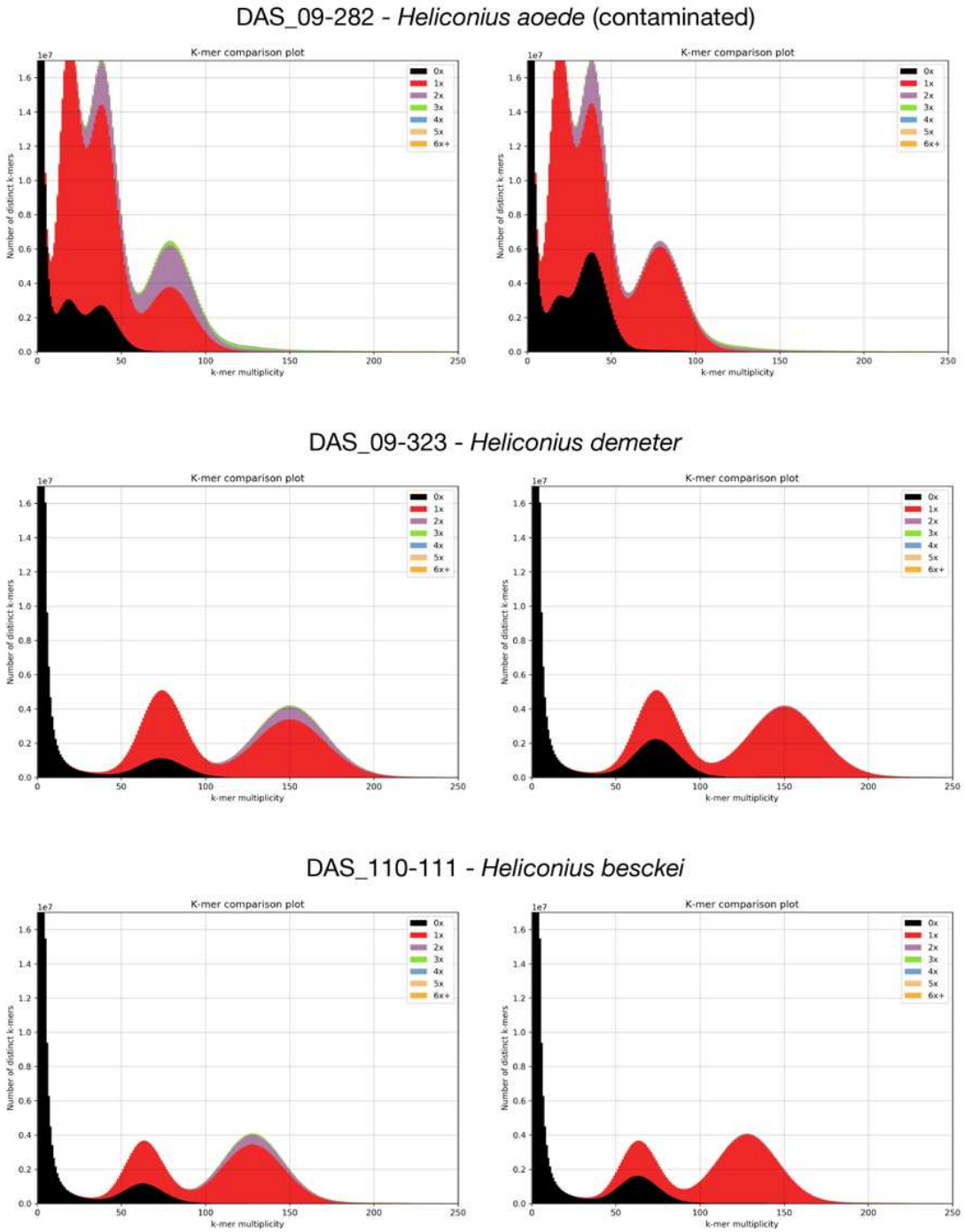

Fig. S1 K-mer spectra for all *de novo* assemblies.

The x-axis of each plot corresponds to the multiplicity of distinct k-mers in the raw reads. The first peak, near zero, corresponds to contaminants, the second peak corresponds to heterozygous content, and the third to homozygous content. The colors represent the number of times those k-mers are present in the genome assembly. Ideally, none of the contaminants would be assembled, half of the heterozygous content would be present as a single copy, and all of the homozygous content would be present as a single copy. For each species, the plot on the left shows the initial assembly, and the plot on the right shows the final assembly.

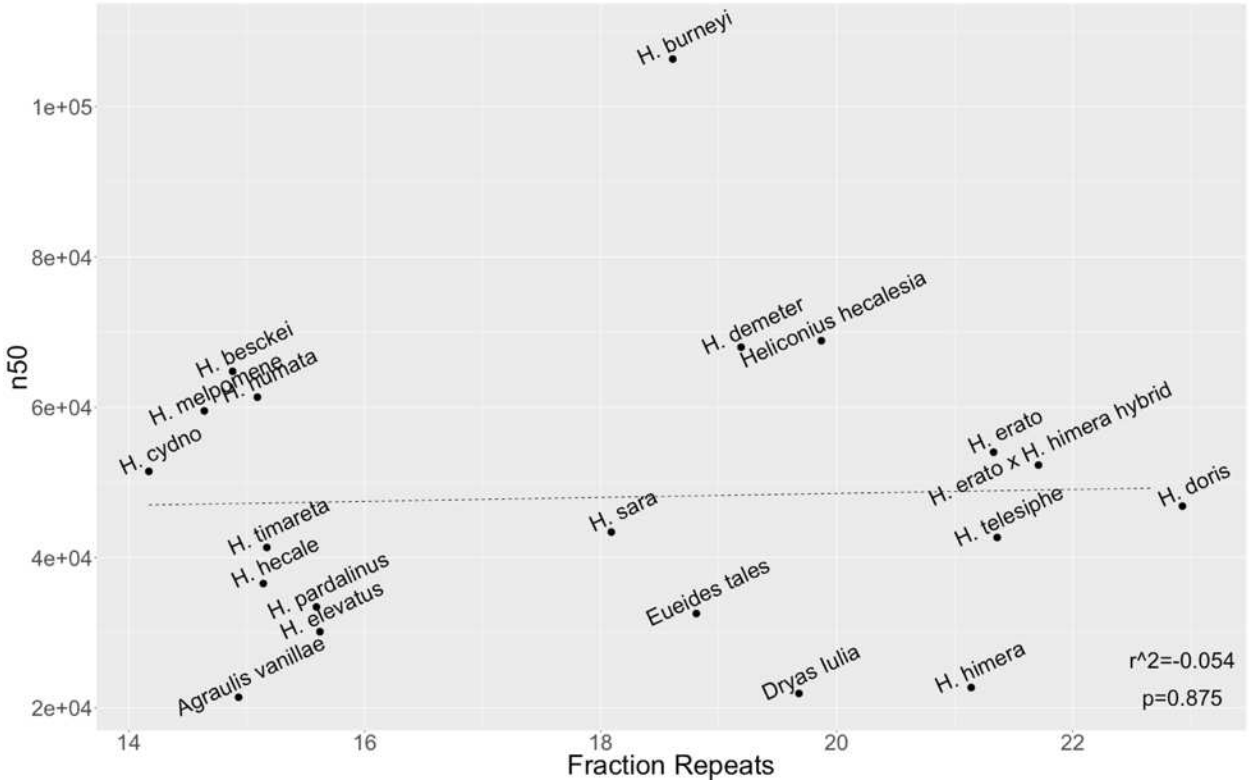

Fig. S2 Relationship of N50 to repeat content

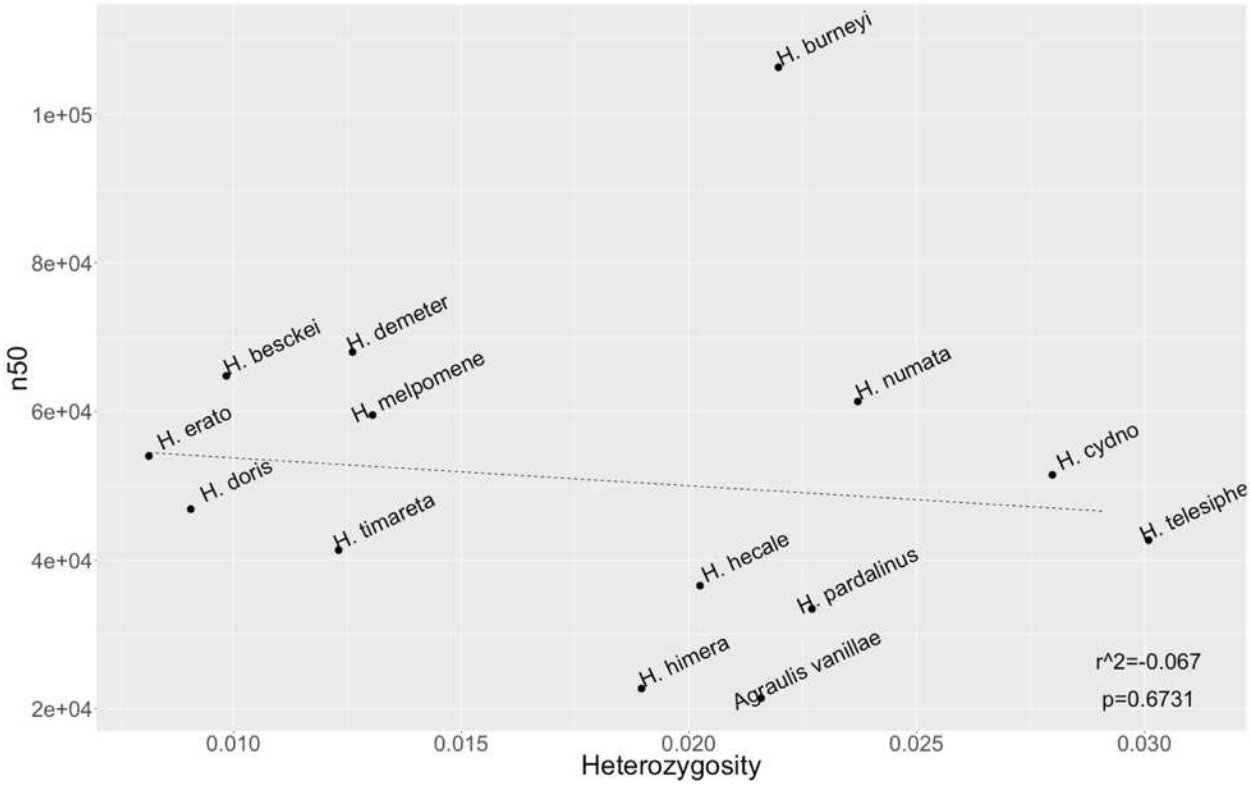

Fig. S3 Relationship of N50 to heterozygosity

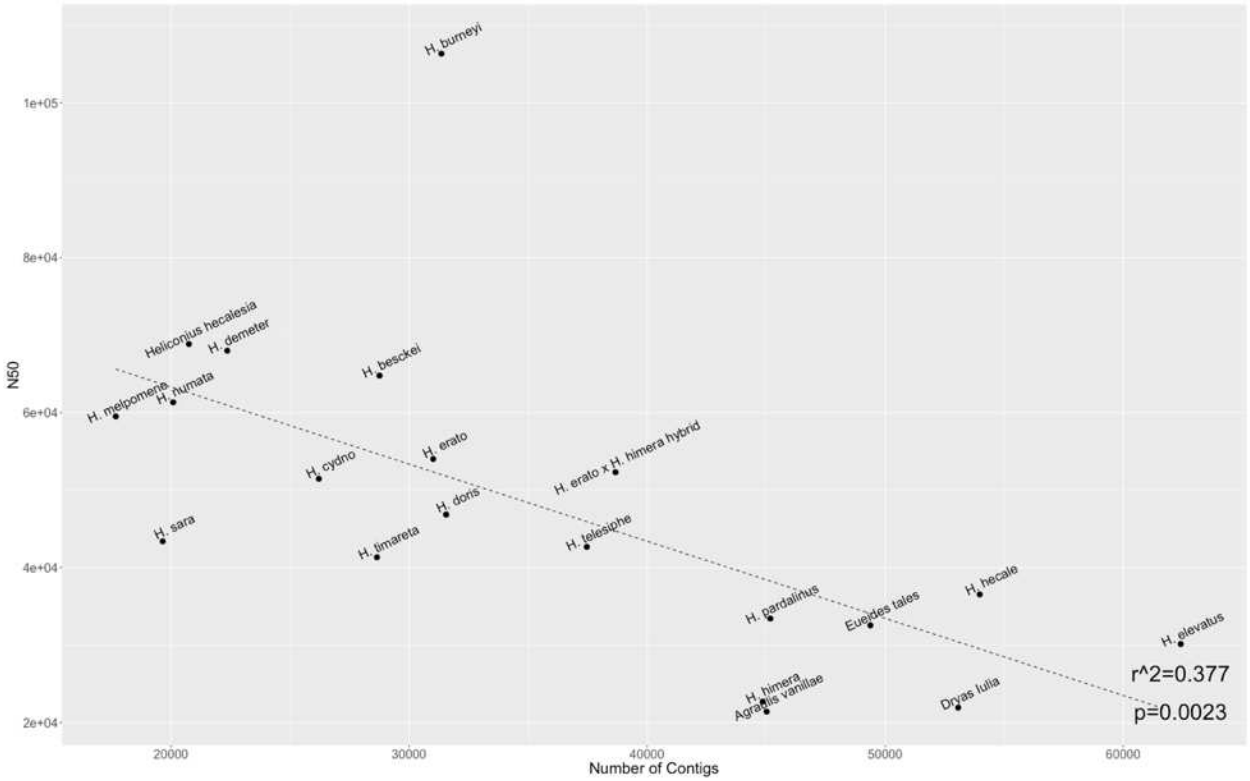

Fig. S4 Relationship of N50 to number of contigs

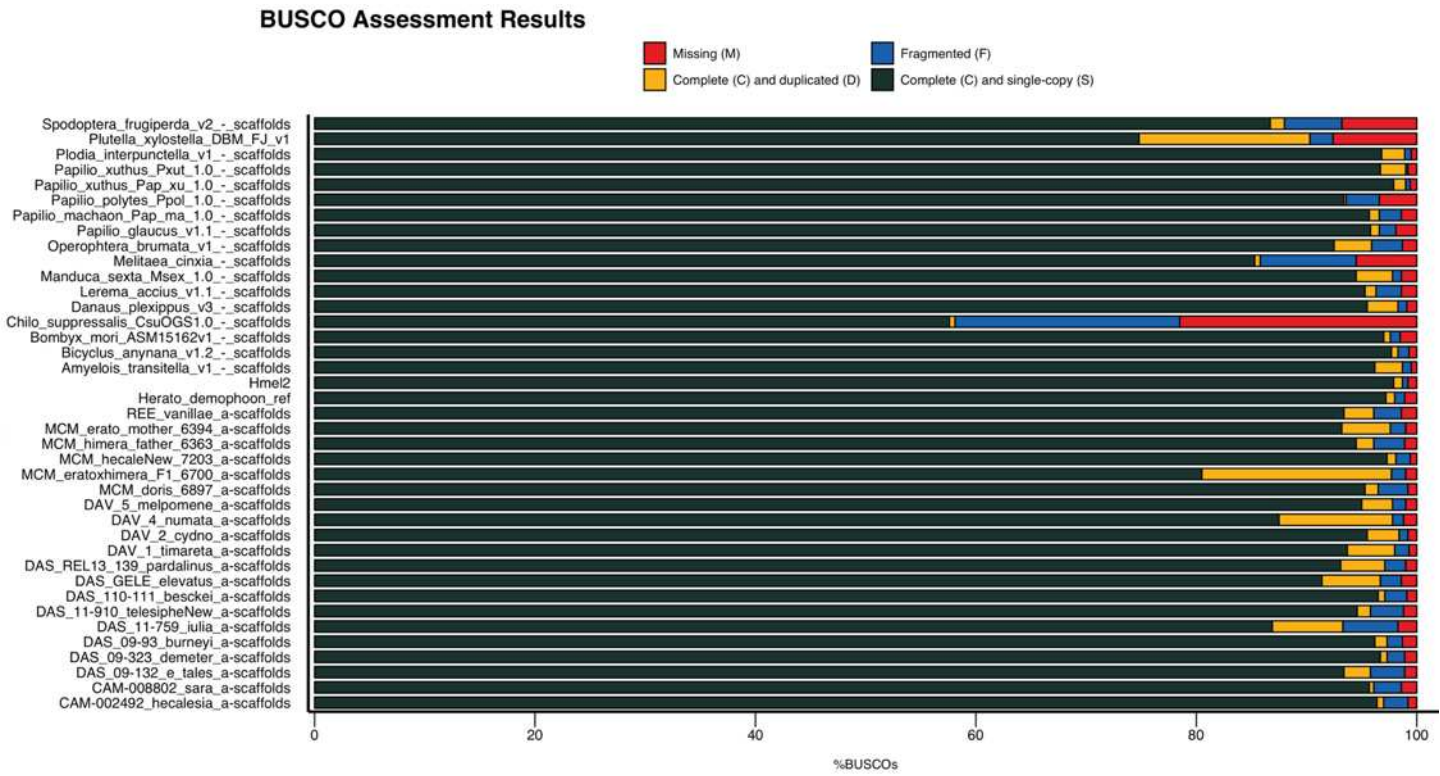

Fig. S5 BUSCO gene content

This plot displays BUSCO results from all de novo *genomes assembled here, as well as other lepidopteran genomes obtained from lepbase.org. All bars below "*Herato_demophoon_ref*" are results of this study. Gene content is comparable between the w2rap assemblies and other lepidopteran assemblies, though the percentage of complete genes identified in w2rap genomes is slightly lower, and percent duplicated slightly higher, than the highest quality reference Lepidoptera genomes.*

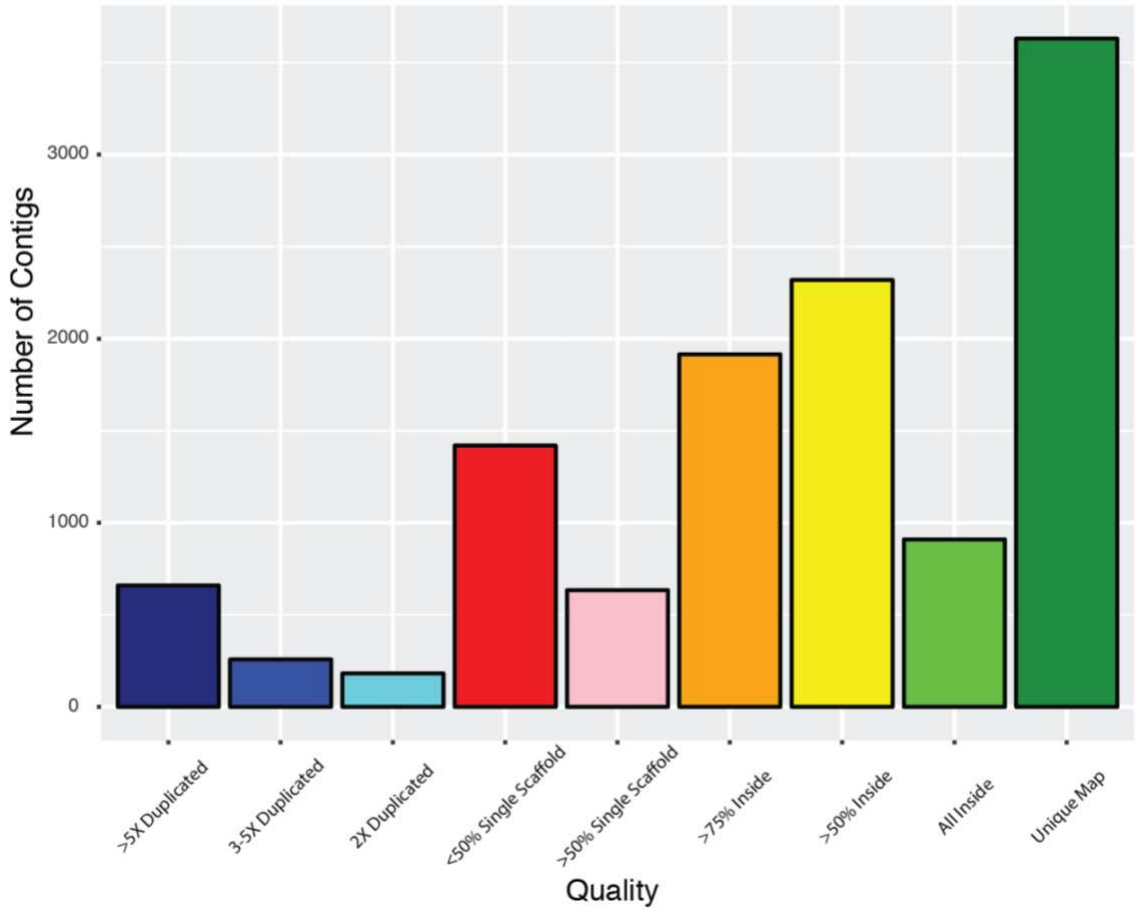

Fig. S6 *H. melpomene* w2rap to Hmel2 contig alignment quality

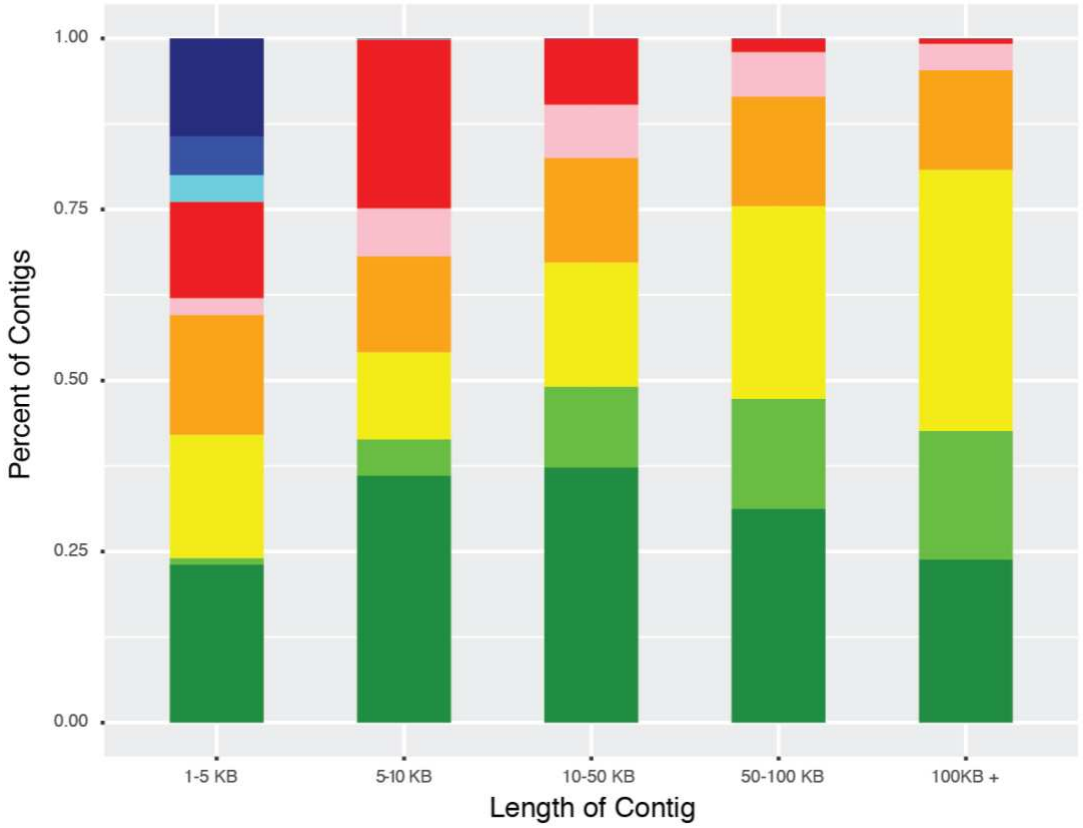

Fig. S7 Contig alignment quality by contig size

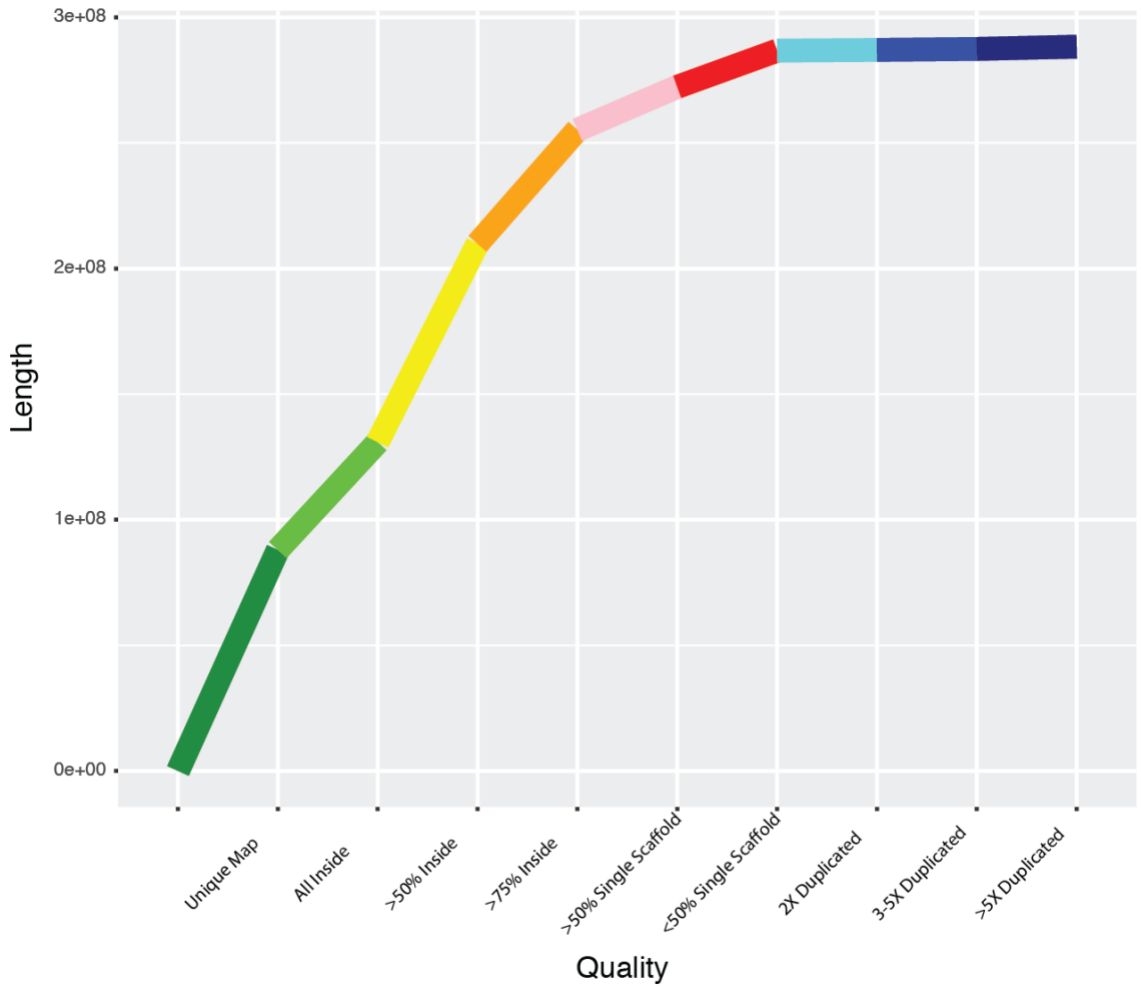

Fig. S8 Cumulative alignment length by quality

Fig. S9 Scaffolding with DISCOVAR flow chart

Required input files are outlined with red boxes, intermediate data files are outlined with gold boxes, and final outputs are outlined with green boxes. Blue diamonds adjacent to arrowed lines hold scripts used to convert the file(s) at the base of the arrow to the file(s) at the tips. Many of these rely on previously published tools (fasta-splitter.pl was written by K. Kryukov; many scripts rely on bedtools). Further details about each step are given in the text above.

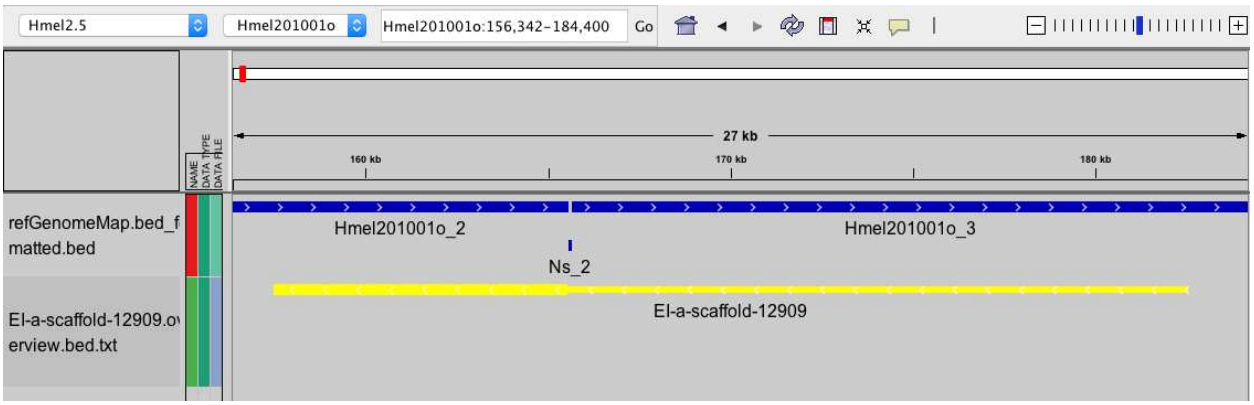

Fig. S10 Example overview alignment

This screenshot from IGV shows a 27 kb region of Hmel2.5 chromosome 1. The blue track displays the location of reference contigs Hmel201001o_2 and Hmel201001o_3, as well as the stretch of Ns that separates them. The yellow track shows the longest sub-alignment of the de novo H. melpomene *genome contig EI-a-scaffold-12909, which overlaps with Hmel201001o_2 (thick line). When we project the remainder of EI-a-scaffold-12909 based on the location of the sub-alignment (thin line), we see that it is expected to continue on to Hmel201001o_3. This overview is colored yellow, indicating that more than 75% of the sub-alignments of this contig are found within the projected area, as can be seen in* Fig. S11.

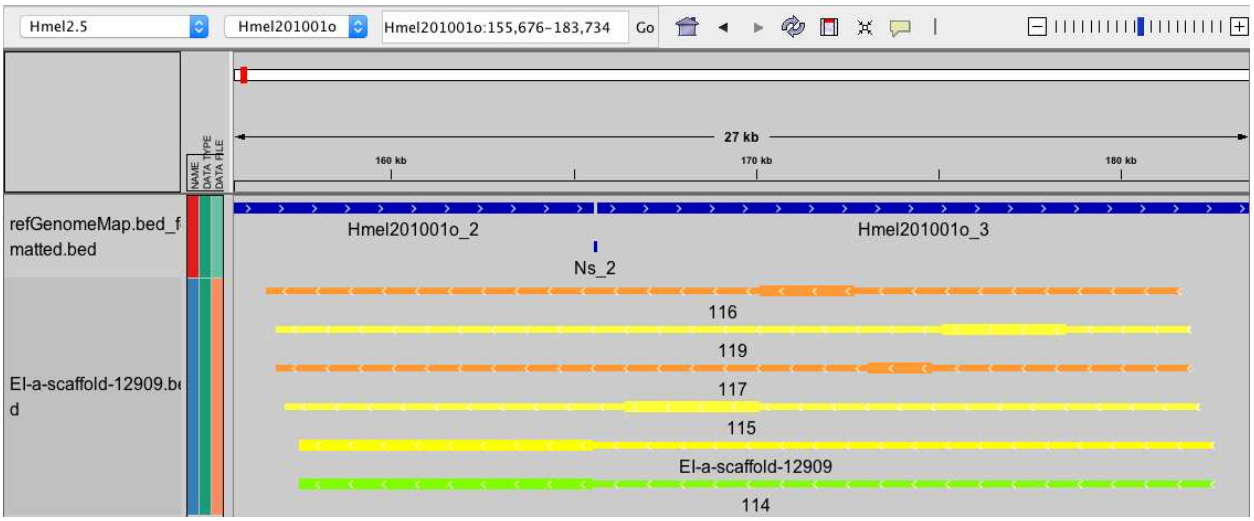

Fig. S11 Example full contig alignment

Here, the remaining sub-alignments of EI-a-scaffold-12909 are displayed in the same manner as the overview – the thick lines indicate the location of the sub-alignment, while the thin lines project the position of the contig based on the aligned region. One can see that the sub-alignments are located in positions expected if Hmel201001o_2 and Hmel201001o_3 are in fact contiguous. The alignments labeled 114-119 are the sub-alignments, and their colors are simply an indication of size relative to the full contig.

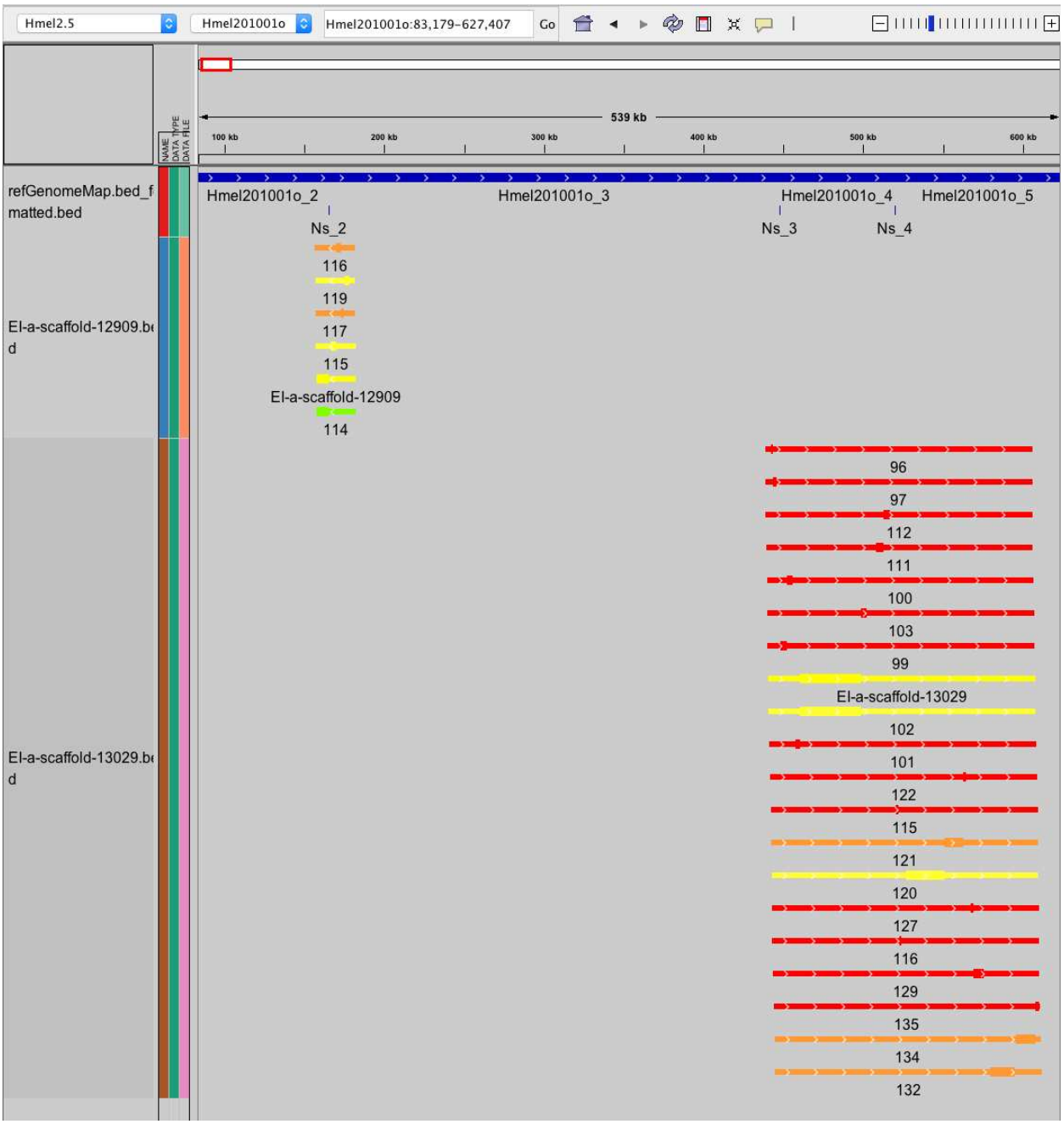

Fig. S12 Example full group alignment

Here, we see that EI-a-scaffold-13029 maps to reference contig Hmel201001o_3 as well, and also connects to Hmel201001o_4 and Hmel201001o_5. These regions are treated as a group, and are joined into a single super-scaffold, keeping as much of the reference contigs as possible but joining them together with the filler contigs (See Table S5*). Three regions of the* de novo *filler genome (names beginning with EI) were used to connect the four reference contigs (names beginning with Hmel) in the group. Each of these regions is between 500 and 1300 base pairs, and replaces fewer than 1000 bp of any individual reference contig.*

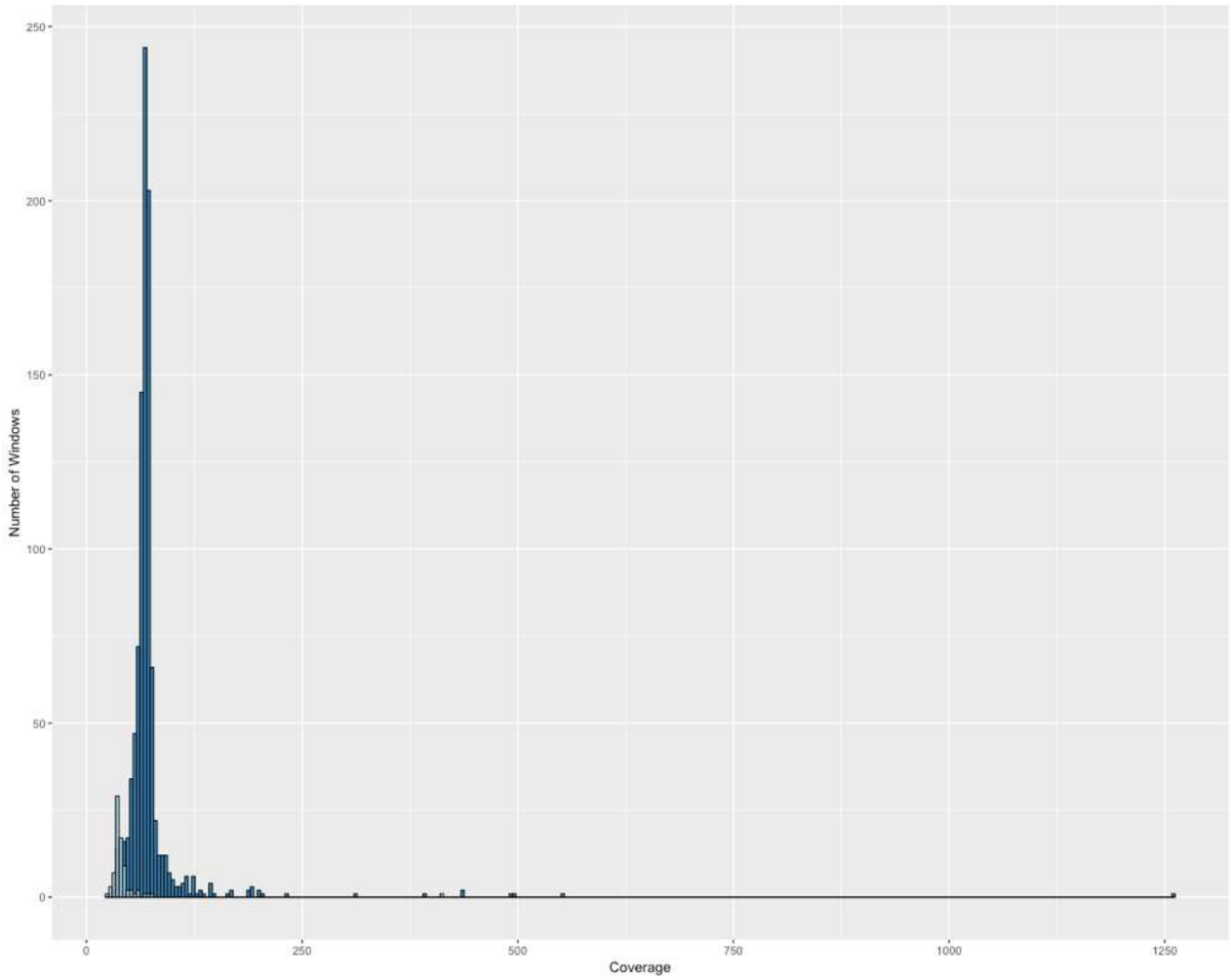

Fig. S13 Coverage of gap-filled regions

Histogram of mean coverage in 10 kb windows overlapping gap-filled regions. Light blue is the Z chromosome, and dark blue is autosomes.

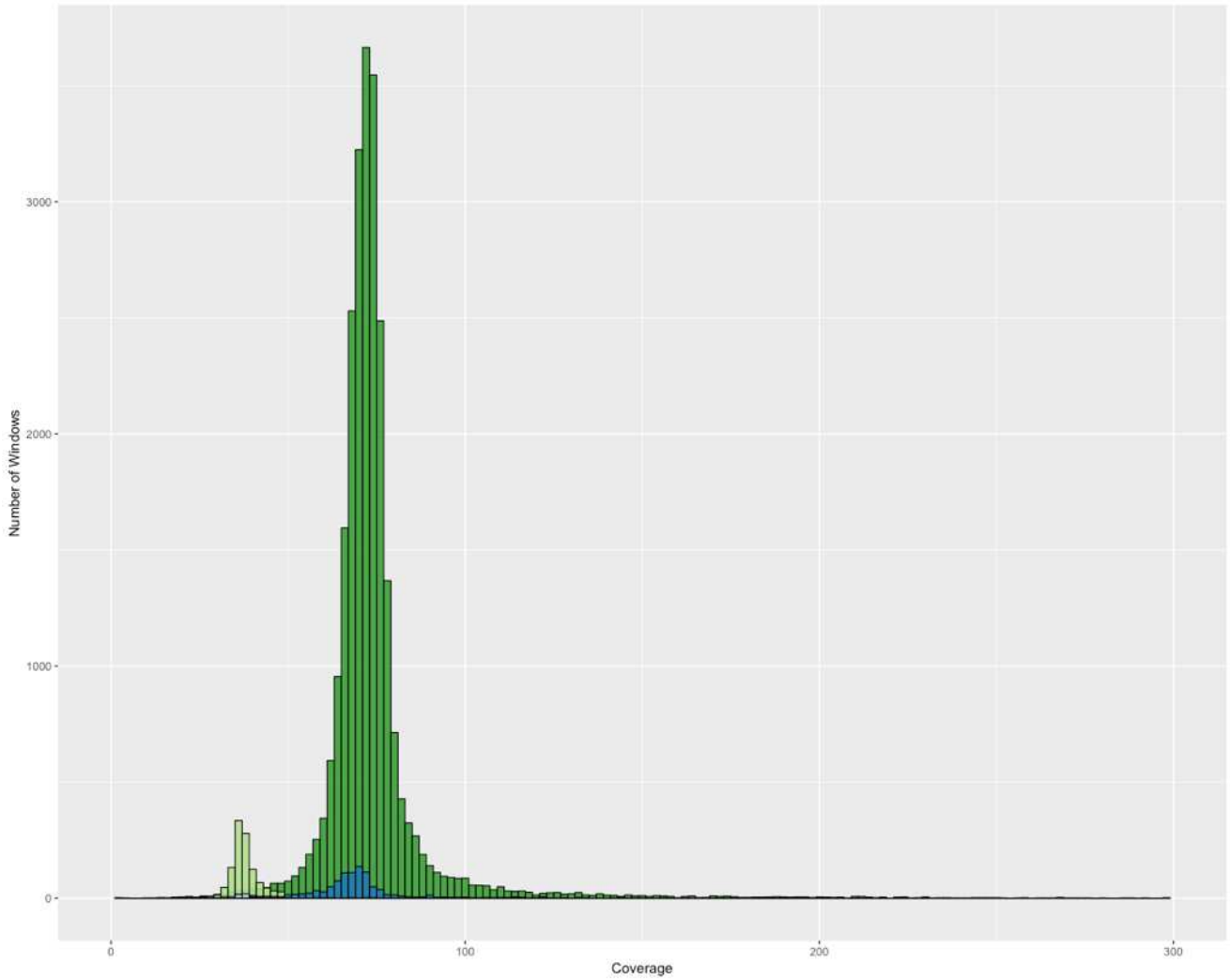

Fig. S14 Coverage of gap-filled and non gap-filled regions

Histogram of mean coverage in 10 kb windows. Blues are the same data as Fig. S13*, light green is non gap-filled Z chromosome, and dark green is non gap-filled autosomes*

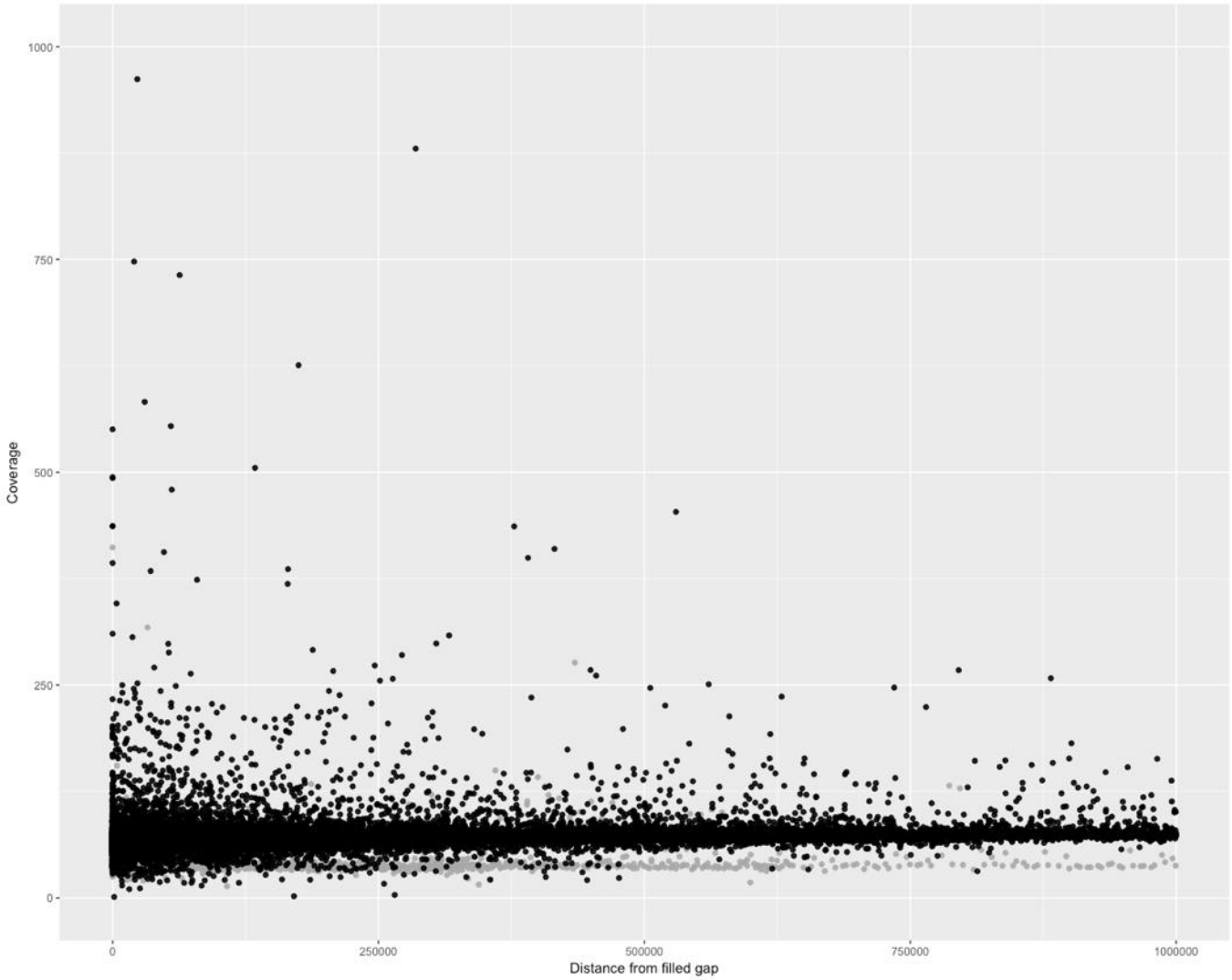

Fig. S15 Coverage with distance from filled gap

Histogram of mean coverage in 10 kb windows with distance from the nearest filled gap on the x-axis. Gaps tend to be in repetitive regions, as seen by increased coverage near zero, but the increase in coverage begins well before the filled gap itself.

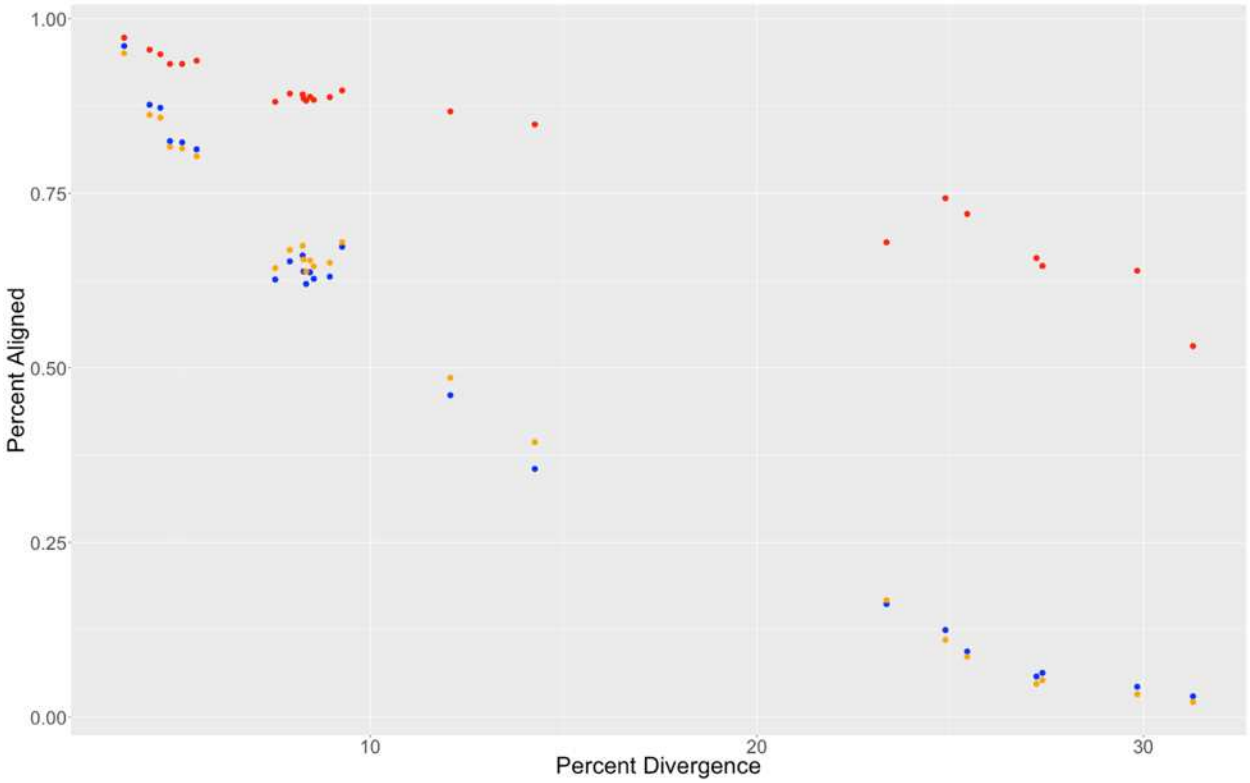

Fig. S16 Pairwise alignment depth

Fig. S16 and Table S7 Pairwise coverage*show the pairwise alignment depth between other Lepidoptera and Hmel2.5 in the progressiveCactus alignment. The "percent divergence" metric is the pairwise distance in concatenated non-coding regions aligned among all species. Exons are shown in red, introns in orange, and intergenic regions in blue.*

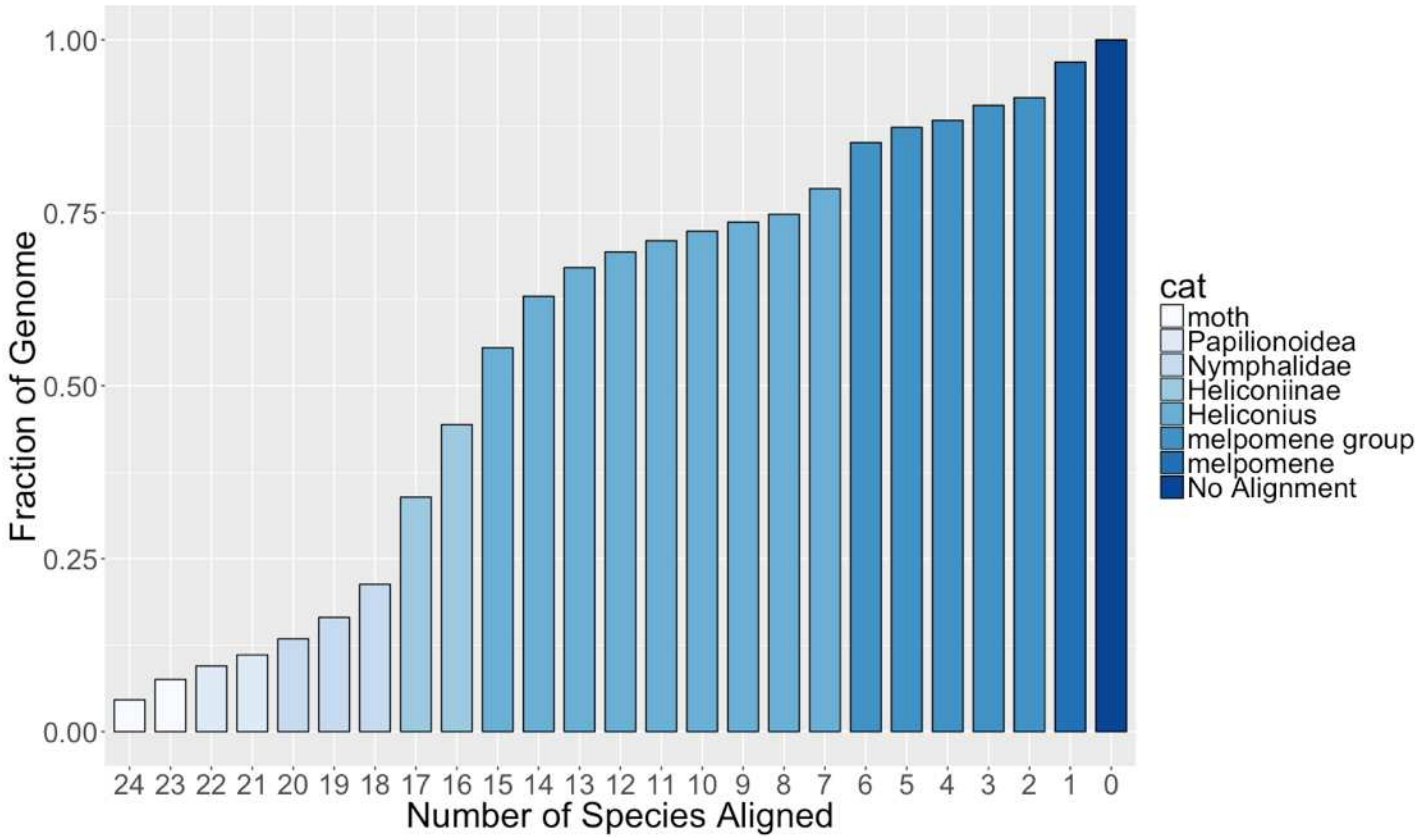

Fig. S17 Cumulative alignment depth to *H. melpomene* Hmel2.5

The Y-axis shows the percentage of Hmel2.5 sites that are aligned at least once among at least the number of species indicated on the X-axis. Colors represent the narrowest taxonomic category that corresponds to each number of species. For example, there are 15 Heliconius *species not including Hmel2. Critically, however, the values of each bar correspond to number of species. The colors are therefore only a qualitative visual aid.*

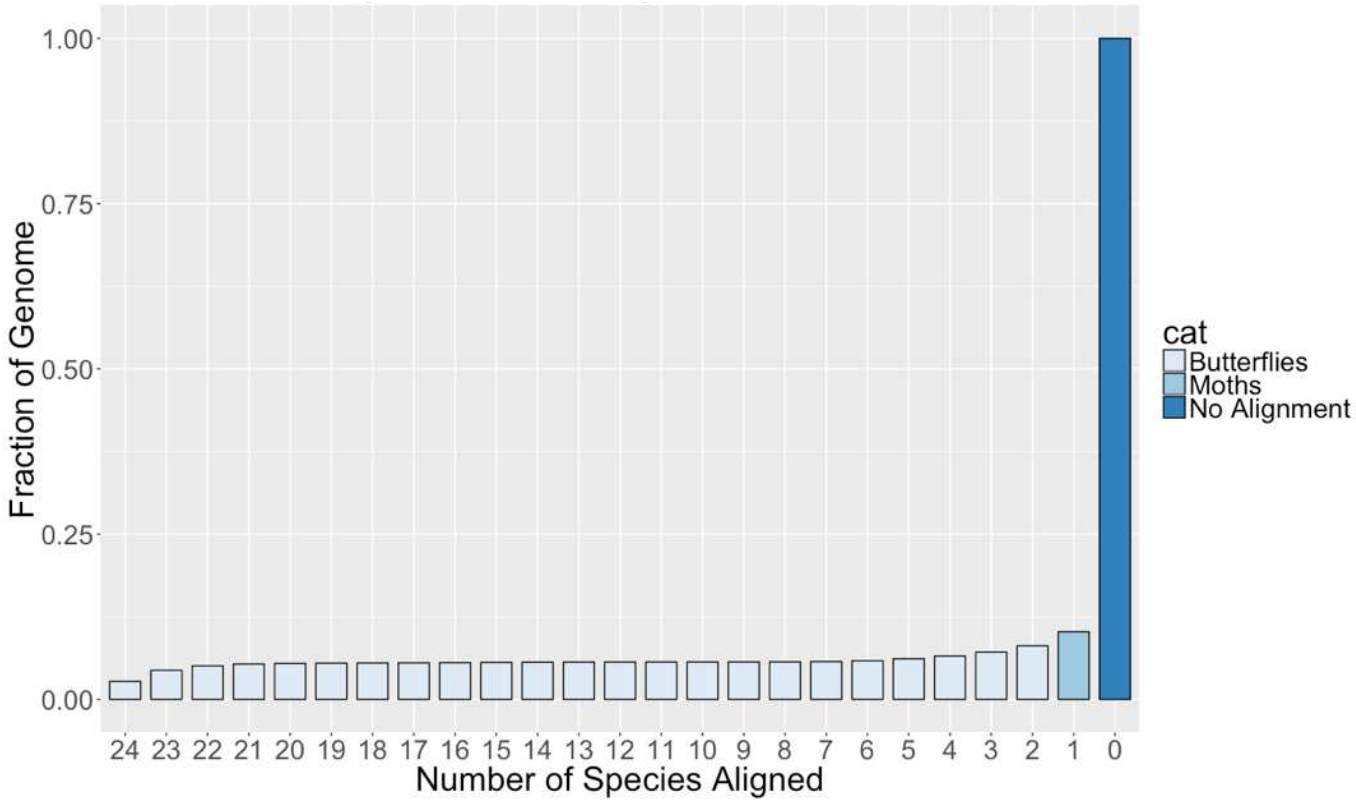

Fig. S18 Cumulative alignment depth to *B. mori*

Same as Fig. S17*, but using* B. mori *as the reference genome. Very little of the* B. mori *genome aligns to any other lepidopteran genome assemblies employed here.*

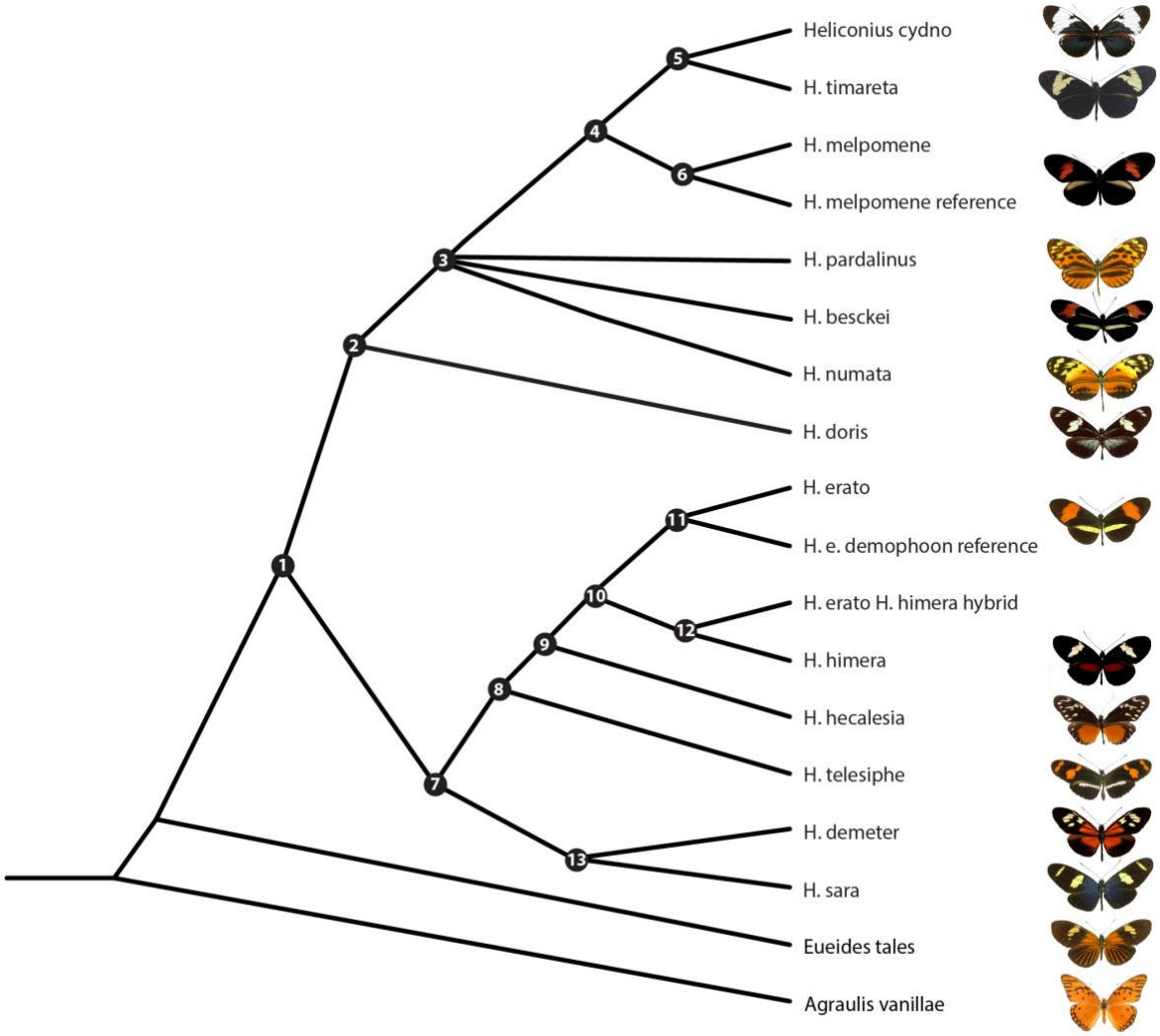

Fig. S19 Consensus phylogeny

Numbers on nodes correspond to Fig. S20

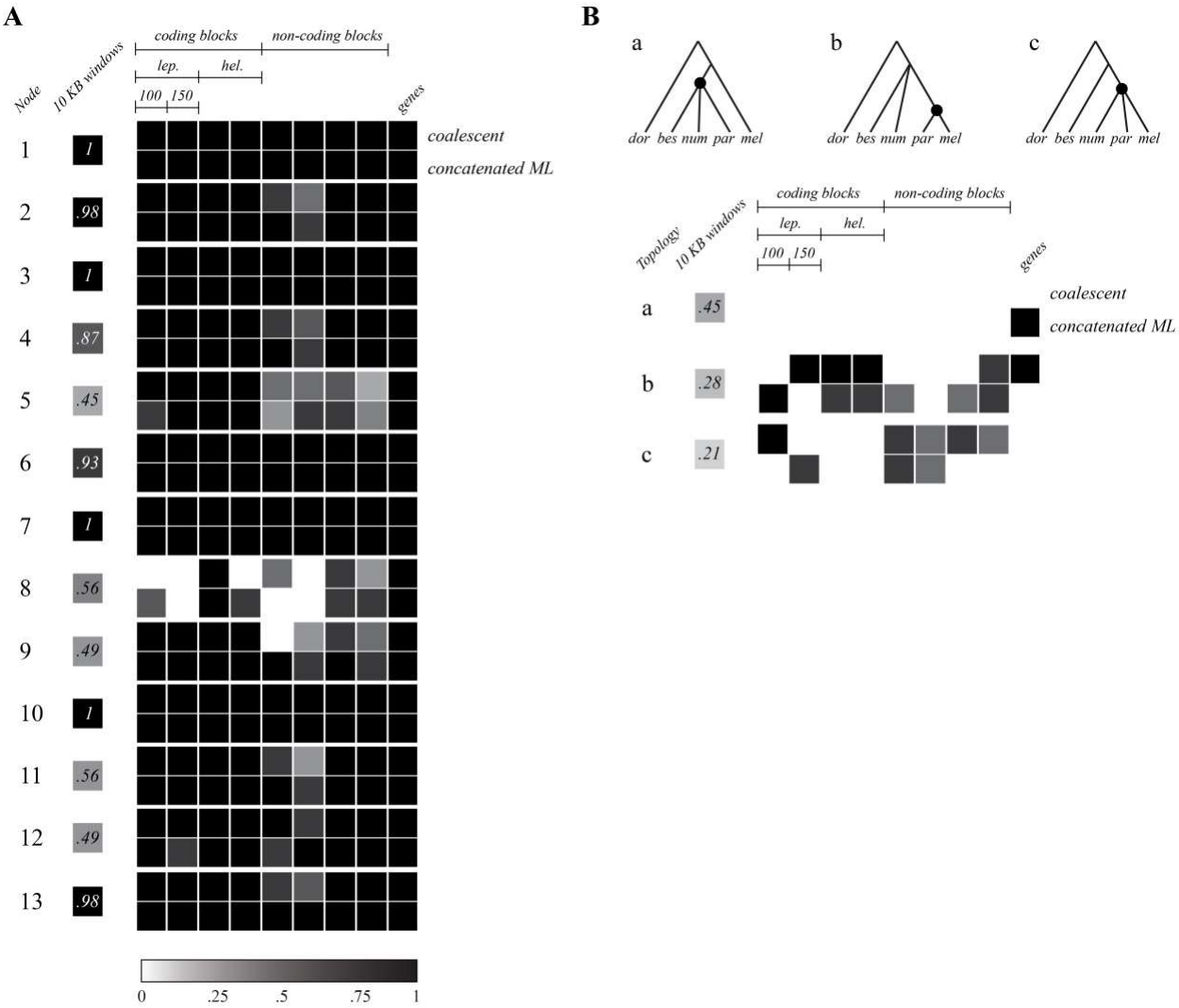

Fig. S20 Summary of node support

A*. Each set of 19 squares corresponds to a node numbered as in* Fig. S19 *above. The first column, 10 kb windows, shows the percent of 10 kb windows that recover the given node. These values correspond to the grey scale in main text Fig. 1A. The remaining blocks indicate support for the given node in the species tree reconstruction method indicated above each column. If a square is filled, that node was recovered in the corresponding species tree reconstruction. Grey scale indicates level of support as bootstrap value (concatenated methods) or node support value (coalescent methods).* ***B.*** *Because no topology was overwhelmingly supported for the silvaniform clade, it was maintained as a polytomy in Fig. 1A. Topologies (a) – (c) illustrate the three supported species groupings. The grids below show relative support for each topology, and are arranged as in* ***A****.*

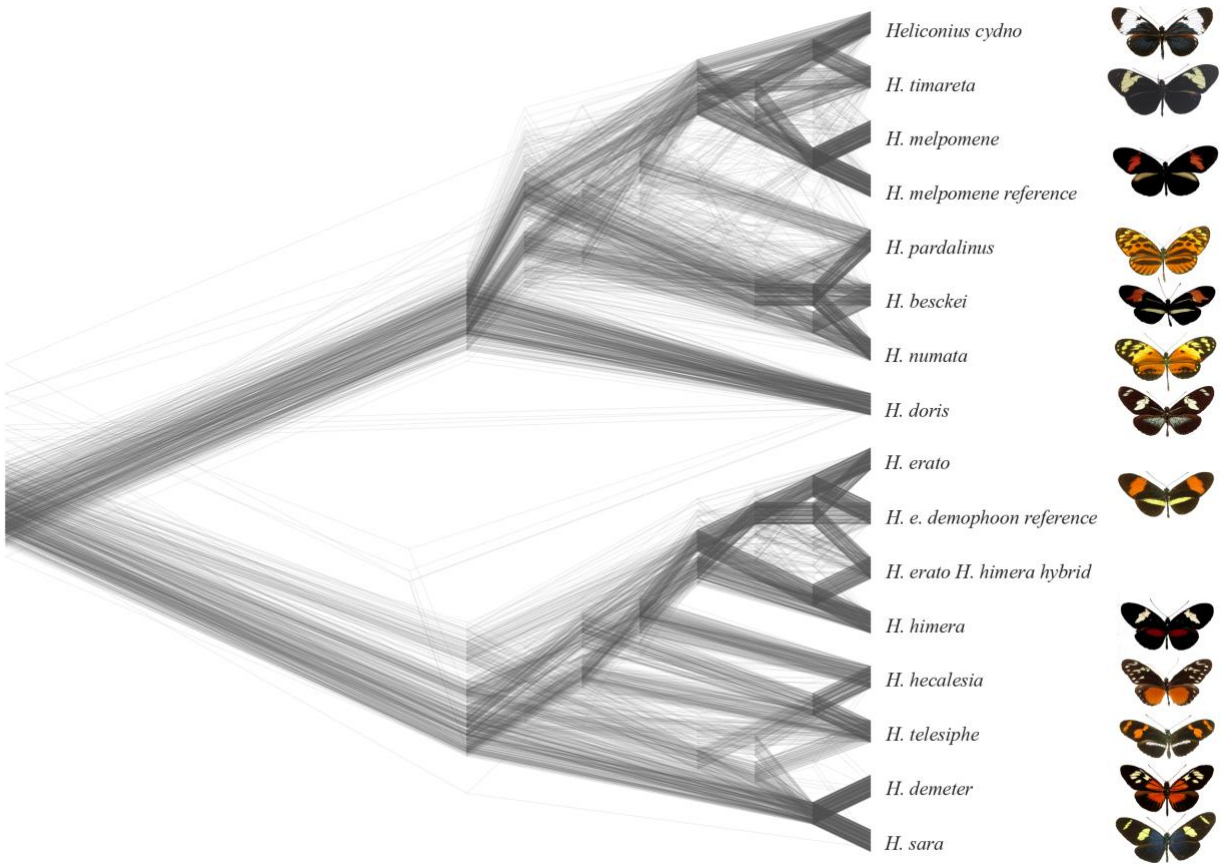

Fig. S21 DensiTree plot with normalized branch lengths

Trees are calculated from 10 kb windows, and are the same subset as in main text Fig. 1A. Branch length information has been removed, so that the depth of each node is based only on its order in the topology.

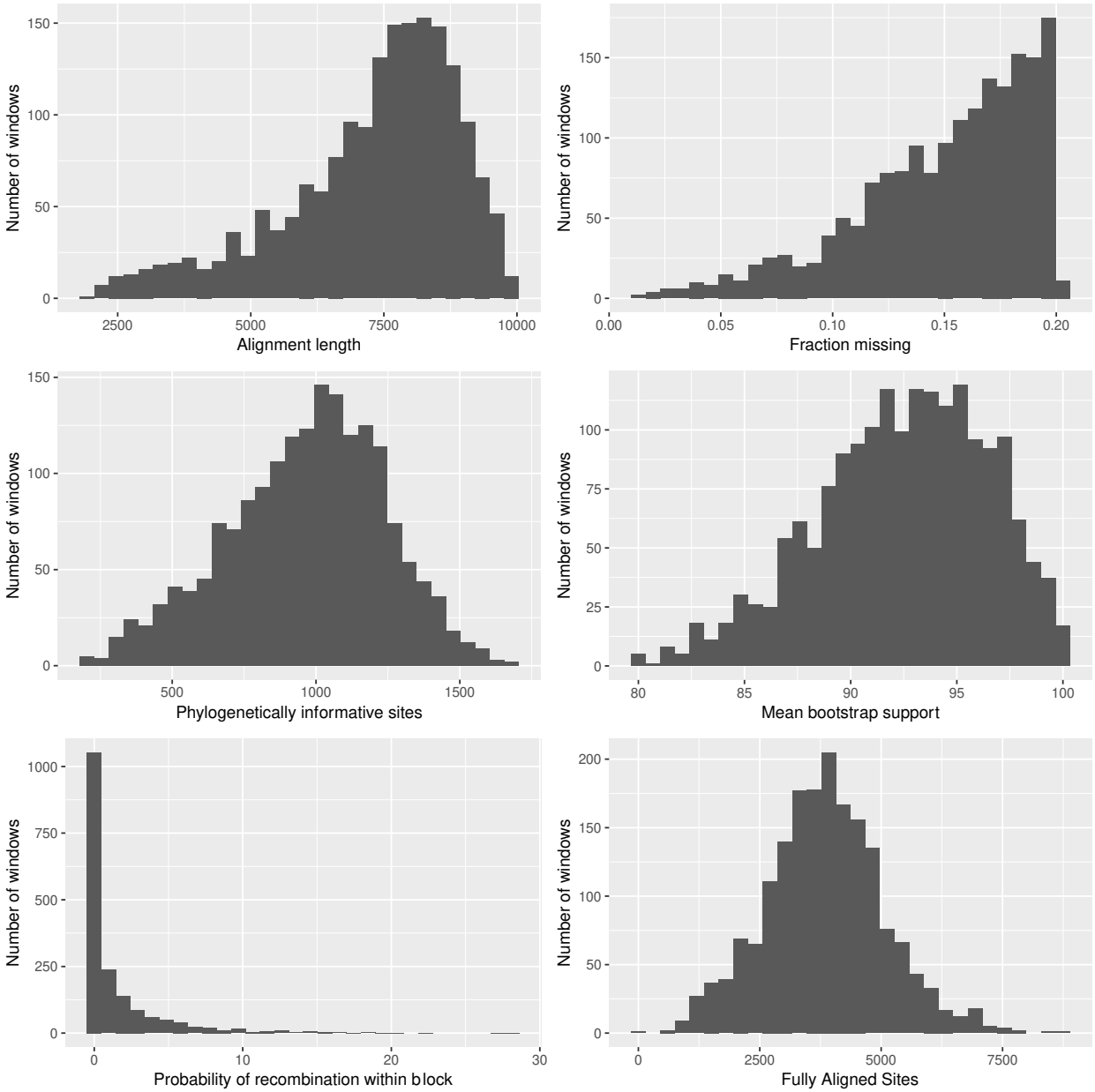

Fig. S22 *Heliconiini* 10 kb block statistics

Basic statistics for trees used to generate DensiTrees in Fig. 1A. Alignment length refers to the final length of the alignment, filtered for only single-copy regions. Fraction missing is the sum of all gaps divided by total base pairs. Phylogenetically informative sites is number of positions where >= 2 species carry the alternate allele. Probability of recombination within block is -log10(p) value for presence of a recombination event as calculated in (81). Fully Aligned Sites is number of sites in which every species is represented by a non-gap character.

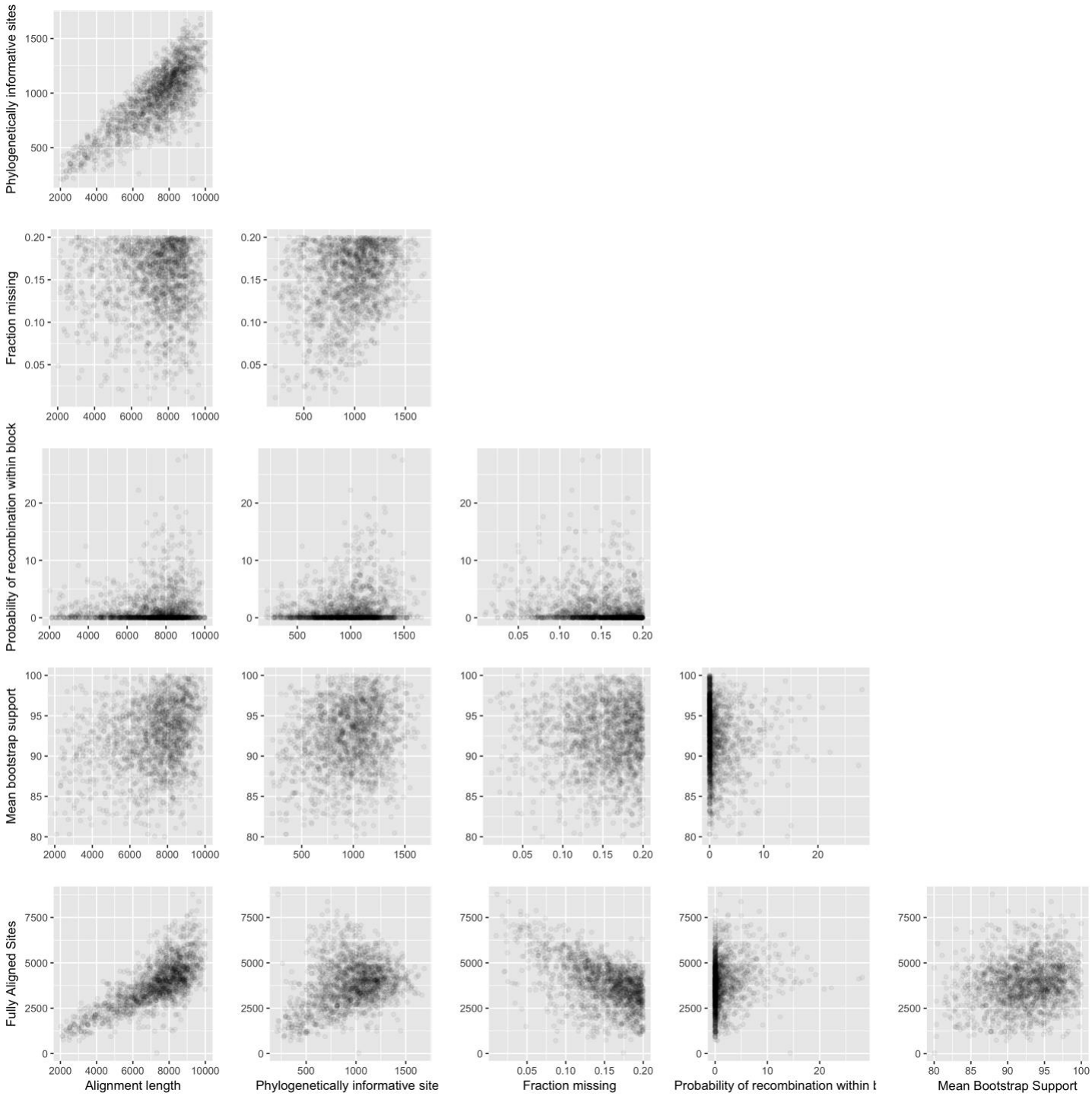

Fig. S23 *Heliconiini* 10 kb block pairwise statistics

Correlations between each pair of window statistics in Fig. S22

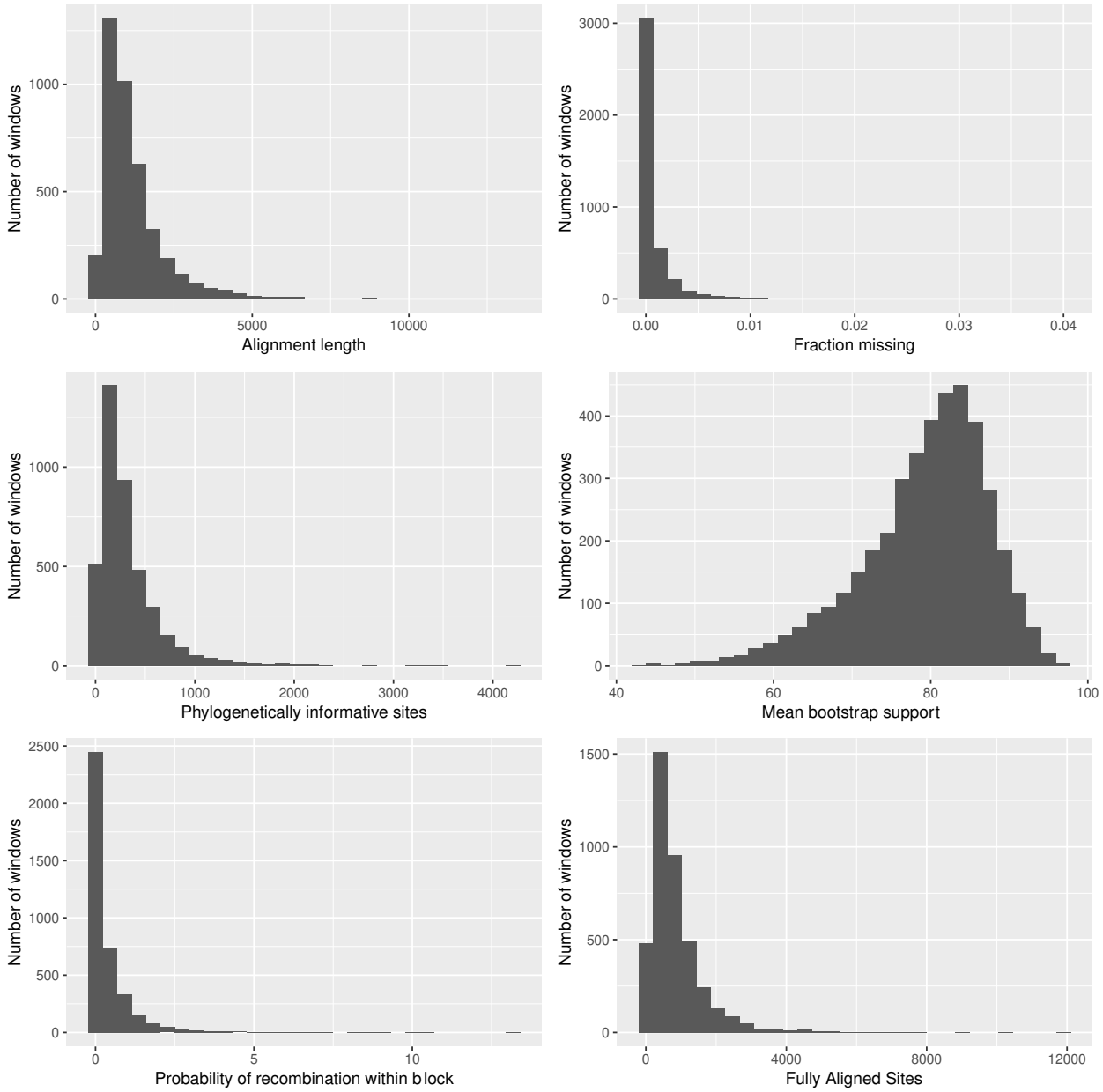

Fig. S24 gene alignment statistics

Basic statistics for gene alignments and resulting trees. Statistics as in Fig. S22

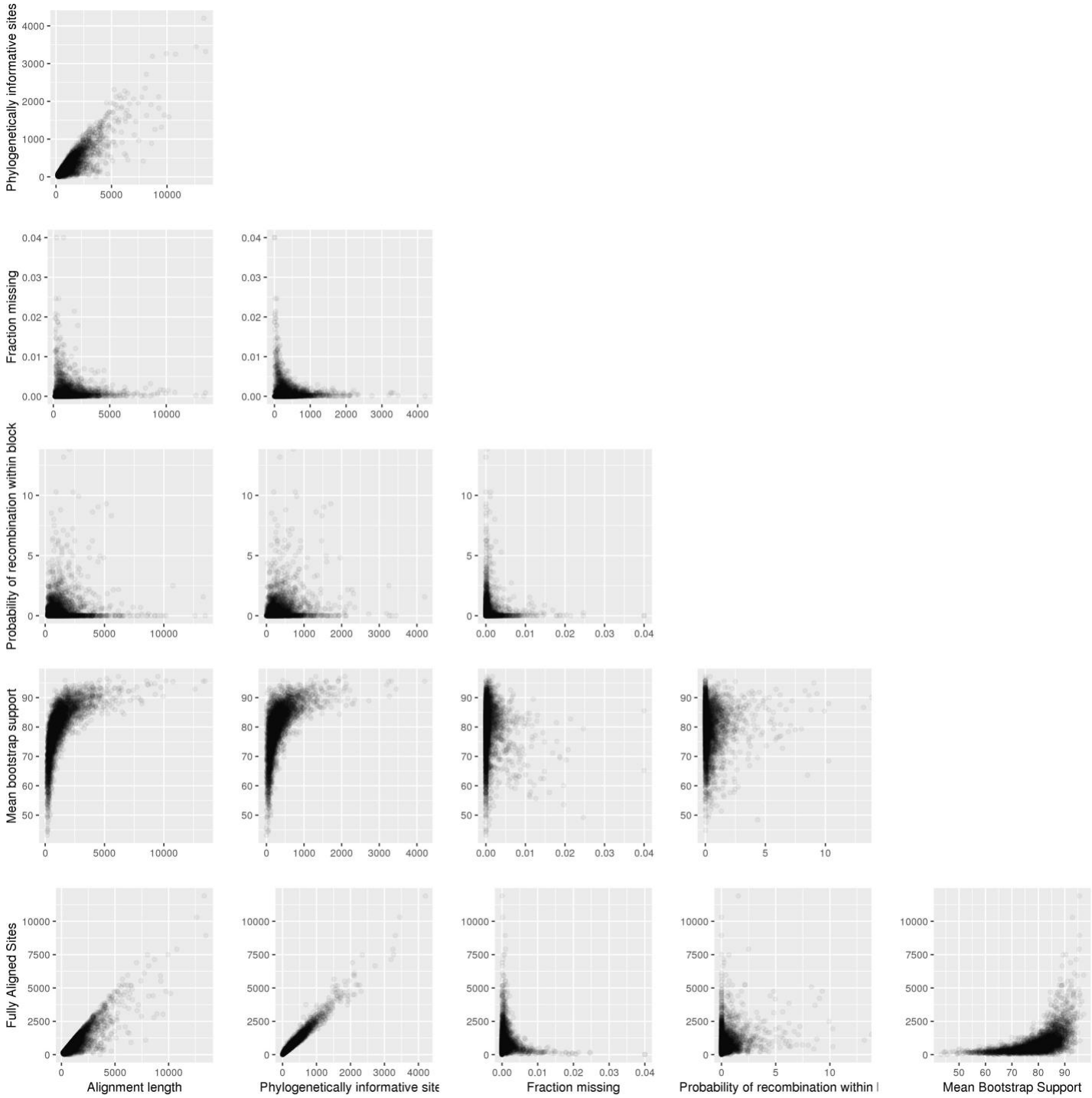

Fig. S25 Pairwise gene statistics

Correlations between each pair of window statistics in Fig. S24

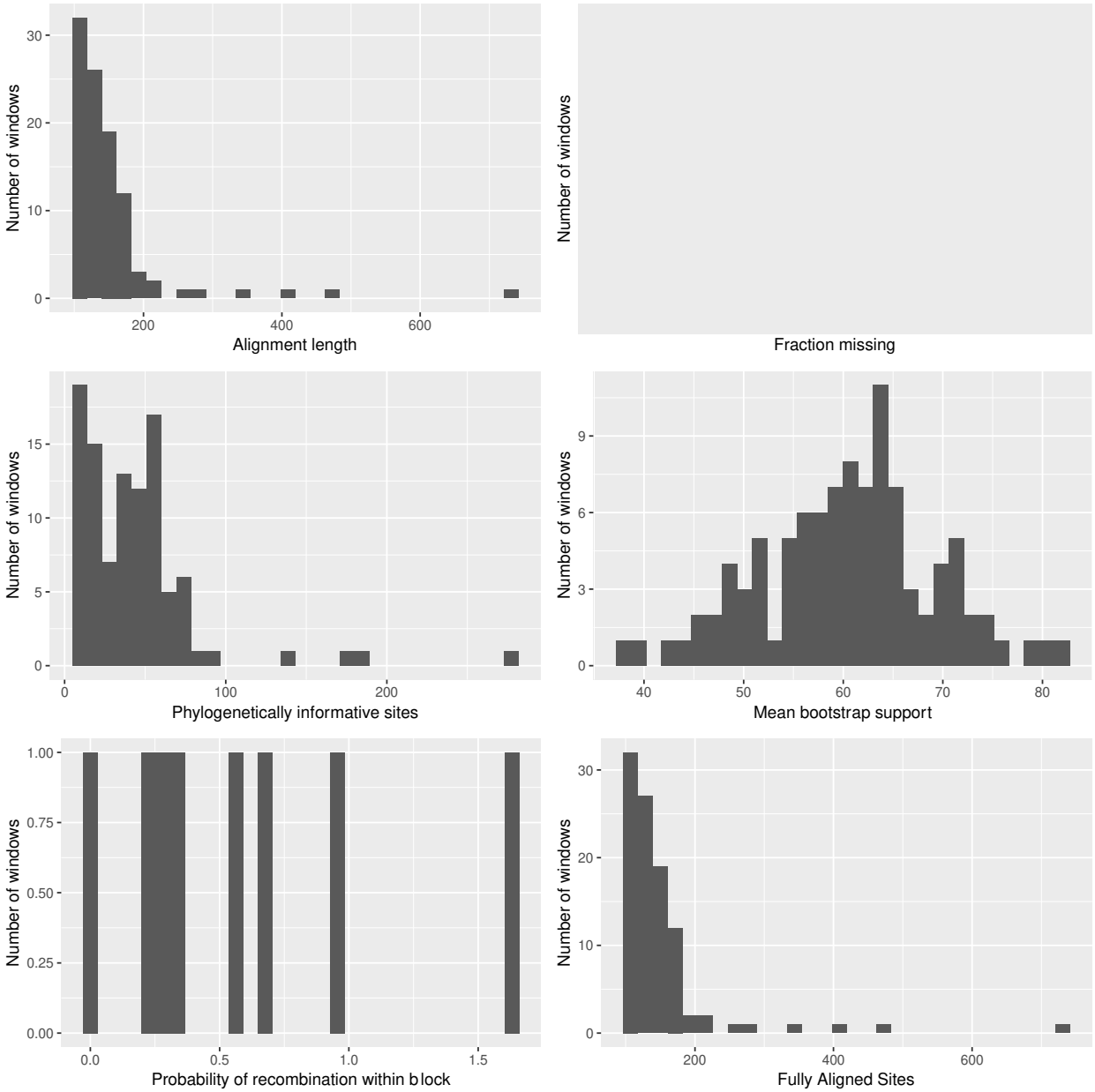

Fig. S26 All species, non-coding block statistics

Basic statistics for non-coding blocks and resulting trees in the full alignment. Statistics as in Fig. S22

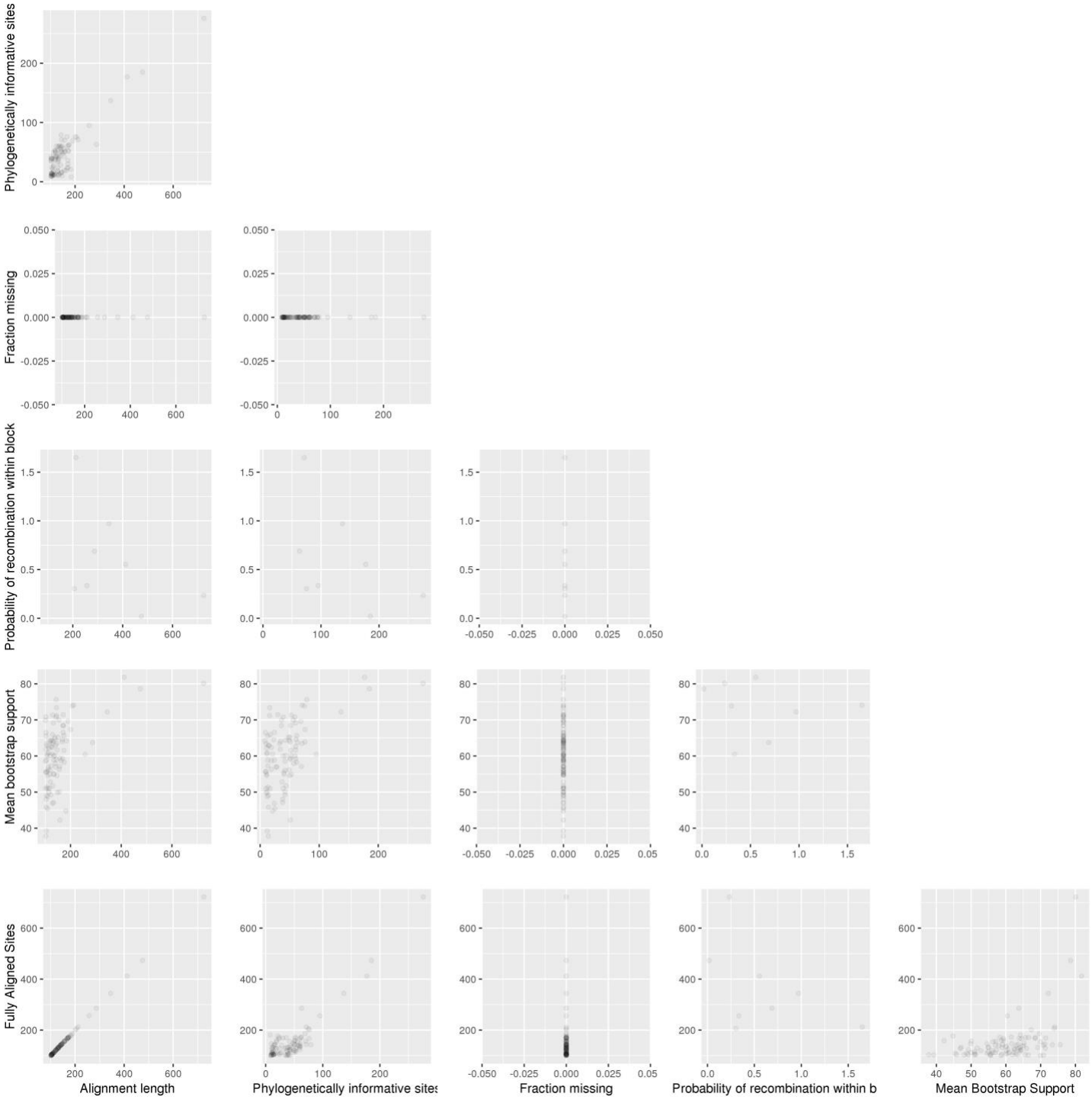

Fig. S27 All species, noncoding blocks pairwise statistics

Correlations between each pair of window statistics in Fig. S26

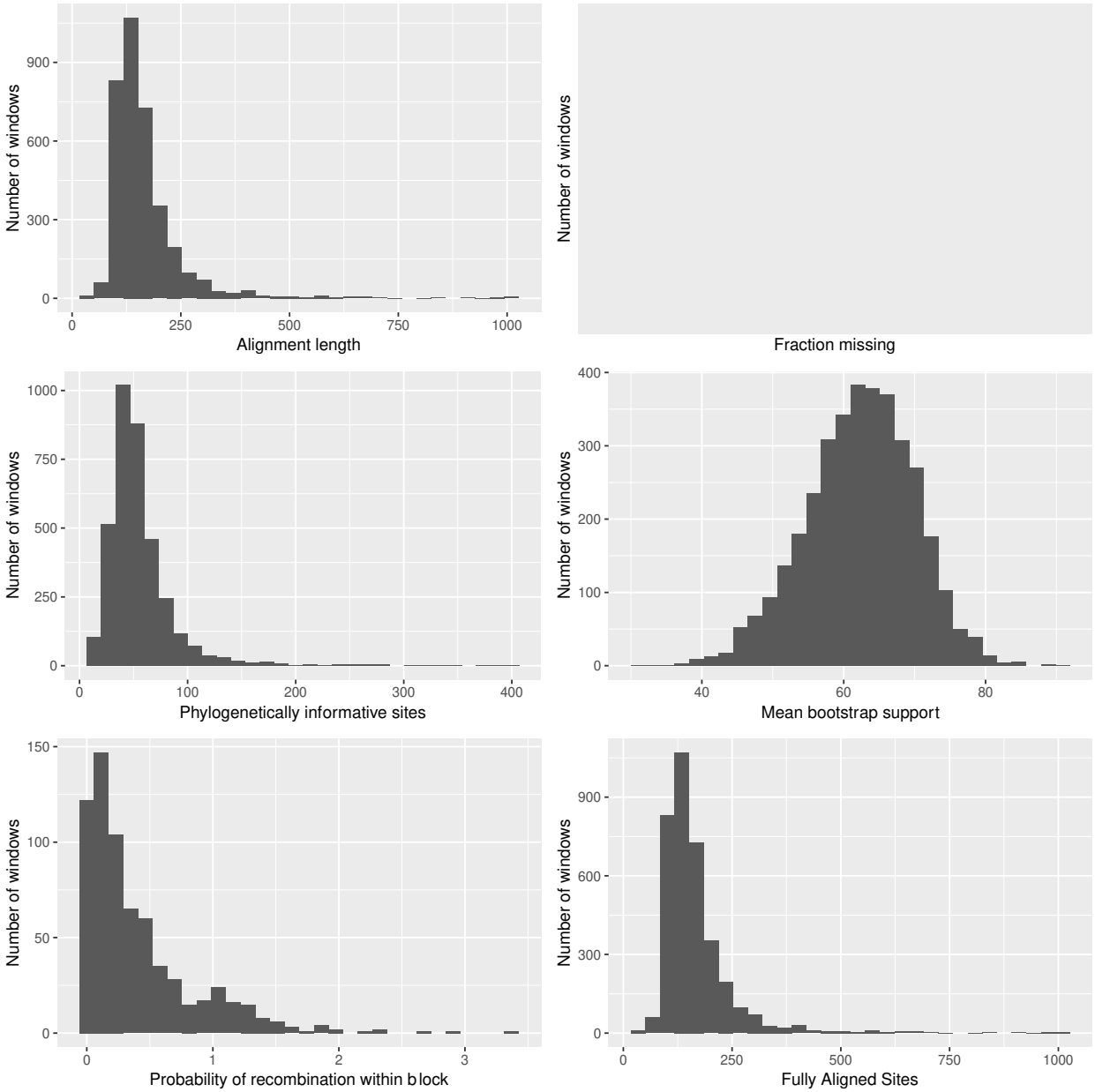

Fig. S28 All species, coding block statistics

Basic statistics for coding blocks and resulting trees in the full alignment. Statistics as in Fig. S22-S24.

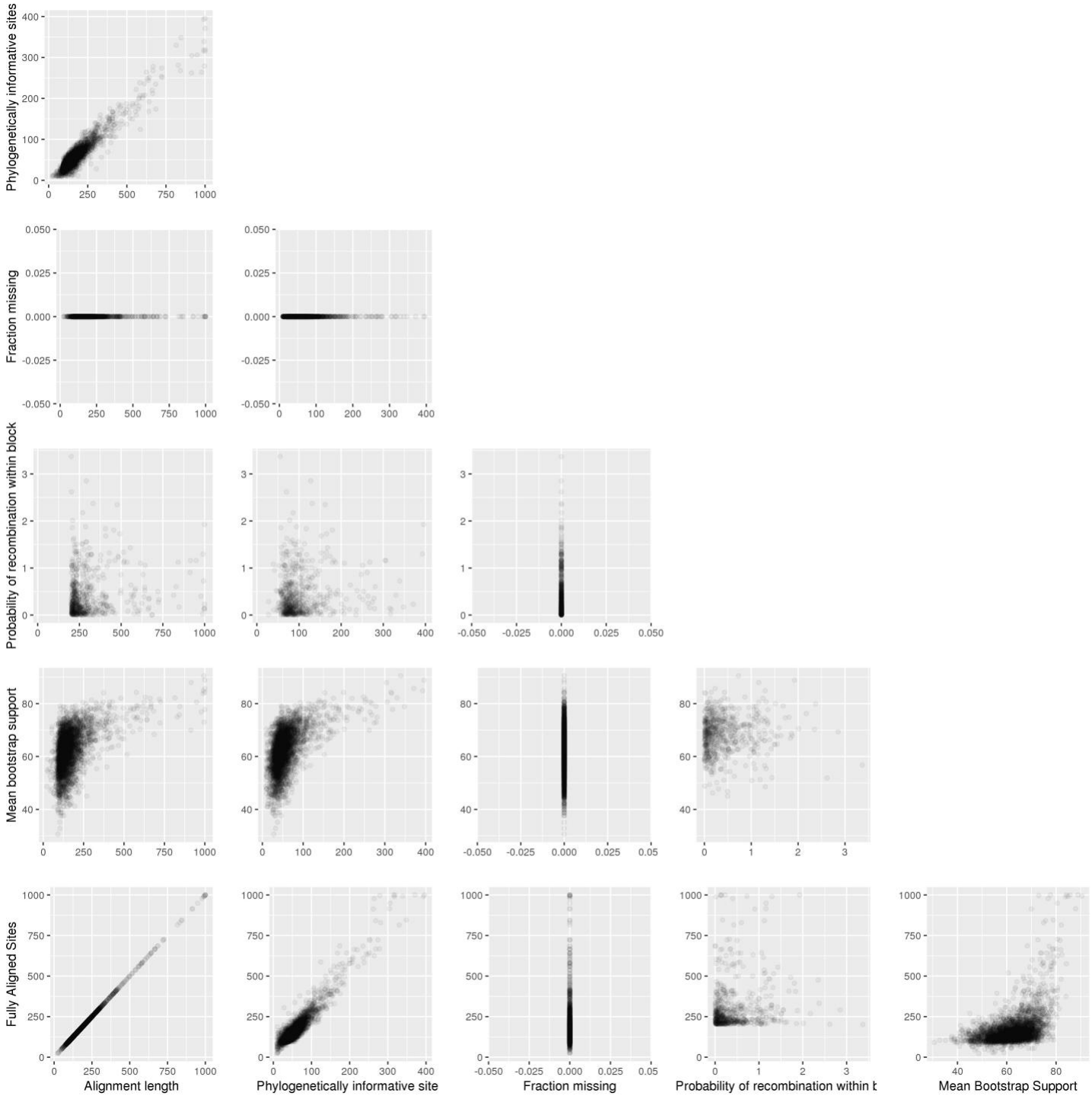

Fig. S29 All species coding block pairwise statistics

Correlations between each pair of window statistics in Fig. S28

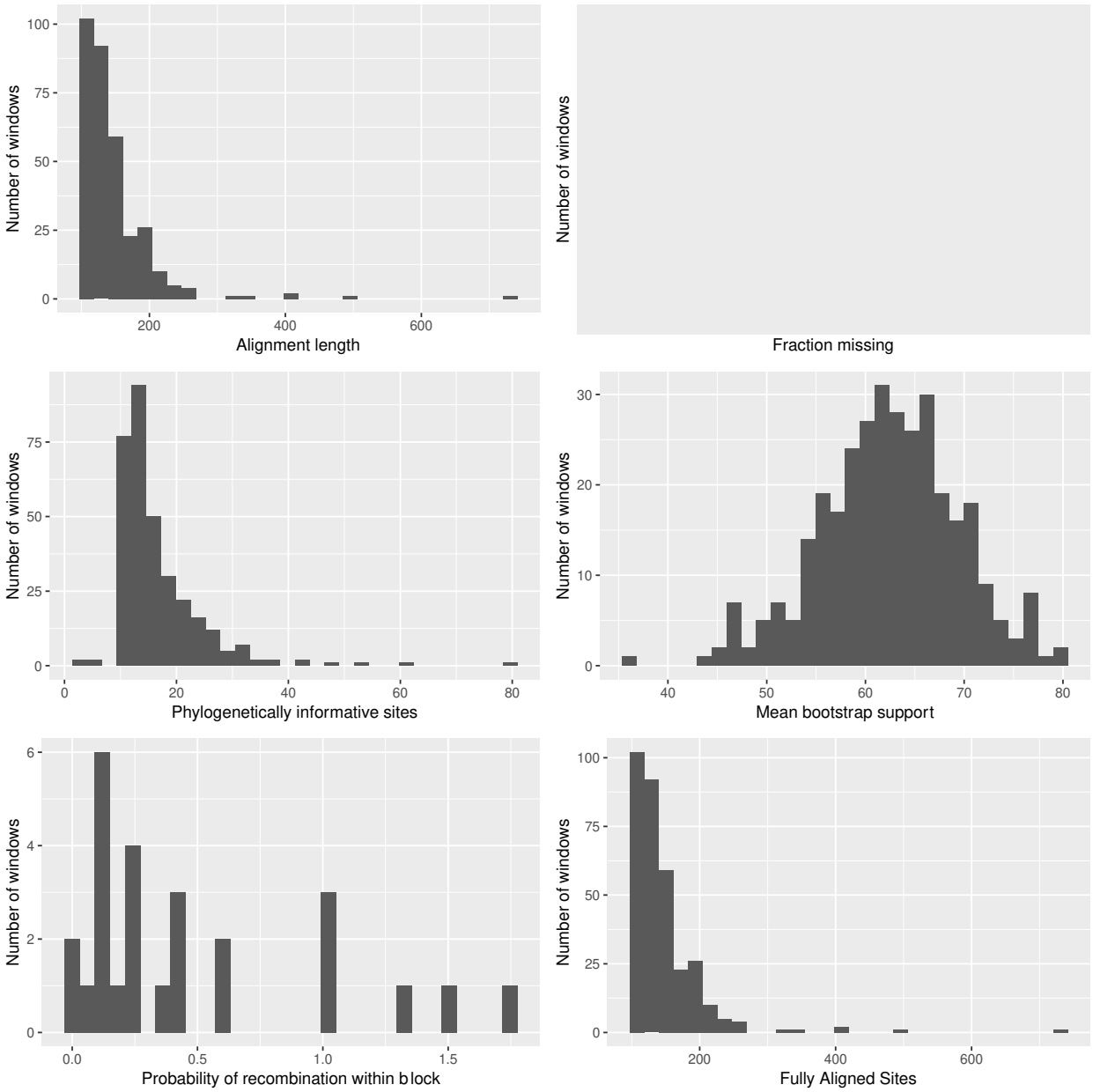

Fig. S30 *Heliconius* species noncoding block statistics

Basic statistics for non-coding blocks and resulting trees in Heliconius *species. Statistics as in* Fig. S22

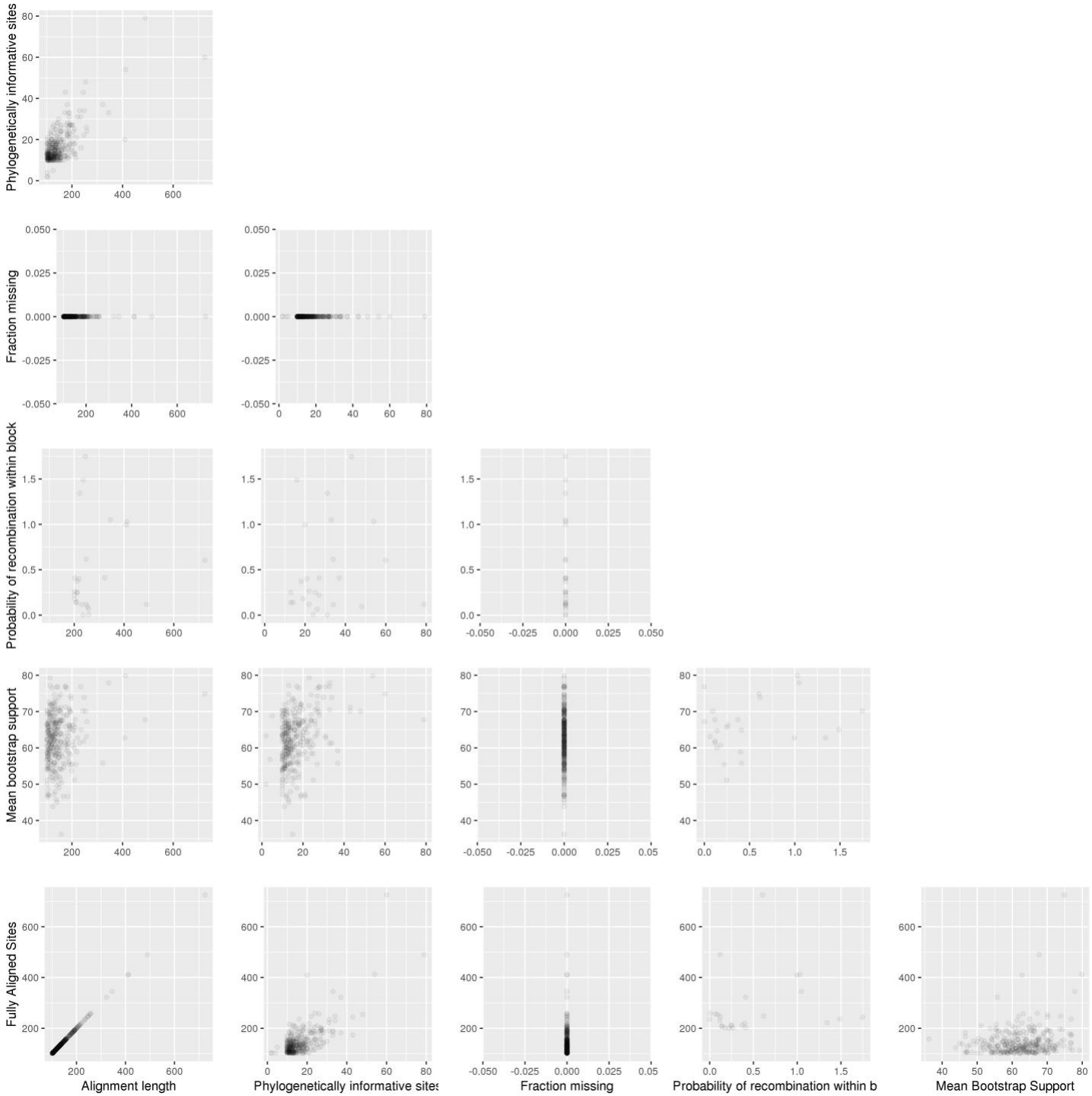

Fig. S31 *Heliconius* species non-coding pairwise statistics

Correlations between each pair of window statistics in Fig. S30

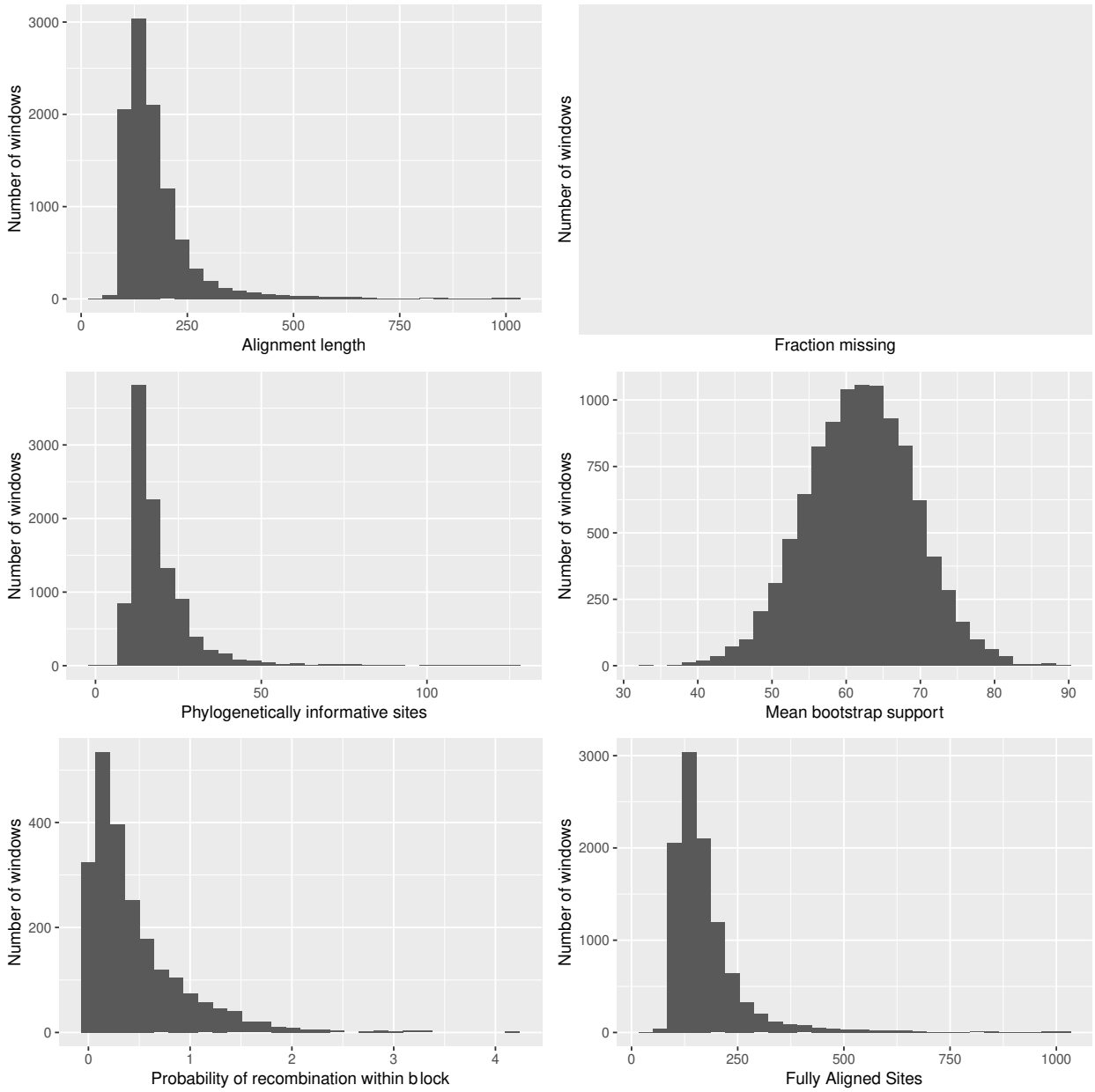

Fig. S32 *Heliconius* coding block statistics

Basic statistics for coding blocks in Heliconius *species and resulting trees. Statistics as in* Fig. S22

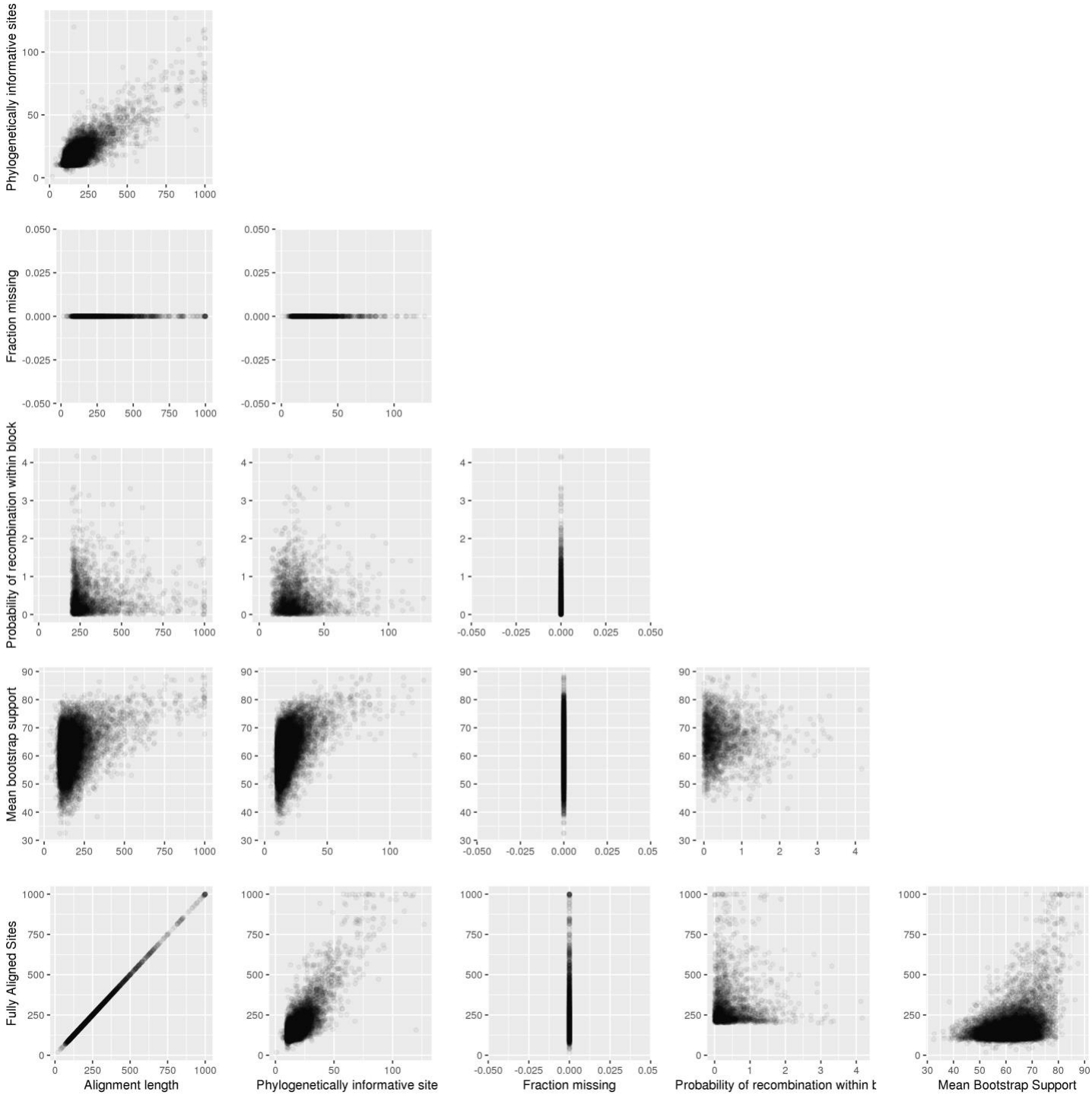

Fig. S33 Heliconius coding block pairwise statistics

Correlations between each pair of window statistics in Fig. S32

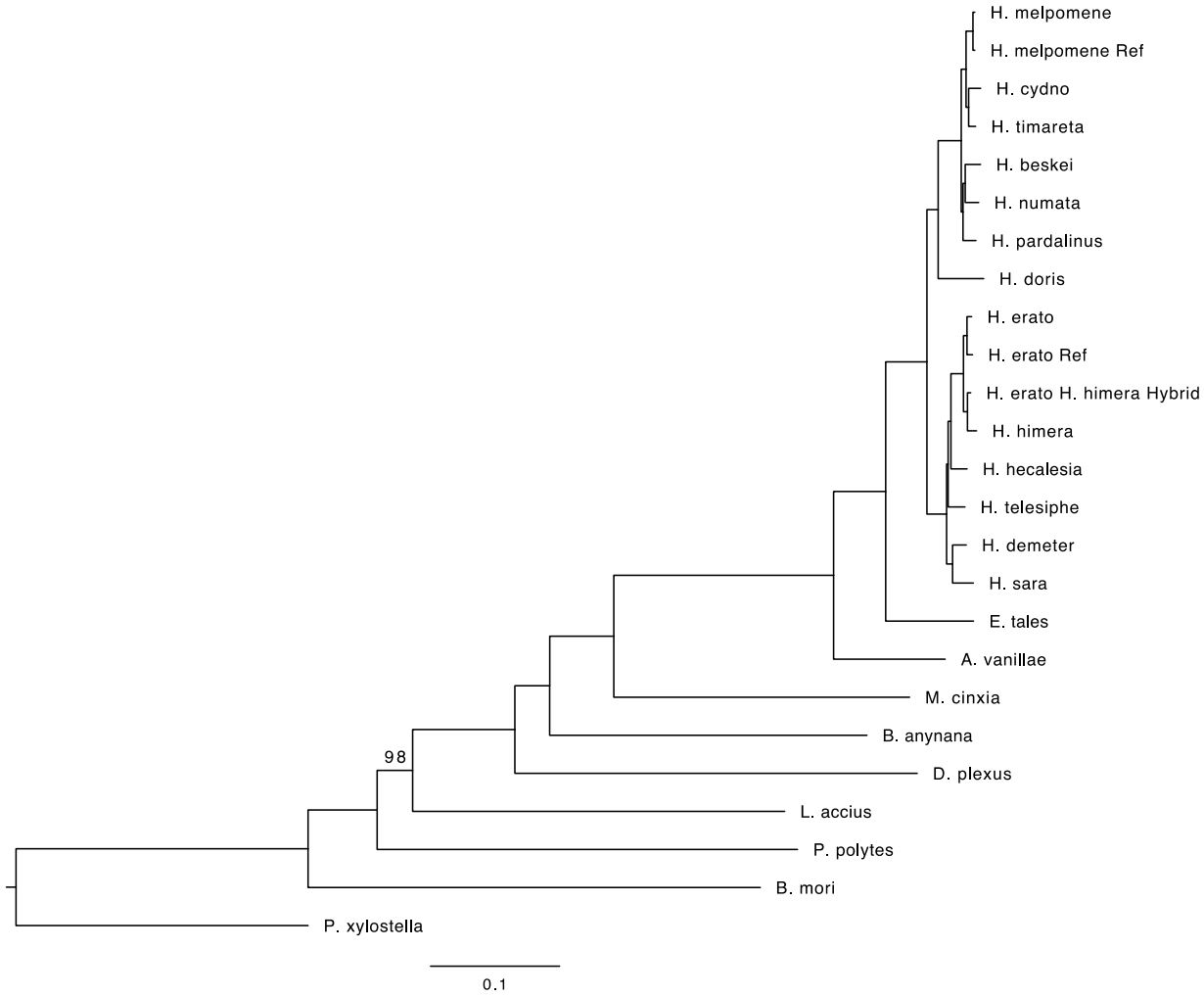

Fig. S34 Maximum likelihood concatenated tree for genes generated in IQtree.

Bootstrap support values are shown for nodes with less than 100% support. The scale bar represents branch lengths, which correspond to the mean number of substitutions per site in the alignment.

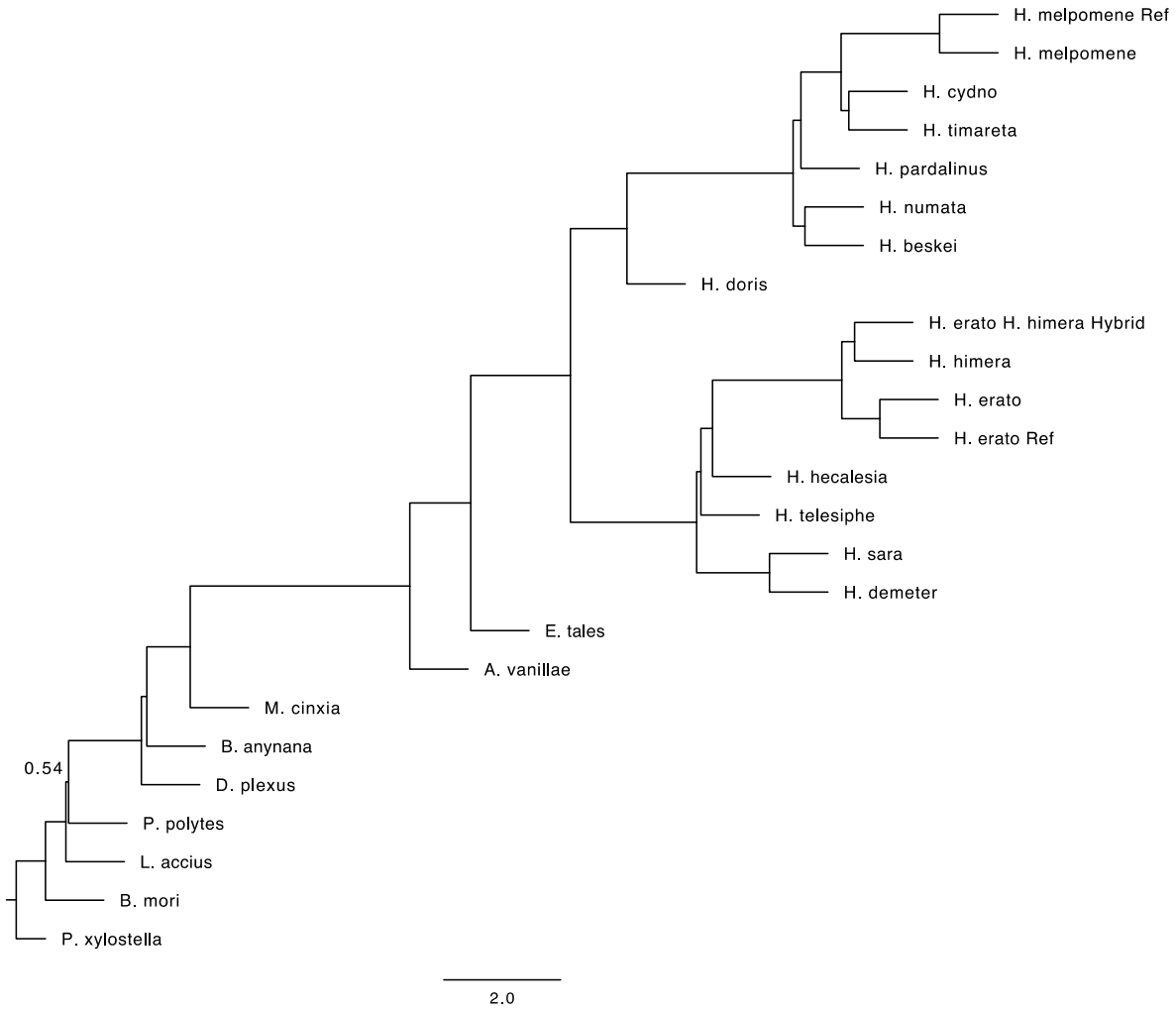

Fig. S35 ASTRAL tree for genes. Species tree generated in ASTRAL for gene alignments.

ASTRAL support values for each node are 1.0. The scale bar represents branch lengths, which correspond to coalescent units.

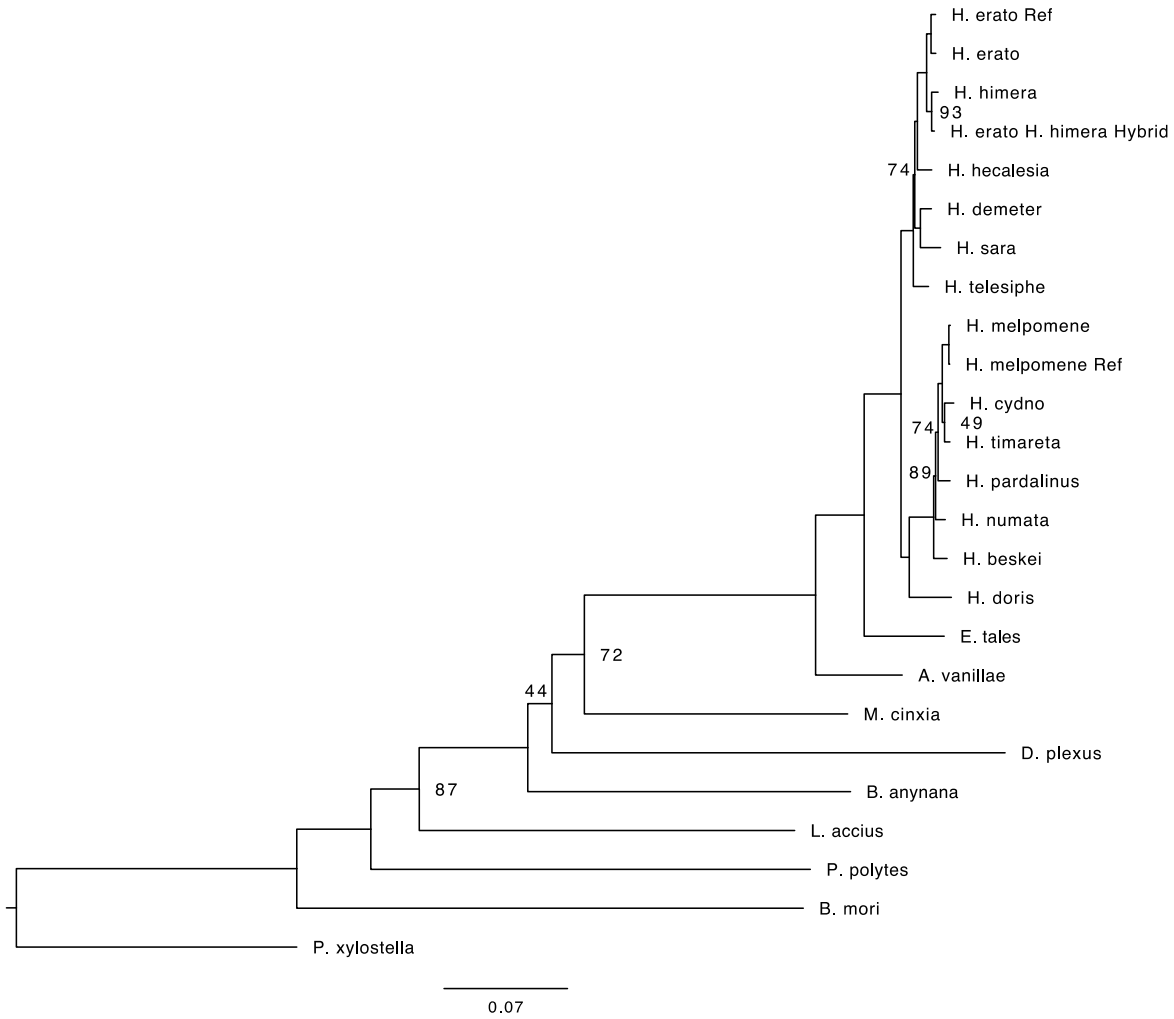

Fig. S36 Concatenated tree for noncoding, fully aligned blocks greater than or equal to 100 bp.

Bootstrap support values are shown for nodes with less than 100% support. The scale bar represents branch lengths, which correspond to the mean number of substitutions per site in the alignment.

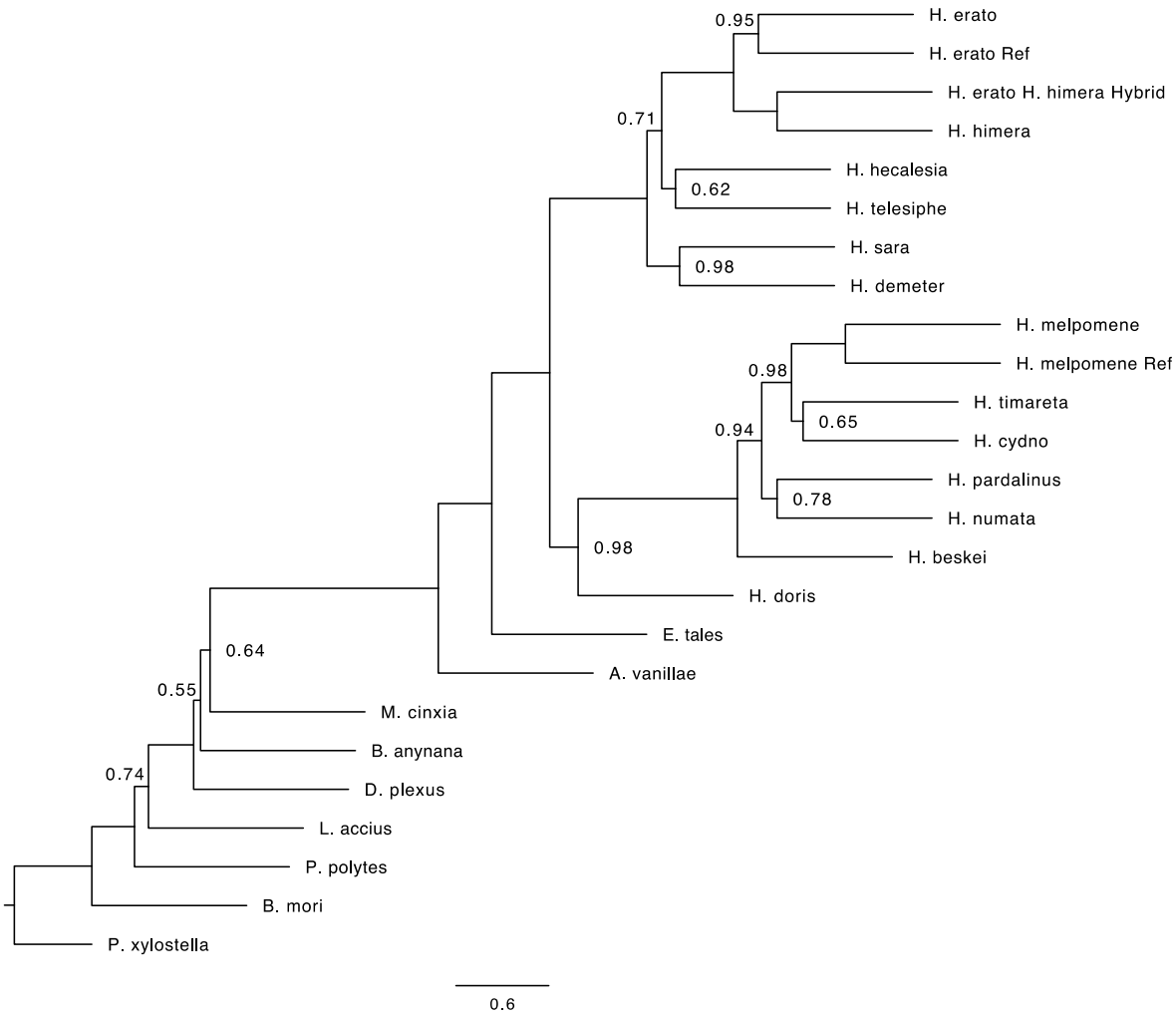

Fig. S37 ASTRAL tree for noncoding, fully aligned blocks greater than or equal to 100 bp.

Astral support values are shown for nodes with less than 1.0 support. Branch lengths in coalescent units.

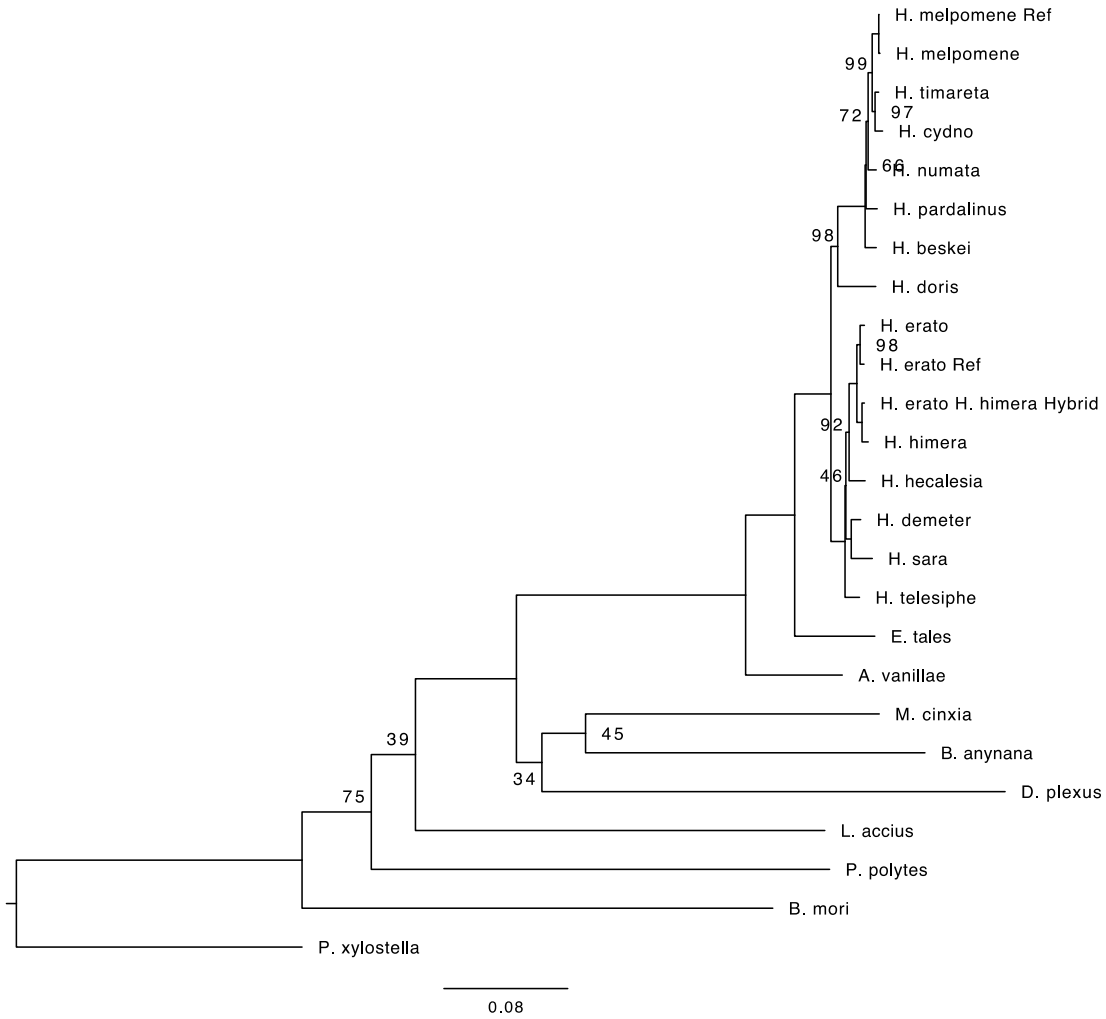

Fig. S38 Concatenated tree for noncoding, fully aligned blocks greater than or equal to 150 bp.

Bootstrap support values are shown for nodes with less than 100% support. The scale bar represents branch lengths, which correspond to the mean number of substitutions per site in the alignment.

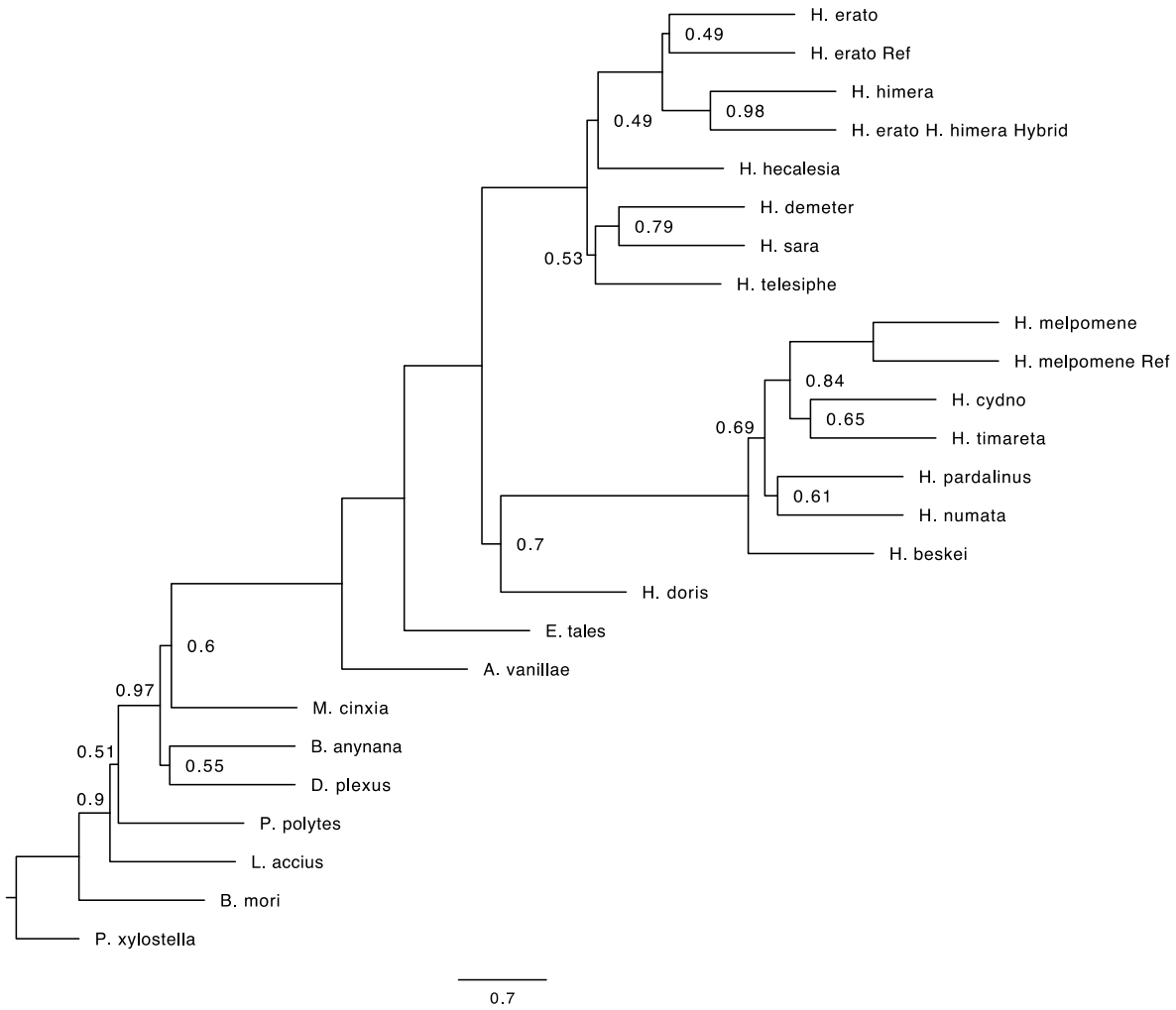

Fig. S39 ASTRAL tree for noncoding, fully aligned blocks greater than or equal to 150 bp.

Astral support values are shown for nodes with less than 1.0 support. Branch lengths in coalescent units.

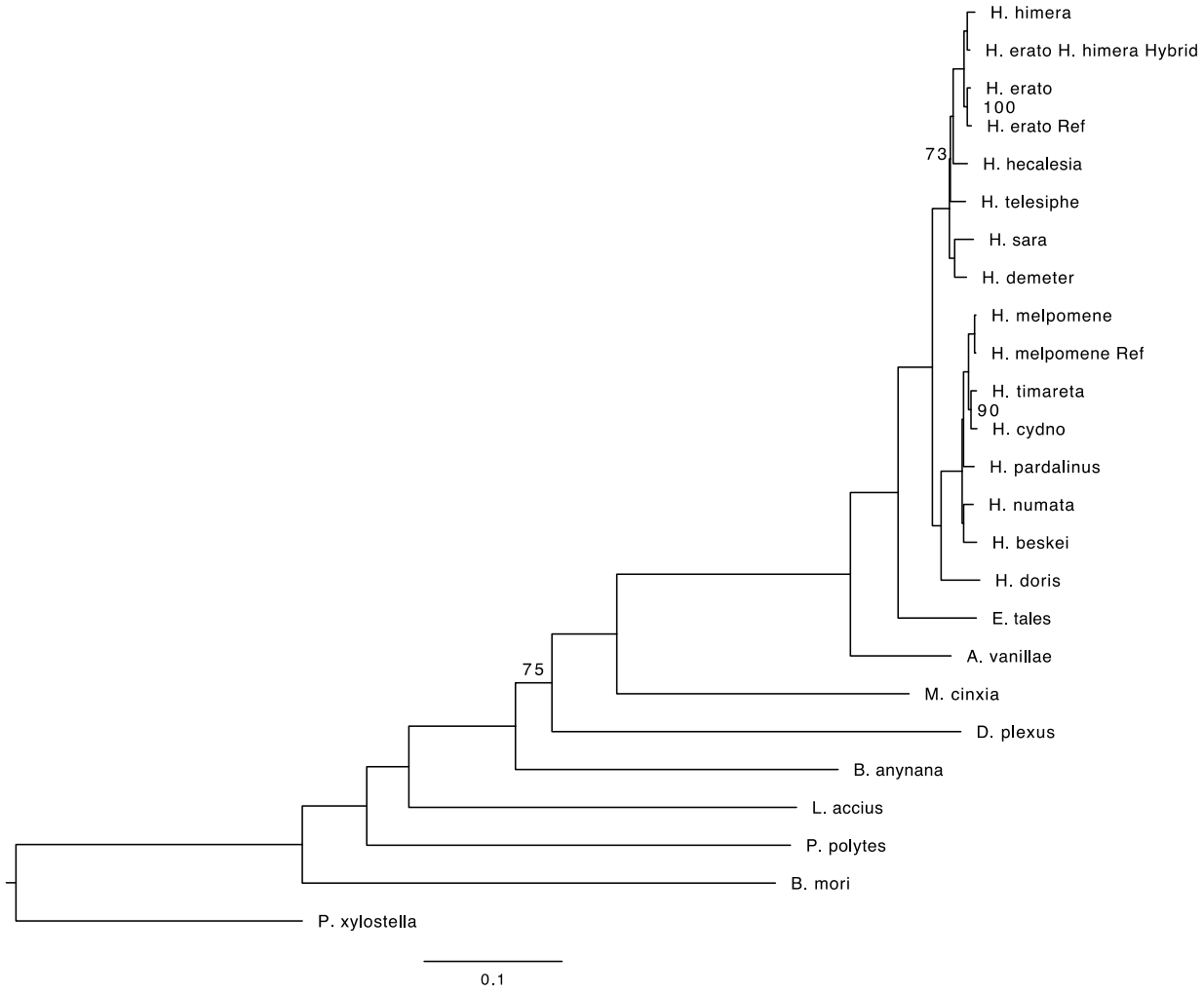

Fig. S40 Concatenated tree for coding, fully aligned blocks greater than or equal to 100 bp.

Bootstrap support values are shown for nodes with less than 100% support. The scale bar represents branch lengths, which correspond to the mean number of substitutions per site in the alignment.

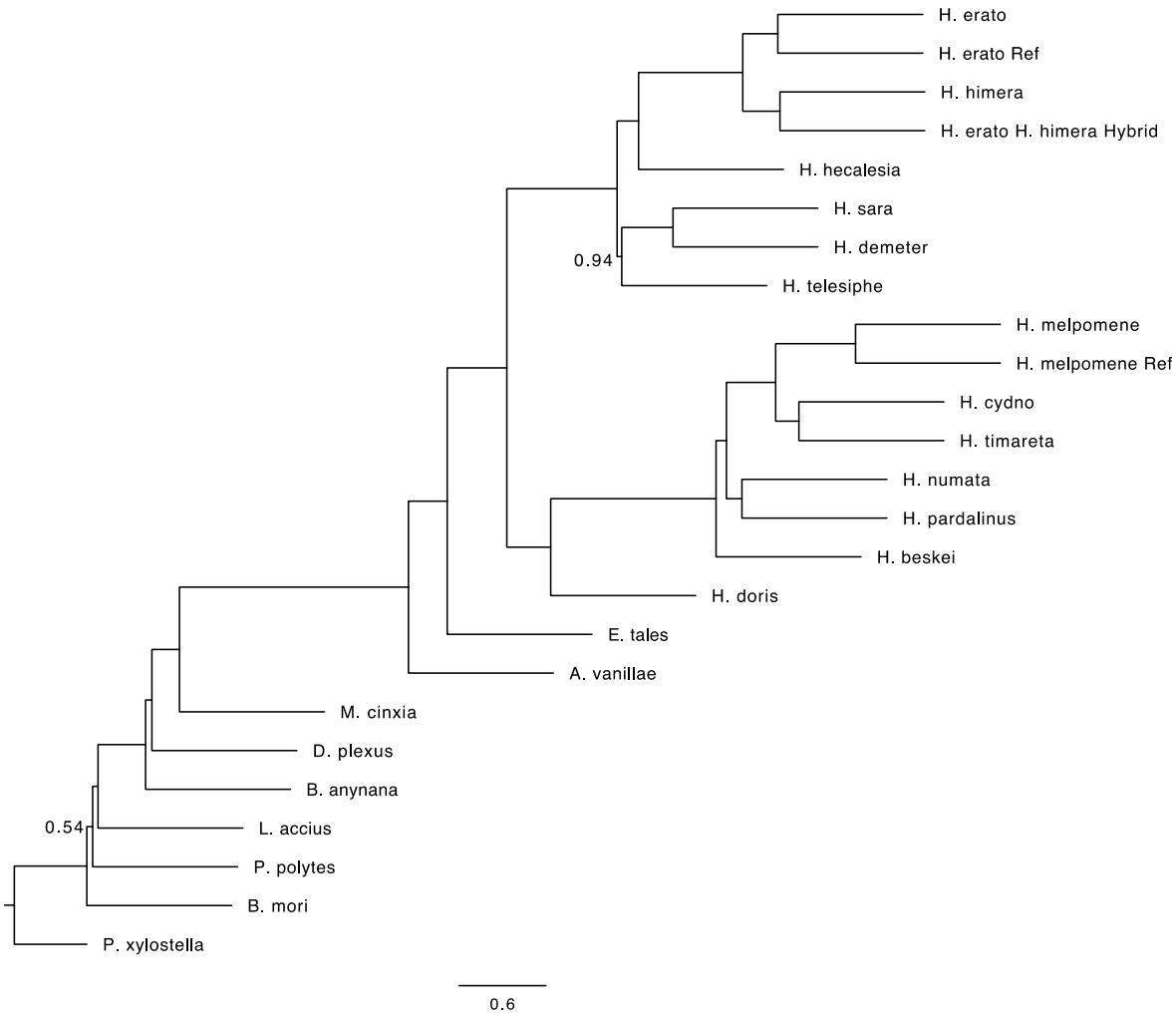

Fig. S41 ASTRAL tree for coding, fully aligned blocks greater than or equal to 100 bp.

Astral support values are shown for nodes with less than 1.0 support. Branch lengths in coalescent units.

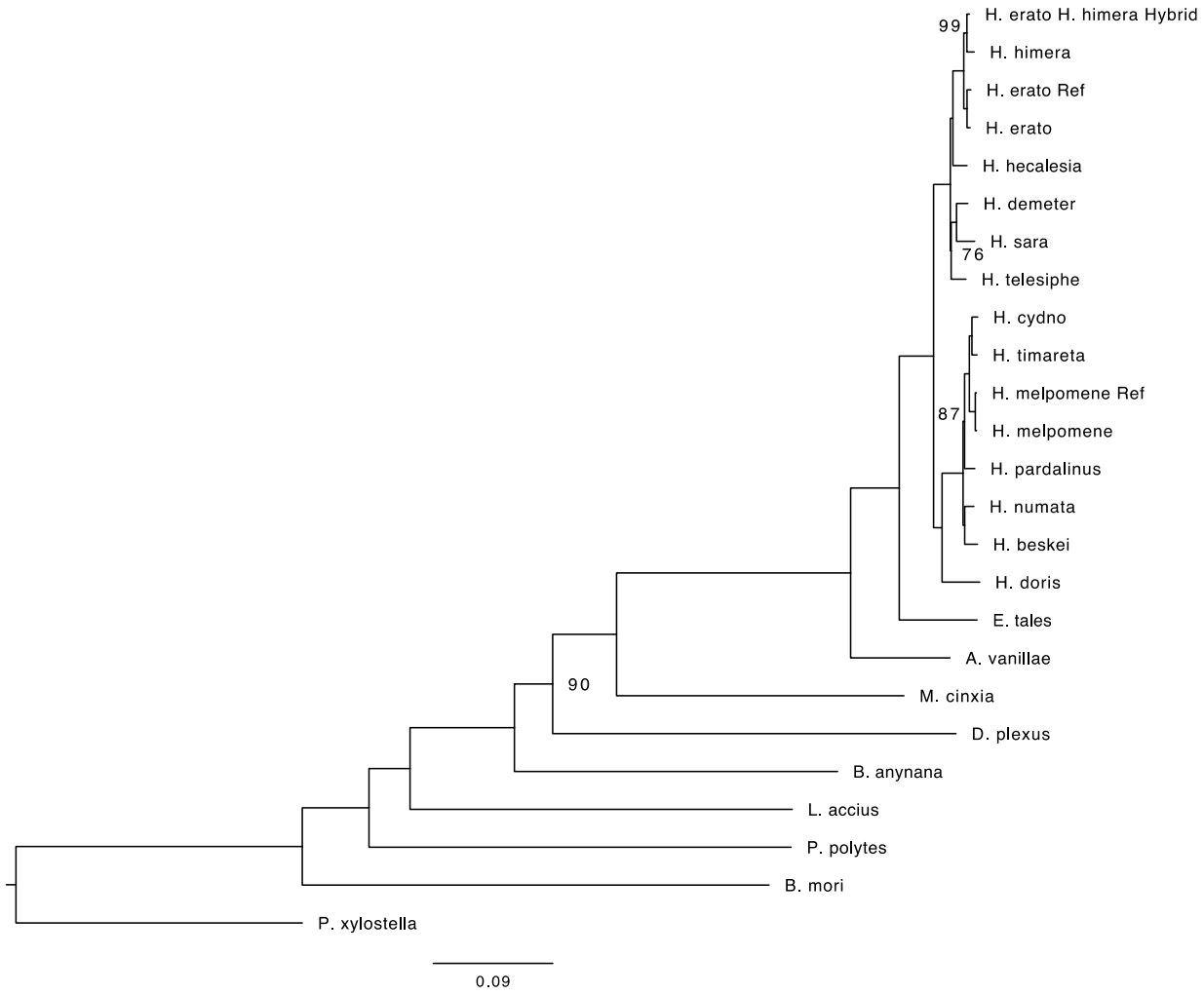

Fig. S42 Concatenated tree for coding, fully aligned blocks greater than or equal to 150 bp.

Bootstrap support values are shown for nodes with less than 100% support. The scale bar represents branch lengths, which correspond to the mean number of substitutions per site in the alignment.

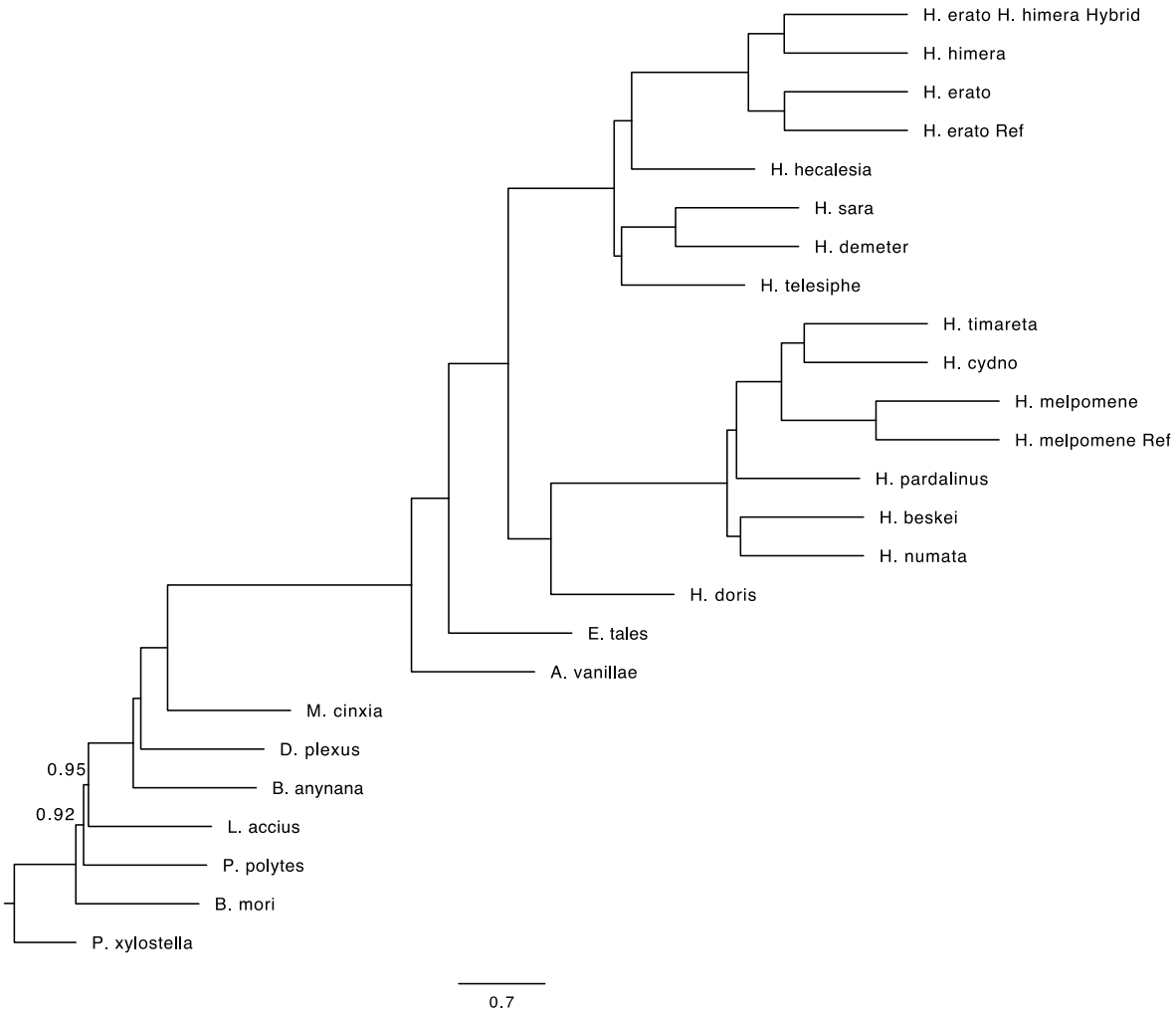

Fig. S43 ASTRAL tree for coding, fully aligned blocks greater than or equal to 150 bp.

Astral support values are shown for nodes with less than 1.0 support. Branch lengths in coalescent units.

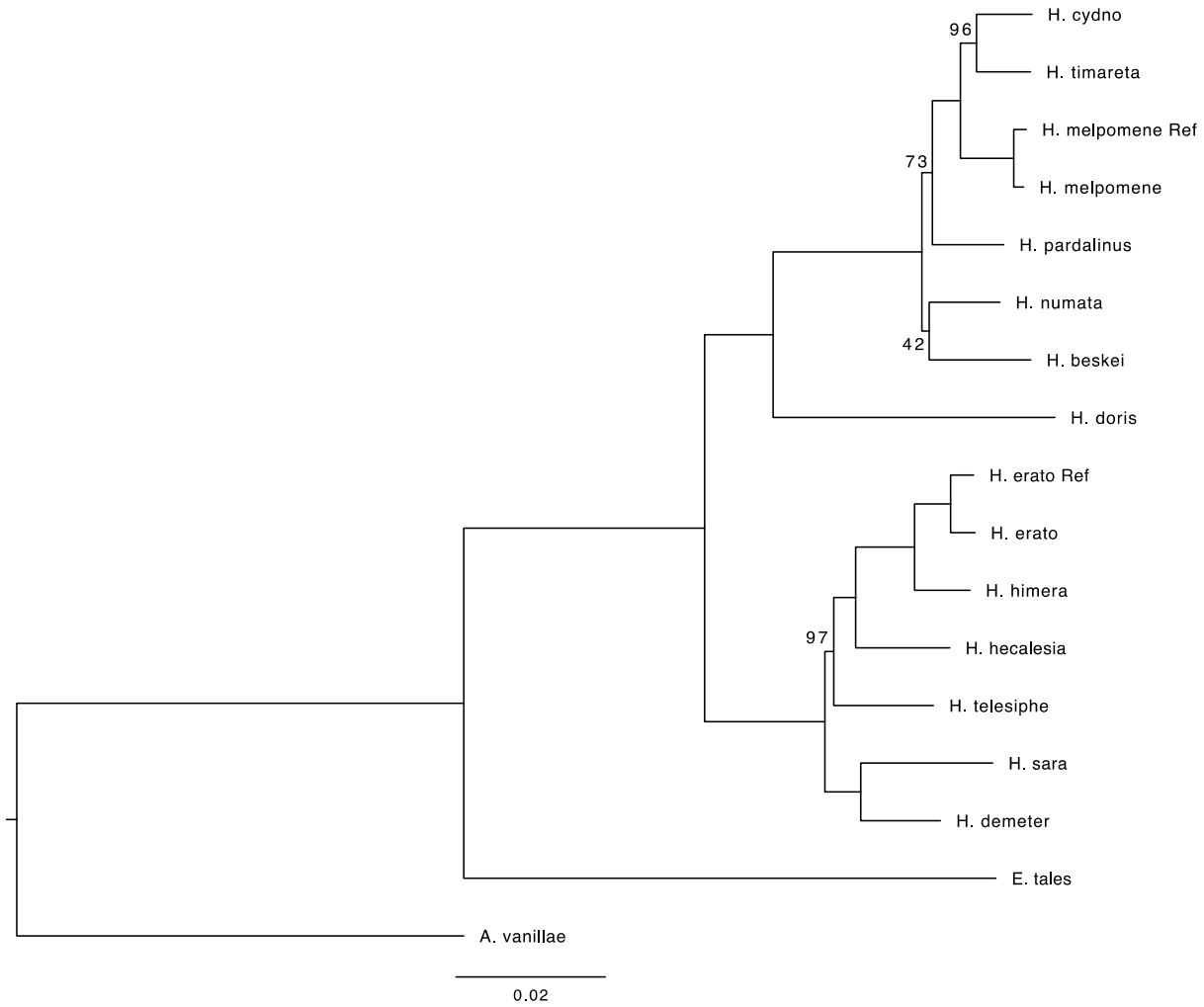

Fig. S44 Concatenated tree for noncoding, fully aligned blocks among Heliconiini that are greater than or equal to 100 bp.

Bootstrap support values are shown for nodes with less than 100% support. The scale bar represents branch lengths, which correspond to the mean number of substitutions per site in the alignment.

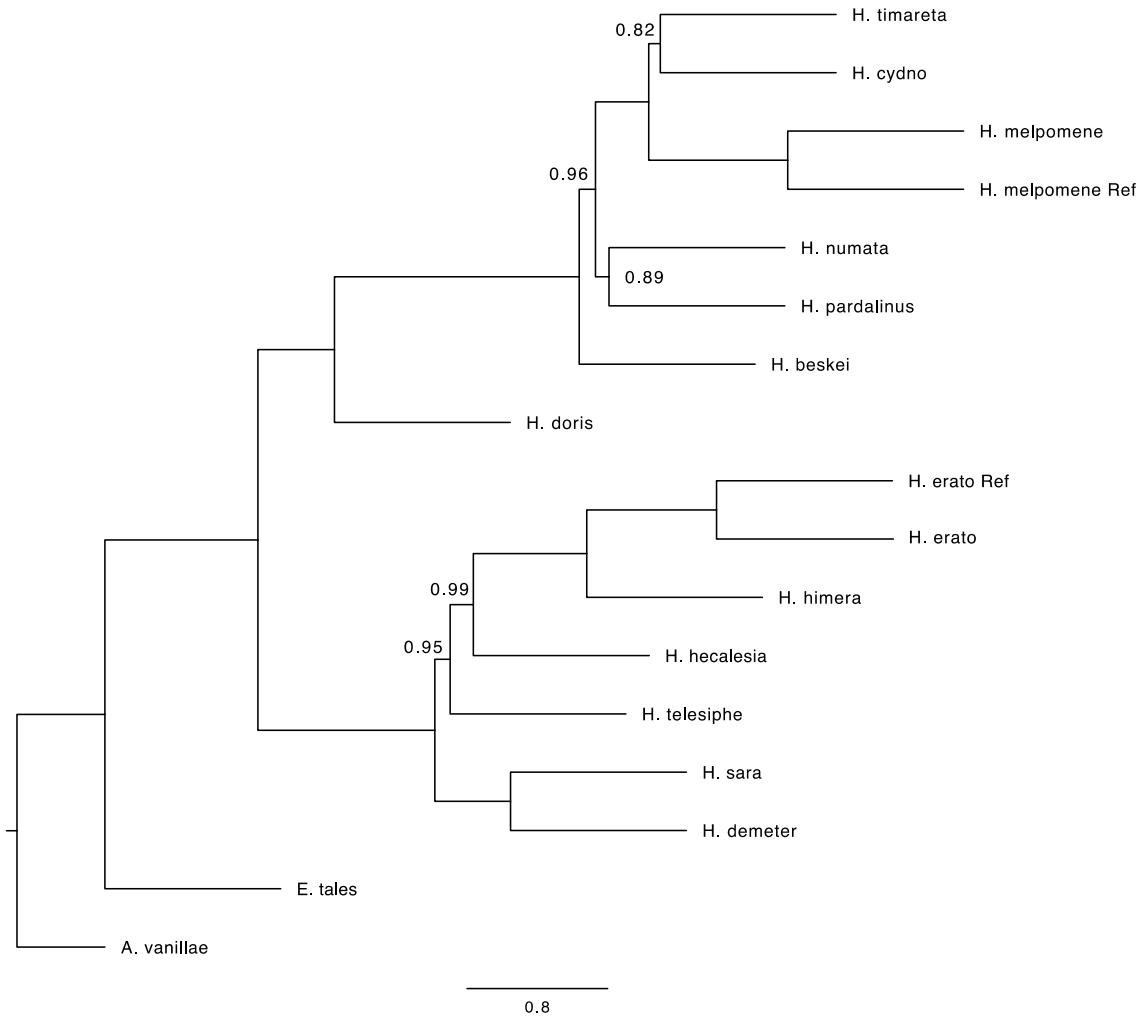

Fig. S45 ASTRAL tree for noncoding, fully aligned blocks among Heliconiini that are greater than or equal to 100 bp.

Astral support values are shown for nodes with less than 1.0 support. Branch lengths in coalescent units.

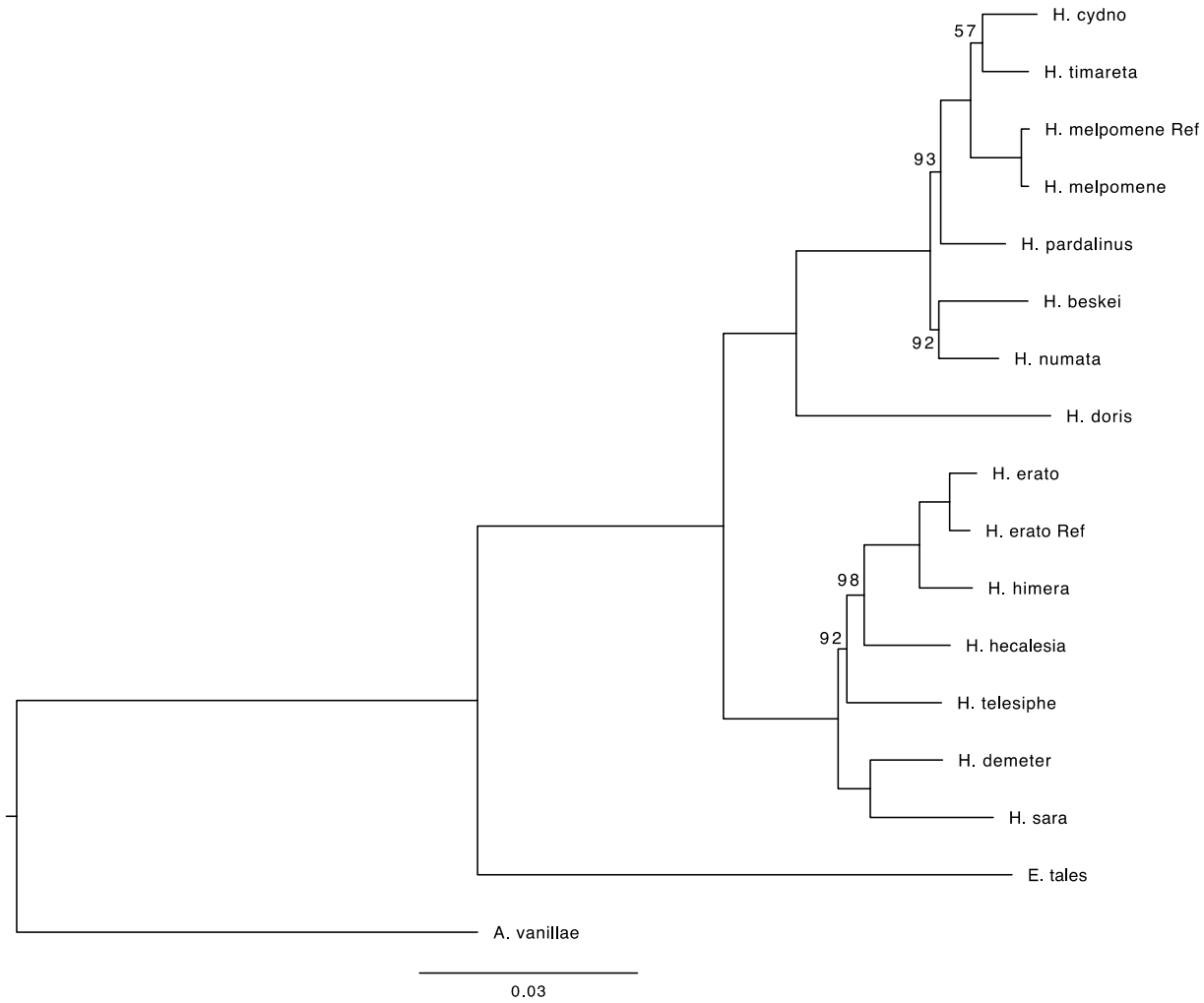

Fig. S46 Concatenated tree for noncoding, fully aligned blocks among Heliconiini that are greater than or equal to 150 bp.

Bootstrap support values are shown for nodes with less than 100% support. The scale bar represents branch lengths, which correspond to the mean number of substitutions per site in the alignment.

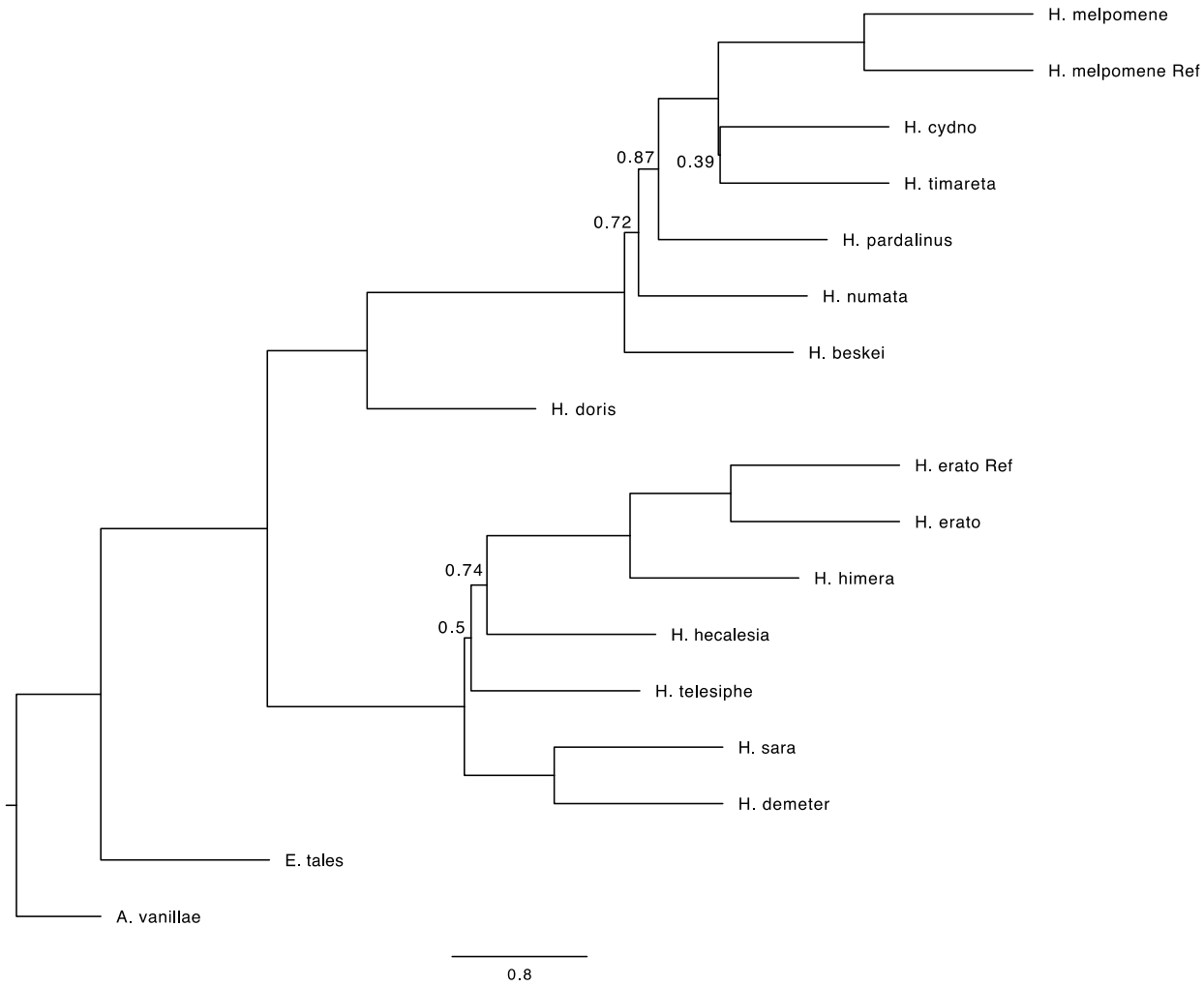

Fig. S47 ASTRAL tree for noncoding, fully aligned blocks among Heliconiini that are greater than or equal to 150 bp.

Astral support values are shown for nodes with less than 1.0 support. Branch lengths in coalescent units.

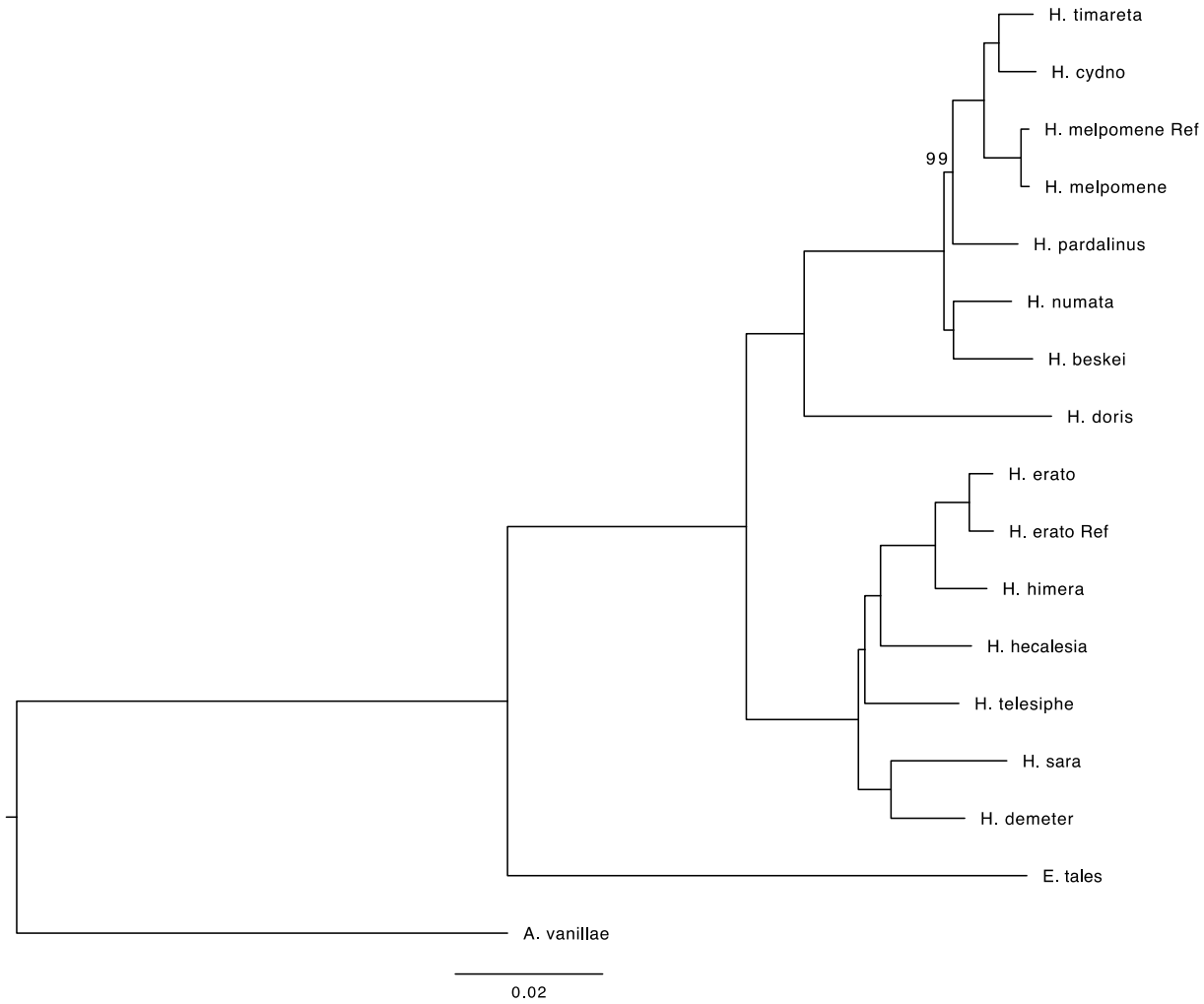

Fig. S48 Concatenated tree for coding, fully aligned blocks among Heliconiini that are greater than or equal to 100 bp.

Bootstrap support values are shown for nodes with less than 100% support. The scale bar represents branch lengths, which correspond to the mean number of substitutions per site in the alignment.

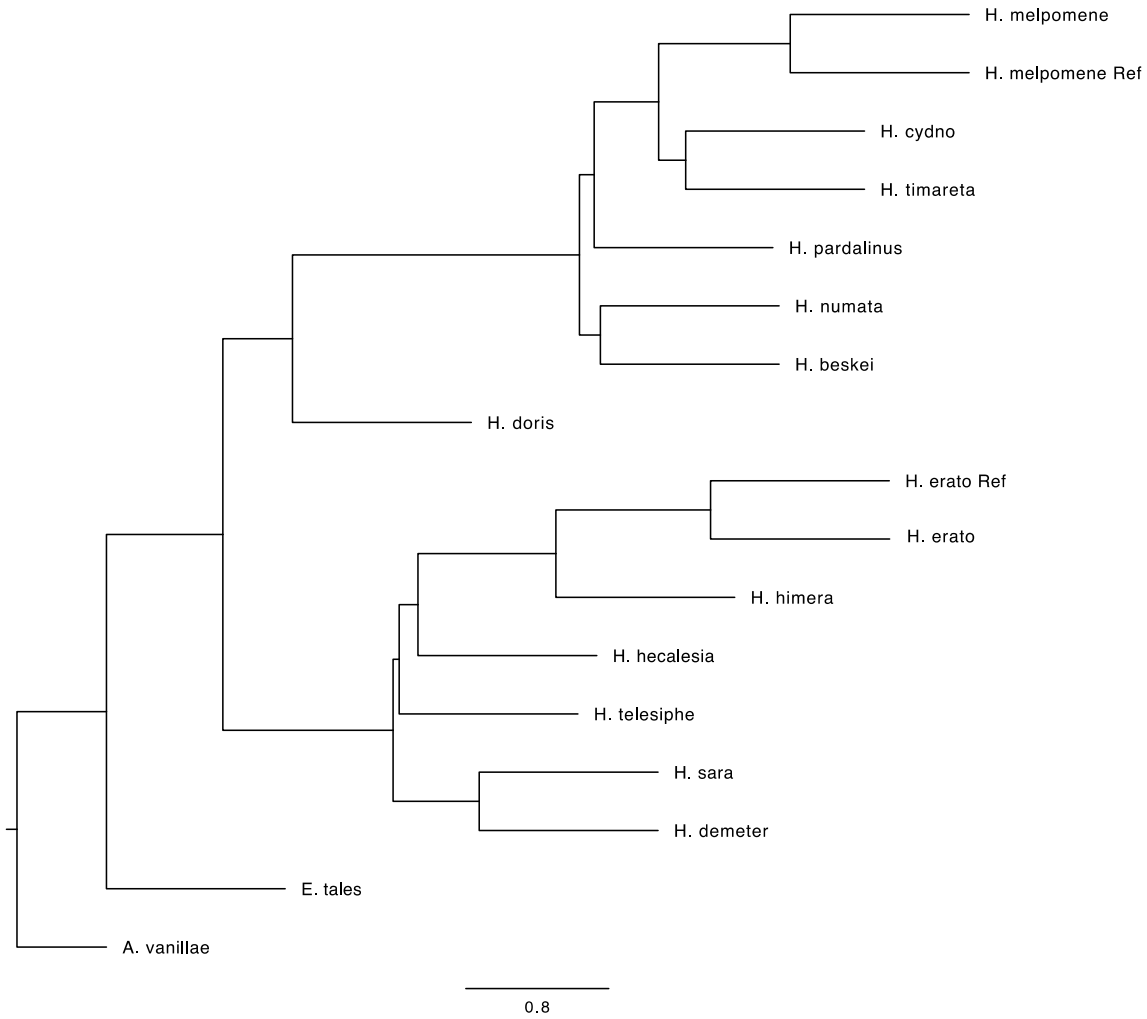

Fig. S49 ASTRAL tree for coding, fully aligned blocks among Heliconiini that are greater than or equal to 100 bp.

Astral support values are shown for nodes with less than 1.0 support. Branch lengths in coalescent units.

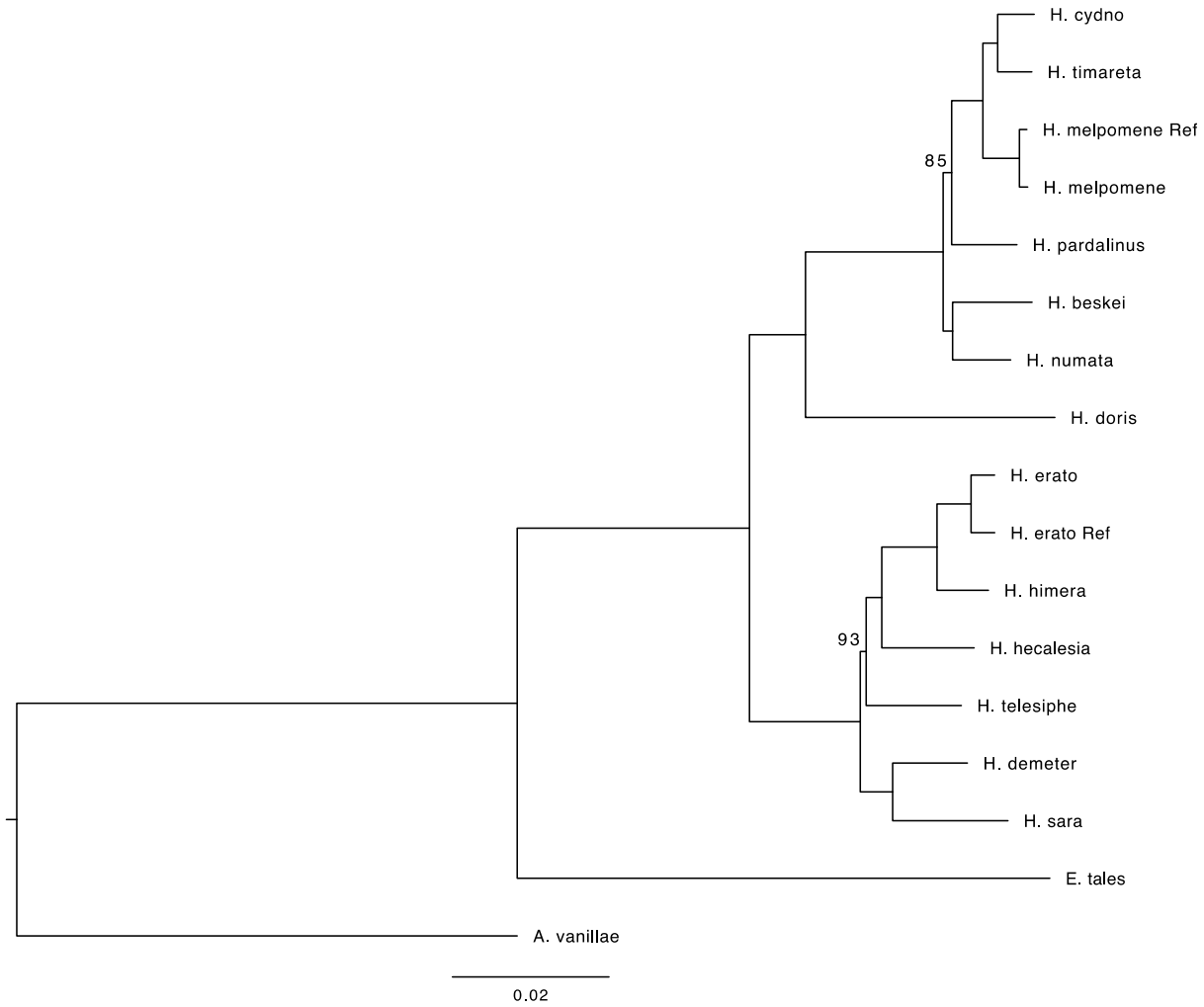

Fig. S50 Concatenated tree for coding, fully aligned blocks among Heliconiini that are greater than or equal to 150 bp.

Bootstrap support values are shown for nodes with less than 100% support. The scale bar represents branch lengths, which correspond to the mean number of substitutions per site in the alignment.

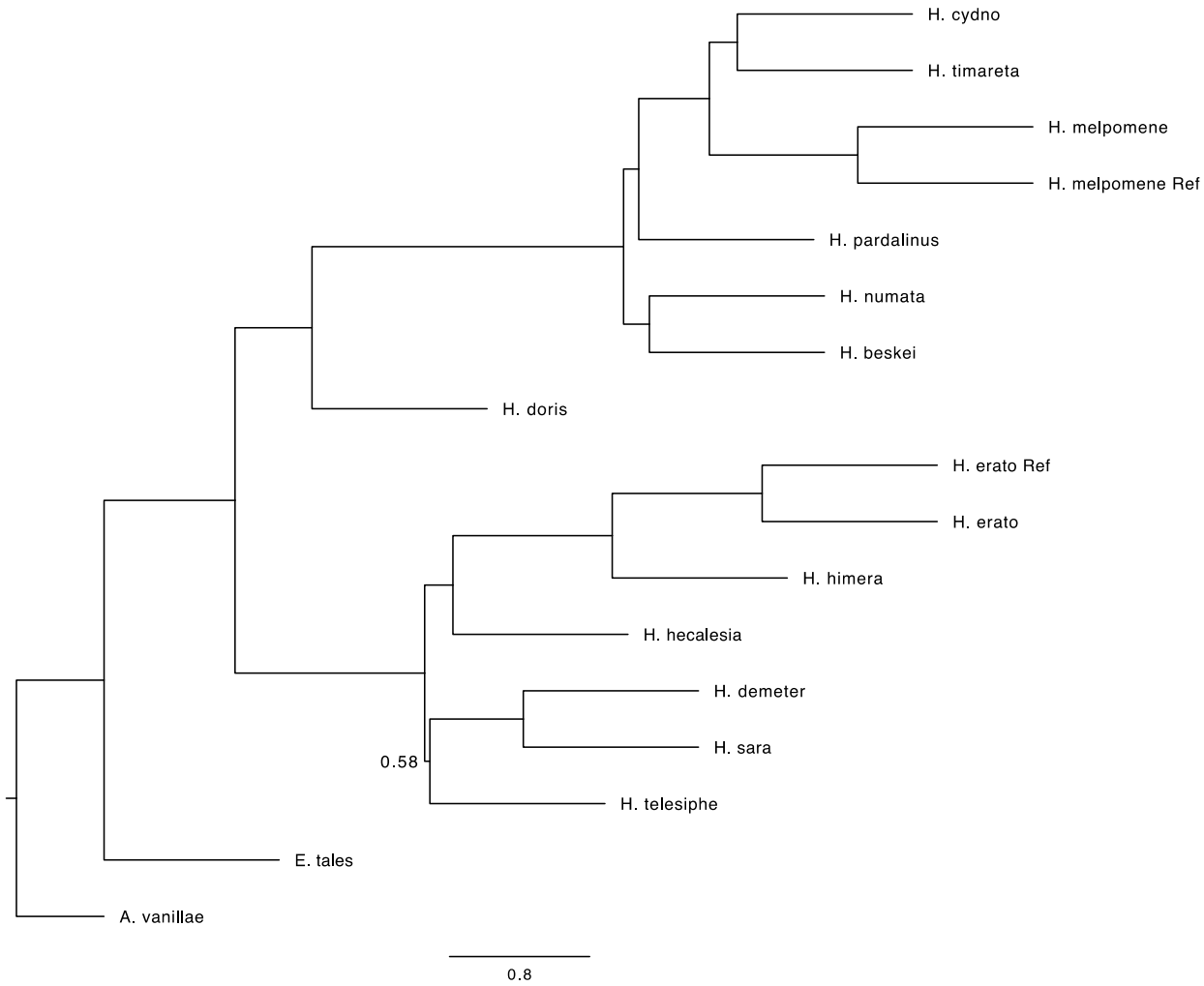

Fig. S51 ASTRAL tree for coding, fully aligned blocks among Heliconiini that are greater than or equal to 150 bp.

Astral support values are shown for nodes with less than 1.0 support. Branch lengths in coalescent units.

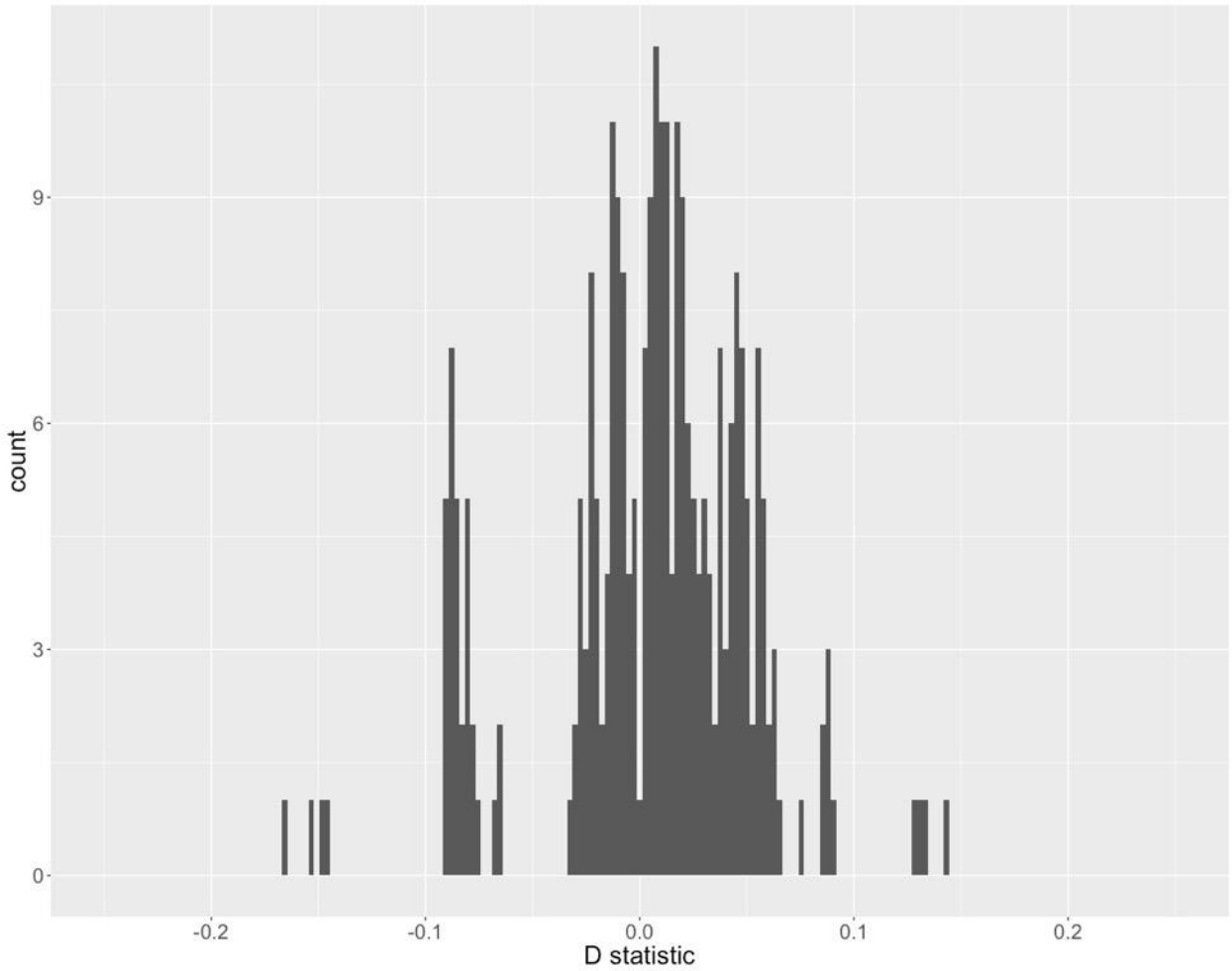

Fig. S52 *D*-statistic values for all triplets.

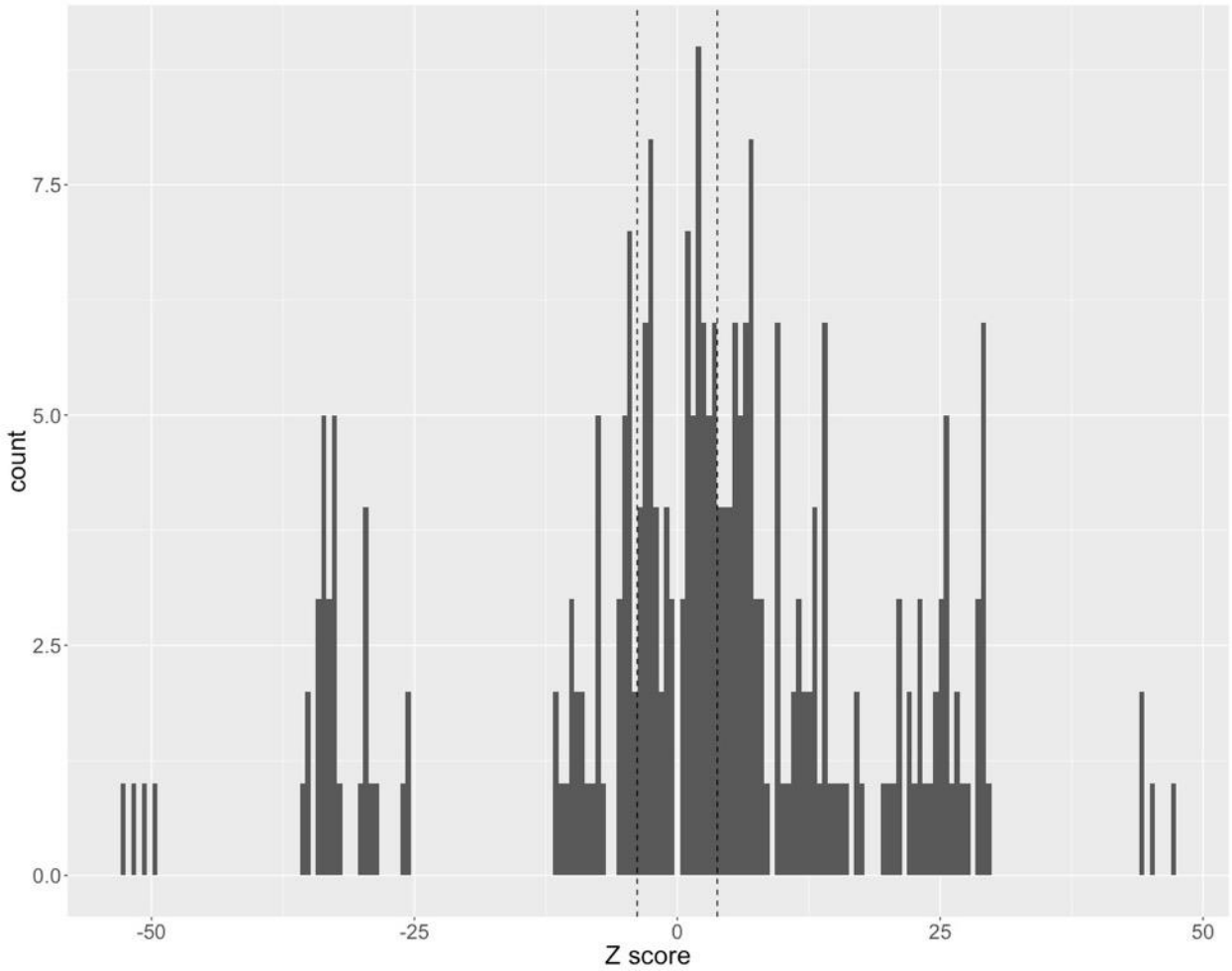

Fig. S53 Z-values for *D*-statistics for all triplets

This histogram shows the Z-values for all comparisons shown in Fig. S52. *The dotted lines represent significance at a .05 level after applying a Bonferroni correction.*

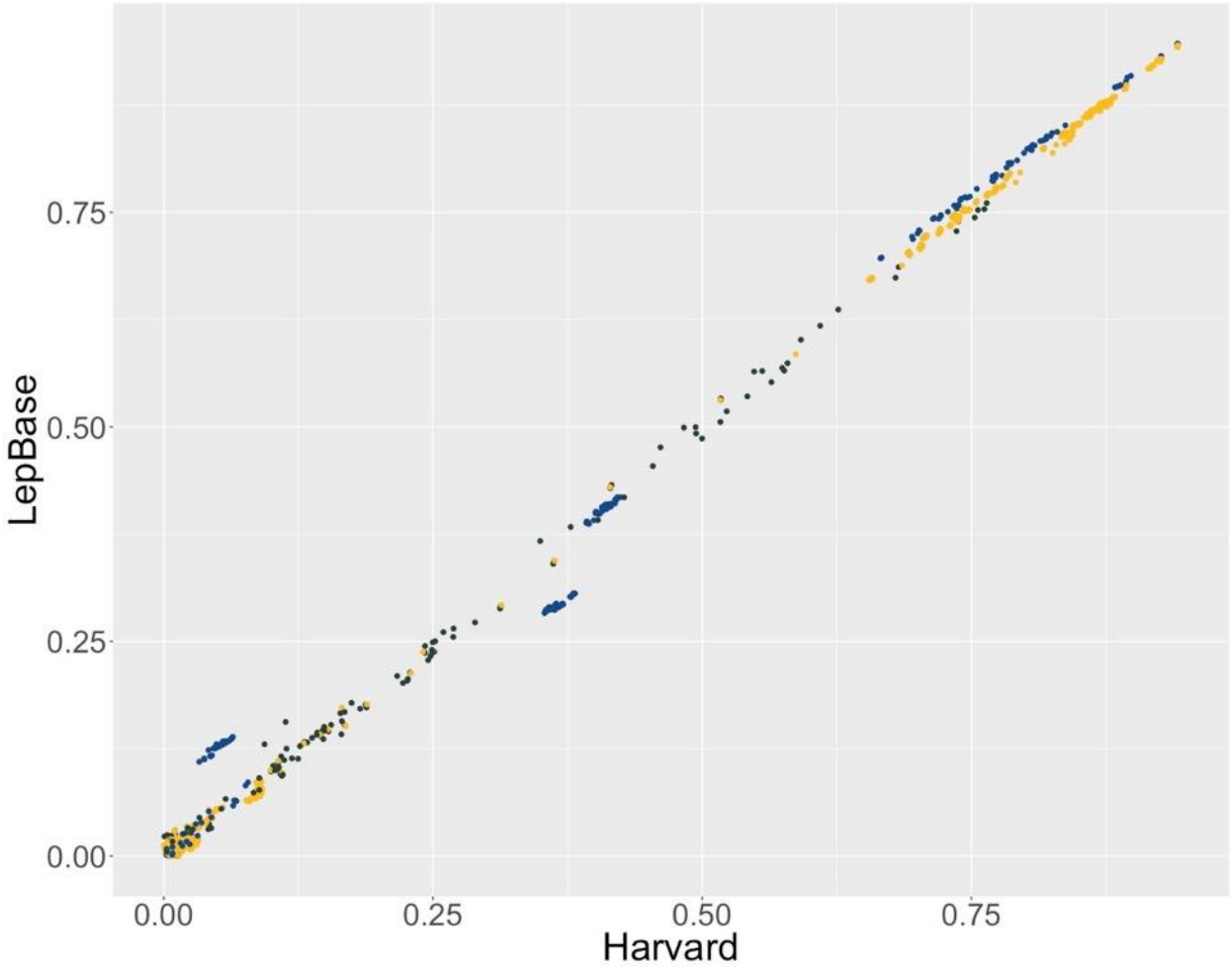

Fig. S54 *D*-statistics are consistent between alignments

These plots show a comparison of the absolute value of D-statistics computed from the full-Lepidoptera alignment described here (x-axis, "Harvard"), and the Heliconiini alignment generated by lepbase.org (y-axis, "LepBase"). Dark green points are inter-clade comparisons, yellow are between clade, and blue are those involving H. doris. *Both groups of* H. doris *points off the 1:1 line are inter-clade comparisons. Values are shown for all triplet topologies, not only the lowest value per triplet.*

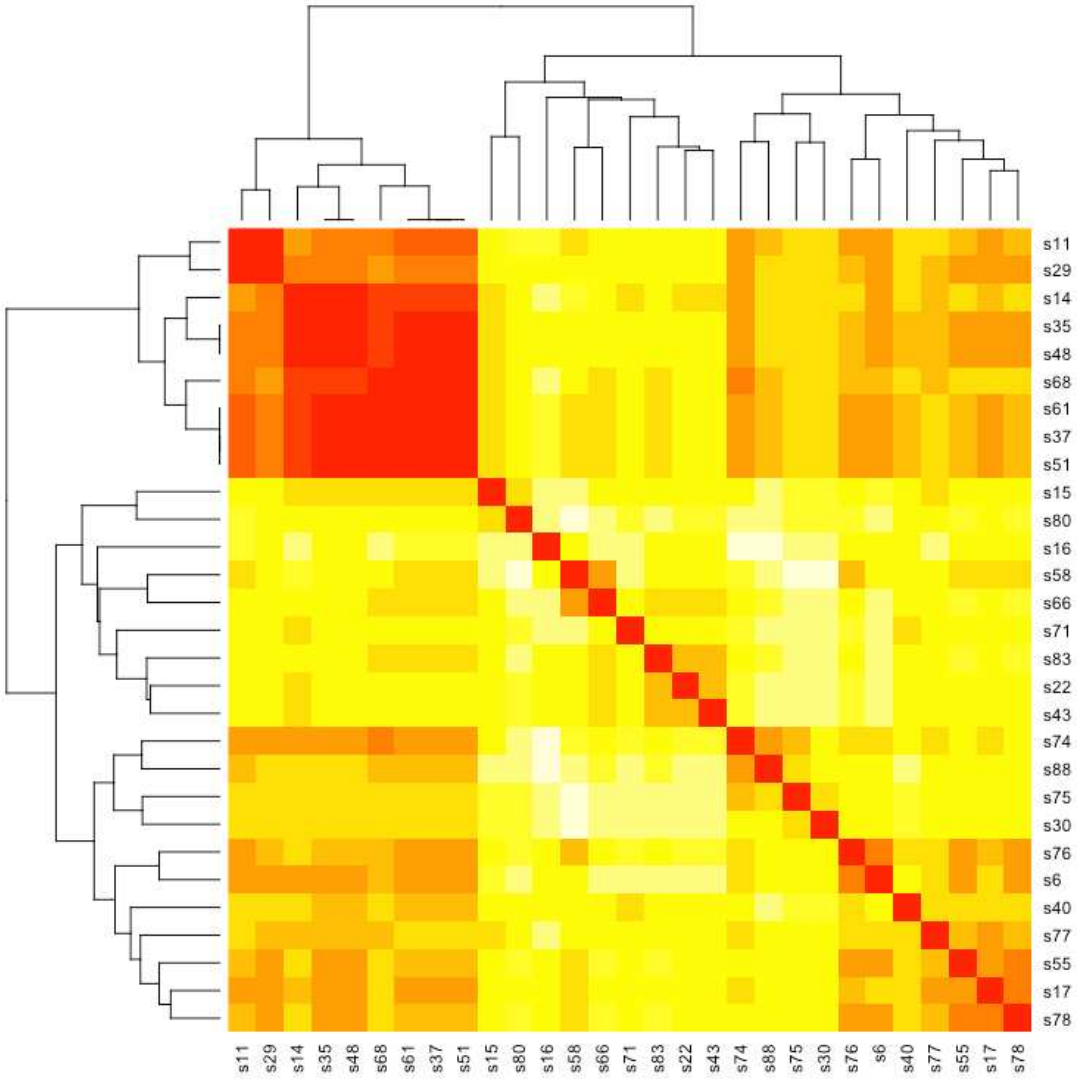

Fig. S55 *melpomene*-silvaniform clade phylogenetic network clustering.

Matrix is symmetrical, and each row or column represents the most likely network in a single run of PhyloNet MCMC_Seq. The branch lengths of the dendrograms represent Luay Nakhleh's reduced phylogenetic network distance metri c(88), where 0 means the networks are identical. The top left section is populated by 9 very similar networks, while the remaining 20 networks are quite different from one another. The consensus network shown in the main text Fig. 1C was generated by summarizing the contents of the networks in the top left corner.

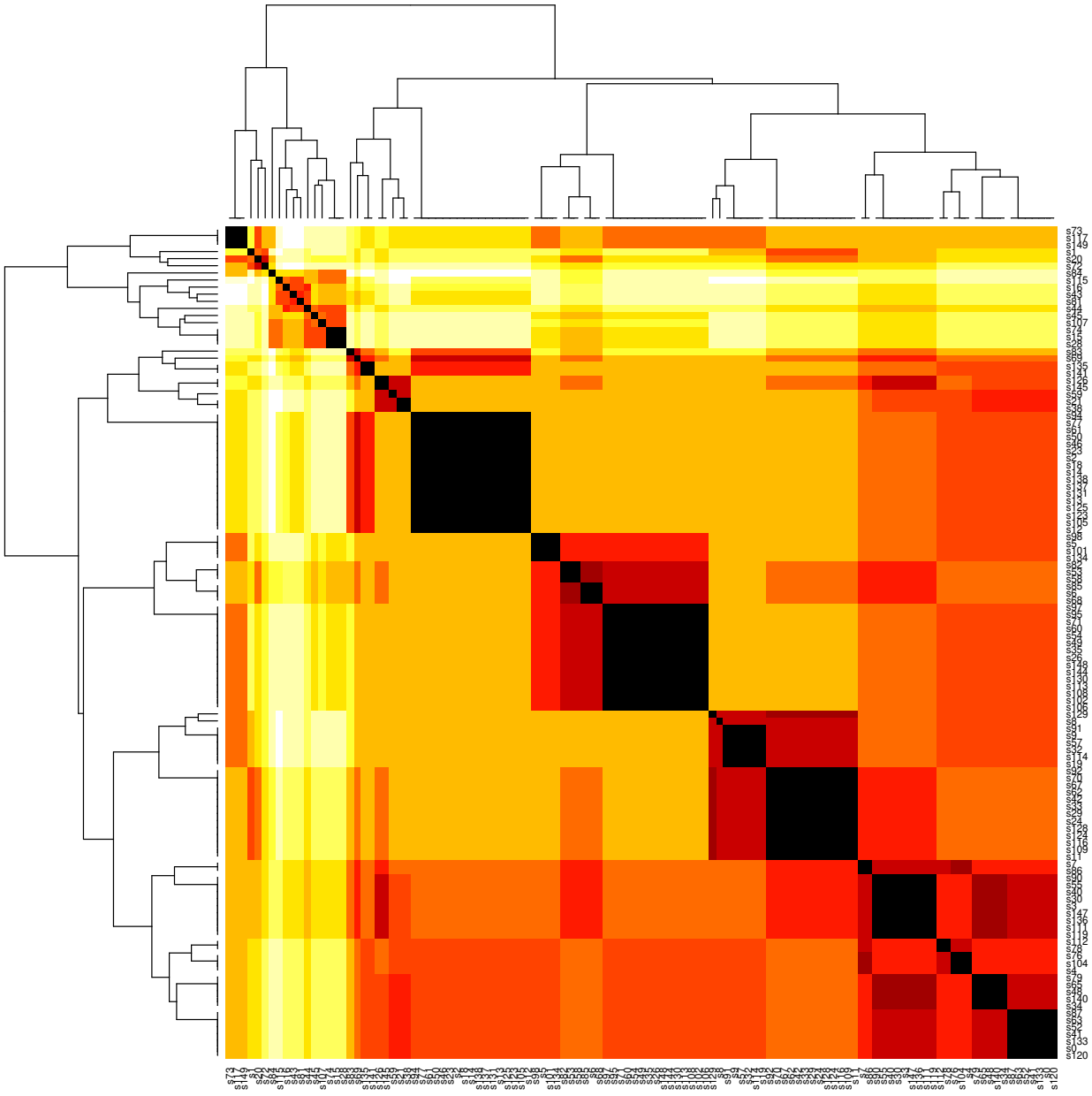

Fig. S56 *erato-sara* clade phylogenetic network clustering.

Format of the matrix is identical to that in Fig. S55. *We identify four well-represented regions of tree space among* erato *clade PhyloNet MCMC_Seq runs.*

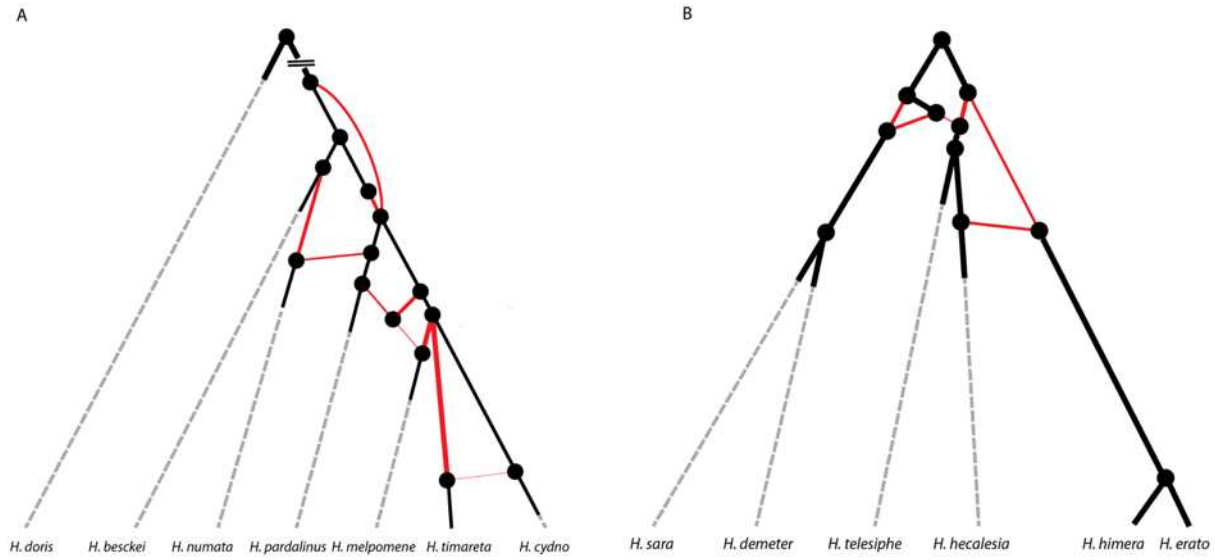

Fig. S57 phylogenetic networks using PhyloNet Infer_Network_MPL.

A. melpomene-*silvaniform clade network.* ***B.*** erato-sara *clade network*

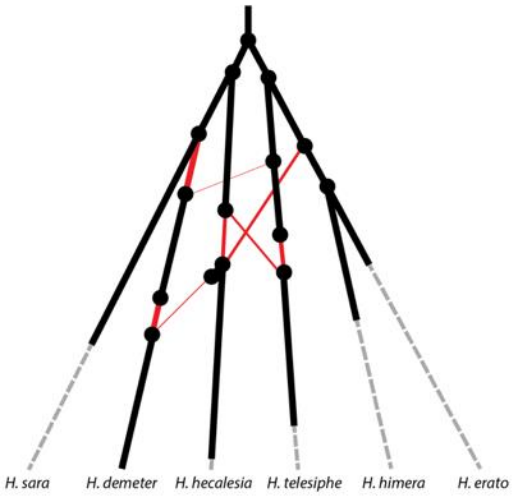

Fig. S58 *erato* clade phylogenetic network using qpGraph

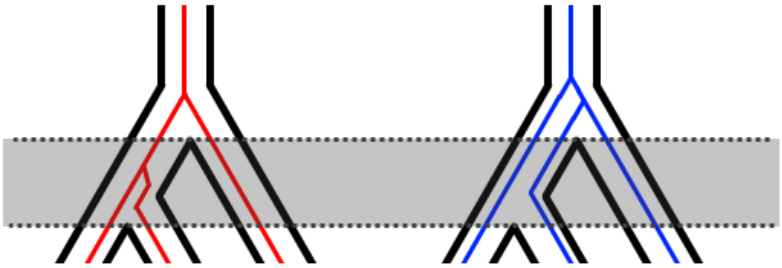

Fig. S59 Coalescent framework

In gene trees matching the species tree topology (left, red), there is an additional window of time in between speciation events (highlighted in grey) where coalescence can occur. However, for non-matching topologies (right, blue) coalescence can only occur in the MRCA.

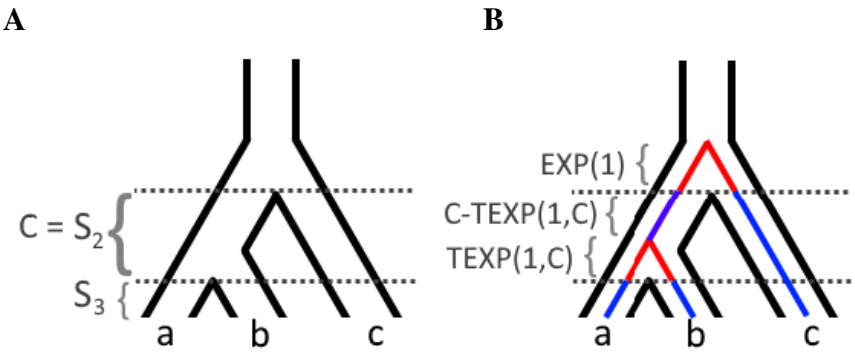

Fig. S60 Branch length components

***A** One sample tree for three species, with the relevant times between speciation events labeled. **B** Given a sample gene tree, we can split the branches into components based on their generating distribution.*

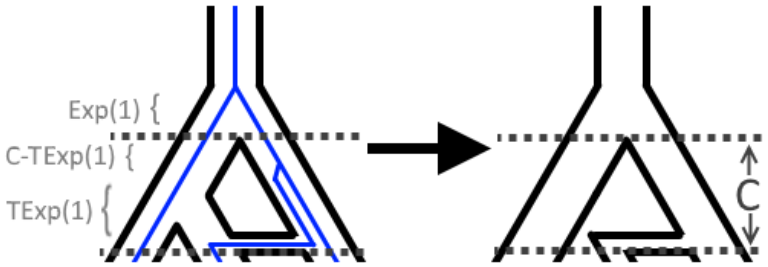

Fig. S61 Branch length components of introgression topologies

If a gene tree follows an introgression path in the species graph, the species history that particular locus experiences can still be described completely as a tree. As a result, the internal branch distribution is of the form EXP(1)+C-TEXP(1;C) . In this case, C is the time from the introgression event back to the common ancestor of all three species. Using the notation in table S13, we have C = S2+S3-H for this example.

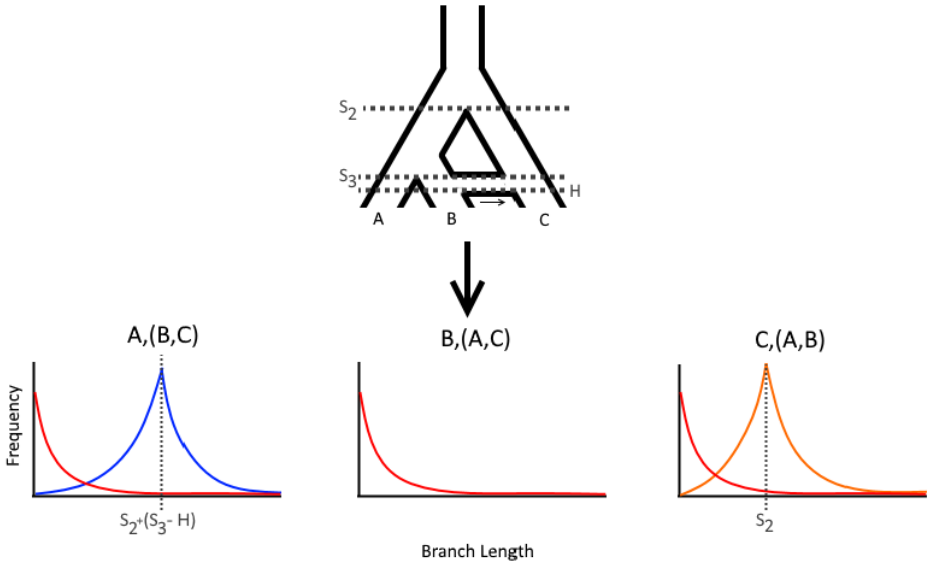

Fig. S62 Expected triplet branch length distributions

A species triplet with an introgression event indicated by the black arrow showing the direction of gene flow backwards in time generates a characteristic branch length distribution. For the topology generated by introgression, ***A, (B,C)*** *, a fraction of gene trees result from introgression (with distribution shown in blue) with* ***C = S2 + (S3 -H)*** *. Similarly for the concordant gene tree topology, a portion of gene trees are generated by speciation with* ***C =S2*** *(shown in orange). In all three topologies, ILS generates trees following an exponential distribution (red).*

Algorithm: Triplet Topology EM

Input: X the set of branch lengths for a given gene tree triplet topology.

$K \leftarrow 2$
$C_1 \leftarrow 0$
$C_2 \leftarrow 1$
$\pi_k \leftarrow 1/K$
$\lambda \leftarrow \bar{x_i}$
$L_1, L_2 \leftarrow 0, |L(\{x_i\}, \{C_k\}, \lambda)|$
while $L_2 - L_1 > 10^{-6} * L_1$ **do**
  $q_{C\lambda}(x_i) \leftarrow \pi_k f(x; C, \lambda) / \Sigma_k^K \pi_k f(x; C, \lambda)$
  $C_2\lambda \leftarrow \text{argmax}_{C\lambda} \Sigma_{i=1}^n q_{C_k}(x_i) ln(f(x; C, \lambda))$ ▷ Find $C\lambda|\lambda$, detailed in 5.1.1
  $\lambda \leftarrow \text{argmax}_{\lambda} \Sigma_{i=1}^n q_{C_k}(x_i) ln(f(x; C, \lambda))$ ▷ Find $\lambda|C\lambda$, detailed in 5.1.2
  $\pi_k \leftarrow mean_{x_i}(q_{C_k\lambda}(x_i))$ ▷ Update proportions to the mean of the soft assignments
  $L_1 \leftarrow L_2$
  $L_2 \leftarrow |L(\{x_i\}, \{C_k\}, \lambda)|$
end
return $C_2, \lambda, \{\pi_k\}$

Fig. S63 Branch length test EM algorithm

Our expectation maximization implementation for inferring the mixture components of a triplet gene tree branch length distributions. Sections refer to sub-sections of supplemental information section 7.

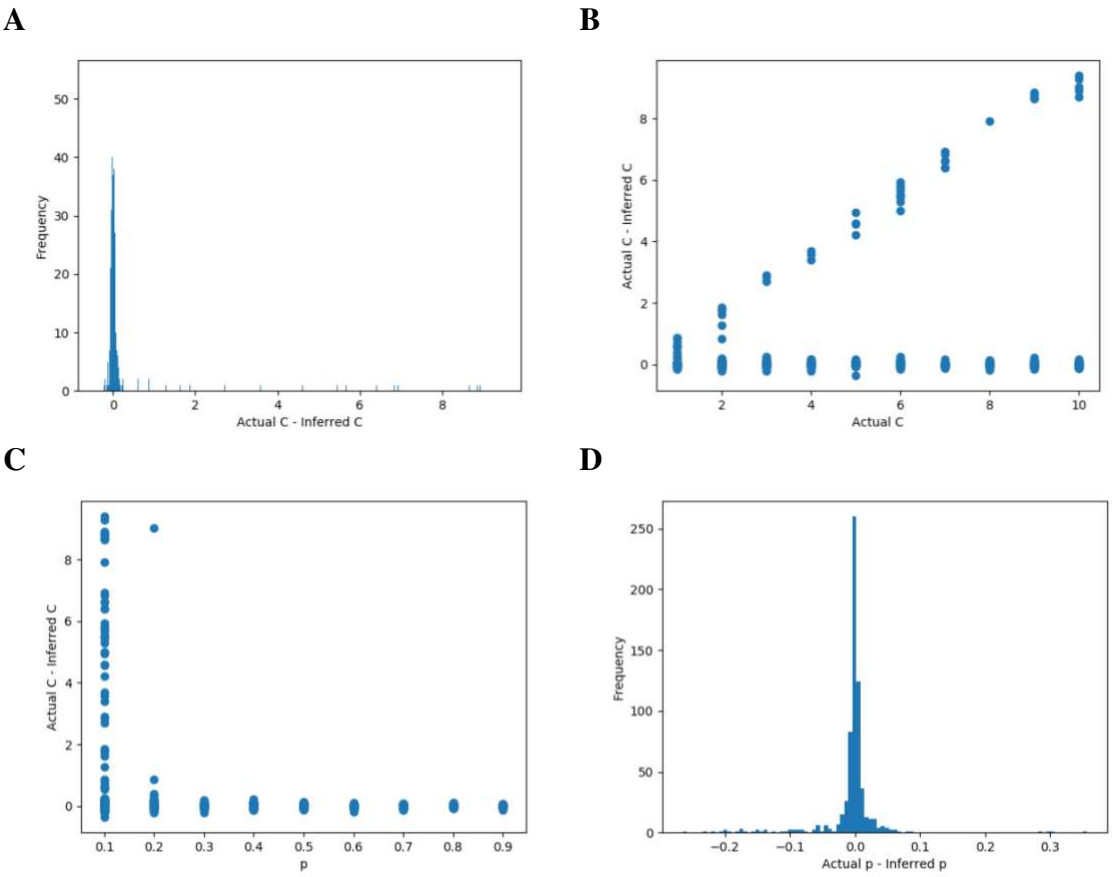

Fig. S64 Tree simulation results

Set of plots describing the behavior of the error in parameter estimates for a set of 650 coalescent trees each for 90 parameter combinations with 10 replicates each. ***A*** *Plot of the error in the estimate of the C.* ***B*** *Errors demonstrating the lack of false positives in C estimates.* ***C*** *Error in C as a function of mixing proportion, showing the error is due to a detection threshold.* ***D*** *Plot of the error in the estimate of the mixing proportion of the non-exponential distribution,* ***p****.*

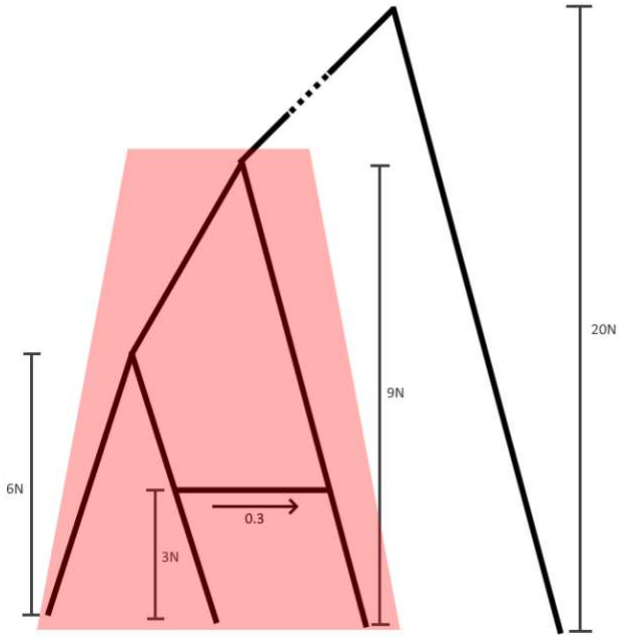

Fig. S65 Sequence simulation demographic model

The demographic model used for the coalescent simulations to test the noise in sequence generation alone, with the triplet of interest highlighted in red. This model was used for simulations generating the results of Fig. S66*. We used N = 1E6, and a probability of following the introgression branch of 0. 3, with direction of gene flow backwards in time shown by the arrow. For the discordant introgression topology, this corresponds to 78.3% of loci resulting from introgression, with a C-value of 3.*

A **B**

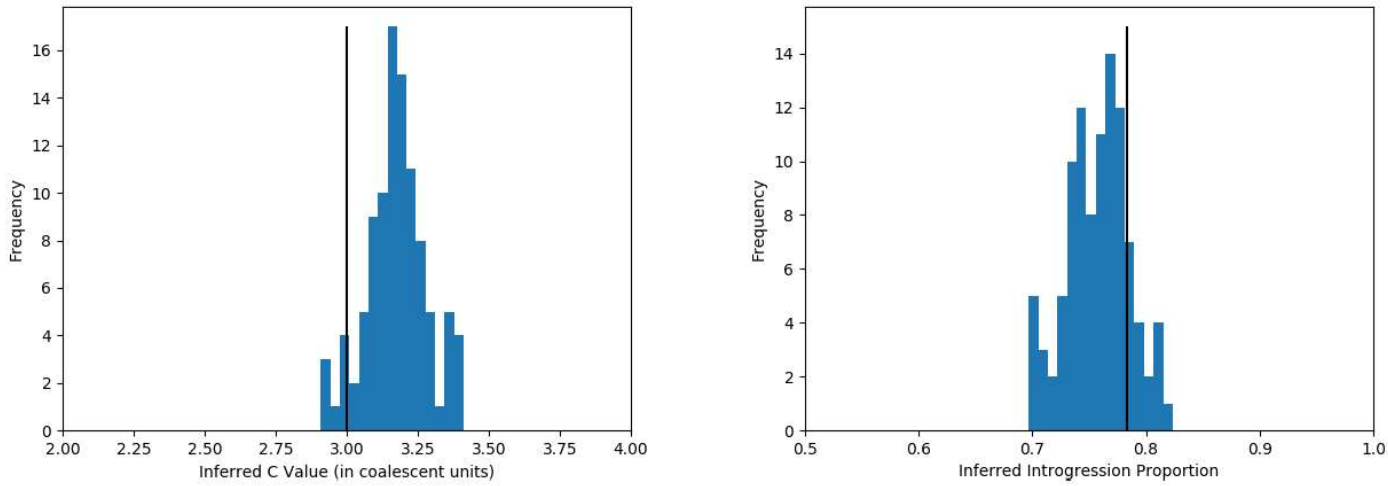

Fig. S66 Sequence simulation results

The estimates of C and p for the introgression distribution from 100 replicates of sequence simulations using the same underlying set of true gene genealogies at 1000 loci. The true values are indicated by the vertical black line. Slight inflation in C causes an underestimate of the introgression probability. ***A*** *Estimated C values.* ***B*** *Estimated introgression probabilities.*

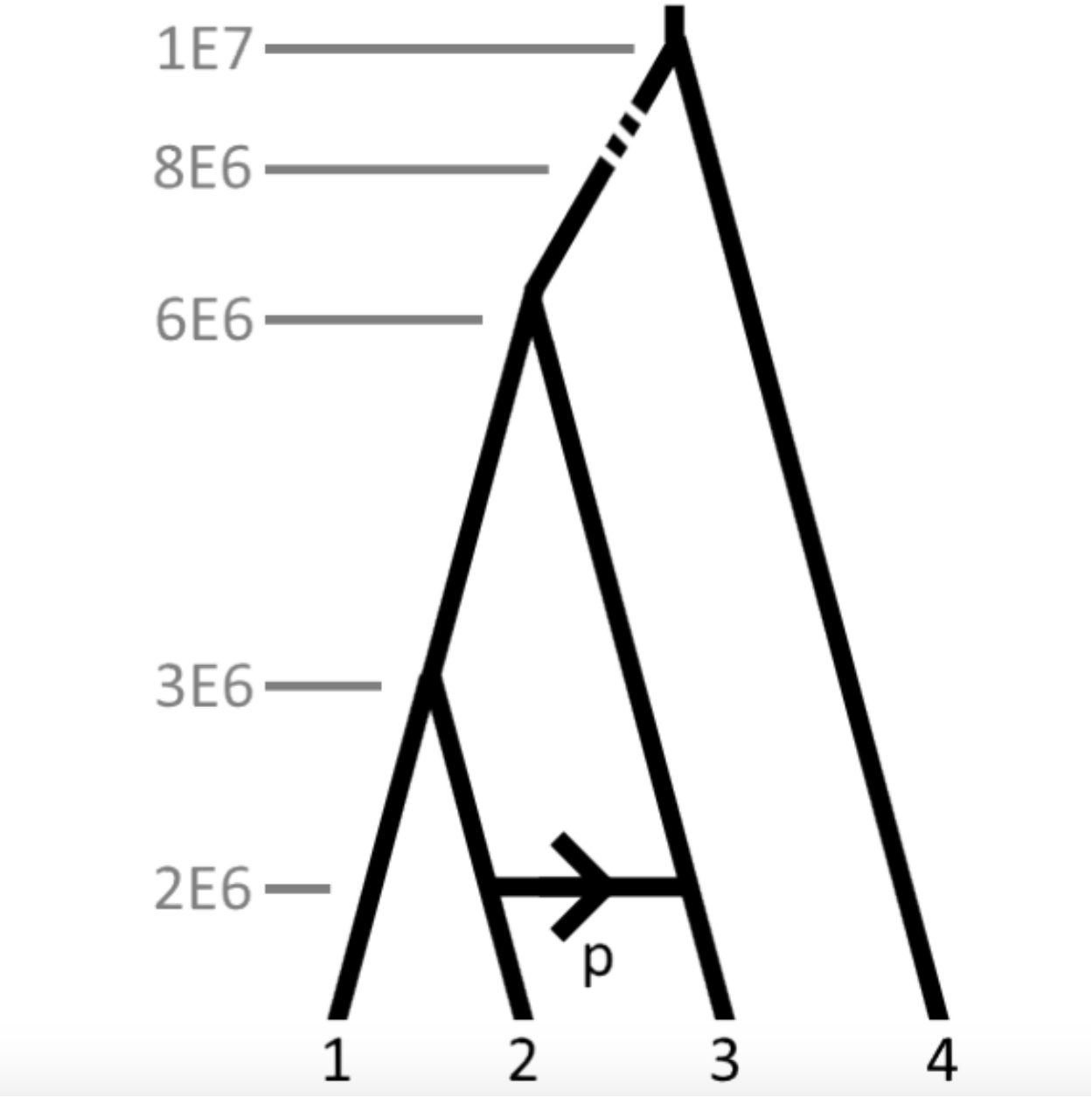

Fig. S67 Null demographic model used for simulations of demographic effects

This model was used in simulations to generate Fig. S68-S69 and Fig. S74-Fig. S75. *The arrow shows the direction of introgression backwards in time. All time units are listed in generations.*

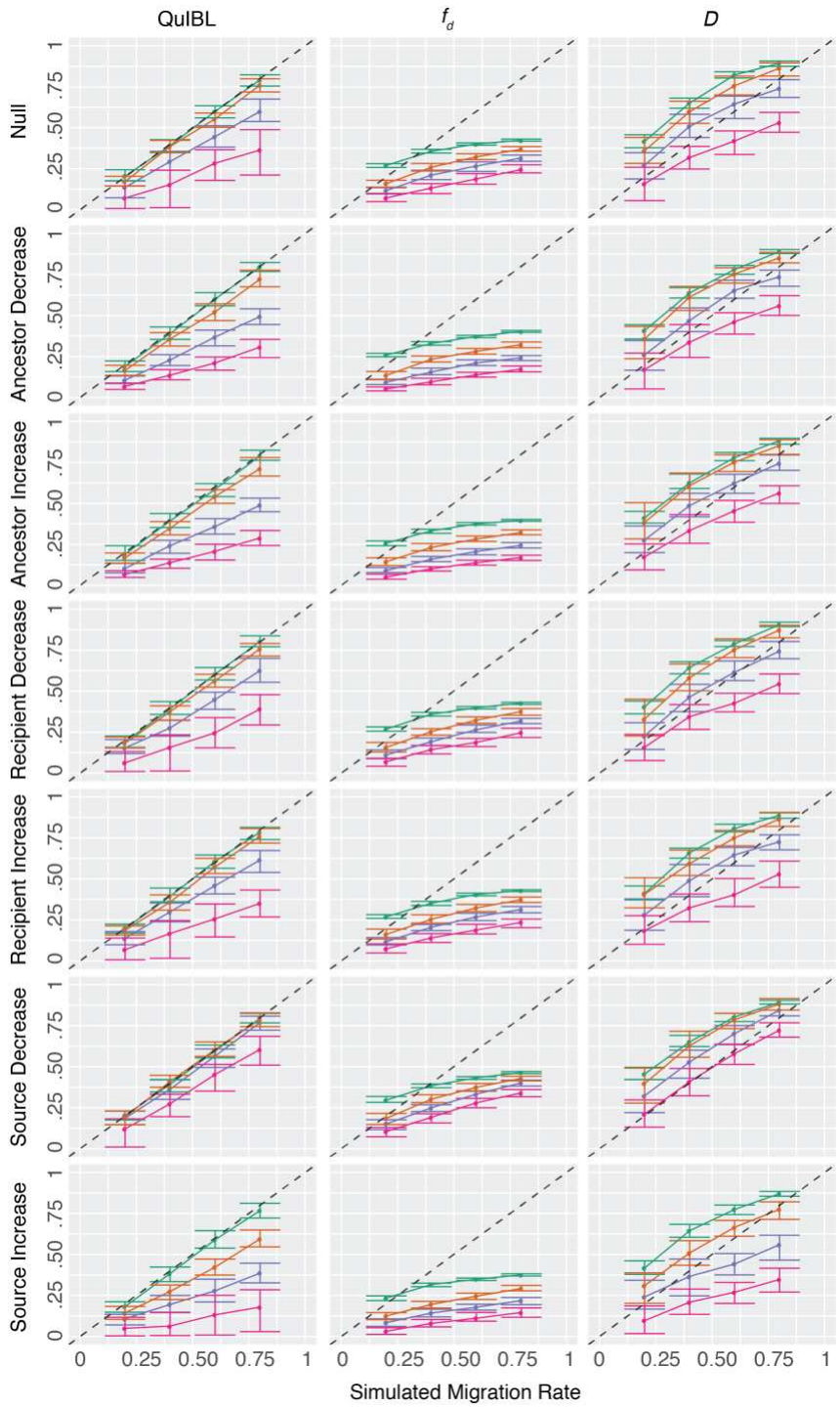

Fig. S68 Effects of changing demography

Each row represents a different demographic scenario. The null model is as described in Fig. S65. *Each "increase" represents a multiplication of population size by a factor of 2 for the relevant branch, and each "decrease" represents a halving of population size for the relevant branch. Base population sizes are represented by colors. Green: 250,000; Orange: 500,000; Blue: 1,000,000; Magenta: 2,000,000*

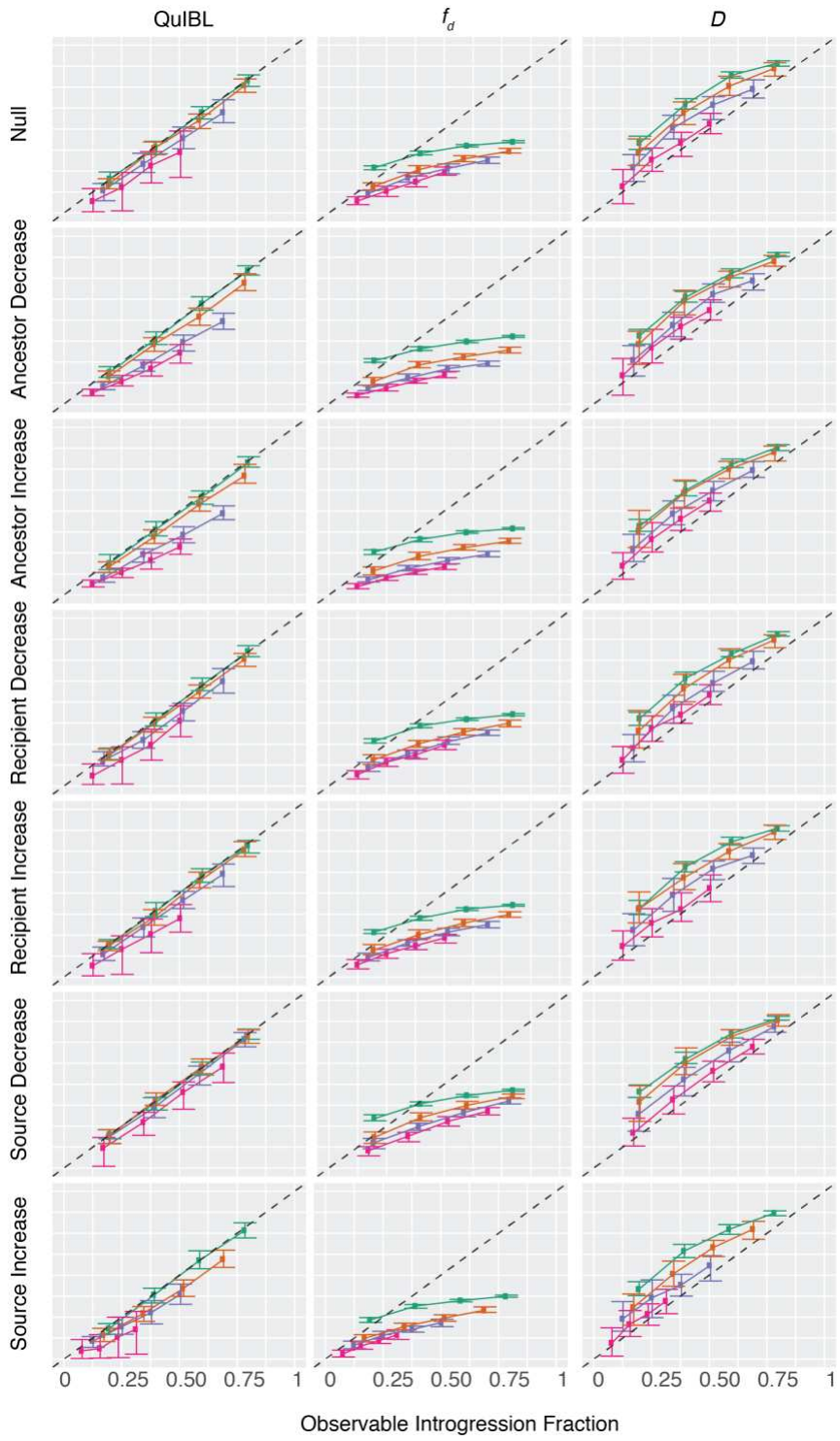

Fig. S69 Effects of changing demography; observable introgression fraction

Demographic scenarios are as in Fig. S68. *The x-axis here represents the observable introgression fraction, or proportion of lineages that experience introgression and do not experience ILS. Base population sizes are represented by colors. Green: 250,000; Orange: 500,000; Blue: 1,000,000; Magenta: 2,000,000*

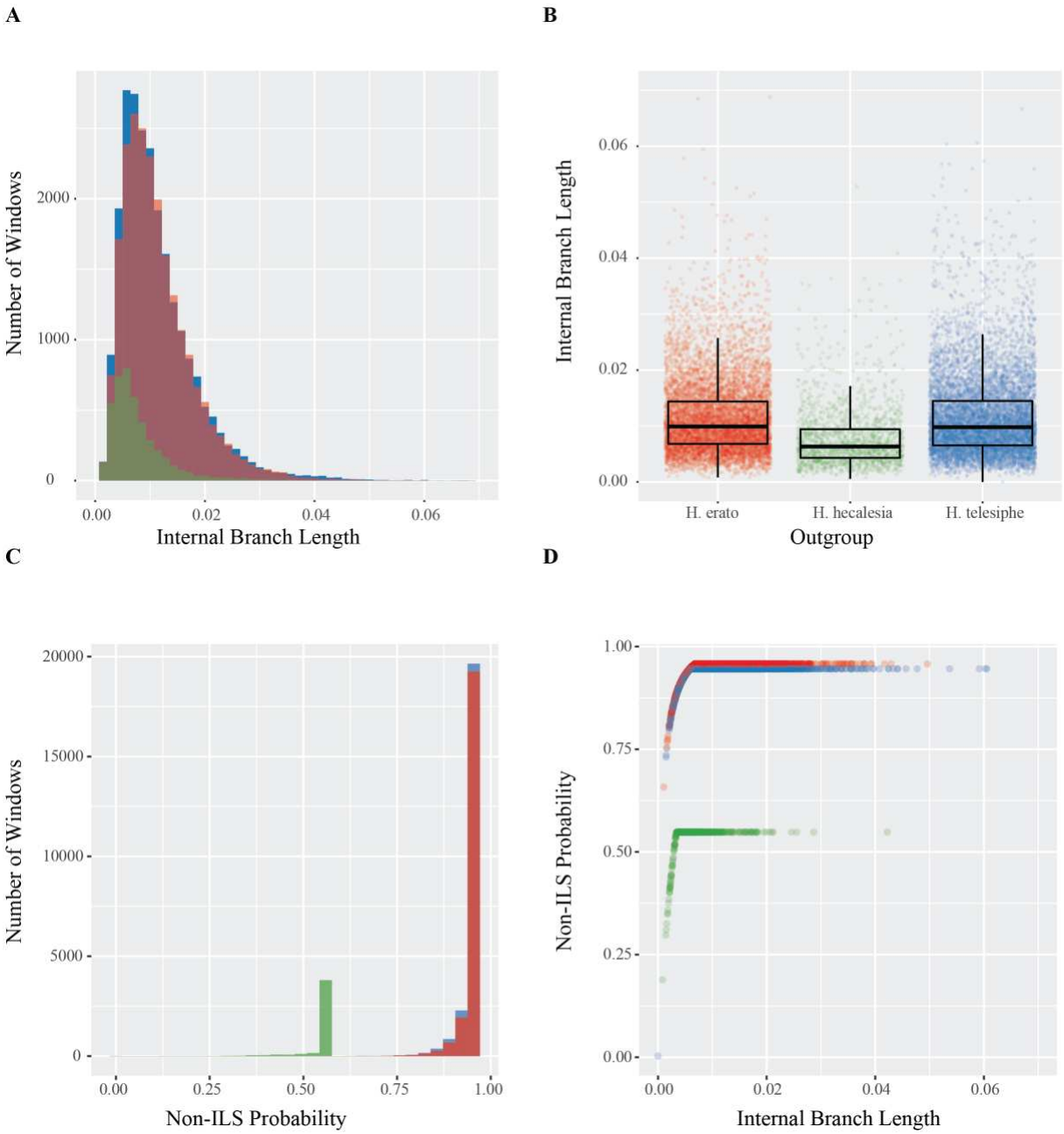

Fig. S70 Representative branch length test

This figure shows the input and output for the internal branch length test with the triplet H. erato + H. hecalesia + H. telesiphe. ***A*** *Distribution of internal branch lengths, colored by topology. In all panels, blue represents the topology* where H. telesiphe *is the outgroup (concordant with species tree), red is* H. erato *as outgroup (consistent with introgression between* H. telesiphe *and* H. hecalesia *or ILS), and green is* H. hecalesia *as outgroup (consistent with introgression between* H. telesiphe *and* H. erato *or ILS).* ***B*** *Boxplot of internal branch lengths, showing the strongly reduced mean branch length when* H. hecalesia *is the outgroup.* ***C*** *Distribution of non-ILS probability for each topology.* ***D.*** *Relationship between internal branch length and probability of belonging to the non-ILS (speciation or introgression) distribution.*

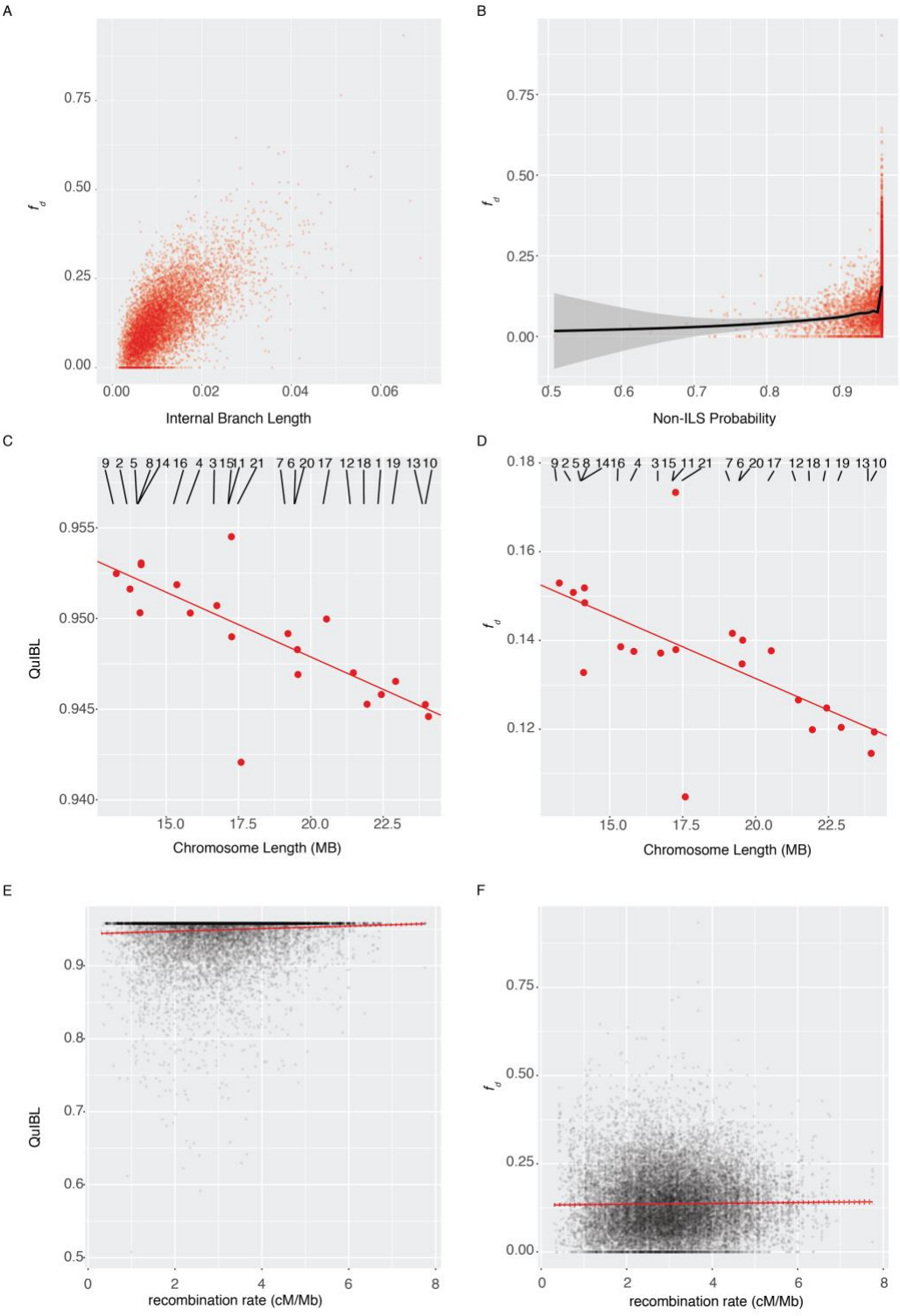

Fig. S71 Comparison of introgression topology branch length test to f_d

All plots use only those windows of the triplet shown in Fig. S70 in which H. erato *is inferred to be the outgroup, consistent with introgression between* H. telesiphe *and* H. hecalesia*.* ***A*** *Internal branch length is strongly, positively correlated with f_d.* ***B*** *Inferred non-ILS probability is correlated with positively correlated with f_d. However, a large proportion of non-ILS probability*

values are equal to the maximum value, in this case 0.96. ***C*** *shows the correlation between chromosome length and non-ILS probability, while* ***D*** *shows the correlation between chromosome length and* f_d*. Both metrics are significantly correlated with chromosome length, but the correlation non-ILS probability is stronger (see Section 8).* ***E*** *shows the correlation between local recombination rate and non-ILS probability, while* ***D*** *shows the correlation between local recombination rate and* f_d*. Both metrics are significantly correlated with local recombination rate, but the correlation non-ILS probability is again stronger (see Section 8).*

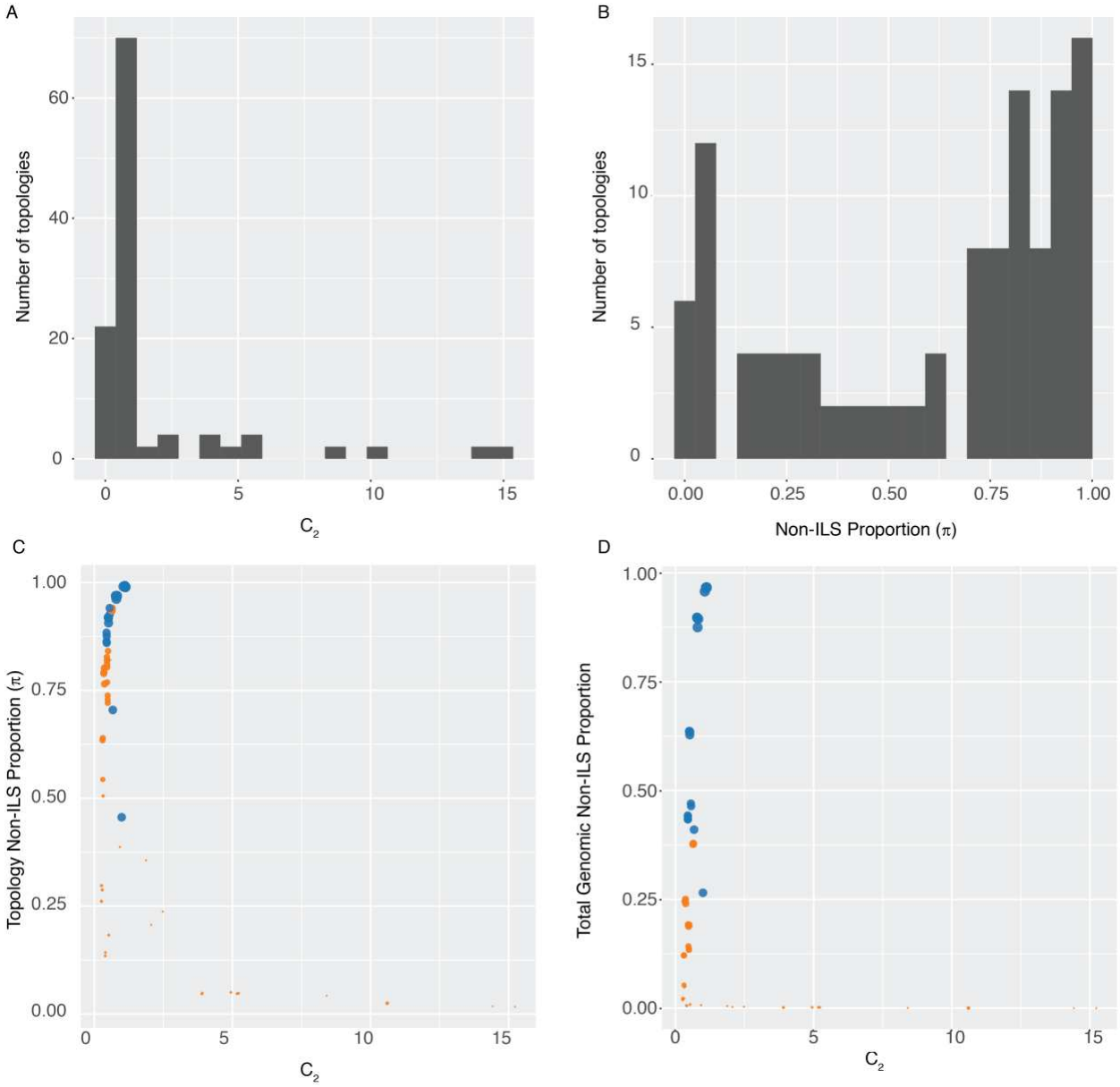

Fig. S72 Branch length test, all *erato* clade triplets

A. *Distribution of inferred internal branch lengths. X-axis is in coalescent units ($2N_e$).* ***B***. *Distribution of inferred non-ILS proportion. This represents either speciation branches or introgression branches.* ***C*** *Relationship between internal branch length (C_2) and non-ILS proportion of each topology. Size of each point corresponds to the proportion of trees in the respective triplet that recover the topology. Circles represent topologies significant for a non-ILS component, and diamonds represent those that are not significant. Blue triplets are concordant with the species tree.* ***D*** *Relationship between internal branch length (C_2) and proportion of non-ILS trees of each topology present in the genome. This value was obtained by multiplying the probability that each topology corresponds to introgression by its genomic frequency.*

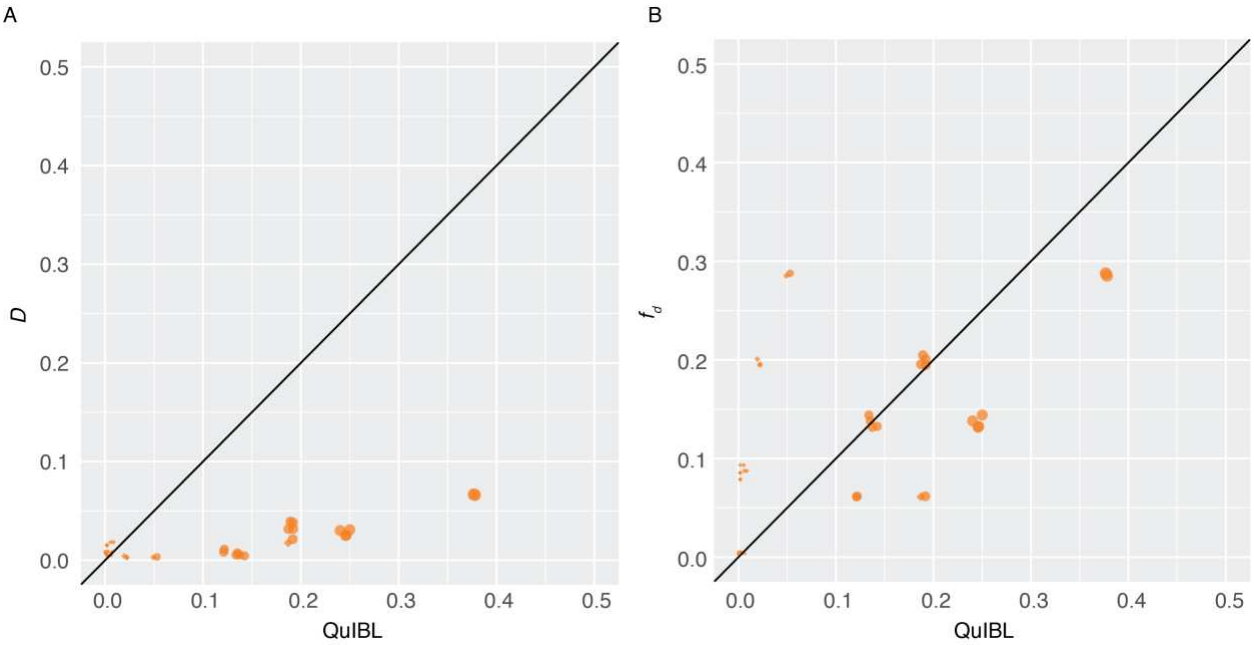

Fig. S73 All topologies, comparison of branch length test to *D* and f_d

Comparison of all concordant erato *clade triplet topologies non-ILS proportions to* ***A*** *the absolute value of the mean D statistic and* ***B*** *the mean value of* f_d. *Size, shape, and color of points are as in Fig. S72 C and D.*

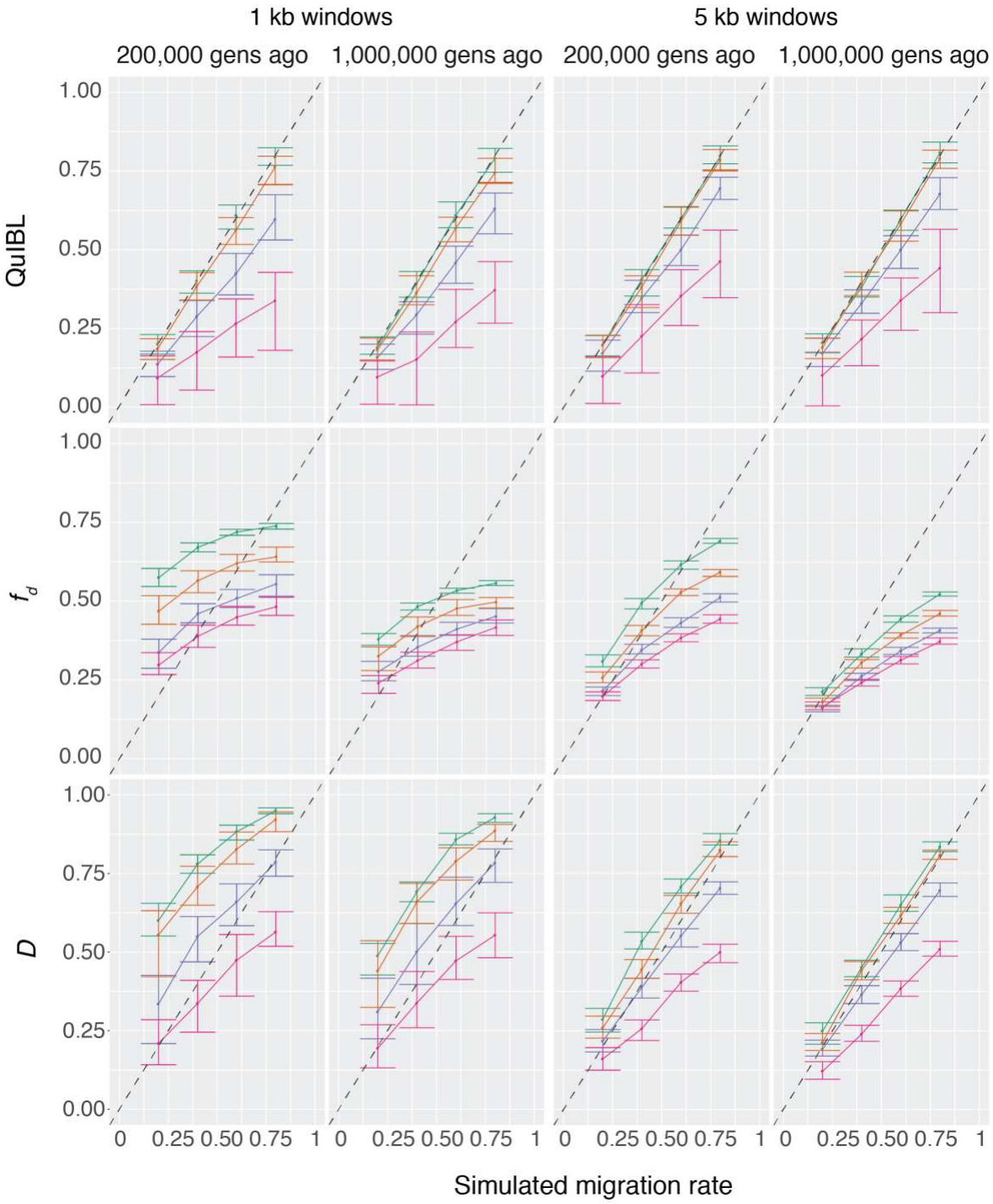

Fig. S74 Effects of timing of introgression on migration rate estimation

Backbone tree is as in Fig. S67. *Introgression occurs either 200,000 generations in the past or 1,000,000 generation in the past. Window sizes of 1 kb or 5kb demonstrate the effect of noise in the inference. In these simulations, there is no recombination. Population sizes are represented by colors. Green: 250,000; Orange: 500,000; Blue: 1,000,000; Magenta: 2,000,000*

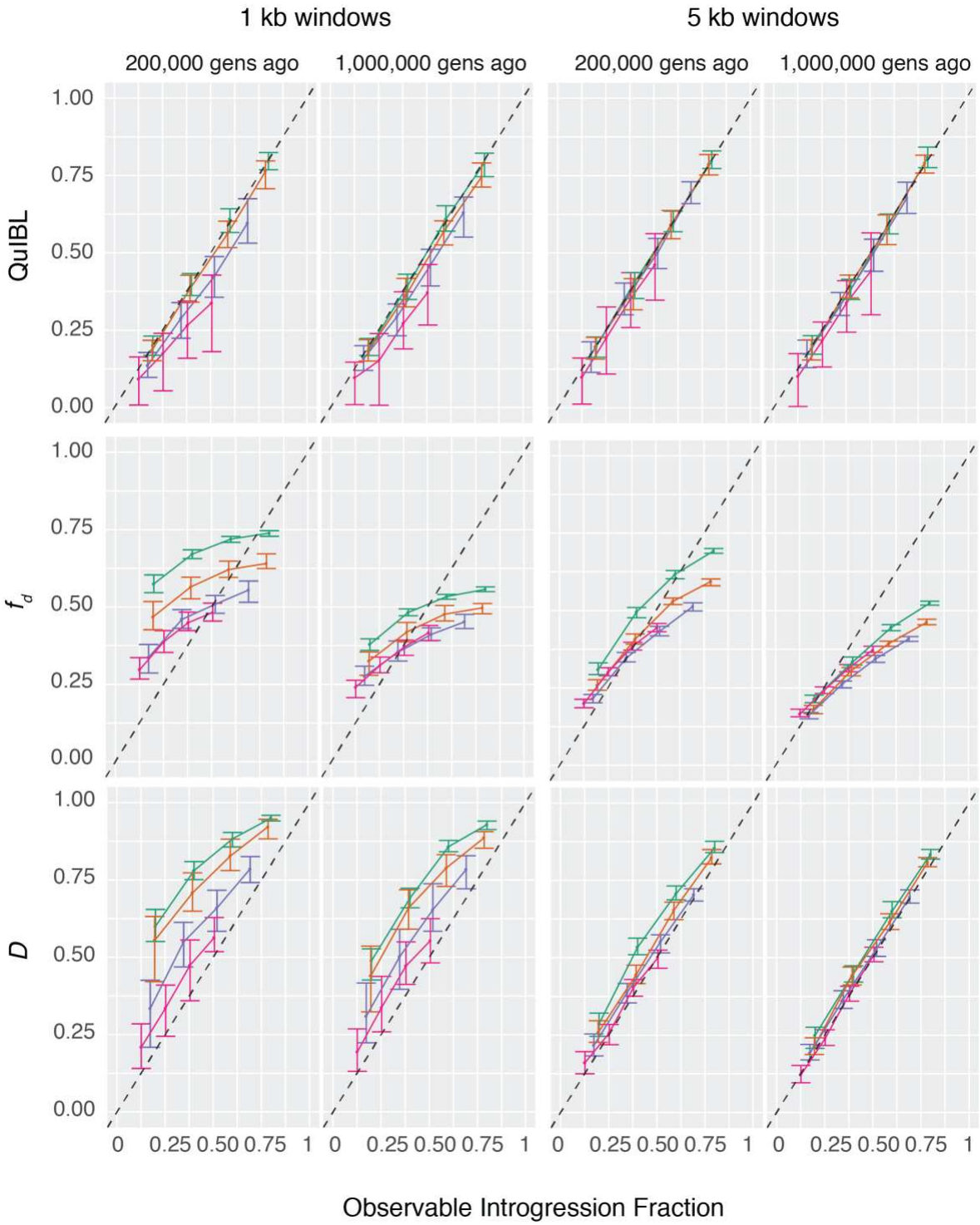

Fig. S75 Effects of introgression timing on observable introgression fraction estimation

See Fig. S74 *above. Here, inferred statistics are compared to observable introgression fraction. Population sizes are represented by colors. Green: 250,000; Orange: 500,000; Blue: 1,000,000; Magenta: 2,000,000*

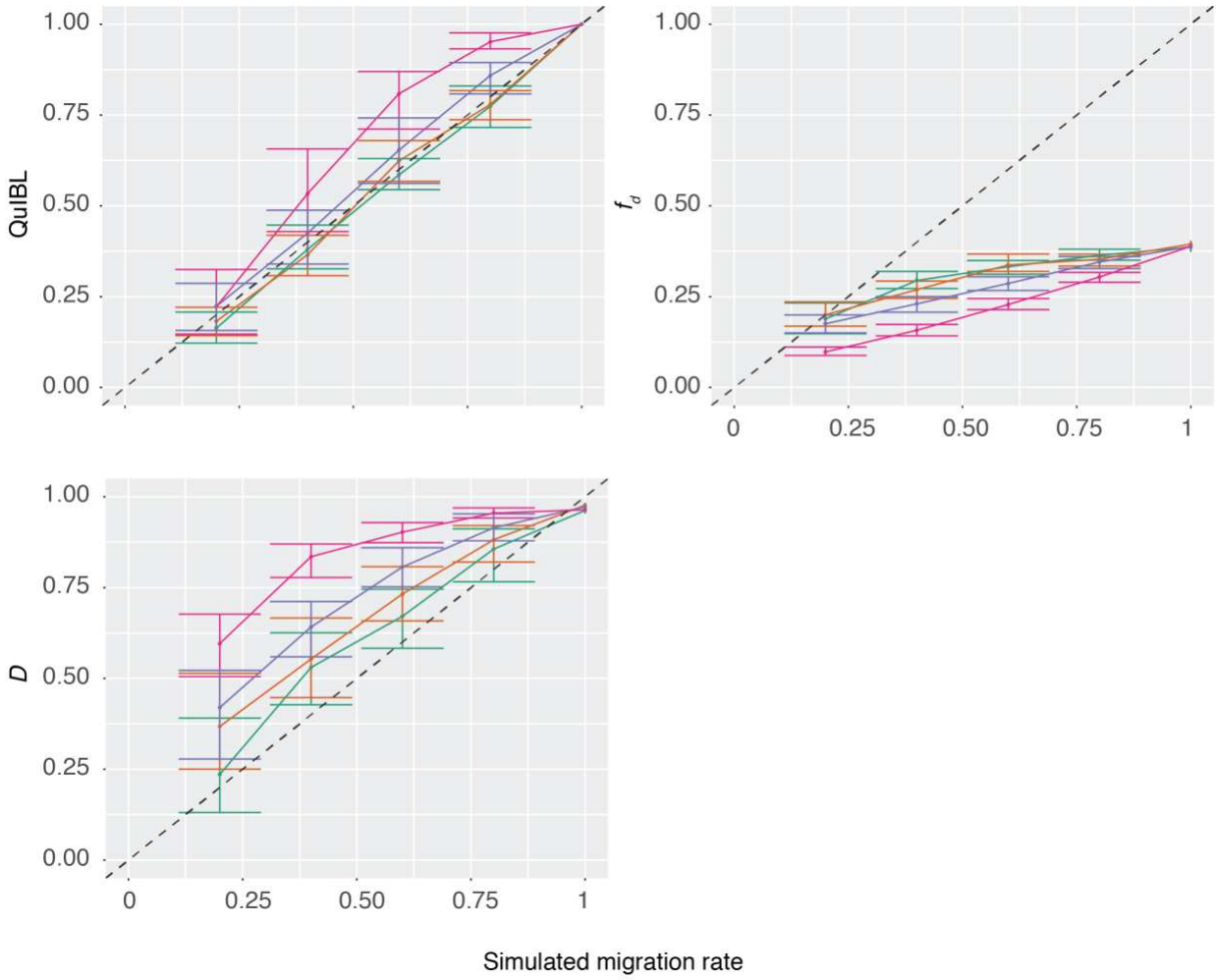

Fig. S76 Effects of recombination

Here, branch lengths correspond to estimates of divergence times for H. erato, H. hecalesia, H. telesiphe, *and* H. melpomene, *calculated from 5 kb windows. Values for introgression time is 0.5* time since divergence of* H. erato *and* H. hecalesia*, estimated as 4.5 million years. Population size is estimated at 500,000. Per-base pair recombination rate, r, is varied as a fraction of mutation rate, μ, and indicated by colors – Green: r= μ *.01; Orange: μ *.1; Blue: r= μ ; Magenta: r= μ*10*

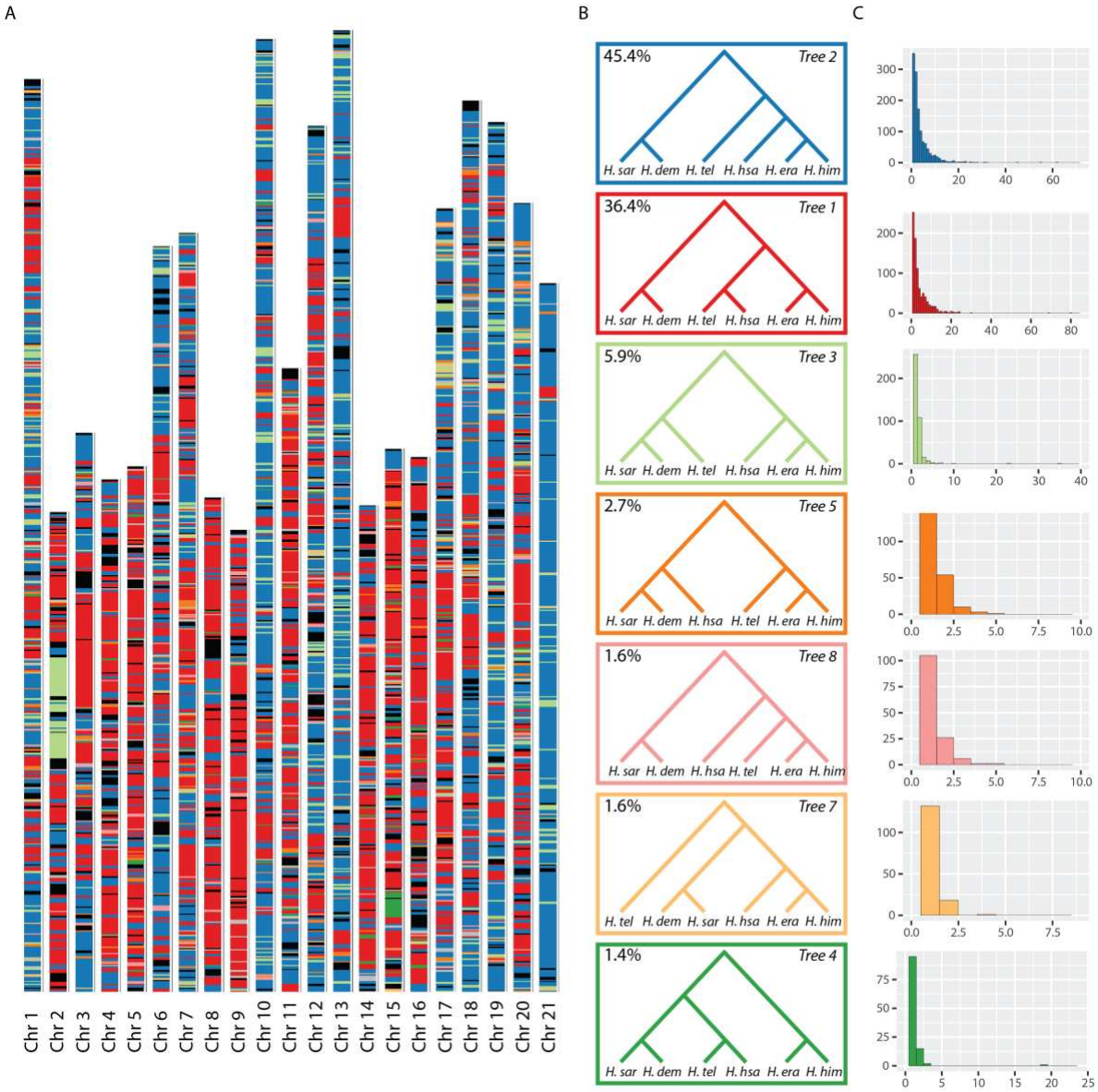

Fig. S77 Heterogeneity of *erato-sara* clade evolutionary history across the *H. melpomene* genome

A. Distribution of topologies across the genome. *For each 50 kb window, the colored bar represents the topology recovered from that region. Colors correspond to topologies in* ***B.*** *Coordinates are in terms of the* H. melpomene *Hmel2.5 reference, and topologies for all windows were reconstructed with PhyML. Black regions are missing data.* ***B. Common topologies.*** *The eight most common phylogenies are shown. The value in the top left corner of each topology is the percentage of all 50 kb windows that recovers that topology. The tree labels correspond to those in the main text Fig. 2B* ***C. Tree block length distribution*** *Each histogram corresponds to the topology of the same color in* ***B*** *and shows the distribution of the number of consecutive 50 kb windows that recover that topology.*

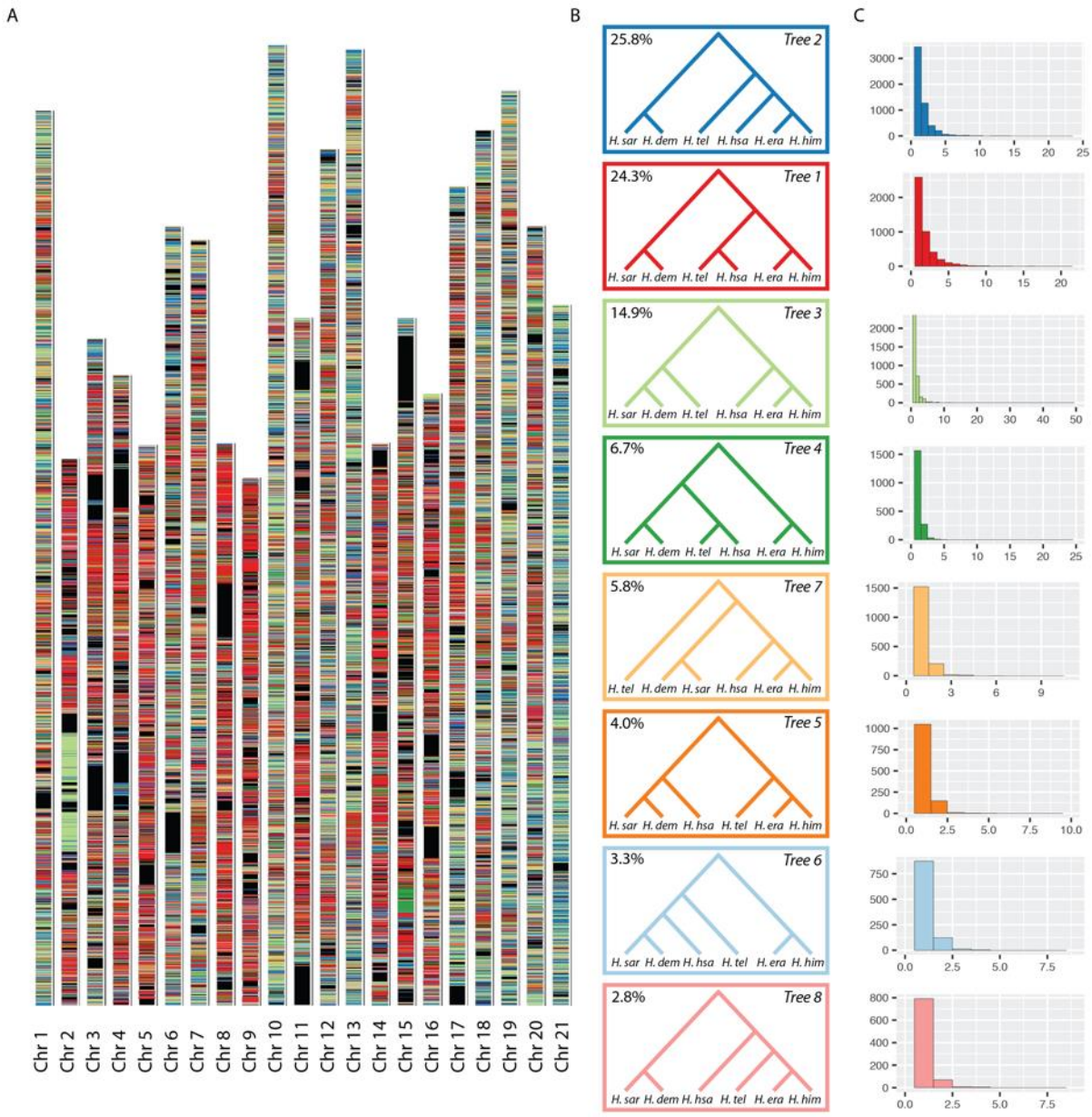

Fig. S78 Heterogeneity of evolutionary history across the *erato* genome, 10 kb windows

For each 10 kb window, the colored bar represents the topology recovered from that region. Colors correspond to topologies in B. Coordinates are in terms of the H. erato demophoon *v1 reference, and topologies for all windows were constructed with PhyML. Black regions are missing data. B. Common topologies. The eight most common phylogenies are shown. The value in the top left corner of each topology is the percentage of all 10 kb windows that recover that topology. The tree labels correspond to those in the main text Fig. 2B. C. Tree block length distribution. Each histogram corresponds to the topology of the same color in B and shows the distribution of the number of consecutive 10 kb windows that recover that topology.*

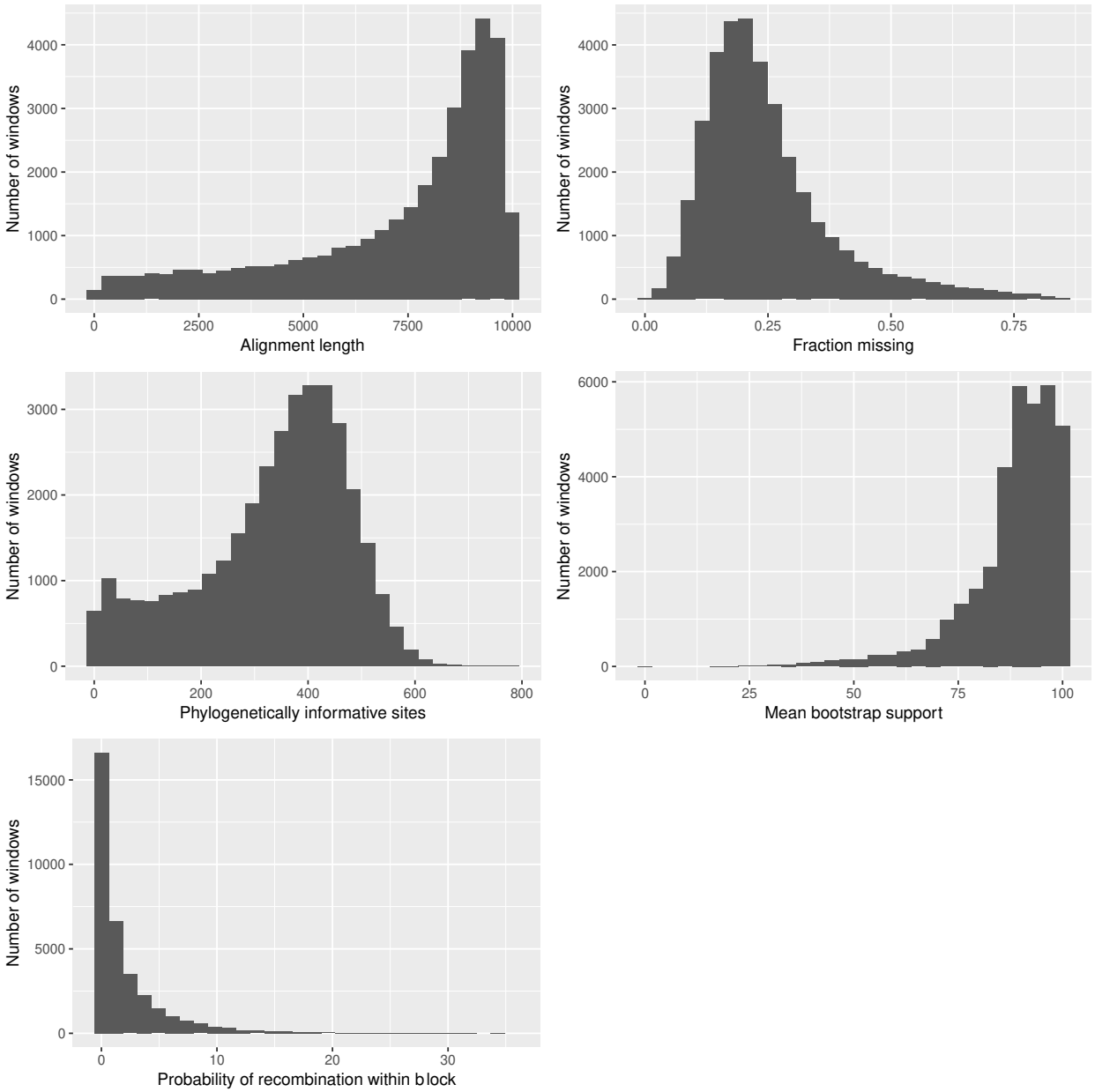

Fig. S79 Basic alignment statistics

Distributions of basic alignment statistics are shown for 10 kb windows of erato *clade alignments. Only windows with Alignment length >2000 bp were included. Statistics are as defined in* Fig. S24

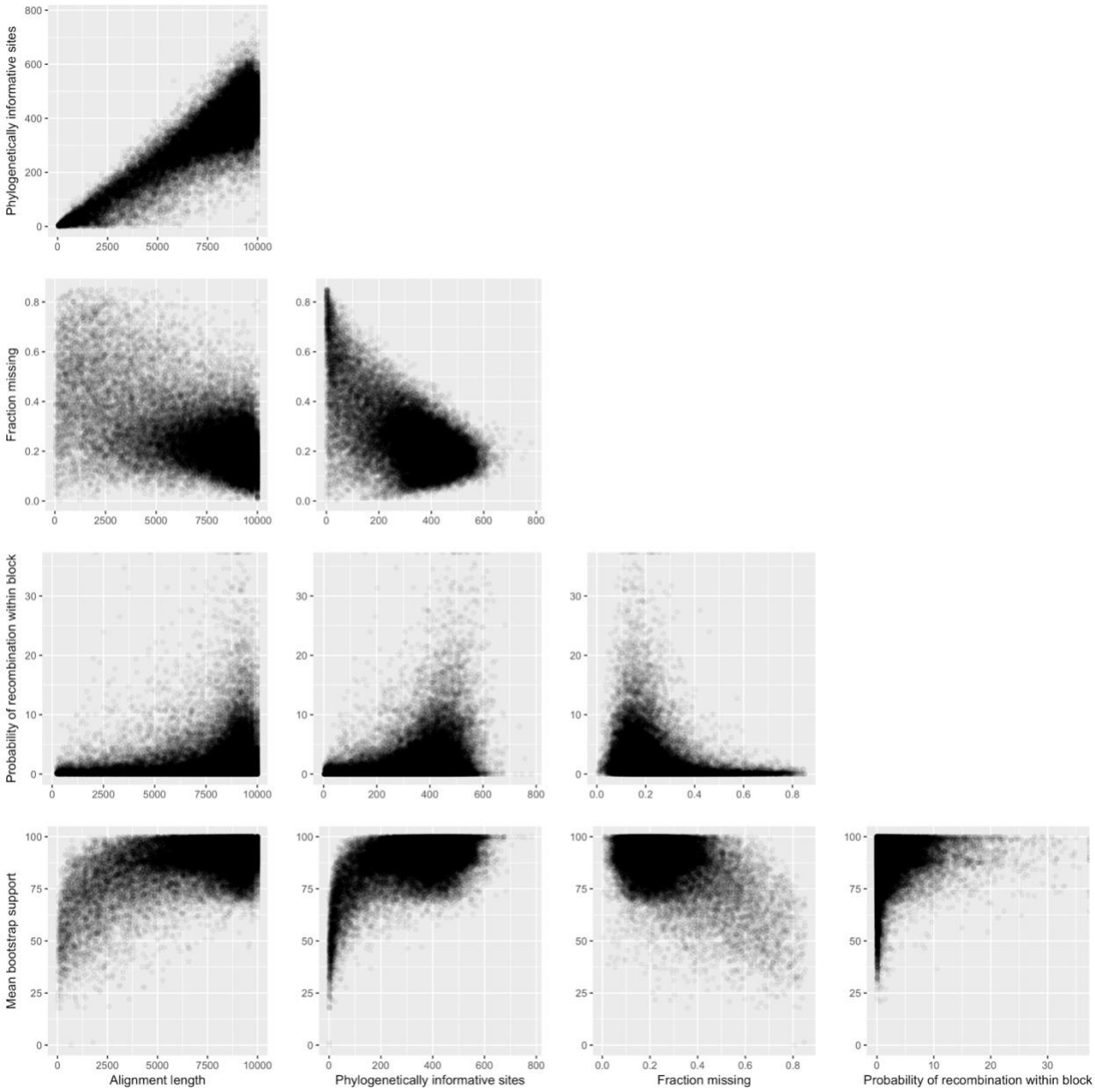

Fig. S80 Correlation between statistics

Pairwise correlations between all statistics shown in Fig. S79

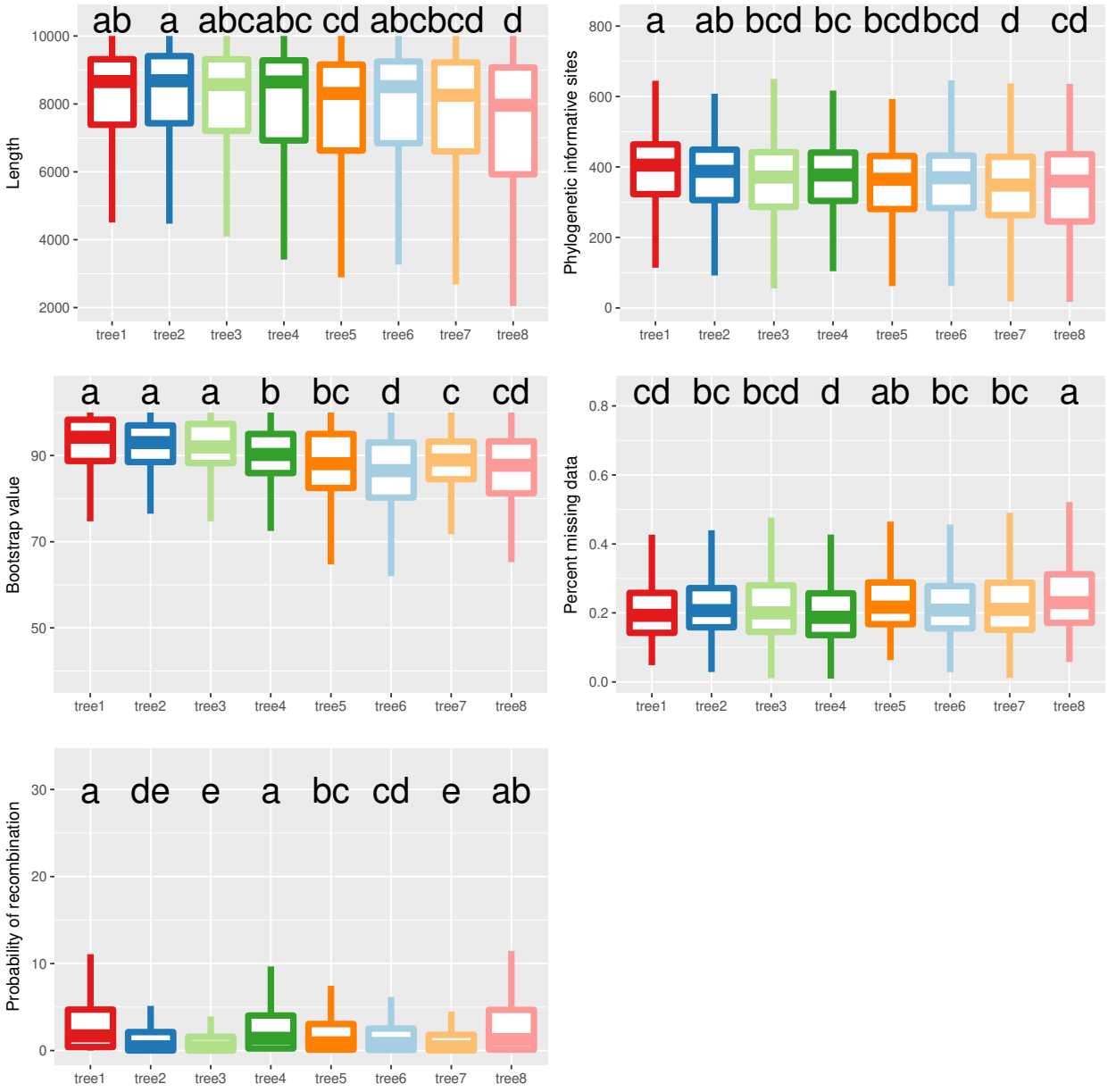

Fig. S81 Alignment statistics by tree topology

Windows were subsampled from each topology to that the number of windows from each was equal. Letters above bars indicate significance based on a Kruskal-Wallace test, using a Bonferroni correction for multiple comparisons. Statistics are as defined in Fig. S24

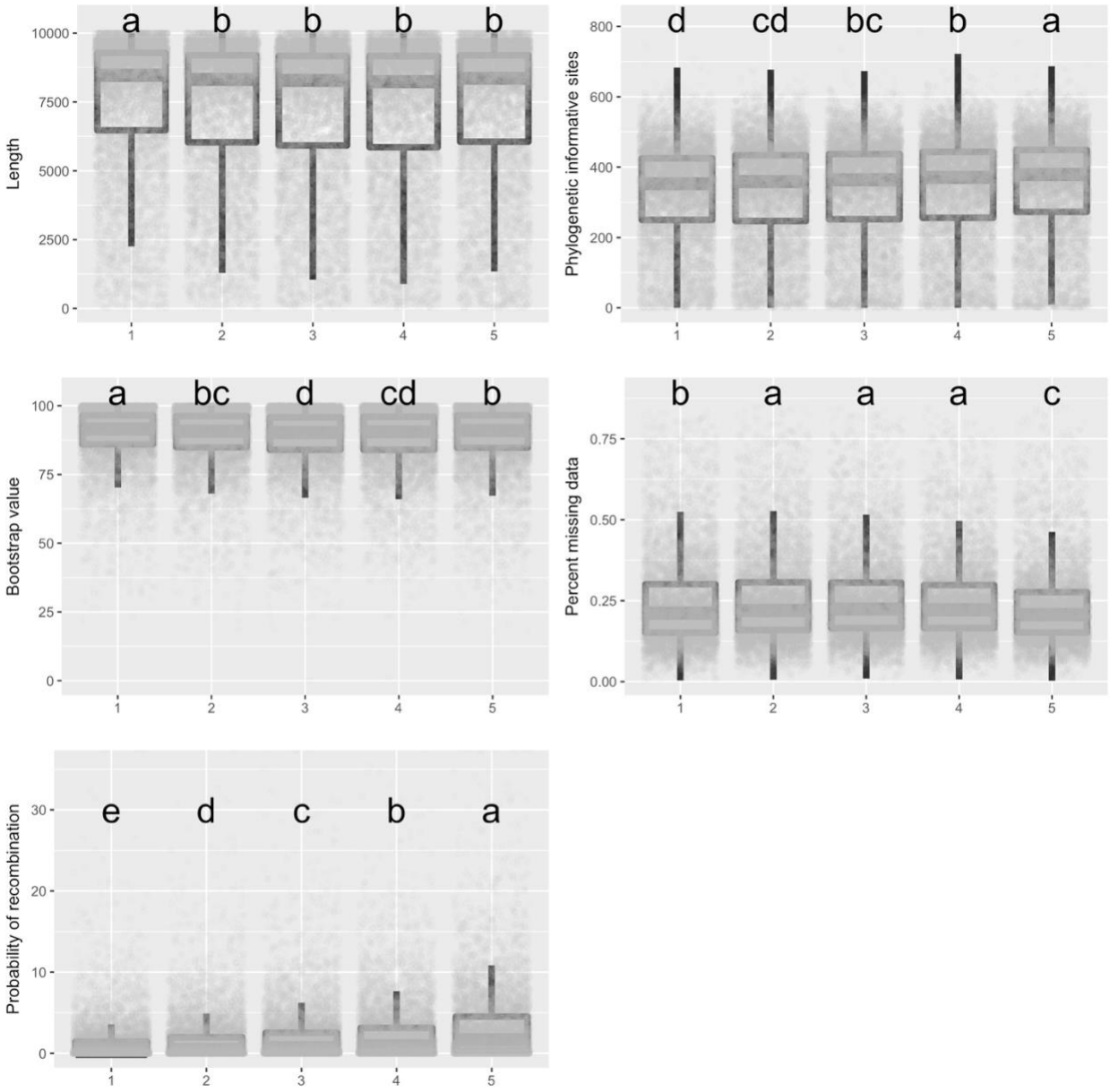

Fig. S82 Alignment statistics by recombination rate quintile

Letters above bars indicate significance based on a Kruskal-Wallace test, using a Bonferroni correction for multiple comparisons. Statistics are as defined in Fig. S24

Fig. S83 Relationship of recombination rate to number of coding base pairs per window

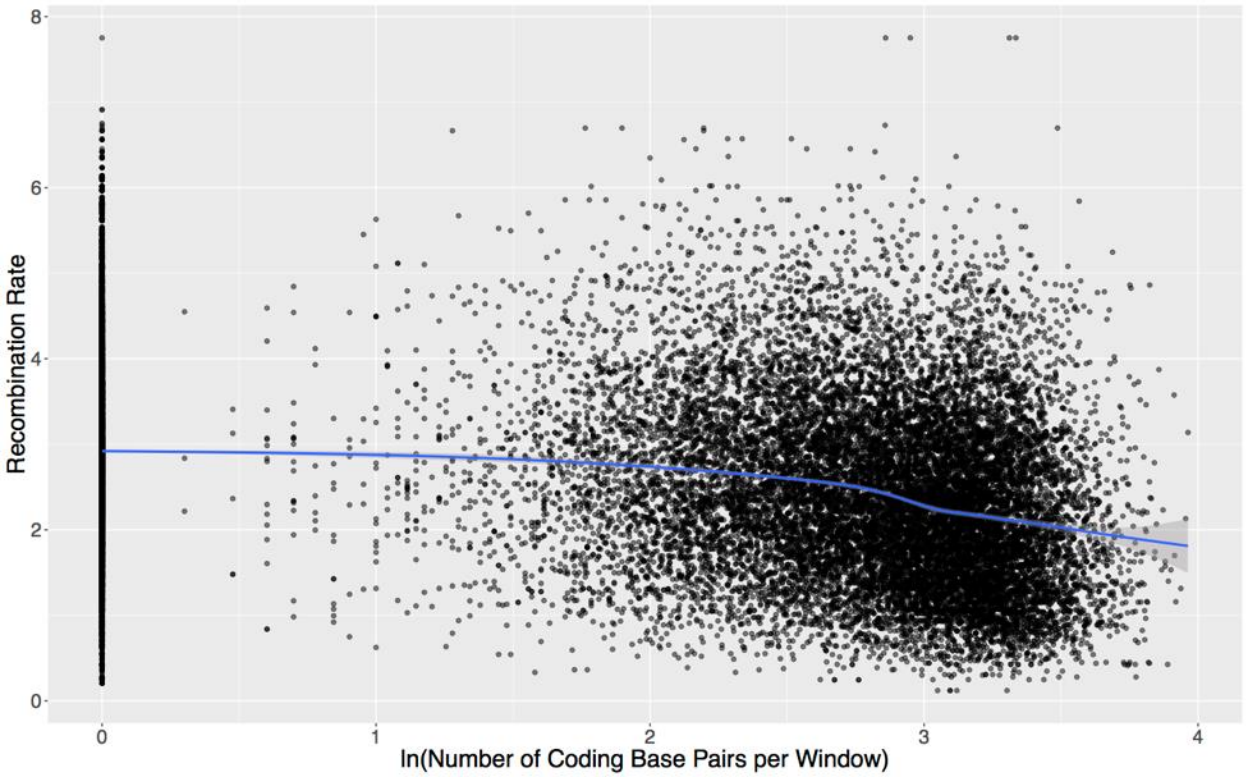

Fig. S84 Relationship of recombination rate to log number of coding base pairs per window

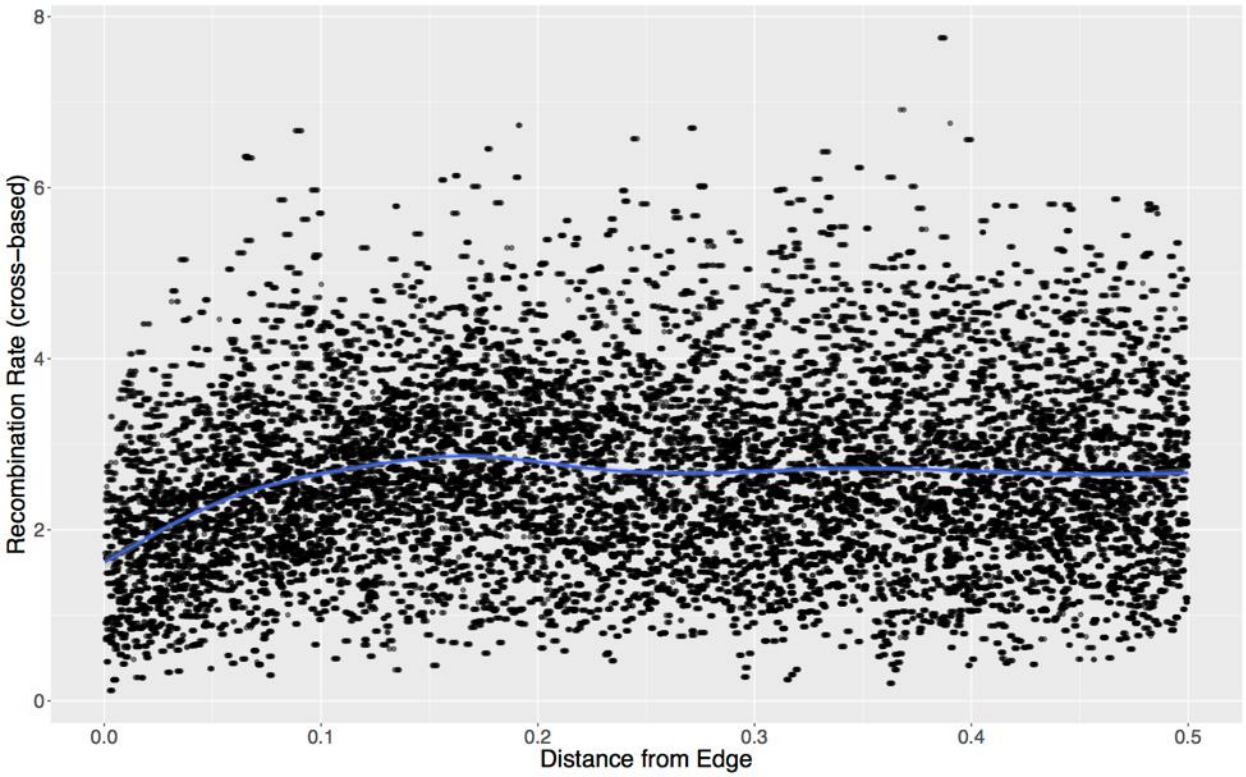

Fig. S85 Relationship of chromosomal position to recombination rate in *H. erato*

Local recombination rates for the H. erato demophoon *genome were calculated in 50 kb windows. Because topologies in this study were reconstructed in 10 kb windows, adjacent windows often share the same recombination rate estimate.*

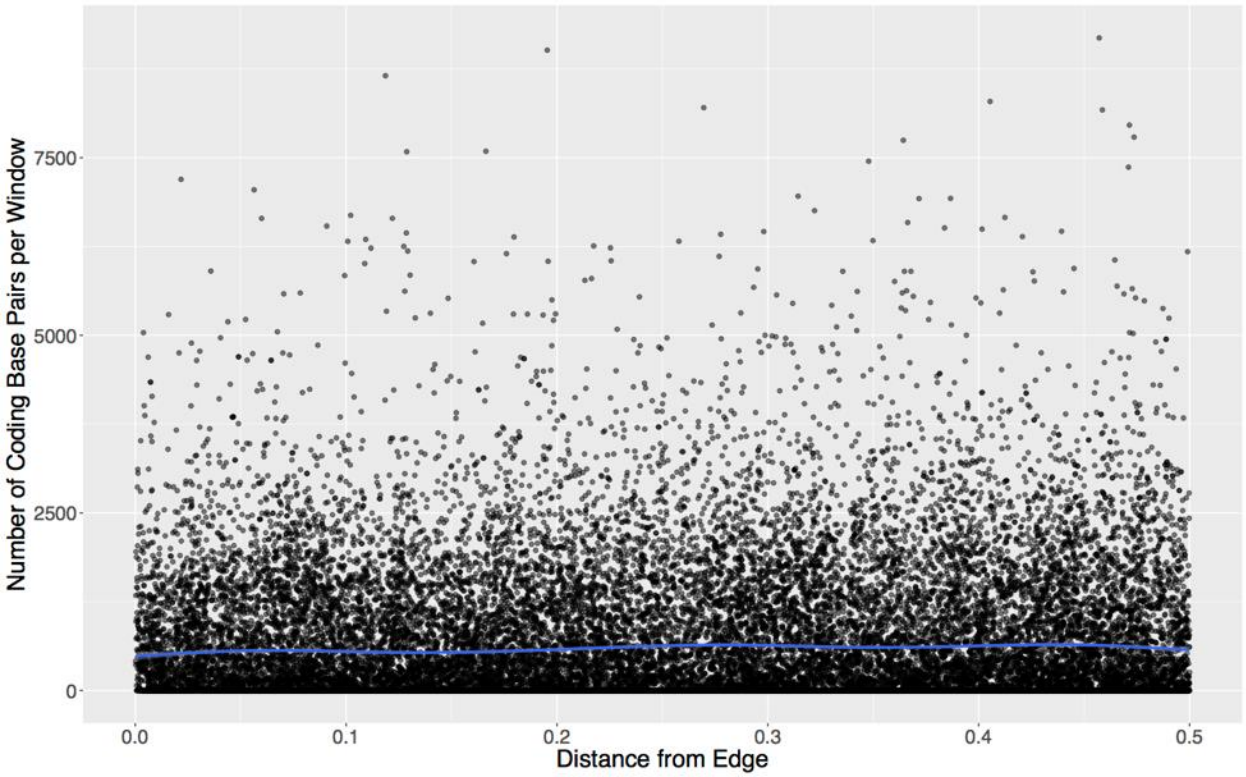

Fig. S86 Relationship of chromosomal position to number of coding bases per window

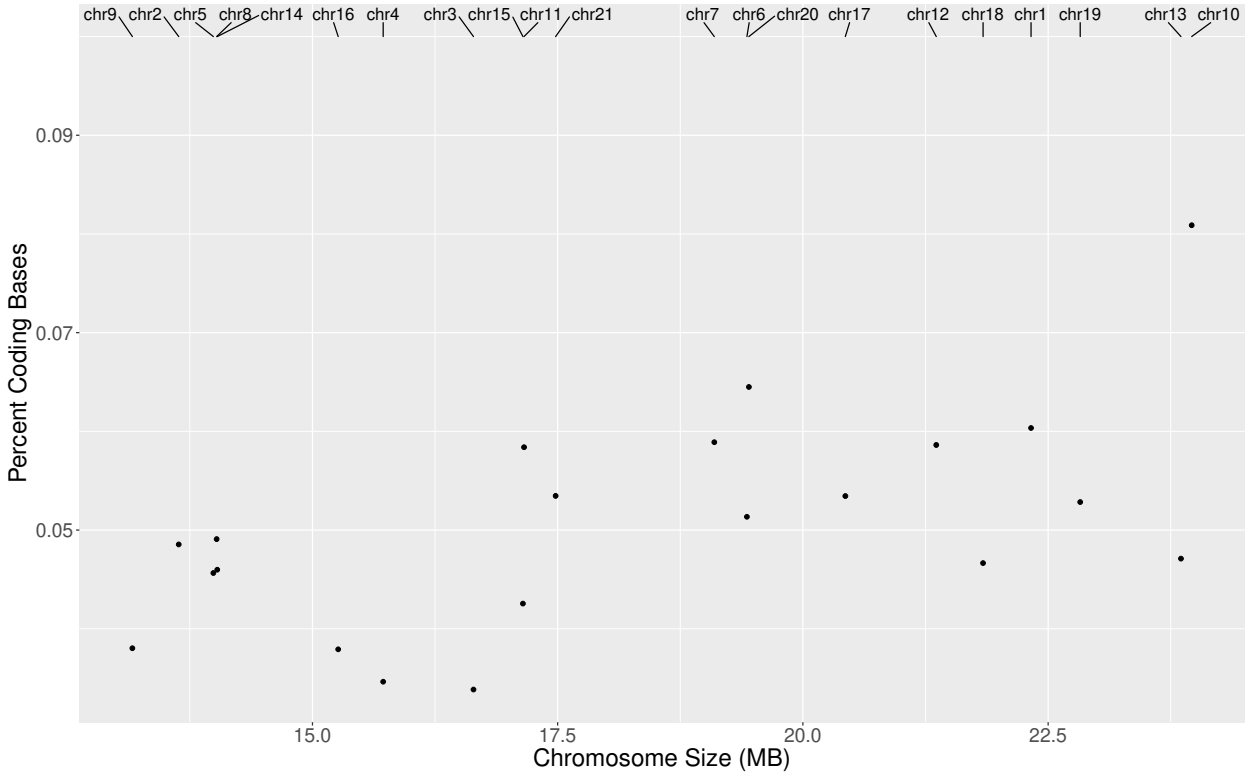

Fig. S87 Relationship of chromosome size in *H. erato* to fraction of coding bases

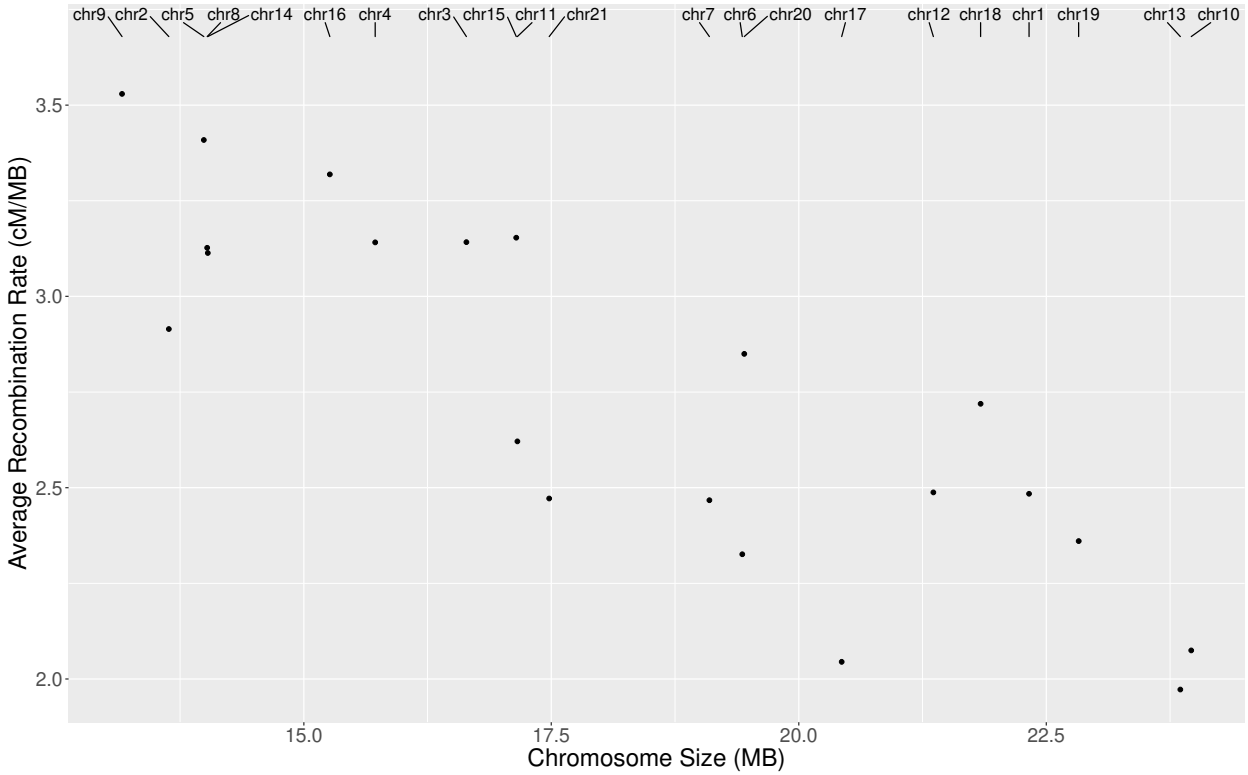

Fig. S88 Relationship of chromosome size to average recombination rate in *H. erato*

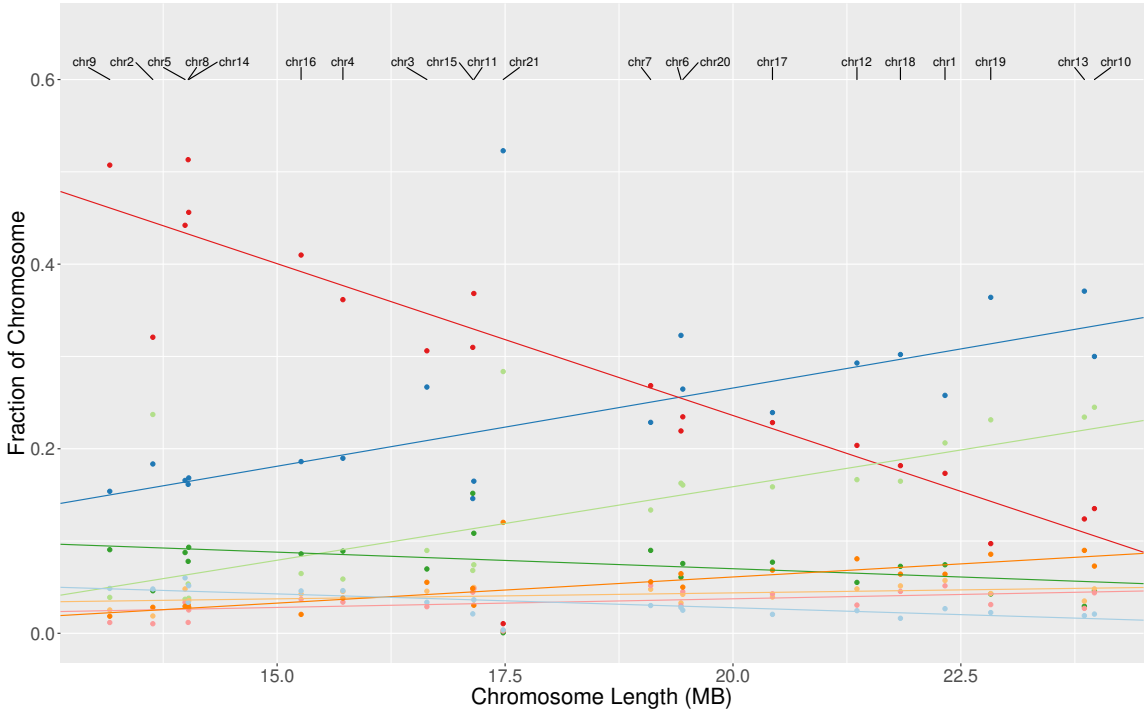

Fig. S89 Relationship of topology fraction to chromosome length in *H. erato*.

Colors as in Fig. S77 *and* Fig. S78. *Trees were reconstructed from 10 kb abutting windows.*

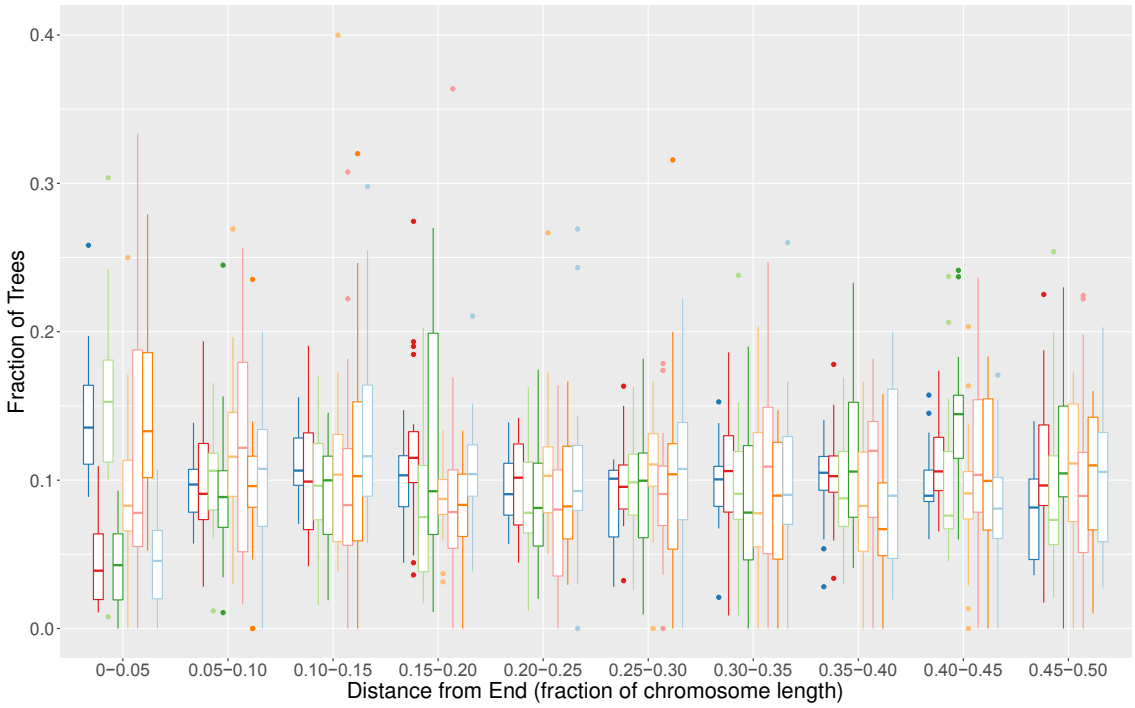

Fig. S90 Relationship of topology to *H. erato* chromosomal position, per tree

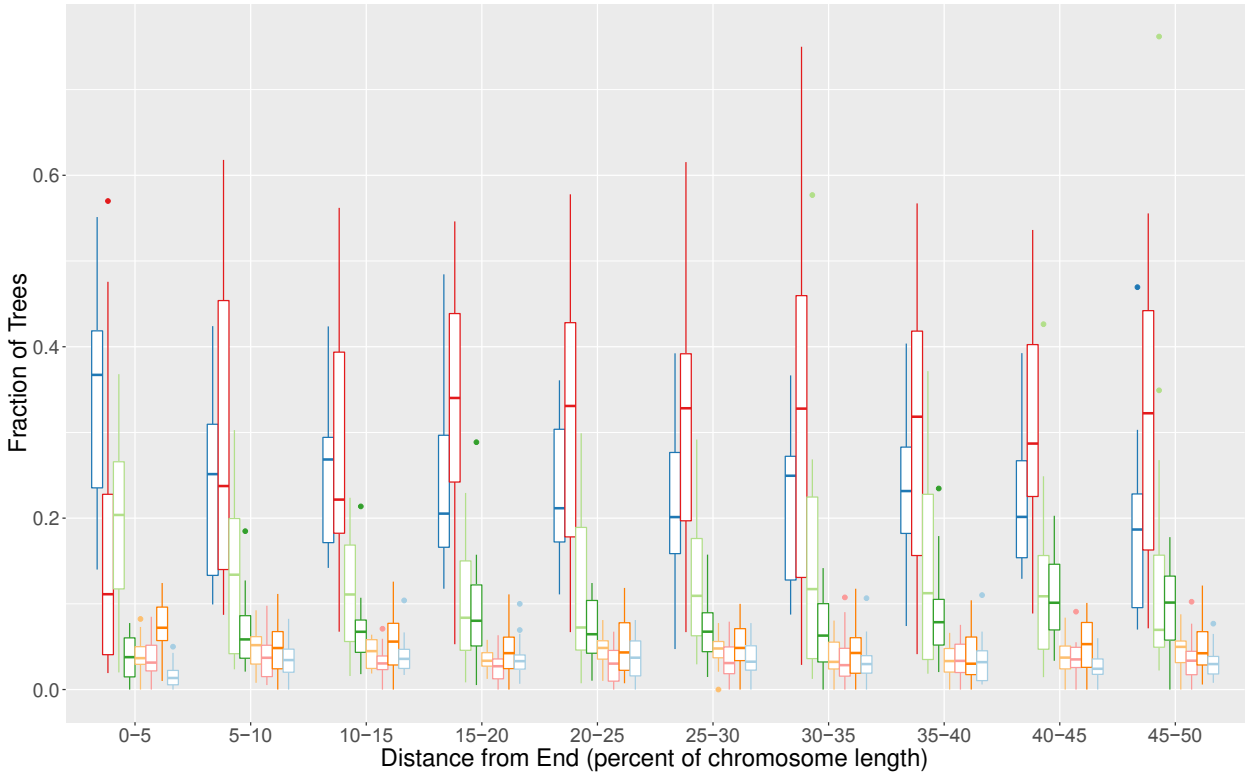

Fig. S91 Relationship of topology to *H. erato* chromosomal position, per position bin

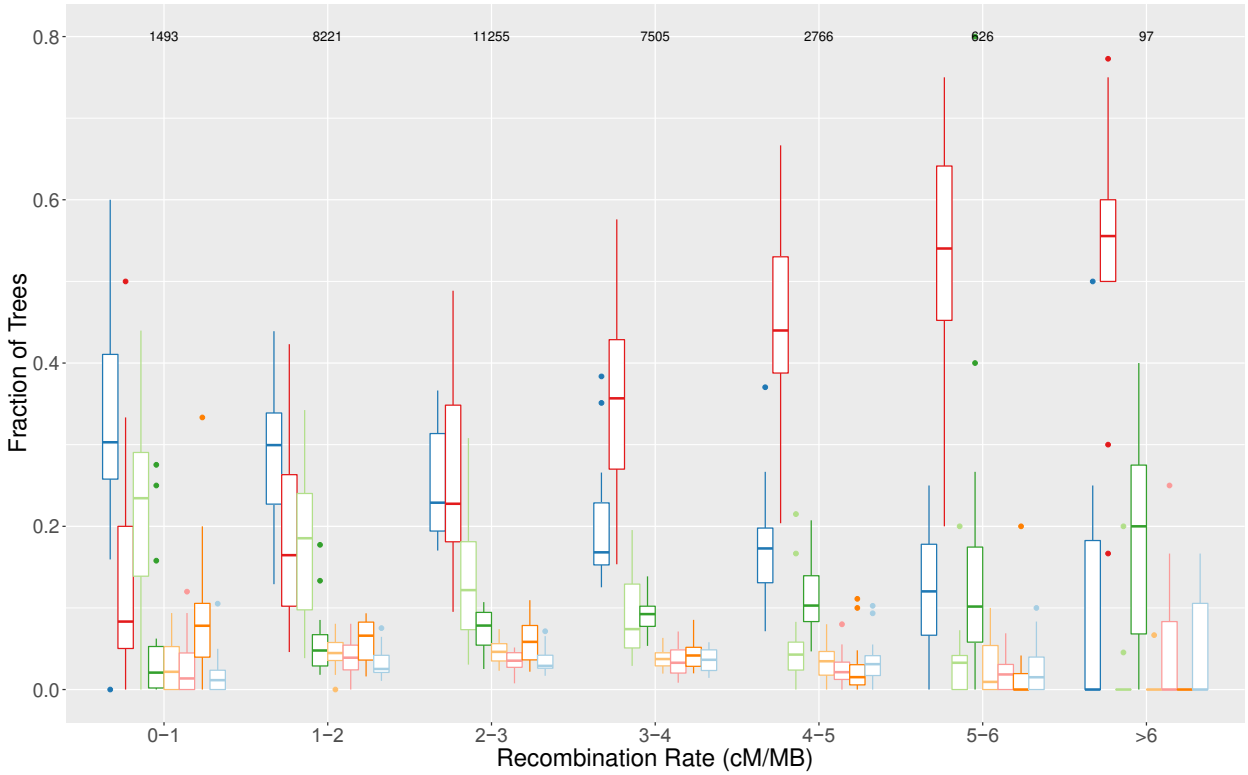

Fig. S92 Relationship of topology to local recombination rate in *H. erato*

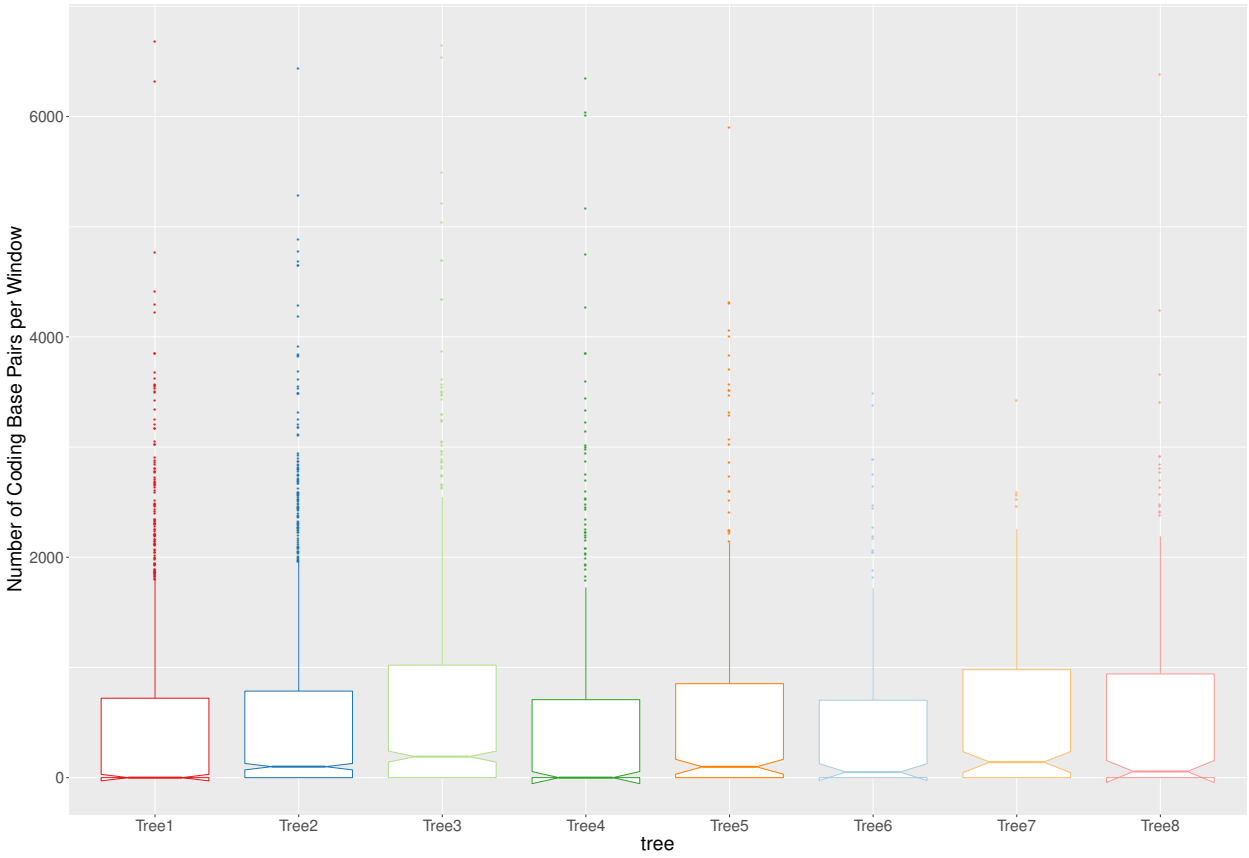

Fig. S93 Relationship of topology to number of coding base pairs per window

Central lines show median number of coding bases per window that recovers given topology. Box edges correspond to the inter-quartile range (IQR), and the minimum value they can take is 0. The notches represent $1.58 * \frac{IQR}{\sqrt{n}}$ *, and can therefore take values less than zero as seen in Trees 1, 4, 6, and 8. Tree labels correspond to those in main text Fig. 2B.*

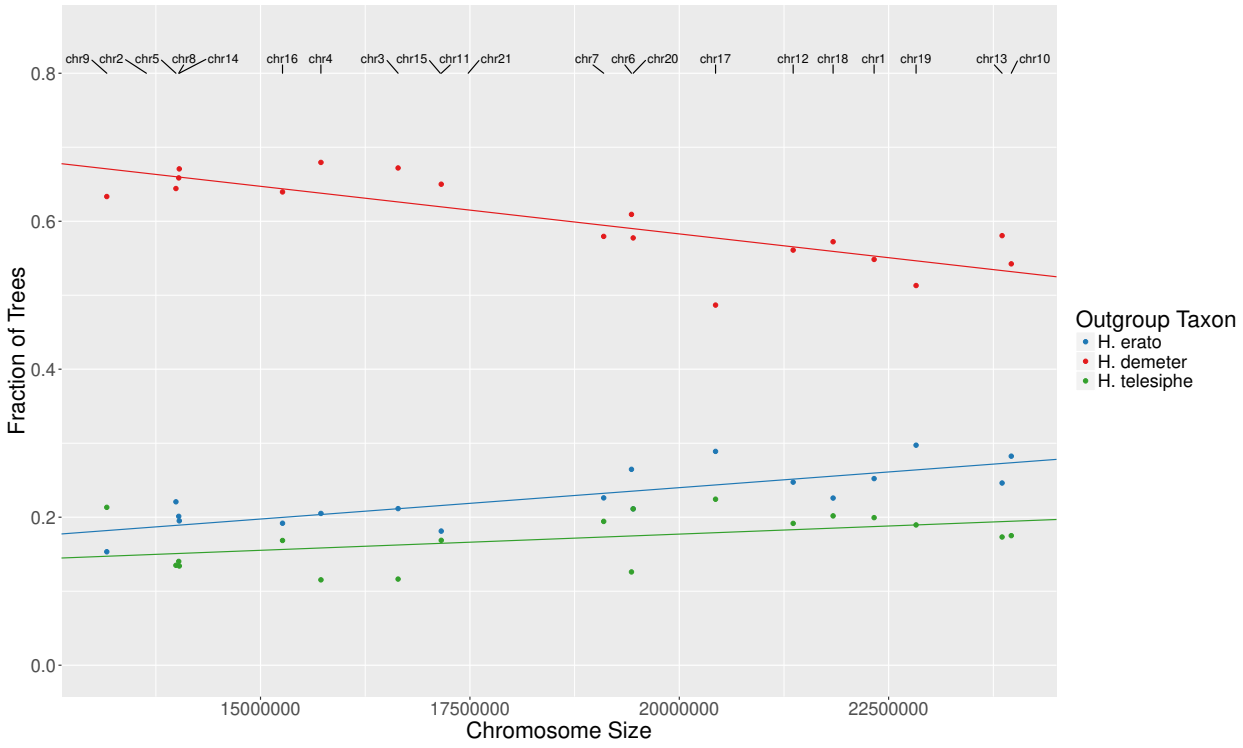

Fig. S94 Relationships of triplet topologies with chromosome length in *H. erato* clade.

The slight negative correlation of the expected species tree (red) in this triplet might be interpreted as evidence that H. telesiphe *is sister to* H. demeter *and* H. sara*, since it goes against the prevailing evidence with the full tree data (main text Fig. 2 Tree 2, and Fig.3A) Trees were reconstructed from 10 kb abutting windows.*

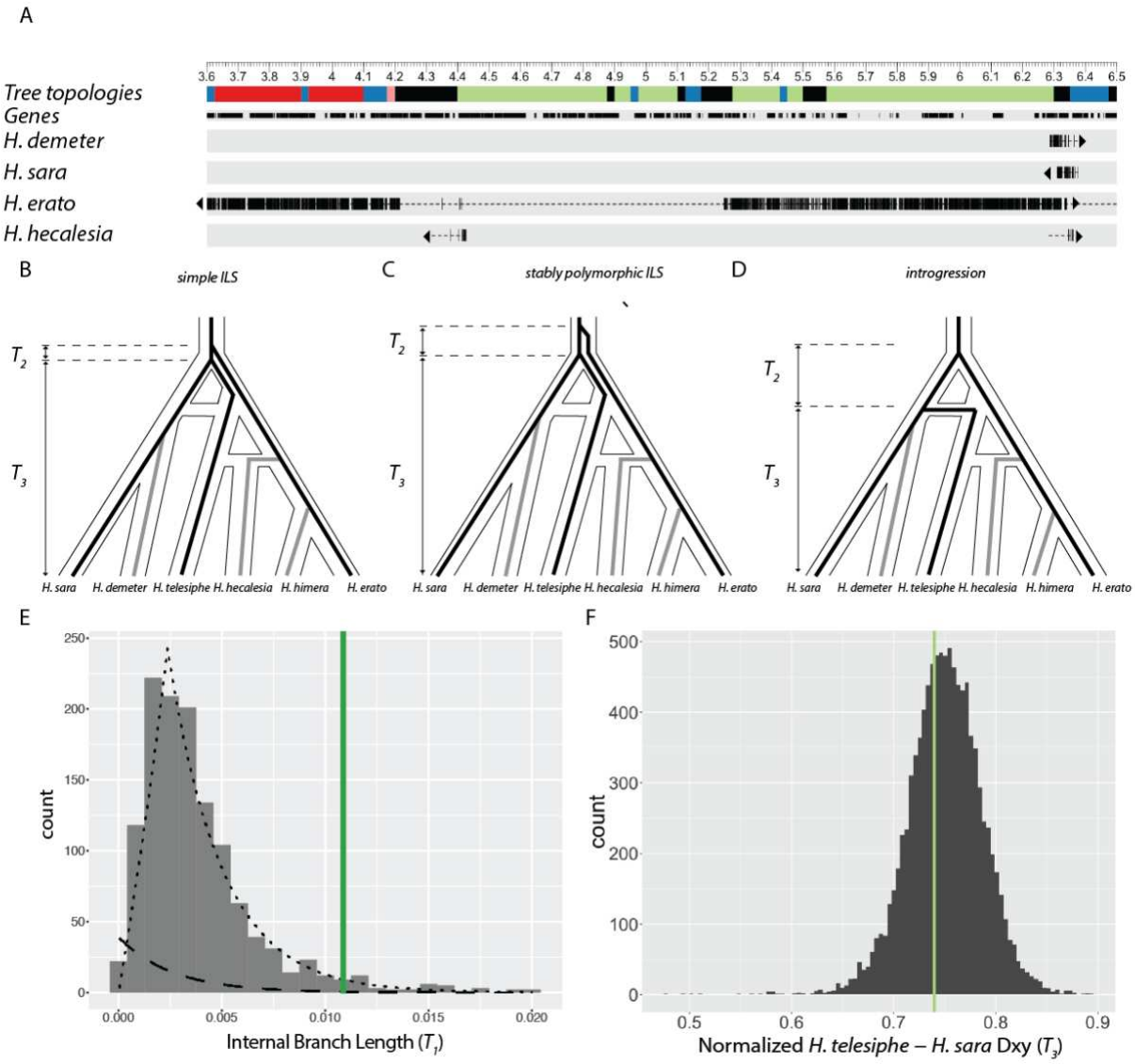

Fig. S95 An inversion on chromosome 2.

A. *Map of 3 Mb region on chromosome 2. Coordinates are in terms of the Hmel 2.5 reference order, and ticks are in Mb. Colors correspond to those in Fig. 2B. Genes are shown as black rectangles. Each line below shows the mapping of a single scaffold. Aligned sections of each scaffold are shown as thick bars, while unaligned sections are shown as dotted lines to indicate the relative position of the alignment within the scaffold. Only regions that were not identified as multiple-copy or repetitive are shown. Arrows indicate direction of alignment.* ***B-D.*** *Hypothetical evolutionary histories. In all cases, the histories of the three species used in the "triplet gene tree" method –* H. erato*,* H. telesiphe*, and* H. sara *– are shown as black lines, while lineages not included are shown as grey lines.* ***B*** *shows the scenario expected in the case of simple ILS.* ***C*** *shows another scenario of ILS, but in this case the inversion is polymorphic for some time in the common ancestor, leading to a longer internal branch for the inversion.* ***D*** *shows the case of introgression from the* H. sara+H. demeter *ancestor into the* H. telesiphe+H. hecalesia *ancestor.* ***E.*** *Distribution of internal branch lengths. Histogram is of internal branch lengths (*T_2*) in the* H.

erato,(H. telesiphe, H. sara*) topology. The inferred ILS distribution is shown as a dashed line, and the inferred introgression distribution is shown as a dotted line. The average internal branch length in the inversion is shown as a green vertical line.* ***F. Normalized*** **H. telesiphe-H. sara** ***D_{XY}.*** *Normalized D_{XY} (T_3) is calculated* as H. telesiphe-H. sara *D_{XY} divided by the mean pairwise D_{XY} among all species in each region. Mean normalized D_{XY} in the inversion is shown as a green vertical line.*

Tablse S1: Sample Info. This table provides basic information about each individual sequenced.

BROAD ID	Species	Subspecies	Labeled Sex	Sequenced 2x?	Supplier	Supplier ID	Extraction method	Tissue	Field/Lab/Inbred	Site of origin	Karyotype, n (Brown 1982 & since)
SM-5BSJW	H. timareta	linaresi	F	Y	Davey/Jiggins/Salazar	D1, RPI_2013_04	Qiagen Magattract	Whole thorax	Inbred Lab	Colombia	21
SM-62OYT	H. cydno	chioneus	F	Y	Davey/Jiggins/Merrill	D2, Merrill RNAlater 67, insectary 723	Qiagen Magattract	1/4 thorax + proximal third of abdomen	Field (Parent of lab cross)	Panama	21
SM-62OYS	H. hecale sisyphus	sisyphus	F	N, replaced	Davey/Jiggins/Joron/Chouteau	D3, MC13-103	Qiagen Magattract	larva whole body	Inbred F3	Peru: Madre de Dios: Los Amigos Res. Stn.	21
SM-5BSJY	H. numata	staudingeri	F	Y	Davey/Jiggins/Joron/Chouteau	D4, MC13-99	Qiagen Magattract	Antennae, brain and proximal abdomen	Inbred F3	Peru: Loreto: Shucshuyacu	21
SM-5BSJX	H. melpomene	melpomene	F	Y	Davey/Jiggins/Joron	D5	Qiagen Magattract	Proximal half of abdomen	Inbred F4, Genome strain	Panama	21
SM-6OSJP	H. himera x H. erato	F1 interspecific hybrid	M	Y	McMillan	6700	Qiagen DNeasy	thorax	Lab hybrid	F1 hybrid	21
SM-6OSJQ	H. himera Father		M	N, replaced	McMillan	6363	Qiagen DNeasy	1/2 thorax	Inbred	Ecuador	21
SM-6OSJR	H. erato Mother	demophoon	F	Y	McMillan	6394	Qiagen DNeasy	1/2 thorax	Inbred	Panama	21
SM-6OSJO	H. doris	viridis	M	Y	McMillan	6897	Qiagen DNeasy	thorax	Lab raised	Panama	19-32
SM-6OSJN	A. vanillae	vanillae	M	Y	Reed	none	Qiagen DNeasy	thorax	Purchased lab stock	USA	31
SM-5BSJR	H. besckei		M	Y	Moreira/Dasmahapatra	110-111	Qiagen Magattract	thorax	Field	SE Brazil	21
SM-5BSJS	N. aoede	cupidineus	F	Y, cross-contaminated	Dasmahapatra	09-282	Qiagen Magattract	thorax	Field	Peru	21-23
SM-5BSJT	E. tales	michaeli	F	Y	Dasmahapatra	09-132	Qiagen Magattract	thorax	Field	Peru	31
SM-5BSJU	H. telesiphe	telesiphe	M	Y, cross-contaminated	Dasmahapatra	09-229	Qiagen Magattract	thorax	Field	Peru	21
SM-6OSKN	H. pardalinus		F	Y	Dasmahapatra	REL13-139	Qiagen Magattract	thorax	Inbred, sib x sib offspring	Peru	21
SM-6OSKO	H. burneyi		M	Y	Dasmahapatra	09-93	Qiagen Magattract	thorax	Field	Peru	21
SM-6OSKP	H. demeter		F	Y	Dasmahapatra	09-323	Qiagen Magattract	thorax	Field	Peru	21
SM-5BSJV	H. elevatus		F	Y	Dasmahapatra	GELE	Qiagen Magattract	thorax	Lab	Peru	21
SM-79XF2	H. himera		M	N, 2015 replacement	McMillan	6900	Qiagen Magattract	thorax	Inbred	Ecuador	21
SM-79XF3	H. hecale		F	N, 2015 replacement	McMillan/Joron/Chouteau	7203	Qiagen Magattract	thorax	field	Peru	21
SM-ADRBN	H. sara	magdalena	M	N, 2016 addition	Jiggins	CAM008802	Qiagen DNeasy	thorax	lab, inbred	Panama	21
SM-ADRBM	H. hecalesia	formosus	F	N, 2016 addition	Jiggins	CAM002492	Qiagen DNeasy	thorax	field	Panama	21
SM-ADRBQ	H. telesiphe	telesiphe	M	N, 2016, replacement	Dasmahapatra	11-919	Qiagen Magattract	thorax	field	Peru	21
SM-ADRBP	D. iulia	iulia	F	N, 2016 addition	Dasmahapatra	11-759	Qiagen Magattract	thorax	field	Peru	31

Table S2: Assembly Statistics. This table provides metrics for each stage of the assembly pipeline.

		Initial contigs						Filtered contigs						Scaffolds soap						Scaffolds modified soap							
Sample	Taxon	n	n:500	N80	N50	N20	Total content	n	n:500	N80	N50	N20	sum	n	n:500	N80	N50	N20	sum	n	n:500	N80	N50	N20	sum	Pct Repeats	Heterozygosity
CAM-002492	Heliconius hecalesia	207020	77058	5884	14985	34541	542,600,000	148332	43003	8573	20205	43342	380,900,000	130323	29029	15285	36588	72956	381,500,000	20753	20753	28416	68761	140411	380,700,000	19.87	NA
CAM-008802	H. sara	167549	60185	6880	17282	37392	495,500,000	115985	31231	10101	23061	46278	339,400,000	102661	20196	18596	43055	81201	339,500,000	19649	19649	18735	43353	80206	339,300,000	18.09	NA
DAS_09-132	Eueides tales	418860	131109	4650	12344	25930	773,400,000	348961	84569	5379	14697	30005	538,800,000	340185	77490	6162	16682	34145	539,200,000	49376	49376	11337	32484	76183	538,300,000	18.81	NA
DAS_09-229	H. telesiphe (contaminated)	1031124	359289	1185	5342	63730	821,500,000	1006511	349216	1039	2870	61466	682,300,000	1001087	346139	1047	2934	69841	683,000,000	295933	295933	1275	3631	237585	681,400,000	NA	NA
DAS_09-282	N. aoede (contaminated)	378579	164605	5001	13117	29750	1,056,000,000	295111	114377	6327	15886	33353	864,000,000	281774	104207	7161	17805	36697	864,500,000	75256	75256	10860	28705	63304	863,400,000	NA	NA
DAS_09-323	H. demeter	247161	66358	5918	17609	45434	458,800,000	209934	43155	8624	23402	52141	366,500,000	203389	39455	9821	25998	56518	367,300,000	22362	22362	27453	67916	138168	366,200,000	19.19	0.012612
DAS_09-93	H. burneyi	258587	72288	8355	23488	50187	528,600,000	231151	52551	10442	29075	59154	382,100,000	224566	49446	11577	33002	66154	383,300,000	31357	31357	33996	106212	230656	381,600,000	18.61	0.0219661
DAS_110-111	H. besckei	244773	68537	4137	16849	46621	351,600,000	218898	49470	6223	22340	51023	299,900,000	213955	47335	6804	23685	53378	300,800,000	28758	28758	21561	64748	137215	299,500,000	19.68	NA
DAS_11-759	Dryas iulia	262564	126548	4655	10717	21379	758,300,000	181690	84166	5384	12329	24030	566,800,000	171280	76244	6059	13988	27176	567,300,000	53067	53067	9200	21881	44369	566,300,000	21.36	0.03009445
DAS_11-919	H. telesiphe	284514	127668	3876	9876	23834	652,500,000	183345	75422	5031	13162	29987	463,700,000	168094	64146	6218	16255	35553	464,400,000	37467	37467	13919	42637	93056	463,200,000	14.88	0.00984165
DAS_GELE	H. elevatus	353019	110138	4991	16636	36549	589,800,000	326497	89196	4639	18082	40369	444,200,000	320260	85726	4949	19584	44177	445,100,000	62414	62414	7710	30092	68093	443,400,000	15.62	NA
DAS_REL13_139	H. pardalinus	265243	84702	5628	18361	42998	514,800,000	241231	66861	5815	20855	48145	400,100,000	234897	62915	6409	22957	53453	400,900,000	45174	45174	9770	33387	76003	399,400,000	15.59	0.0227013
DAV_1_timareta	H. timareta	198294	60476	5598	17498	46888	383,200,000	179591	45771	7102	21606	54861	318,500,000	343031	82052	8203	23886	56035	638,900,000	28649	28649	13854	41310	86120	318,100,000	15.17	0.0123072
DAV_2_cydno	H. cydno	176072	63050	7935	20382	40977	501,700,000	150896	40970	9573	25497	49079	321,300,000	293925	76755	10688	28486	54179	643,200,000	26207	26207	18569	51460	109017	320,900,000	14.17	0.0279814
DAV_3_hecale	H. hecale	336937	151231	1545	4255	16864	389,700,000	225349	100723	2069	5755	20818	325,300,000	224707	100267	2084	5807	20892	325,400,000	96141	96141	2197	6223	21638	325,200,000	NA	NA
DAV_4_numata	H. numata	105488	36353	15823	40235	87601	459,200,000	94732	27893	18825	48647	103825	349,300,000	187476	54797	18979	48049	97720	699,000,000	20089	20089	24869	61332	119220	349,000,000	15.09	0.02370745
DAV_5_melpomene	H. melpomene	100495	39945	9339	25391	64861	365,200,000	87278	28778	12362	31653	76161	293,400,000	171385	55379	13150	33008	74748	587,100,000	17678	17678	23034	59409	122385	293,100,000	14.64	0.01305165
MCM_doris_6897	H. doris	221409	91245	3680	14833	37585	468,000,000	154482	60204	5618	18626	41275	404,800,000	145759	54304	6597	20760	44847	405,400,000	31556	31556	16578	46801	94078	404,300,000	22.93	0.00906053
MCM_eratowhimera_F1_6700	H. erato H. himera hybrid	265842	68706	13463	34266	70239	769,700,000	242010	53910	14725	39037	78715	587,700,000	-	-	-	-	-	-	38670	38670	20397	52193	108055	587,200,000	21.71	NA
MCM_hecale_7203	H. hecale	323789	118425	2970	9064	23151	461,000,000	275976	85856	3327	11325	27610	351,100,000	264792	80086	3693	12717	30065	352,600,000	53970	53970	6678	36514	86999	350,700,000	15.14	0.0202421
MCM_himera_6900	H. himera	153046	60424	6375	22399	56740	445,900,000	115595	43543	8637	26174	61020	399,600,000	109520	39498	9746	28271	64226	400,300,000	25411	25411	19084	48640	103581	399,400,000	NA	NA
MCM_himera_father_6363	H. himera	230072	98626	3658	10957	28898	485,300,000	162340	63948	5083	13737	32463	410,800,000	160831	62908	5187	14014	32848	411,000,000	44859	44859	8244	22685	48666	410,600,000	21.14	0.0189574
MCM_erato_mother_6394	H. erato	225412	60910	10121	27480	60804	564,600,000	201668	46728	12032	32668	70038	447,700,000	196452	43501	13478	35816	75008	448,500,000	31014	31014	20626	53995	112169	447,200,000	21.33	0.00813964
REE_vanillae	A. vanillae	419913	135877	3212	7439	16053	595,500,000	335233	79931	3698	9223	19317	390,500,000	-	-	-	-	-	-	45022	45022	7954	21374	47700	390,100,000	14.93	0.0215847

Table S3: Mapping to reference. This table provides statistics on the reciprocal mapping coverage of *de novo* genomes and previously published reference genome assemblies.

Genome	Total Size	Total Sequences > 1KB	Fraction Aligned *	Fraction Single Copy	fraction repeats	single copy + repeats	coding aligned	non-coding aligned	Alignment Target
H. melpomene reference (Hmel2)	275198219	794	0.942361	0.814264045	0.1473	0.961564045	NA	NA	H. melpomene w2rap
H. melpomene w2rap	289529429	12179	0.957001	0.851926705	0.1464	0.998326705	0.993	0.953	H. melpomene reference (Hmel2)
H. erato demophoon reference	382828983	195	0.883146	0.658102687	0.2015	0.859602687	NA	NA	H. erato w2rap
H. erato w2rap	441457298	21969	0.925971	0.749634089	0.2133	0.962934089	0.985	0.919	H. erato demophoon reference

* this value is the percent of the alignment target covered at least 1X by the query genome

Table S4: Scaffolding With DISCOVAR filled gap. This is an example output for the SWD pipeline showing a group of three filled gaps.

Scaffold	Group	Contig	Start	End	Strand
Hmel201001o	3	Hmel201001o_2	0	92309	+
Hmel201001o	3	EI-a-scaffold-12909	8072	9336	-
Hmel201001o	3	Hmel201001o_3	761	280226	+
Hmel201001o	3	EI-a-scaffold-13029	6832	7959	+
Hmel201001o	3	Hmel201001o_4	639	69269	+
Hmel201001o	3	EI-a-scaffold-13029	77551	78099	+
Hmel201001o	3	Hmel201001o_5	555	491511	+

Table S5: Gap-filling output. This table is a comparison of summary statistics for the Hmel2.5 genome and that same genome after gaps were filled with SWD.

Genome	Contigs	Total Contig Length	Mean contig	Contig N50	Gaps	Total Gap Length	Mean Gap Length	Gap N50
Hmel2.5	3111	274214515	88143	329606	2990	1031298	371	2233
Hmel2.5, gap-filled	2423	274117371	113131	458152	2091	795323	380	1466

w2rap melpomene full genome

```
================================================
sequences:         12179
total length:  289529429 bp  (289477054 bp excl N/X-runs)
GC level:         32.74 %
bases masked:   42390139 bp ( 14.64 %)
================================================
                number of      length   percentage
                elements*    occupied  of sequence
------------------------------------------------
Retroelements        18032      4390549 bp    1.52 %
   SINEs:              684        34049 bp    0.01 %
   Penelope              2          155 bp    0.00 %
   LINEs:            12167      3257088 bp    1.12 %
    CRE/SLACS            0            0 bp    0.00 %
     L2/CR1/Rex       6128      1511859 bp    0.52 %
     R1/LOA/Jockey    2340       674824 bp    0.23 %
     R2/R4/NeSL       1459       468411 bp    0.16 %
     RTE/Bov-B        1740       483943 bp    0.17 %
     L1/CIN4            12          624 bp    0.00 %
   LTR elements:      5181      1099412 bp    0.38 %
     BEL/Pao           633       144481 bp    0.05 %
     Ty1/Copia         178        40374 bp    0.01 %
     Gypsy/DIRS1      3862       807954 bp    0.28 %
       Retroviral        0            0 bp    0.00 %

DNA transposons     231972     30820377 bp   10.64 %
   hobo-Activator     8196      1506936 bp    0.52 %
   Tc1-IS630-Pogo   123631     15828698 bp    5.47 %
   En-Spm                0            0 bp    0.00 %
   MuDR-IS905            0            0 bp    0.00 %
   PiggyBac             88        35700 bp    0.01 %
   Tourist/Harbinger    11         1563 bp    0.00 %
   Other (Mirage,      146         7447 bp    0.00 %
    P-element, Transib)

Rolling-circles          0            0 bp    0.00 %

Unclassified:         1997       282672 bp    0.10 %

Total interspersed repeats:    35493598 bp   12.26 %


Small RNA:             790        49738 bp    0.02 %

Satellites:            331        18247 bp    0.01 %
Simple repeats:     128725      5687070 bp    1.96 %
Low complexity:      25791      1246843 bp    0.43 %
```

w2rap sequences inserted across gaps

```
================================================
sequences:           792
total length:    1909413 bp  (1908113 bp excl N/X-runs)
GC level:         32.90 %
bases masked:     600714 bp ( 31.46 %)
================================================
                number of      length   percentage
                elements*    occupied  of sequence
------------------------------------------------
Retroelements         1805       299637 bp   15.69 %
   SINEs:             1432       179734 bp    9.41 %
   Penelope             15         7175 bp    0.38 %
   LINEs:              274        91167 bp    4.77 %
    CRE/SLACS            0            0 bp    0.00 %
     L2/CR1/Rex         84        29195 bp    1.53 %
     R1/LOA/Jockey      23         5461 bp    0.29 %
     R2/R4/NeSL         19         7326 bp    0.38 %
     RTE/Bov-B          71        24710 bp    1.29 %
     L1/CIN4             0            0 bp    0.00 %
   LTR elements:        99        28736 bp    1.50 %
     BEL/Pao             9         2630 bp    0.14 %
     Ty1/Copia           5          322 bp    0.02 %
     Gypsy/DIRS1        45        10596 bp    0.55 %
       Retroviral        0            0 bp    0.00 %

DNA transposons         620        90142 bp    4.72 %
   hobo-Activator        41         8030 bp    0.42 %
   Tc1-IS630-Pogo       371        40697 bp    2.13 %
   En-Spm                 0            0 bp    0.00 %
   MuDR-IS905             0            0 bp    0.00 %
   PiggyBac              51        10913 bp    0.57 %
   Tourist/Harbinger      0            0 bp    0.00 %
   Other (Mirage,         9          704 bp    0.04 %
    P-element, Transib)

Rolling-circles          0            0 bp    0.00 %

Unclassified:          652       174562 bp    9.14 %

Total interspersed repeats:     564341 bp   29.56 %


Small RNA:            1431       179655 bp    9.41 %

Satellites:              7          338 bp    0.02 %
Simple repeats:        695        30687 bp    1.61 %
Low complexity:        137         6194 bp    0.32 %
```

Table S6 Comparison of general *H melpomene* de novo repeat content with repeat content of regions used to fill gaps in Hmel2.

Table S7: Pairwise coverage. This table provides a summary of pairwise coverage between the indicated genome and H. melpomene (Hmel2.5) in the progressiveCactus multiple sequence alignment.

Species	Exonic Aligned Bases	Intronic Aligned Bases	Intergenic Aligned Bases	Total Aligned Bases	Total fraction Aligned Bases	Percent Identity with Hmel2.5
A. vanillae	24097265	28989986	66553755	119641006	0.434742028	85.744
B. anynana	21097464	10153992	18682837	49934293	0.181447286	75.122
B. mori	18148815	3531535	5495058	27175408	0.098747849	70.161
D. plexippus	20456742	7653762	14576915	42687419	0.155114168	74.559
E. tales	24621153	37597605	82128987	144347745	0.524519422	87.93
H. besckei	26688422	66337604	135787543	228813569	0.831444655	94.493
H. cydno	26949426	71193415	145130181	243273022	0.883986272	95.431
H. demeter	25348301	53240913	113086551	191675765	0.696496239	92.083
H. erato de novo	25098699	51204203	109130872	185433774	0.673814586	91.463
H. erato/H. himera hybrid	25152324	52063794	110781241	187997359	0.683129938	91.725
H. erato reference	25014475	51118217	108693122	184825814	0.671605429	92.461
H. himera	25064348	50612316	107874008	183550672	0.666971919	91.661
H. hecalesia	25215400	51964526	110511018	187690944	0.682016512	91.559
H. melpomene de novo	27622639	78415264	160715437	266753340	0.969307195	96.367
H. numata	26557912	67149274	137656437	231363623	0.840710839	94.867
H. pardalinus	26559866	67296306	138047997	231904169	0.842675033	95.183
H. sara	25205144	51454453	109981601	186641198	0.678202028	91.047
H. telesiphe	25320375	53937353	114098714	193356442	0.70260335	91.75
H. timareta	27134044	71545070	145798364	244477478	0.888362929	95.71
L. accius	18662013	4727985	8021427	31411425	0.114140352	72.767
H. doris	25476851	54956304	114965325	195398480	0.710023547	90.728
M. cinxia	19301595	13207459	28287896	60796950	0.22091915	76.646
P. polytes	18342885	5153458	8888529	32384872	0.117677587	72.614
P. xytostella	15083665	2414768	3610607	21109040	0.07670436	68.717

Table S8: Phylogeny Datasets. This table provides a summary of all datasets used to construct species trees.

Data set	Number of taxa	Number of loci used in ASTRAL analyses	Number of characters used in concatenated analysis
Genes	25	4090	4,955,181
Noncoding blocks (100 bp or longer)	25	100	15,144
Noncoding blocks (150 bp or longer)	25	30	6640
Coding blocks (100 bp or longer)	25	3572	596,163
Coding blocks (150 bp or longer)	25	1641	367,915
Heliconini only noncoding blocks (100 bp or longer)	17	328	47,945
Heliconini only noncoding blocks (150 bp or longer)	17	102	20,368
Heliconini only coding blocks (100 bp or longer)	17	10,473	1,870,808
Heliconini only coding blocks (150 bp or longer)	17	5441	1,258,140

Outgroup	P3	P2	P1	D	SE	Z	BABA	ABBA	Total SNPs
Etal	Htel	Hhsa	Hera	-0.2427	0.003064	-79.224	58235	95569	6671421
Etal	Htel	Hhsa	Hhim	-0.2426	0.00309	-78.502	57923	95029	6671421
Etal	Hdem	Hhsa	Hera	-0.1554	0.002941	-52.818	61308	83862	6671421
Etal	Hdem	Hhsa	Hhim	-0.1529	0.002966	-51.551	61093	83144	6671421
Etal	Hsar	Hhsa	Hera	-0.1476	0.002905	-50.819	63018	84849	6671421
Etal	Hsar	Hhsa	Hhim	-0.1458	0.002946	-49.495	62823	84273	6671421
Etal	Htel	Hsar	Hdem	0.1427	0.003014	47.344	66620	49980	6671421
Etal	Hhsa	Hsar	Hdem	0.1332	0.002961	44.98	69992	53537	6671421
Etal	Hhim	Hsar	Hdem	0.1304	0.002939	44.375	68700	52846	6671421
Etal	Hera	Hsar	Hdem	0.1293	0.002931	44.107	68706	52974	6671421
Etal	Hdem	Htel	Hera	-0.109	0.002801	-38.905	69053	85941	6671421
Etal	Hdem	Htel	Hhim	-0.1061	0.002827	-37.543	68989	85374	6671421
Etal	Hsar	Htel	Hera	-0.1016	0.002781	-36.532	70651	86631	6671421
Etal	Hsar	Htel	Hhim	-0.0995	0.002806	-35.455	70600	86199	6671421
Etal	Hsar	Htel	Hhsa	0.0421	0.003168	13.296	72375	66524	6671421
Etal	Hdem	Htel	Hhsa	0.0414	0.003197	12.954	71248	65582	6671421
Etal	Hdem	Hera	Hhim	0.007	0.003845	1.832	35957	35454	6671421
Etal	Hhsa	Hera	Hhim	0.0055	0.003732	1.465	38612	38192	6671421
Etal	Hsar	Hera	Hhim	0.0052	0.003787	1.376	36735	36354	6671421
Etal	Htel	Hera	Hhim	0.0032	0.003803	0.828	36298	36070	6671421

Table S9 *erato* clade *D*-statistics given species tree

These erato *clade D-statistic values are ordered by absolute value, and assume the species tree shown in Fig. 1A.*

Outgroup	P3	P2	P1	D	SE	Z	BABA	ABBA	Total SNPs
Etal	Hmel	Hbes	Hpar	0.2691	0.003107	86.621	93490	53839	6671421
Etal	Htim	Hbes	Hpar	0.2491	0.003073	81.045	91074	54755	6671421
Etal	Hpar	Hbes	Hnum	0.2267	0.003089	73.392	84703	53395	6671421
Etal	Hcyd	Hbes	Hpar	0.2168	0.003118	69.537	86650	55771	6671421
Etal	Hbes	Hpar	Hmel	-0.1679	0.003451	-48.639	53839	75559	6671421
Etal	Hmel	Hpar	Hnum	-0.1655	0.003587	-46.143	52575	73431	6671421
Etal	Hmel	Hbes	Hnum	0.1490	0.00316	47.159	72458	53663	6671421
Etal	Htim	Hpar	Hnum	-0.1482	0.003544	-41.827	53024	71480	6671421
Etal	Htim	Hbes	Hnum	0.1421	0.003149	45.131	71777	53914	6671421
Etal	Hcyd	Hbes	Hnum	0.1265	0.003135	40.339	69857	54172	6671421
Etal	Hcyd	Hpar	Hnum	-0.1248	0.003575	-34.899	53294	68488	6671421
Etal	Hbes	Hpar	Hnum	0.1191	0.003539	33.665	67839	53395	6671421
Etal	Hpar	Hcyd	Hmel	0.1140	0.004143	27.509	51848	41239	6671421
Etal	Hcyd	Htim	Hmel	-0.1132	0.005137	-22.040	51004	64028	6671421
Etal	Hnum	Hbes	Hpar	0.1106	0.003456	31.989	84703	67839	6671421
Etal	Hpar	Htim	Hcyd	-0.0887	0.004067	-21.798	38607	46118	6671421
Etal	Hnum	Hcyd	Hmel	0.0575	0.004007	14.358	45466	40519	6671421
Etal	Hnum	Htim	Hcyd	-0.0535	0.004005	-13.364	37568	41817	6671421
Etal	Ldor	Hbes	Hcyd	0.0442	0.00308	14.339	55903	51174	6671421
Etal	Ldor	Hbes	Hnum	0.0418	0.003251	12.857	49650	45666	6671421
Etal	Ldor	Hbes	Htim	0.0349	0.003114	11.193	55385	51654	6671421
Etal	Hpar	Htim	Hmel	0.0331	0.004243	7.812	48280	45182	6671421
Etal	Ldor	Hpar	Hcyd	0.0315	0.003312	9.508	47857	44935	6671421
Etal	Ldor	Hbes	Hmel	0.0298	0.003121	9.562	55457	52243	6671421
Etal	Hbes	Htim	Hcyd	-0.0271	0.00399	-6.797	37145	39216	6671421
Etal	Ldor	Hpar	Hnum	0.0253	0.003432	7.373	44106	41929	6671421
Etal	Ldor	Hcyd	Hmel	-0.0242	0.004009	-6.042	30517	32032	6671421
Etal	Hbes	Hcyd	Hmel	0.0222	0.003958	5.601	42353	40516	6671421
Etal	Ldor	Hpar	Htim	0.0212	0.003382	6.259	46405	44481	6671421
Etal	Hmel	Htim	Hcyd	-0.0198	0.004771	-4.151	51004	53065	6671421
Etal	Ldor	Hbes	Hpar	0.0175	0.003143	5.581	52407	50600	6671421
Etal	Ldor	Htim	Hcyd	0.0173	0.004163	4.162	29300	28302	6671421
Etal	Ldor	Hpar	Hmel	0.0156	0.003434	4.542	45806	44399	6671421
Etal	Ldor	Htim	Hmel	-0.0083	0.004034	-2.047	31053	31570	6671421
Etal	Hnum	Htim	Hmel	0.0081	0.004022	2.014	43439	42741	6671421
Etal	Ldor	Hnum	Hmel	-0.0081	0.003328	-2.423	47369	48139	6671421
Etal	Ldor	Hnum	Hcyd	0.0078	0.00324	2.408	48121	47376	6671421
Etal	Hbes	Htim	Hmel	-0.0028	0.00396	-0.717	41097	41331	6671421
Etal	Ldor	Hnum	Htim	-0.0027	0.003309	-0.803	47464	47717	6671421

Table S10 *melpomene* clade *D*-statistics given species tree

These melpomene *clade D-statistic values are ordered by absolute value and assume the species tree shown in Fig. 1A. Values for all topologies are shown when they include the silvaniform clade polytomy.*

Table S11: D statistics. This table shows the raw output of the D statistic calculations using the full Lepidooptera alignment and the Heliconiini-only alignment

				Lepidoptera Alignment (Harvard)							Heliconiini Alignment (Lepbase)						
Outgroup	*P3*	*P2*	*P1*	*|D|*	*SE*	*|Z|*	*best*	*BABA sites*	*ABBA sites*	*Total SNPs*	*|D|*	*SE*	*|Z|*	*best*	*BABA sites*	*ABBA sites*	*Total SNPs*
Etal	Htel	Hhsa	Hera	0.2431	0.015724	15.459	-	58235	95569	6671421	0.2426	0.011299	21.474	-	28766	47179	3242509
Etal	Hhsa	Htel	Hera	0.007	0.032702	0.214	best	96921	95569	6671421	0.0056	0.021243	0.262	best	46658	47179	3242509
Etal	Hera	Htel	Hhsa	0.2496	0.016523	15.11	-	96921	58235	6671421	0.2374	0.010306	23.033	-	46658	28766	3242509
Etal	Htel	Hhsa	Hhim	0.2429	0.016322	14.884	-	57923	95029	6671421	0.2344	0.012196	19.218	-	28687	46231	3242509
Etal	Hhsa	Htel	Hhim	0.0092	0.032859	0.28	best	96801	95029	6671421	0.0038	0.021894	0.175	best	46590	46231	3242509
Etal	Hhim	Htel	Hhsa	0.2516	0.016492	15.255	-	96801	57923	6671421	0.238	0.010465	22.739	-	46590	28687	3242509
Etal	Htel	Hhsa	HeraHhimHyl	0.241	0.015971	15.093	-	58040	94840	6671421	0.2354	0.011828	19.904	-	28673	46312	3242509
Etal	Hhsa	Htel	HeraHhimHyl	0.0101	0.032771	0.31	best	96789	94840	6671421	0.0036	0.021585	0.168	best	46651	46312	3242509
Etal	HeraHhimHyl	Htel	Hhsa	0.2506	0.016728	14.98	-	96789	58040	6671421	0.2388	0.010526	22.688	-	46651	28673	3242509
Etal	Htel	Hhsa	Hsar	0.2892	0.019022	15.206	-	66524	120626	6671421	0.2706	0.012806	21.134	-	33628	58570	3242509
Etal	Hhsa	Htel	Hsar	0.2502	0.015011	16.666	-	72375	120626	6671421	0.2375	0.011128	21.344	-	36097	58570	3242509
Etal	Hsar	Htel	Hhsa	0.0421	0.009787	4.297	best	72375	66524	6671421	0.0354	0.006844	5.169	best	36097	33628	3242509
Etal	Htel	Hhsa	Hdem	0.2224	0.022406	9.925	-	65582	103044	6671421	0.1993	0.015746	12.656	-	33147	49630	3242509
Etal	Hhsa	Htel	Hdem	0.1827	0.017541	10.413	-	71248	103044	6671421	0.171	0.013243	12.912	-	35149	49630	3242509
Etal	Hdem	Htel	Hhsa	0.0413	0.010152	4.071	best	71248	65582	6671421	0.0293	0.007614	3.844	best	35149	33147	3242509
Etal	Htel	Hhsa	Ldor	0.7787	0.005388	100	-	58556	470383	6671421	0.7925	0.003556	100	-	28649	247396	3242509
Etal	Hhsa	Htel	Ldor	0.7828	0.00523	100	-	57333	470383	6671421	0.8019	0.003507	100	-	27196	247396	3242509
Etal	Ldor	Htel	Hhsa	0.0106	0.002427	4.35	best	57333	58556	6671421	0.026	0.003757	6.926	best	27196	28649	3242509
Etal	Htel	Hhsa	Hbes	0.7784	0.005516	100	-	57308	459805	6671421	0.7794	0.003836	100	-	28817	232385	3242509
Etal	Hhsa	Htel	Hbes	0.782	0.005467	100	-	56257	459805	6671421	0.7886	0.003714	100	-	27467	232385	3242509
Etal	Hbes	Htel	Hhsa	0.0093	0.002785	3.322	best	56257	57308	6671421	0.024	0.003989	6.015	best	27467	28817	3242509
Etal	Htel	Hhsa	Hpar	0.7794	0.005347	100	-	56683	457032	6671421	0.7801	0.003866	100	-	28485	230557	3242509
Etal	Hhsa	Htel	Hpar	0.7821	0.005318	100	-	55902	457032	6671421	0.7893	0.003735	100	-	27151	230557	3242509
Etal	Hpar	Htel	Hhsa	0.0069	0.002895	2.395	best	55902	56683	6671421	0.024	0.003798	6.314	best	27151	28485	3242509
Etal	Htel	Hhsa	Hnum	0.779	0.00541	100	-	56522	454845	6671421	0.7802	0.003846	100	-	28366	229645	3242509
Etal	Hhsa	Htel	Hnum	0.7823	0.005438	100	-	55574	454845	6671421	0.789	0.003649	100	-	27096	229645	3242509
Etal	Hnum	Htel	Hhsa	0.0085	0.003277	2.58	best	55574	56522	6671421	0.0229	0.004108	5.576	best	27096	28366	3242509
Etal	Htel	Hhsa	Htim	0.7798	0.005353	100	-	56339	455127	6671421	0.7809	0.003771	100	-	28311	230022	3242509
Etal	Hhsa	Htel	Htim	0.7828	0.005378	100	-	55464	455127	6671421	0.79	0.003697	100	-	26985	230022	3242509
Etal	Htim	Htel	Hhsa	0.0078	0.003345	2.338	best	55464	56339	6671421	0.024	0.004014	5.974	best	26985	28311	3242509
Etal	Htel	Hhsa	Hcyd	0.7796	0.005356	100	-	56314	454456	6671421	0.7812	0.003758	100	-	28218	229634	3242509
Etal	Hhsa	Htel	Hcyd	0.783	0.00542	100	-	55320	454456	6671421	0.7905	0.003659	100	-	26870	229634	3242509
Etal	Hcyd	Htel	Hhsa	0.0089	0.003246	2.74	best	55320	56314	6671421	0.0245	0.003941	6.21	best	26870	28218	3242509
Etal	Htel	Hhsa	Hmel	0.7796	0.005363	100	-	56467	455855	6671421	0.7811	0.003827	100	-	28306	230241	3242509
Etal	Hhsa	Htel	Hmel	0.7832	0.005465	100	-	55439	455855	6671421	0.7914	0.003643	100	-	26820	230241	3242509
Etal	Hmel	Htel	Hhsa	0.0092	0.002893	3.172	best	55439	56467	6671421	0.027	0.004144	6.506	best	26820	28306	3242509
Etal	Htel	Hera	Hhim	0.0031	0.004158	0.755	best	36298	36070	6671421	0.0247	0.005638	4.373	best	18038	17169	3242509
Etal	Hera	Htel	Hhim	0.7377	0.005732	100	-	238914	36070	6671421	0.7395	0.004525	100	-	114634	17169	3242509
Etal	Hhim	Htel	Hera	0.7362	0.005454	100	-	238914	36298	6671421	0.7281	0.004018	100	-	114634	18038	3242509
Etal	Htel	Hera	HeraHhimHyl	0.01	0.004787	2.085	best	26890	26356	6671421	0.0299	0.006517	4.588	best	13319	12545	3242509
Etal	Hera	Htel	HeraHhimHyl	0.8288	0.00706	100	-	281375	26356	6671421	0.8304	0.005122	100	-	135390	12545	3242509
Etal	HeraHhimHyl	Htel	Hera	0.8256	0.00658	100	-	281375	26890	6671421	0.8209	0.005004	100	-	135390	13319	3242509
Etal	Htel	Hera	Hsar	0.0883	0.007139	12.363	best	86631	103399	6671421	0.0701	0.006021	11.636	best	43348	49877	3242509
Etal	Hera	Htel	Hsar	0.1882	0.005951	31.623	-	70651	103399	6671421	0.1734	0.005348	32.412	-	35142	49877	3242509
Etal	Hsar	Htel	Hera	0.1016	0.00449	22.631	-	70651	86631	6671421	0.1046	0.004471	23.388	-	35142	43348	3242509
Etal	Htel	Hera	Hdem	0.0008	0.008587	0.092	best	85941	86069	6671421	0.0229	0.007354	3.111	best	43065	41135	3242509
Etal	Hera	Htel	Hdem	0.1098	0.007428	14.775	-	69053	86069	6671421	0.0928	0.006708	13.835	-	34152	41135	3242509
Etal	Hdem	Htel	Hera	0.109	0.004531	24.052	-	69053	85941	6671421	0.1154	0.004865	23.728	-	34152	43065	3242509
Etal	Htel	Hera	Ldor	0.7365	0.00312	100	-	66996	441489	6671421	0.7548	0.002401	100	-	32538	232872	3242509
Etal	Hera	Htel	Ldor	0.7397	0.003302	100	-	66066	441489	6671421	0.7643	0.002084	100	-	31108	232872	3242509
Etal	Ldor	Htel	Hera	0.007	0.003031	2.306	best	66066	66996	6671421	0.0225	0.00379	5.929	best	31108	32538	3242509
Etal	Htel	Hera	Hbes	0.7366	0.003244	100	-	65291	430454	6671421	0.7395	0.002822	100	-	32610	217765	3242509
Etal	Hera	Htel	Hbes	0.7342	0.003287	100	-	65978	430454	6671421	0.7447	0.00238	100	-	31871	217765	3242509
Etal	Hbes	Htel	Hera	0.0052	0.00343	1.528	best	65978	65291	6671421	0.0115	0.004833	2.372	best	31871	32610	3242509
Etal	Htel	Hera	Hpar	0.7373	0.003193	100	-	64681	427696	6671421	0.7402	0.002932	100	-	32241	215900	3242509
Etal	Hera	Htel	Hpar	0.733	0.003157	100	-	65911	427696	6671421	0.7446	0.002369	100	-	31615	215900	3242509
Etal	Hpar	Htel	Hera	0.0094	0.00302	3.12	best	65911	64681	6671421	0.0098	0.004688	2.093	best	31615	32241	3242509
Etal	Htel	Hera	Hnum	0.737	0.003347	100	-	64405	425394	6671421	0.7398	0.002846	100	-	32153	215019	3242509
Etal	Hera	Htel	Hnum	0.7322	0.003299	100	-	65784	425394	6671421	0.744	0.002325	100	-	31562	215019	3242509
Etal	Hnum	Htel	Hera	0.0106	0.003138	3.376	best	65784	64405	6671421	0.0093	0.004683	1.982	best	31562	32153	3242509
Etal	Htel	Hera	Htim	0.7373	0.003179	100	-	64393	425847	6671421	0.7405	0.002888	100	-	32120	215418	3242509
Etal	Hera	Htel	Htim	0.7345	0.00321	100	-	65189	425847	6671421	0.746	0.002376	100	-	31345	215418	3242509
Etal	Htim	Htel	Hera	0.0061	0.003178	1.934	best	65189	64393	6671421	0.0122	0.00462	2.645	best	31345	32120	3242509
Etal	Htel	Hera	Hcyd	0.7373	0.00321	100	-	64290	425098	6671421	0.741	0.002901	100	-	31986	214989	3242509
Etal	Hera	Htel	Hcyd	0.7343	0.00325	100	-	65131	425098	6671421	0.746	0.002457	100	-	31284	214989	3242509
Etal	Hcyd	Htel	Hera	0.0065	0.003267	1.991	best	65131	64290	6671421	0.0111	0.004901	2.265	best	31284	31986	3242509
Etal	Htel	Hera	Hmel	0.7373	0.003157	100	-	64514	426568	6671421	0.741	0.002913	100	-	32077	215599	3242509
Etal	Hera	Htel	Hmel	0.734	0.003302	100	-	65438	426568	6671421	0.7465	0.002435	100	-	31297	215599	3242509
Etal	Hmel	Htel	Hera	0.0071	0.003304	2.154	best	65438	64514	6671421	0.0123	0.004738	2.599	best	31297	32077	3242509
Etal	Htel	Hhim	HeraHhimHyl	0.0072	0.005164	1.394	best	21533	21227	6671421	0.0046	0.006698	0.685	best	10147	10242	3242509
Etal	Hhim	Htel	HeraHhimHyl	0.8695	0.003494	100	-	303977	21227	6671421	0.8691	0.003494	100	-	146247	10242	3242509
Etal	HeraHhimHyl	Htel	Hhim	0.8677	0.00407	100	-	303977	21533	6671421	0.8703	0.004004	100	-	146247	10147	3242509
Etal	Htel	Hhim	Hsar	0.0898	0.007122	12.603	best	86199	103195	6671421	0.08	0.005203	15.383	best	42533	49931	3242509
Etal	Hhim	Htel	Hsar	0.1876	0.0055	34.106	-	70600	103195	6671421	0.1765	0.005515	31.997	-	34954	49931	3242509
Etal	Hsar	Htel	Hhim	0.0995	0.004757	20.915	-	70600	86199	6671421	0.0978	0.003961	24.694	-	34954	42533	3242509
Etal	Htel	Hhim	Hdem	0.0021	0.008548	0.248	best	85374	85730	6671421	0.0127	0.00637	1.993	best	42177	41116	3242509
Etal	Hhim	Htel	Hdem	0.1083	0.007272	14.888	-	68989	85730	6671421	0.0952	0.00633	15.039	-	33972	41116	3242509
Etal	Hdem	Htel	Hhim	0.1062	0.004938	21.5	-	68989	85374	6671421	0.1078	0.00421	25.596	-	33972	42177	3242509
Etal	Htel	Hhim	Ldor	0.7377	0.003125	100	-	66614	441335	6671421	0.759	0.002168	100	-	31948	233151	3242509
Etal	Hhim	Htel	Ldor	0.7405	0.003264	100	-	65803	441335	6671421	0.766	0.0023	100	-	30890	233151	3242509
Etal	Ldor	Htel	Hhim	0.0061	0.003235	1.894	best	65803	66614	6671421	0.0168	0.004005	4.205	best	30890	31948	3242509
Etal	Htel	Hhim	Hbes	0.7376	0.003238	100	-	64990	430381	6671421	0.744	0.002447	100	-	31998	218022	3242509
Etal	Hhim	Htel	Hbes	0.7333	0.003042	100	-	66222	430381	6671421	0.7457	0.002298	100	-	31764	218022	3242509
Etal	Hbes	Htel	Hhim	0.0094	0.002934	3.201	best	66222	64990	6671421	0.0037	0.004679	0.785	best	31764	31998	3242509
Etal	Htel	Hhim	Hpar	0.7382	0.003144	100	-	64426	427669	6671421	0.7446	0.002584	100	-	31647	216175	3242509
Etal	Hhim	Htel	Hpar	0.7324	0.00301	100	-	66074	427669	6671421	0.7448	0.002317	100	-	31620	216175	3242509
Etal	Hpar	Htel	Hhim	0.0126	0.002439	5.178	best	66074	64426	6671421	0.0004	0.004664	0.093	best	31620	31647	3242509
Etal	Htel	Hhim	Hnum	0.7379	0.003306	100	-	64153	425370	6671421	0.7445	0.002432	100	-	31530	215265	3242509
Etal	Hhim	Htel	Hnum	0.7323	0.003183	100	-	65733	425370	6671421	0.7454	0.002273	100	-	31402	215265	3242509
Etal	Hnum	Htel	Hhim	0.0122	0.002694	4.515	best	65733	64153	6671421	0.002	0.004456	0.457	best	31402	31530	3242509
Etal	Htel	Hhim	Htim	0.7384	0.003251	100	-	64071	425753	6671421	0.7453	0.002491	100	-	31467	215634	3242509
Etal	Hhim	Htel	Htim	0.734	0.003052	100	-	65308	425753	6671421	0.7465	0.002299	100	-	31303	215634	3242509
Etal	Htim	Htel	Hhim	0.0096	0.002906	3.291	best	65308	64071	6671421	0.0026	0.00442	0.592	best	31303	31467	3242509
Etal	Htel	Hhim	Hcyd	0.7382	0.00324	100	-	64019	425055	6671421	0.7457	0.002487	100	-	31348	215220	3242509
Etal	Hhim	Htel	Hcyd	0.7343	0.003122	100	-	65127	425055	6671421	0.7467	0.00235	100	-	31212	215220	3242509
Etal	Hcyd	Htel	Hhim	0.0086	0.002977	2.883	best	65127	64019	6671421	0.0022	0.004708	0.462	best	31212	31348	3242509

Etal	Htel	Hhim	Hmel	0.7383	0.003143	100	-	64204	426486	6671421	0.7458	0.002465	100	-	31428	215819	3242509
Etal	Hhim	Htel	Hmel	0.734	0.003101	100	-	65430	426486	6671421	0.7473	0.002327	100	-	31221	215819	3242509
Etal	Hmel	Htel	Hhim	0.0095	0.002686	3.522	best	65430	64204	6671421	0.0033	0.004506	0.734	best	31221	31428	3242509
Etal	Htel	HeraHhimHy	Hsar	0.0914	0.007569	12.072	best	86047	103349	6671421	0.0788	0.005949	13.251	best	42684	49987	3242509
Etal	HeraHhimHyl	Htel	Hsar	0.1887	0.005948	31.733	-	70534	103349	6671421	0.1766	0.005723	30.862	-	34983	49987	3242509
Etal	Hsar	Htel	HeraHhimHyl	0.0991	0.00488	20.306	-	70534	86047	6671421	0.0992	0.004248	23.341	-	34983	42684	3242509
Etal	Htel	HeraHhimHy	Hdem	0.0039	0.00916	0.427	best	85266	85928	6671421	0.0138	0.0073	1.89	best	42342	41186	3242509
Etal	HeraHhimHyl	Htel	Hdem	0.1099	0.007671	14.332	-	68913	85928	6671421	0.0964	0.006811	14.151	-	33948	41186	3242509
Etal	Hdem	Htel	HeraHhimHyl	0.1061	0.004917	21.574	-	68913	85266	6671421	0.11	0.004807	22.89	-	33948	42342	3242509
Etal	Htel	HeraHhimHy	Ldor	0.7383	0.003244	100	-	66490	441517	6671421	0.7587	0.002323	100	-	31981	233089	3242509
Etal	HeraHhimHyl	Htel	Ldor	0.7404	0.003243	100	-	65870	441517	6671421	0.7652	0.002237	100	-	31002	233089	3242509
Etal	Ldor	Htel	HeraHhimHyl	0.0047	0.003137	1.493	best	65870	66490	6671421	0.0155	0.00403	3.858	best	31002	31981	3242509
Etal	Htel	HeraHhimHy	Hbes	0.7382	0.003434	100	-	64857	430554	6671421	0.7434	0.002642	100	-	32092	218021	3242509
Etal	HeraHhimHyl	Htel	Hbes	0.7344	0.003125	100	-	65942	430554	6671421	0.7459	0.002383	100	-	31728	218021	3242509
Etal	Hbes	Htel	HeraHhimHyl	0.0083	0.00329	2.522	best	65942	64857	6671421	0.0057	0.004651	1.228	best	31728	32092	3242509
Etal	Htel	HeraHhimHy	Hpar	0.7387	0.003301	100	-	64320	427869	6671421	0.744	0.00276	100	-	31737	216170	3242509
Etal	HeraHhimHyl	Htel	Hpar	0.7333	0.003126	100	-	65852	427869	6671421	0.7454	0.002297	100	-	31540	216170	3242509
Etal	Hpar	Htel	HeraHhimHyl	0.0118	0.00285	4.131	best	65852	64320	6671421	0.0031	0.004667	0.669	best	31540	31737	3242509
Etal	Htel	HeraHhimHy	Hnum	0.7386	0.003485	100	-	63978	425501	6671421	0.7437	0.002658	100	-	31643	215283	3242509
Etal	HeraHhimHyl	Htel	Hnum	0.733	0.003213	100	-	65561	425501	6671421	0.7457	0.002276	100	-	31357	215283	3242509
Etal	Hnum	Htel	HeraHhimHyl	0.0122	0.002684	4.553	best	65561	63978	6671421	0.0045	0.004613	0.985	best	31357	31643	3242509
Etal	Htel	HeraHhimHy	Htim	0.739	0.003417	100	-	63945	425933	6671421	0.7445	0.002669	100	-	31580	215652	3242509
Etal	HeraHhimHyl	Htel	Htim	0.7348	0.003109	100	-	65129	425933	6671421	0.7464	0.002315	100	-	31317	215652	3242509
Etal	Htim	Htel	HeraHhimHyl	0.0092	0.003109	2.952	best	65129	63945	6671421	0.0042	0.004442	0.943	best	31317	31580	3242509
Etal	Htel	HeraHhimHy	Hcyd	0.739	0.003393	100	-	63835	425177	6671421	0.7451	0.002642	100	-	31442	215219	3242509
Etal	HeraHhimHyl	Htel	Hcyd	0.7353	0.003202	100	-	64868	425177	6671421	0.7472	0.00239	100	-	31147	215219	3242509
Etal	Hcyd	Htel	HeraHhimHyl	0.008	0.003155	2.545	best	64868	63835	6671421	0.0047	0.004536	1.04	best	31147	31442	3242509
Etal	Htel	HeraHhimHy	Hmel	0.7389	0.003338	100	-	64072	426660	6671421	0.7451	0.002675	100	-	31526	215822	3242509
Etal	HeraHhimHyl	Htel	Hmel	0.7347	0.003264	100	-	65272	426660	6671421	0.7475	0.00237	100	-	31187	215822	3242509
Etal	Hmel	Htel	HeraHhimHyl	0.0093	0.003047	3.046	best	65272	64072	6671421	0.0054	0.004628	1.169	best	31187	31526	3242509
Etal	Htel	Hsar	Hdem	0.1427	0.003556	40.131	best	66620	49980	6671421	0.145	0.005177	28.012	best	33393	24934	3242509
Etal	Hsar	Htel	Hdem	0.4939	0.003608	100	-	147531	49980	6671421	0.5001	0.003856	100	-	74829	24934	3242509
Etal	Hdem	Htel	Hsar	0.3778	0.00349	100	-	147531	66620	6671421	0.3829	0.004339	88.236	-	74829	33393	3242509
Etal	Htel	Hsar	Ldor	0.6957	0.002924	100	-	78228	435953	6671421	0.719	0.002642	100	-	37882	231687	3242509
Etal	Hsar	Htel	Ldor	0.734	0.002136	100	-	66872	435953	6671421	0.7579	0.002048	100	-	31903	231687	3242509
Etal	Ldor	Htel	Hsar	0.0783	0.003507	22.314	best	66872	78228	6671421	0.0857	0.003694	23.192	best	31903	37882	3242509
Etal	Htel	Hsar	Hbes	0.6929	0.002908	100	-	77231	425626	6671421	0.7005	0.00292	100	-	38182	216808	3242509
Etal	Hsar	Htel	Hbes	0.7353	0.002109	100	-	64915	425626	6671421	0.7417	0.002217	100	-	32157	216808	3242509
Etal	Hbes	Htel	Hsar	0.0866	0.003828	22.635	best	64915	77231	6671421	0.0857	0.004195	20.42	best	32157	38182	3242509
Etal	Htel	Hsar	Hpar	0.6929	0.002763	100	-	76740	422987	6671421	0.7008	0.003044	100	-	37814	214944	3242509
Etal	Hsar	Htel	Hpar	0.736	0.002323	100	-	64325	422987	6671421	0.7411	0.002412	100	-	31968	214944	3242509
Etal	Hpar	Htel	Hsar	0.088	0.003752	23.455	best	64325	76740	6671421	0.0838	0.004389	19.091	best	31968	37814	3242509
Etal	Htel	Hsar	Hnum	0.692	0.002843	100	-	76605	420826	6671421	0.7003	0.002967	100	-	37732	214069	3242509
Etal	Hsar	Htel	Hnum	0.7365	0.002401	100	-	63858	420826	6671421	0.7414	0.002383	100	-	31797	214069	3242509
Etal	Hnum	Htel	Hsar	0.0907	0.003504	25.901	best	63858	76605	6671421	0.0854	0.003921	21.771	best	31797	37732	3242509
Etal	Htel	Hsar	Htim	0.6928	0.002875	100	-	76416	421102	6671421	0.7011	0.002873	100	-	37676	214445	3242509
Etal	Hsar	Htel	Htim	0.7363	0.002276	100	-	63963	421102	6671421	0.7426	0.002297	100	-	31677	214445	3242509
Etal	Htim	Htel	Hsar	0.0887	0.003863	22.962	best	63963	76416	6671421	0.0865	0.003902	22.171	best	31677	37676	3242509
Etal	Htel	Hsar	Hcyd	0.6927	0.002783	100	-	76321	420361	6671421	0.7012	0.002842	100	-	37605	214079	3242509
Etal	Hsar	Htel	Hcyd	0.7367	0.002284	100	-	63742	420361	6671421	0.743	0.002313	100	-	31561	214079	3242509
Etal	Hcyd	Htel	Hsar	0.0898	0.003759	23.891	best	63742	76321	6671421	0.0874	0.003827	22.835	best	31561	37605	3242509
Etal	Htel	Hsar	Hmel	0.6932	0.002754	100	-	76433	421719	6671421	0.7018	0.00298	100	-	37610	214603	3242509
Etal	Hsar	Htel	Hmel	0.7362	0.00223	100	-	64074	421719	6671421	0.7432	0.002354	100	-	31621	214603	3242509
Etal	Hmel	Htel	Hsar	0.088	0.003789	23.212	best	64074	76433	6671421	0.0865	0.004222	20.49	best	31621	37610	3242509
Etal	Htel	Hdem	Ldor	0.746	0.002043	100	-	63726	438091	6671421	0.7674	0.001932	100	-	30646	232910	3242509
Etal	Hdem	Htel	Ldor	0.7551	0.002076	100	-	61144	438091	6671421	0.7774	0.001814	100	-	29169	232910	3242509
Etal	Ldor	Htel	Hdem	0.0207	0.00278	7.437	best	61144	63726	6671421	0.0247	0.003277	7.537	best	29169	30646	3242509
Etal	Htel	Hdem	Hbes	0.7447	0.002157	100	-	62572	427607	6671421	0.7519	0.002192	100	-	30865	217950	3242509
Etal	Hdem	Htel	Hbes	0.7541	0.001973	100	-	59961	427607	6671421	0.7609	0.001962	100	-	29595	217950	3242509
Etal	Hbes	Htel	Hdem	0.0213	0.00269	7.919	best	59961	62572	6671421	0.021	0.004748	4.424	best	29595	30865	3242509
Etal	Htel	Hdem	Hpar	0.7449	0.002001	100	-	62157	425044	6671421	0.7523	0.002209	100	-	30548	216137	3242509
Etal	Hdem	Htel	Hpar	0.7543	0.001972	100	-	59526	425044	6671421	0.7621	0.001966	100	-	29178	216137	3242509
Etal	Hpar	Htel	Hdem	0.0216	0.002674	8.086	best	59526	62157	6671421	0.0229	0.004079	5.623	best	29178	30548	3242509
Etal	Htel	Hdem	Hnum	0.7441	0.002024	100	-	62060	422921	6671421	0.7521	0.002107	100	-	30457	215253	3242509
Etal	Hdem	Htel	Hnum	0.7544	0.002128	100	-	59207	422921	6671421	0.7619	0.001915	100	-	29090	215253	3242509
Etal	Hnum	Htel	Hdem	0.0235	0.002441	9.638	best	59207	62060	6671421	0.023	0.003787	6.062	best	29090	30457	3242509
Etal	Htel	Hdem	Htim	0.7453	0.002118	100	-	61755	423081	6671421	0.7535	0.002139	100	-	30304	215532	3242509
Etal	Hdem	Htel	Htim	0.7548	0.002099	100	-	59130	423081	6671421	0.7623	0.001914	100	-	29078	215532	3242509
Etal	Htim	Htel	Hdem	0.0217	0.00283	7.672	best	59130	61755	6671421	0.0206	0.003807	5.424	best	29078	30304	3242509
Etal	Htel	Hdem	Hcyd	0.7452	0.002084	100	-	61660	422340	6671421	0.7538	0.002129	100	-	30196	215129	3242509
Etal	Hdem	Htel	Hcyd	0.7546	0.00219	100	-	59084	422340	6671421	0.7623	0.002044	100	-	29020	215129	3242509
Etal	Hcyd	Htel	Hdem	0.0213	0.00295	7.233	best	59084	61660	6671421	0.0199	0.003988	4.979	best	29020	30196	3242509
Etal	Htel	Hdem	Hmel	0.7453	0.00201	100	-	61859	423785	6671421	0.754	0.002226	100	-	30247	215699	3242509
Etal	Hdem	Htel	Hmel	0.755	0.002142	100	-	59165	423785	6671421	0.7633	0.001923	100	-	28962	215699	3242509
Etal	Hmel	Htel	Hdem	0.0223	0.002921	7.622	best	59165	61859	6671421	0.0217	0.003757	5.777	best	28962	30247	3242509
Etal	Htel	Ldor	Hbes	0.0375	0.003423	10.96	best	129023	119693	6671421	0.1128	0.003796	29.718	best	74872	59693	3242509
Etal	Ldor	Htel	Hbes	0.395	0.004535	87.099	-	275941	119693	6671421	0.3873	0.004082	94.892	-	135163	59693	3242509
Etal	Hbes	Htel	Ldor	0.3628	0.004187	86.656	-	275941	129023	6671421	0.2871	0.004001	71.747	-	135163	74872	3242509
Etal	Htel	Ldor	Hpar	0.0468	0.003446	13.584	best	128363	116885	6671421	0.126	0.00354	35.594	best	74514	57839	3242509
Etal	Ldor	Htel	Hpar	0.4034	0.004318	93.418	-	274940	116885	6671421	0.3989	0.003818	100	-	134602	57839	3242509
Etal	Hpar	Htel	Ldor	0.3635	0.003887	93.504	-	274940	128363	6671421	0.2874	0.004009	71.673	-	134602	74514	3242509
Etal	Htel	Ldor	Hnum	0.0557	0.003489	15.967	best	127964	114460	6671421	0.1335	0.004239	31.504	best	74138	56670	3242509
Etal	Ldor	Htel	Hnum	0.4118	0.004349	94.681	-	274692	114460	6671421	0.4071	0.004231	96.207	-	134484	56670	3242509
Etal	Hnum	Htel	Ldor	0.3644	0.003976	91.652	-	274692	127964	6671421	0.2893	0.003933	73.558	-	134484	74138	3242509
Etal	Htel	Ldor	Htim	0.0539	0.00337	15.99	best	127506	114467	6671421	0.1301	0.003813	34.113	best	74013	56977	3242509
Etal	Ldor	Htel	Htim	0.4114	0.004053	100	-	274446	114467	6671421	0.4047	0.004049	99.936	-	134436	56977	3242509
Etal	Htim	Htel	Ldor	0.3656	0.003892	93.928	-	274446	127506	6671421	0.2899	0.004083	70.999	-	134436	74013	3242509
Etal	Htel	Ldor	Hcyd	0.0569	0.003321	17.117	best	127210	113525	6671421	0.1329	0.003646	36.467	best	73846	56515	3242509
Etal	Ldor	Htel	Hcyd	0.4149	0.004154	99.871	-	274502	113525	6671421	0.4078	0.004003	100	-	134360	56515	3242509
Etal	Hcyd	Htel	Ldor	0.3667	0.003938	93.107	-	274502	127210	6671421	0.2907	0.003978	73.061	-	134360	73846	3242509
Etal	Htel	Ldor	Hmel	0.0513	0.003541	14.484	best	127491	115052	6671421	0.1286	0.004013	32.039	best	73790	56978	3242509
Etal	Ldor	Htel	Hmel	0.4094	0.004439	92.219	-	274514	115052	6671421	0.4043	0.00409	98.873	-	134331	56978	3242509
Etal	Hmel	Htel	Ldor	0.3657	0.003881	94.244	-	274514	127491	6671421	0.2909	0.004016	72.443	-	134331	73790	3242509
Etal	Htel	Hbes	Hpar	0.023	0.002419	9.513	best	47735	45587	6671421	0.0328	0.004623	7.09	best	23565	22069	3242509
Etal	Hbes	Htel	Hpar	0.8576	0.001511	100	-	594582	45587	6671421	0.8626	0.002063	100	-	299033	22069	3242509
Etal	Hpar	Htel	Hbes	0.8514	0.001624	100	-	594582	47735	6671421	0.8539	0.002088	100	-	299033	23565	3242509
Etal	Htel	Hbes	Hnum	0.0482	0.003477	13.873	best	45362	41188	6671421	0.0537	0.005083	10.566	best	22453	20164	3242509
Etal	Hbes	Htel	Hnum	0.8725	0.001927	100	-	604627	41188	6671421	0.8757	0.002263	100	-	304130	20164	3242509
Etal	Hnum	Htel	Hbes	0.8604	0.002261	100	-	604627	45362	6671421	0.8625	0.002315	100	-	304130	22453	3242509
Etal	Htel	Hbes	Htim	0.0381	0.003171	12.011	best	50548	46839	6671421	0.0389	0.004189	9.277	best	24816	22959	3242509

Etal	Hbes	Htel	Htim	0.8492	0.001532	100	-	574348	46839	6671421	0.853	0.002027	100	-	289322	22959	3242509
Etal	Htim	Htel	Hbes	0.8382	0.001932	100	-	574348	50548	6671421	0.842	0.002113	100	-	289322	24816	3242509
Etal	Htel	Hbes	Hcyd	0.0447	0.003362	13.308	best	50844	46489	6671421	0.0451	0.004522	9.963	best	24960	22808	3242509
Etal	Hbes	Htel	Hcyd	0.8497	0.001664	100	-	571927	46489	6671421	0.8533	0.002109	100	-	288036	22808	3242509
Etal	Hcyd	Htel	Hbes	0.8367	0.001865	100	-	571927	50844	6671421	0.8405	0.002189	100	-	288036	24960	3242509
Etal	Htel	Hbes	Hmel	0.0316	0.003655	8.658	best	50669	47560	6671421	0.0343	0.005144	6.661	best	24643	23010	3242509
Etal	Hbes	Htel	Hmel	0.8472	0.001797	100	-	574835	47560	6671421	0.8528	0.002109	100	-	289526	23010	3242509
Etal	Hmel	Htel	Hbes	0.838	0.001774	100	-	574835	50669	6671421	0.8431	0.002087	100	-	289526	24643	3242509
Etal	Htel	Hpar	Hnum	0.0259	0.002232	11.608	best	40118	38092	6671421	0.0206	0.00525	3.925	best	19634	18841	3242509
Etal	Hpar	Htel	Hnum	0.8836	0.001659	100	-	616247	38092	6671421	0.8848	0.002121	100	-	308191	18841	3242509
Etal	Hnum	Htel	Hpar	0.8778	0.00181	100	-	616247	40118	6671421	0.8802	0.001952	100	-	308191	19634	3242509
Etal	Htel	Hpar	Htim	0.0189	0.002452	7.695	best	42136	40575	6671421	0.009	0.004564	1.966	best	20297	19936	3242509
Etal	Hpar	Htel	Htim	0.8738	0.002398	100	-	602255	40575	6671421	0.8762	0.002195	100	-	301968	19936	3242509
Etal	Htim	Htel	Hpar	0.8693	0.002502	100	-	602255	42136	6671421	0.8741	0.002242	100	-	301968	20297	3242509
Etal	Htel	Hpar	Hcyd	0.0261	0.003136	8.33	best	43337	41130	6671421	0.016	0.004746	3.375	best	20792	20136	3242509
Etal	Hpar	Htel	Hcyd	0.8708	0.002501	100	-	595299	41130	6671421	0.8736	0.002367	100	-	298460	20136	3242509
Etal	Hcyd	Htel	Hpar	0.8643	0.002532	100	-	595299	43337	6671421	0.8698	0.002299	100	-	298460	20792	3242509
Etal	Htel	Hpar	Hmel	0.0117	0.003487	3.355	best	41564	40603	6671421	0.0035	0.005162	0.676	best	19712	19575	3242509
Etal	Hpar	Htel	Hmel	0.8743	0.002146	100	-	605381	40603	6671421	0.8789	0.002162	100	-	303598	19575	3242509
Etal	Hmel	Htel	Hpar	0.8715	0.002232	100	-	605381	41564	6671421	0.8781	0.002187	100	-	303598	19712	3242509
Etal	Htel	Hnum	Htim	0.0054	0.002479	2.174	best	42938	43403	6671421	0.0103	0.005446	1.884	best	20828	21260	3242509
Etal	Hnum	Htel	Htim	0.8618	0.001698	100	-	584601	43403	6671421	0.8652	0.001753	100	-	294029	21260	3242509
Etal	Htim	Htel	Hnum	0.8632	0.001757	100	-	584601	42938	6671421	0.8677	0.001963	100	-	294029	20828	3242509
Etal	Htel	Hnum	Hcyd	0.0021	0.003181	0.655	best	43497	43316	6671421	0.0032	0.004798	0.675	best	21058	21195	3242509
Etal	Hnum	Htel	Hcyd	0.8611	0.001705	100	-	580265	43316	6671421	0.8646	0.00177	100	-	291898	21195	3242509
Etal	Hcyd	Htel	Hnum	0.8605	0.001617	100	-	580265	43497	6671421	0.8654	0.001904	100	-	291898	21058	3242509
Etal	Htel	Hnum	Hmel	0.0123	0.00387	3.175	best	42845	43910	6671421	0.0158	0.004767	3.306	best	20498	21154	3242509
Etal	Hnum	Htel	Hmel	0.8606	0.001906	100	-	585806	43910	6671421	0.866	0.001888	100	-	294654	21154	3242509
Etal	Hmel	Htel	Hnum	0.8637	0.001603	100	-	585806	42845	6671421	0.8699	0.001876	100	-	294654	20498	3242509
Etal	Htel	Htim	Hcyd	0.0123	0.004388	2.813	best	26534	25888	6671421	0.0117	0.00592	1.983	best	12695	12400	3242509
Etal	Htim	Htel	Hcyd	0.9258	0.002286	100	-	672175	25888	6671421	0.9291	0.002093	100	-	337137	12400	3242509
Etal	Hcyd	Htel	Htim	0.9241	0.002364	100	-	672175	26534	6671421	0.9274	0.002028	100	-	337137	12695	3242509
Etal	Htel	Htim	Hmel	0.0105	0.005572	1.887	best	28138	28738	6671421	0.0081	0.006521	1.242	best	13716	13940	3242509
Etal	Htim	Htel	Hmel	0.9171	0.001799	100	-	664062	28738	6671421	0.9193	0.001655	100	-	331329	13940	3242509
Etal	Hmel	Htel	Htim	0.9187	0.001895	100	-	664062	28138	6671421	0.9205	0.001643	100	-	331329	13716	3242509
Etal	Htel	Hcyd	Hmel	0.0219	0.004473	4.901	best	27779	29025	6671421	0.0189	0.006343	2.972	best	13499	14018	3242509
Etal	Hcyd	Htel	Hmel	0.916	0.001638	100	-	661642	29025	6671421	0.9185	0.001577	100	-	329879	14018	3242509
Etal	Hmel	Htel	Hcyd	0.9194	0.00167	100	-	661642	27779	6671421	0.9214	0.001606	100	-	329879	13499	3242509
Etal	Hhsa	Hera	Hhim	0.0055	0.003708	1.474	best	38612	38192	6671421	0.0236	0.005216	4.53	best	19047	18167	3242509
Etal	Hera	Hhsa	Hhim	0.6825	0.003872	100	-	202350	38192	6671421	0.6865	0.004007	100	-	97740	18167	3242509
Etal	Hhim	Hhsa	Hera	0.6795	0.003556	100	-	202350	38612	6671421	0.6738	0.003433	100	-	97740	19047	3242509
Etal	Hhsa	Hera	HeraHhimHyl	0.0105	0.004143	2.543	best	28463	27866	6671421	0.0314	0.005565	5.646	best	14107	13247	3242509
Etal	Hera	Hhsa	HeraHhimHyl	0.7952	0.007666	100	-	244199	27866	6671421	0.7985	0.005822	100	-	118200	13247	3242509
Etal	HeraHhimHyl	Hhsa	Hera	0.7913	0.006875	100	-	244199	28463	6671421	0.7868	0.005823	100	-	118200	14107	3242509
Etal	Hhsa	Hera	Hsar	0.2262	0.017942	12.609	best	84849	134452	6671421	0.2063	0.012366	16.681	best	42241	64193	3242509
Etal	Hera	Hhsa	Hsar	0.3618	0.009951	36.364	-	63018	134452	6671421	0.3408	0.007148	47.672	-	31566	64193	3242509
Etal	Hsar	Hhsa	Hera	0.1478	0.008539	17.304	-	63018	84849	6671421	0.1447	0.006436	22.481	-	31566	42241	3242509
Etal	Hhsa	Hera	Hdem	0.165	0.019265	8.567	best	83862	117010	6671421	0.1435	0.013448	10.673	best	41658	55618	3242509
Etal	Hera	Hhsa	Hdem	0.3125	0.011035	28.317	-	61308	117010	6671421	0.2881	0.007869	36.612	-	30743	55618	3242509
Etal	Hdem	Hhsa	Hera	0.1555	0.008453	18.395	-	61308	83862	6671421	0.1508	0.006536	23.077	-	30743	41658	3242509
Etal	Hhsa	Hera	Ldor	0.7704	0.00225	100	-	61771	476173	6671421	0.7871	0.001866	100	-	29705	249384	3242509
Etal	Hera	Hhsa	Ldor	0.7694	0.002515	100	-	62064	476173	6671421	0.787	0.001604	100	-	29728	249384	3242509
Etal	Ldor	Hhsa	Hera	0.0024	0.003008	0.786	best	62064	61771	6671421	0.0004	0.003607	0.106	best	29728	29705	3242509
Etal	Hhsa	Hera	Hbes	0.7707	0.002084	100	-	60224	465124	6671421	0.7736	0.002208	100	-	29908	234305	3242509
Etal	Hera	Hhsa	Hbes	0.7649	0.002243	100	-	61962	465124	6671421	0.7695	0.00179	100	-	30519	234305	3242509
Etal	Hbes	Hhsa	Hera	0.0142	0.002601	5.468	best	61962	60224	6671421	0.0101	0.00423	2.389	best	30519	29908	3242509
Etal	Hhsa	Hera	Hpar	0.7713	0.002192	100	-	59682	462164	6671421	0.7744	0.002232	100	-	29560	232445	3242509
Etal	Hera	Hhsa	Hpar	0.7645	0.00238	100	-	61693	462164	6671421	0.7696	0.001886	100	-	30268	232445	3242509
Etal	Hpar	Hhsa	Hera	0.0166	0.002475	6.696	best	61693	59682	6671421	0.0118	0.004084	2.897	best	30268	29560	3242509
Etal	Hhsa	Hera	Hnum	0.7715	0.002334	100	-	59330	459953	6671421	0.7741	0.002227	100	-	29477	231505	3242509
Etal	Hera	Hhsa	Hnum	0.7636	0.002375	100	-	61657	459953	6671421	0.7695	0.001738	100	-	30156	231505	3242509
Etal	Hnum	Hhsa	Hera	0.0192	0.002981	6.451	best	61657	59330	6671421	0.0114	0.00417	2.729	best	30156	29477	3242509
Etal	Hhsa	Hera	Htim	0.7711	0.002325	100	-	59526	460541	6671421	0.7742	0.002337	100	-	29526	232042	3242509
Etal	Hera	Hhsa	Htim	0.7654	0.002417	100	-	61197	460541	6671421	0.7705	0.001843	100	-	30077	232042	3242509
Etal	Htim	Hhsa	Hera	0.0138	0.002616	5.291	best	61197	59526	6671421	0.0092	0.004237	2.18	best	30077	29526	3242509
Etal	Hhsa	Hera	Hcyd	0.7715	0.002234	100	-	59321	459809	6671421	0.7749	0.002229	100	-	29379	231622	3242509
Etal	Hera	Hhsa	Hcyd	0.7652	0.00245	100	-	61156	459809	6671421	0.7705	0.001732	100	-	30025	231622	3242509
Etal	Hcyd	Hhsa	Hera	0.0152	0.002441	6.242	best	61156	59321	6671421	0.0109	0.004128	2.633	best	30025	29379	3242509
Etal	Hhsa	Hera	Hmel	0.7716	0.002254	100	-	59461	461229	6671421	0.7757	0.002204	100	-	29329	232229	3242509
Etal	Hera	Hhsa	Hmel	0.765	0.002511	100	-	61413	461229	6671421	0.771	0.001837	100	-	30035	232229	3242509
Etal	Hmel	Hhsa	Hera	0.0162	0.002535	6.373	best	61413	59461	6671421	0.0119	0.004152	2.864	best	30035	29329	3242509
Etal	Hhsa	Hhim	HeraHhimHyl	0.0039	0.004647	0.849	best	22713	22536	6671421	0.0009	0.006001	0.147	best	10752	10772	3242509
Etal	Hhim	Hhsa	HeraHhimHyl	0.844	0.003011	100	-	266408	22536	6671421	0.8458	0.003986	100	-	128874	10772	3242509
Etal	HeraHhimHyl	Hhsa	Hhim	0.8429	0.003681	100	-	266408	22713	6671421	0.846	0.004277	100	-	128874	10752	3242509
Etal	Hhsa	Hhim	Hsar	0.2289	0.017858	12.818	best	84273	134296	6671421	0.216	0.012391	17.434	best	41437	64269	3242509
Etal	Hhim	Hhsa	Hsar	0.3627	0.010159	35.699	-	62823	134296	6671421	0.3438	0.007314	47.003	-	31389	64269	3242509
Etal	Hsar	Hhsa	Hhim	0.1459	0.008411	17.351	-	62823	84273	6671421	0.138	0.006012	22.958	-	31389	41437	3242509
Etal	Hhsa	Hhim	Hdem	0.168	0.019161	8.767	best	83144	116712	6671421	0.154	0.013467	11.437	best	40764	55604	3242509
Etal	Hhim	Hhsa	Hdem	0.3129	0.011116	28.151	-	61093	116712	6671421	0.2908	0.007994	36.376	-	30557	55604	3242509
Etal	Hdem	Hhsa	Hhim	0.153	0.008519	17.96	-	61093	83144	6671421	0.1432	0.006359	22.516	-	30557	40764	3242509
Etal	Hhsa	Hhim	Ldor	0.7718	0.002222	100	-	61333	476155	6671421	0.7913	0.001671	100	-	29090	249649	3242509
Etal	Hhim	Hhsa	Ldor	0.7704	0.002484	100	-	61745	476155	6671421	0.7887	0.00178	100	-	29485	249649	3242509
Etal	Ldor	Hhsa	Hhim	0.0033	0.003267	1.025	best	61745	61333	6671421	0.0067	0.003826	1.763	best	29485	29090	3242509
Etal	Hhsa	Hhim	Hbes	0.7719	0.001979	100	-	59884	465204	6671421	0.7782	0.001944	100	-	29261	234538	3242509
Etal	Hhim	Hhsa	Hbes	0.7642	0.00224	100	-	62167	465204	6671421	0.7707	0.001819	100	-	30377	234538	3242509
Etal	Hbes	Hhsa	Hhim	0.0187	0.002497	7.494	best	62167	59884	6671421	0.0187	0.004367	4.285	best	30377	29261	3242509
Etal	Hhsa	Hhim	Hpar	0.7723	0.002091	100	-	59406	462308	6671421	0.7789	0.001954	100	-	28922	232687	3242509
Etal	Hhim	Hhsa	Hpar	0.7641	0.002439	100	-	61835	462308	6671421	0.7701	0.001941	100	-	30229	232687	3242509
Etal	Hpar	Hhsa	Hhim	0.02	0.002615	7.665	best	61835	59406	6671421	0.0221	0.004477	4.936	best	30229	28922	3242509
Etal	Hhsa	Hhim	Hnum	0.7726	0.002202	100	-	59037	460080	6671421	0.7788	0.001952	100	-	28810	231718	3242509
Etal	Hhim	Hhsa	Hnum	0.764	0.002309	100	-	61565	460080	6671421	0.7711	0.001836	100	-	29952	231718	3242509
Etal	Hnum	Hhsa	Hhim	0.021	0.002956	7.092	best	61565	59037	6671421	0.0194	0.004463	4.353	best	29952	28810	3242509
Etal	Hhsa	Hhim	Htim	0.7724	0.002189	100	-	59158	460593	6671421	0.779	0.002017	100	-	28848	232244	3242509
Etal	Hhim	Hhsa	Htim	0.7652	0.002395	100	-	61270	460593	6671421	0.7711	0.001879	100	-	30010	232244	3242509
Etal	Htim	Hhsa	Hhim	0.0175	0.002862	6.13	best	61270	59158	6671421	0.0197	0.004435	4.451	best	30010	28848	3242509
Etal	Hhsa	Hhim	Hcyd	0.7726	0.002127	100	-	59002	459910	6671421	0.7795	0.001907	100	-	28726	231849	3242509
Etal	Hhim	Hhsa	Hcyd	0.7654	0.002469	100	-	61104	459910	6671421	0.7713	0.001858	100	-	29938	231849	3242509
Etal	Hcyd	Hhsa	Hhim	0.0175	0.002876	6.089	best	61104	59002	6671421	0.0207	0.004334	4.767	best	29938	28726	3242509
Etal	Hhsa	Hhim	Hmel	0.7729	0.002113	100	-	59101	461289	6671421	0.7805	0.001925	100	-	28660	232440	3242509
Etal	Hhim	Hhsa	Hmel	0.7652	0.00243	100	-	61355	461289	6671421	0.7718	0.001877	100	-	29939	232440	3242509

Etal	Hmel	Hhsa	Hhim	0.0187	0.002535	7.383	best	61355	59101	6671421	0.0218	0.004504	4.845	best	29939	28660	3242509
Etal	Hhsa	HeraHhimHyl	Hsar	0.2298	0.01783	12.888	best	84150	134350	6671421	0.2152	0.012384	17.381	best	41592	64404	3242509
Etal	HeraHhimHyl	Hhsa	Hsar	0.3631	0.010264	35.379	-	62786	134350	6671421	0.3442	0.007278	47.3	-	31422	64404	3242509
Etal	Hsar	Hhsa	HeraHhimHyl	0.1455	0.008366	17.393	-	62786	84150	6671421	0.1393	0.00641	21.739	-	31422	41592	3242509
Etal	Hhsa	HeraHhimHyl	Hdem	0.1689	0.019172	8.809	best	83046	116791	6671421	0.1533	0.013477	11.375	best	40937	55757	3242509
Etal	HeraHhimHyl	Hhsa	Hdem	0.3137	0.01131	27.737	-	61027	116791	6671421	0.2923	0.007903	36.984	-	30541	55757	3242509
Etal	Hdem	Hhsa	HeraHhimHyl	0.153	0.008199	18.655	-	61027	83046	6671421	0.1455	0.006485	22.437	-	30541	40937	3242509
Etal	Hhsa	HeraHhimHyl	Ldor	0.7723	0.002055	100	-	61167	476166	6671421	0.7912	0.001652	100	-	29103	249642	3242509
Etal	HeraHhimHyl	Hhsa	Ldor	0.7704	0.002527	100	-	61770	476166	6671421	0.7881	0.001787	100	-	29577	249642	3242509
Etal	Ldor	Hhsa	HeraHhimHyl	0.0049	0.003095	1.587	best	61770	61167	6671421	0.0081	0.004129	1.957	best	29577	29103	3242509
Etal	Hhsa	HeraHhimHyl	Hbes	0.7727	0.001898	100	-	59638	465135	6671421	0.7777	0.001989	100	-	29331	234588	3242509
Etal	HeraHhimHyl	Hhsa	Hbes	0.7655	0.002158	100	-	61774	465135	6671421	0.7711	0.001907	100	-	30317	234588	3242509
Etal	Hbes	Hhsa	HeraHhimHyl	0.0176	0.002753	6.392	best	61774	59638	6671421	0.0165	0.00443	3.731	best	30317	29331	3242509
Etal	Hhsa	HeraHhimHyl	Hpar	0.7731	0.001975	100	-	59163	462242	6671421	0.7786	0.002023	100	-	28970	232715	3242509
Etal	HeraHhimHyl	Hhsa	Hpar	0.7652	0.002467	100	-	61476	462242	6671421	0.7709	0.001982	100	-	30107	232715	3242509
Etal	Hpar	Hhsa	HeraHhimHyl	0.0192	0.002781	6.898	best	61476	59163	6671421	0.0192	0.004418	4.356	best	30107	28970	3242509
Etal	Hhsa	HeraHhimHyl	Hnum	0.7735	0.002089	100	-	58744	459964	6671421	0.7783	0.002034	100	-	28904	231792	3242509
Etal	HeraHhimHyl	Hhsa	Hnum	0.7649	0.002268	100	-	61275	459964	6671421	0.7716	0.001889	100	-	29888	231792	3242509
Etal	Hnum	Hhsa	HeraHhimHyl	0.0211	0.002849	7.403	best	61275	58744	6671421	0.0167	0.004523	3.7	best	29888	28904	3242509
Etal	Hhsa	HeraHhimHyl	Htim	0.7732	0.002077	100	-	58914	460526	6671421	0.7787	0.00208	100	-	28907	232283	3242509
Etal	HeraHhimHyl	Hhsa	Htim	0.7662	0.002378	100	-	60973	460526	6671421	0.7714	0.001946	100	-	29970	232283	3242509
Etal	Htim	Hhsa	HeraHhimHyl	0.0172	0.003153	5.449	best	60973	58914	6671421	0.0181	0.004553	3.964	best	29970	28907	3242509
Etal	Hhsa	HeraHhimHyl	Hcyd	0.7735	0.001975	100	-	58724	459809	6671421	0.7792	0.001937	100	-	28785	231888	3242509
Etal	HeraHhimHyl	Hhsa	Hcyd	0.7666	0.002476	100	-	60751	459809	6671421	0.772	0.001894	100	-	29838	231888	3242509
Etal	Hcyd	Hhsa	HeraHhimHyl	0.017	0.00308	5.51	best	60751	58724	6671421	0.018	0.004258	4.219	best	29838	28785	3242509
Etal	Hhsa	HeraHhimHyl	Hmel	0.7737	0.002012	100	-	58849	461214	6671421	0.7801	0.001972	100	-	28711	232471	3242509
Etal	HeraHhimHyl	Hhsa	Hmel	0.7661	0.002513	100	-	61077	461214	6671421	0.7724	0.001927	100	-	29858	232471	3242509
Etal	Hmel	Hhsa	HeraHhimHyl	0.0186	0.002771	6.707	best	61077	58849	6671421	0.0196	0.004459	4.392	best	29858	28711	3242509
Etal	Hhsa	Hsar	Hdem	0.1332	0.003745	35.571	best	69992	53537	6671421	0.1334	0.004365	30.548	best	33962	25970	3242509
Etal	Hsar	Hhsa	Hdem	0.4614	0.006919	66.679	-	145237	53537	6671421	0.4773	0.004998	95.5	-	73396	25970	3242509
Etal	Hdem	Hhsa	Hsar	0.3496	0.00674	51.871	-	145237	69992	6671421	0.3673	0.005213	70.468	-	73396	33962	3242509
Etal	Hhsa	Hsar	Ldor	0.6949	0.003823	100	-	80097	444896	6671421	0.7217	0.003041	100	-	38133	235860	3242509
Etal	Hsar	Hhsa	Ldor	0.7282	0.003117	100	-	69964	444896	6671421	0.7506	0.00244	100	-	33607	235860	3242509
Etal	Ldor	Hhsa	Hsar	0.0675	0.003512	19.228	best	69964	80097	6671421	0.0631	0.003458	18.244	best	33607	38133	3242509
Etal	Hhsa	Hsar	Hbes	0.6917	0.004003	100	-	79209	434506	6671421	0.7029	0.003283	100	-	38559	221004	3242509
Etal	Hsar	Hhsa	Hbes	0.7296	0.003268	100	-	67944	434506	6671421	0.7341	0.0027	100	-	33884	221004	3242509
Etal	Hbes	Hhsa	Hsar	0.0766	0.003562	21.495	best	67944	79209	6671421	0.0645	0.003342	19.313	best	33884	38559	3242509
Etal	Hhsa	Hsar	Hpar	0.6912	0.003937	100	-	78829	431708	6671421	0.703	0.003398	100	-	38218	219151	3242509
Etal	Hsar	Hhsa	Hpar	0.7307	0.003478	100	-	67195	431708	6671421	0.7334	0.002845	100	-	33706	219151	3242509
Etal	Hpar	Hhsa	Hsar	0.0797	0.003301	24.14	best	67195	78829	6671421	0.0627	0.003602	17.417	best	33706	38218	3242509
Etal	Hhsa	Hsar	Hnum	0.6908	0.003991	100	-	78576	429596	6671421	0.7025	0.003284	100	-	38128	218204	3242509
Etal	Hsar	Hhsa	Hnum	0.731	0.003415	100	-	66777	429596	6671421	0.7341	0.002858	100	-	33463	218204	3242509
Etal	Hnum	Hhsa	Hsar	0.0812	0.003344	24.275	best	66777	78576	6671421	0.0652	0.003112	20.941	best	33463	38128	3242509
Etal	Hhsa	Hsar	Htim	0.6911	0.004034	100	-	78548	429960	6671421	0.703	0.003305	100	-	38139	218703	3242509
Etal	Hsar	Hhsa	Htim	0.7305	0.003353	100	-	66970	429960	6671421	0.7346	0.002712	100	-	33466	218703	3242509
Etal	Htim	Hhsa	Hsar	0.0796	0.003408	23.346	best	66970	78548	6671421	0.0653	0.003332	19.59	best	33466	38139	3242509
Etal	Hhsa	Hsar	Hcyd	0.6915	0.003999	100	-	78285	429170	6671421	0.7034	0.003258	100	-	38011	218302	3242509
Etal	Hsar	Hhsa	Hcyd	0.731	0.003347	100	-	66700	429170	6671421	0.7352	0.002797	100	-	33315	218302	3242509
Etal	Hcyd	Hhsa	Hsar	0.0799	0.003234	24.71	best	66700	78285	6671421	0.0658	0.003144	20.944	best	33315	38011	3242509
Etal	Hhsa	Hsar	Hmel	0.692	0.003934	100	-	78385	430550	6671421	0.7046	0.003347	100	-	37942	218890	3242509
Etal	Hsar	Hhsa	Hmel	0.7305	0.003343	100	-	67054	430550	6671421	0.735	0.002864	100	-	33439	218890	3242509
Etal	Hmel	Hhsa	Hsar	0.0779	0.003417	22.801	best	67054	78385	6671421	0.0631	0.003367	18.738	best	33439	37942	3242509
Etal	Hhsa	Hdem	Ldor	0.744	0.00306	100	-	65602	446856	6671421	0.7679	0.00242	100	-	31092	236811	3242509
Etal	Hdem	Hhsa	Ldor	0.7486	0.00321	100	-	64243	446856	6671421	0.7681	0.002364	100	-	31068	236811	3242509
Etal	Ldor	Hhsa	Hdem	0.0105	0.003269	3.201	best	64243	65602	6671421	0.0004	0.003396	0.115	best	31068	31092	3242509
Etal	Hhsa	Hdem	Hbes	0.7423	0.003286	100	-	64550	436302	6671421	0.7522	0.002745	100	-	31374	221811	3242509
Etal	Hdem	Hhsa	Hbes	0.7477	0.003061	100	-	62990	436302	6671421	0.7516	0.002421	100	-	31454	221811	3242509
Etal	Hbes	Hhsa	Hdem	0.0122	0.00255	4.799	best	62990	64550	6671421	0.0013	0.00421	0.301	best	31454	31374	3242509
Etal	Hhsa	Hdem	Hpar	0.7419	0.003257	100	-	64268	433602	6671421	0.7524	0.002794	100	-	31088	220013	3242509
Etal	Hdem	Hhsa	Hpar	0.7484	0.003087	100	-	62418	433602	6671421	0.7527	0.002514	100	-	31052	220013	3242509
Etal	Hpar	Hhsa	Hdem	0.0146	0.003085	4.737	best	62418	64268	6671421	0.0006	0.004305	0.136	best	31052	31088	3242509
Etal	Hhsa	Hdem	Hnum	0.7416	0.003286	100	-	64032	431507	6671421	0.7522	0.002682	100	-	30974	219042	3242509
Etal	Hdem	Hhsa	Hnum	0.7483	0.003109	100	-	62127	431507	6671421	0.7529	0.002436	100	-	30877	219042	3242509
Etal	Hnum	Hhsa	Hdem	0.0151	0.002899	5.211	best	62127	64032	6671421	0.0016	0.004118	0.383	best	30877	30974	3242509
Etal	Hhsa	Hdem	Htim	0.7422	0.003336	100	-	63897	431764	6671421	0.7533	0.002737	100	-	30885	219441	3242509
Etal	Hdem	Hhsa	Htim	0.7484	0.003082	100	-	62147	431764	6671421	0.7526	0.00231	100	-	30985	219441	3242509
Etal	Htim	Hhsa	Hdem	0.0139	0.003281	4.235	best	62147	63897	6671421	0.0016	0.003927	0.409	best	30985	30885	3242509
Etal	Hhsa	Hdem	Hcyd	0.7427	0.003347	100	-	63629	430969	6671421	0.754	0.002735	100	-	30722	219005	3242509
Etal	Hdem	Hhsa	Hcyd	0.7483	0.003211	100	-	62047	430969	6671421	0.7528	0.002529	100	-	30894	219005	3242509
Etal	Hcyd	Hhsa	Hdem	0.0126	0.00314	4.012	best	62047	63629	6671421	0.0028	0.003958	0.704	best	30894	30722	3242509
Etal	Hhsa	Hdem	Hmel	0.7428	0.003283	100	-	63835	432455	6671421	0.7546	0.002785	100	-	30723	219663	3242509
Etal	Hdem	Hhsa	Hmel	0.7486	0.003219	100	-	62169	432455	6671421	0.7532	0.002468	100	-	30924	219663	3242509
Etal	Hmel	Hhsa	Hdem	0.0132	0.002948	4.487	best	62169	63835	6671421	0.0033	0.003837	0.848	best	30924	30723	3242509
Etal	Hhsa	Ldor	Hbes	0.0377	0.003342	11.282	best	130775	121273	6671421	0.1126	0.003759	29.957	best	75499	60217	3242509
Etal	Ldor	Hhsa	Hbes	0.3937	0.004498	87.521	-	278744	121273	6671421	0.3898	0.003943	98.862	-	137140	60217	3242509
Etal	Hbes	Hhsa	Ldor	0.3613	0.004178	86.49	-	278744	130775	6671421	0.2899	0.003836	75.575	-	137140	75499	3242509
Etal	Hhsa	Ldor	Hpar	0.048	0.00341	14.072	best	130186	118266	6671421	0.1258	0.003462	36.331	best	75151	58357	3242509
Etal	Ldor	Hhsa	Hpar	0.4024	0.004294	93.719	-	277544	118266	6671421	0.4013	0.003673	100	-	136573	58357	3242509
Etal	Hpar	Hhsa	Ldor	0.3614	0.003935	91.837	-	277544	130186	6671421	0.2901	0.003784	76.663	-	136573	75151	3242509
Etal	Hhsa	Ldor	Hnum	0.0562	0.003519	15.962	best	129562	115783	6671421	0.1338	0.004156	32.201	best	74767	57116	3242509
Etal	Ldor	Hhsa	Hnum	0.4108	0.004269	96.237	-	277238	115783	6671421	0.4097	0.004059	100	-	136383	57116	3242509
Etal	Hnum	Hhsa	Ldor	0.363	0.004116	88.205	-	277238	129562	6671421	0.2918	0.003767	77.467	-	136383	74767	3242509
Etal	Hhsa	Ldor	Htim	0.0546	0.003469	15.746	best	129248	115861	6671421	0.1299	0.00368	35.303	best	74632	57469	3242509
Etal	Ldor	Hhsa	Htim	0.4103	0.004077	100	-	277063	115861	6671421	0.4071	0.003926	100	-	136381	57469	3242509
Etal	Htim	Hhsa	Ldor	0.3638	0.004013	90.661	-	277063	129248	6671421	0.2926	0.003943	74.224	-	136381	74632	3242509
Etal	Hhsa	Ldor	Hcyd	0.0571	0.00339	16.834	best	128885	114971	6671421	0.1327	0.003561	37.265	best	74414	56978	3242509
Etal	Ldor	Hhsa	Hcyd	0.4136	0.004117	100	-	277171	114971	6671421	0.4103	0.003823	100	-	136276	56978	3242509
Etal	Hcyd	Hhsa	Ldor	0.3652	0.003963	92.142	-	277171	128885	6671421	0.2936	0.003808	77.098	-	136276	74414	3242509
Etal	Hhsa	Ldor	Hmel	0.0514	0.003644	14.116	best	129121	116487	6671421	0.1274	0.003905	32.63	best	74237	57458	3242509
Etal	Ldor	Hhsa	Hmel	0.4082	0.004459	91.539	-	277172	116487	6671421	0.4068	0.003979	100	-	136264	57458	3242509
Etal	Hmel	Hhsa	Ldor	0.3644	0.004024	90.552	-	277172	129121	6671421	0.2947	0.003853	76.488	-	136264	74237	3242509
Etal	Hhsa	Hbes	Hpar	0.0255	0.00291	8.776	best	48558	46140	6671421	0.0328	0.004758	6.893	best	23805	22293	3242509
Etal	Hbes	Hhsa	Hpar	0.8563	0.001552	100	-	596186	46140	6671421	0.8619	0.002023	100	-	300607	22293	3242509
Etal	Hpar	Hhsa	Hbes	0.8494	0.001671	100	-	596186	48558	6671421	0.8533	0.001988	100	-	300607	23805	3242509
Etal	Hhsa	Hbes	Hnum	0.0488	0.004124	11.839	best	45941	41664	6671421	0.0551	0.005408	10.186	best	22686	20317	3242509
Etal	Hbes	Hhsa	Hnum	0.8714	0.00186	100	-	606154	41664	6671421	0.8754	0.002152	100	-	305633	20317	3242509
Etal	Hnum	Hhsa	Hbes	0.8591	0.002222	100	-	606154	45941	6671421	0.8618	0.002251	100	-	305633	22686	3242509
Etal	Hhsa	Hbes	Htim	0.0393	0.004052	9.695	best	51392	47507	6671421	0.039	0.004862	8.012	best	25076	23195	3242509
Etal	Hbes	Hhsa	Htim	0.8476	0.001574	100	-	576067	47507	6671421	0.8523	0.002005	100	-	290908	23195	3242509
Etal	Htim	Hhsa	Hbes	0.8362	0.002003	100	-	576067	51392	6671421	0.8413	0.002014	100	-	290908	25076	3242509

Etal	Hhsa	Hbes	Hcyd	0.0447	0.003214	13.897	best	51589	47177	6671421	0.0447	0.00475	9.411	best	25169	23015	3242509
Etal	Hbes	Hhsa	Hcyd	0.848	0.001712	100	-	573666	47177	6671421	0.8528	0.002039	100	-	289593	23015	3242509
Etal	Hcyd	Hhsa	Hbes	0.835	0.001907	100	-	573666	51589	6671421	0.8401	0.002066	100	-	289593	25169	3242509
Etal	Hhsa	Hbes	Hmel	0.0314	0.003775	8.324	best	51398	48266	6671421	0.0312	0.005413	5.758	best	24760	23263	3242509
Etal	Hbes	Hhsa	Hmel	0.8455	0.001777	100	-	576592	48266	6671421	0.852	0.002105	100	-	291129	23263	3242509
Etal	Hmel	Hhsa	Hbes	0.8363	0.001889	100	-	576592	51398	6671421	0.8432	0.00203	100	-	291129	24760	3242509
Etal	Hhsa	Hpar	Hnum	0.0234	0.00287	8.156	best	40638	38779	6671421	0.022	0.005628	3.909	best	19904	19047	3242509
Etal	Hpar	Hhsa	Hnum	0.8819	0.001716	100	-	617715	38779	6671421	0.8841	0.002074	100	-	309731	19047	3242509
Etal	Hnum	Hhsa	Hpar	0.8766	0.001864	100	-	617715	40638	6671421	0.8792	0.001976	100	-	309731	19904	3242509
Etal	Hhsa	Hpar	Htim	0.0174	0.003127	5.579	best	42778	41311	6671421	0.009	0.004526	1.999	best	20577	20208	3242509
Etal	Hpar	Hhsa	Htim	0.8719	0.002359	100	-	603772	41311	6671421	0.8752	0.002076	100	-	303574	20208	3242509
Etal	Htim	Hhsa	Hpar	0.8677	0.002522	100	-	603772	42778	6671421	0.8731	0.002173	100	-	303574	20577	3242509
Etal	Hhsa	Hpar	Hcyd	0.0233	0.002783	8.362	best	43831	41837	6671421	0.0155	0.004632	3.351	best	20998	20356	3242509
Etal	Hpar	Hhsa	Hcyd	0.869	0.002457	100	-	596787	41837	6671421	0.8729	0.002286	100	-	300014	20356	3242509
Etal	Hcyd	Hhsa	Hpar	0.8632	0.002545	100	-	596787	43831	6671421	0.8692	0.002249	100	-	300014	20998	3242509
Etal	Hhsa	Hpar	Hmel	0.0086	0.004146	2.067	best	42039	41325	6671421	0.0004	0.005125	0.073	best	19823	19838	3242509
Etal	Hpar	Hhsa	Hmel	0.8725	0.002092	100	-	606884	41325	6671421	0.878	0.002077	100	-	305195	19838	3242509
Etal	Hmel	Hhsa	Hpar	0.8705	0.002297	100	-	606884	42039	6671421	0.878	0.002127	100	-	305195	19823	3242509
Etal	Hhsa	Hnum	Htim	0.0045	0.002892	1.546	best	43663	44055	6671421	0.0115	0.005834	1.965	best	21053	21541	3242509
Etal	Hnum	Hhsa	Htim	0.8602	0.001758	100	-	586201	44055	6671421	0.8642	0.001832	100	-	295580	21541	3242509
Etal	Htim	Hhsa	Hnum	0.8614	0.001773	100	-	586201	43663	6671421	0.867	0.001897	100	-	295580	21053	3242509
Etal	Hhsa	Hnum	Hcyd	0.0015	0.003294	0.465	best	44128	43993	6671421	0.005	0.005003	1.008	best	21209	21424	3242509
Etal	Hnum	Hhsa	Hcyd	0.8594	0.001739	100	-	581890	43993	6671421	0.8639	0.001809	100	-	293397	21424	3242509
Etal	Hcyd	Hhsa	Hnum	0.859	0.001671	100	-	581890	44128	6671421	0.8652	0.00183	100	-	293397	21209	3242509
Etal	Hhsa	Hnum	Hmel	0.013	0.004346	2.997	best	43396	44541	6671421	0.0207	0.005054	4.105	best	20585	21457	3242509
Etal	Hnum	Hhsa	Hmel	0.859	0.00188	100	-	587385	44541	6671421	0.8649	0.001905	100	-	296227	21457	3242509
Etal	Hmel	Hhsa	Hnum	0.8624	0.001753	100	-	587385	43396	6671421	0.8701	0.001854	100	-	296227	20585	3242509
Etal	Hhsa	Htim	Hcyd	0.0099	0.004761	2.085	best	26907	26380	6671421	0.0108	0.006491	1.659	best	12791	12518	3242509
Etal	Htim	Hhsa	Hcyd	0.9246	0.002224	100	-	673542	26380	6671421	0.9287	0.00212	100	-	338581	12518	3242509
Etal	Hcyd	Hhsa	Htim	0.9232	0.002396	100	-	673542	26907	6671421	0.9272	0.002046	100	-	338581	12791	3242509
Etal	Hhsa	Htim	Hmel	0.013	0.006292	2.061	best	28568	29321	6671421	0.0137	0.005735	2.395	best	13783	14167	3242509
Etal	Htim	Hhsa	Hmel	0.9156	0.001764	100	-	665520	29321	6671421	0.9184	0.001627	100	-	332882	14167	3242509
Etal	Hmel	Hhsa	Htim	0.9177	0.001918	100	-	665520	28568	6671421	0.9205	0.001614	100	-	332882	13783	3242509
Etal	Hhsa	Hcyd	Hmel	0.0222	0.004743	4.674	best	28212	29492	6671421	0.0237	0.00669	3.546	best	13515	14172	3242509
Etal	Hcyd	Hhsa	Hmel	0.9149	0.001629	100	-	663103	29492	6671421	0.918	0.001553	100	-	331381	14172	3242509
Etal	Hmel	Hhsa	Hcyd	0.9184	0.001678	100	-	663103	28212	6671421	0.9216	0.001611	100	-	331381	13515	3242509
Etal	Hera	Hhim	HeraHhimHyl	0.5877	0.03529	16.652	-	70548	18373	6671421	0.5977	0.023922	24.986	-	33947	8567	3242509
Etal	Hhim	Hera	HeraHhimHyl	0.6854	0.017384	39.425	-	98507	18373	6671421	0.697	0.013045	53.428	-	47976	8567	3242509
Etal	HeraHhimHyl	Hera	Hhim	0.165	0.030225	5.46	best	98507	70548	6671421	0.171	0.027196	6.289	best	47976	33947	3242509
Etal	Hera	Hhim	Hsar	0.7642	0.003753	100	-	36354	271946	6671421	0.7614	0.003263	100	-	17583	129783	3242509
Etal	Hhim	Hera	Hsar	0.762	0.003789	100	-	36735	271946	6671421	0.7539	0.003025	100	-	18210	129783	3242509
Etal	Hsar	Hera	Hhim	0.0052	0.004579	1.139	best	36735	36354	6671421	0.0175	0.005722	3.059	best	18210	17583	3242509
Etal	Hera	Hhim	Hdem	0.7561	0.003894	100	-	35454	255314	6671421	0.7531	0.003337	100	-	17121	121569	3242509
Etal	Hhim	Hera	Hdem	0.7531	0.003978	100	-	35957	255314	6671421	0.7442	0.003338	100	-	17829	121569	3242509
Etal	Hdem	Hera	Hhim	0.007	0.003977	1.771	best	35957	35454	6671421	0.0202	0.00508	3.986	best	17829	17121	3242509
Etal	Hera	Hhim	Ldor	0.8937	0.001268	100	-	34397	612664	6671421	0.903	0.001166	100	-	16066	315295	3242509
Etal	Hhim	Hera	Ldor	0.8933	0.001142	100	-	34516	612664	6671421	0.9009	0.001075	100	-	16438	315295	3242509
Etal	Ldor	Hera	Hhim	0.0017	0.003952	0.436	best	34516	34397	6671421	0.0114	0.006142	1.858	best	16438	16066	3242509
Etal	Hera	Hhim	Hbes	0.8937	0.001223	100	-	33741	601061	6671421	0.8971	0.001094	100	-	16246	299605	3242509
Etal	Hhim	Hera	Hbes	0.8921	0.001134	100	-	34286	601061	6671421	0.8941	0.001195	100	-	16751	299605	3242509
Etal	Hbes	Hera	Hhim	0.008	0.003311	2.418	best	34286	33741	6671421	0.0153	0.004681	3.266	best	16751	16246	3242509
Etal	Hera	Hhim	Hpar	0.8935	0.00132	100	-	33643	598272	6671421	0.8977	0.001129	100	-	16051	297801	3242509
Etal	Hhim	Hera	Hpar	0.8923	0.001222	100	-	34061	598272	6671421	0.8941	0.00117	100	-	16650	297801	3242509
Etal	Hpar	Hera	Hhim	0.0062	0.004023	1.534	best	34061	33643	6671421	0.0183	0.005229	3.5	best	16650	16051	3242509
Etal	Hera	Hhim	Hnum	0.8932	0.001259	100	-	33613	596067	6671421	0.8972	0.001058	100	-	16091	297013	3242509
Etal	Hhim	Hera	Hnum	0.8926	0.001193	100	-	33814	596067	6671421	0.8944	0.001189	100	-	16554	297013	3242509
Etal	Hnum	Hera	Hhim	0.003	0.003533	0.842	best	33814	33613	6671421	0.0142	0.005178	2.737	best	16554	16091	3242509
Etal	Hera	Hhim	Htim	0.894	0.001187	100	-	33404	596906	6671421	0.898	0.001091	100	-	15983	297521	3242509
Etal	Hhim	Hera	Htim	0.8927	0.001223	100	-	33845	596906	6671421	0.8943	0.001215	100	-	16594	297521	3242509
Etal	Htim	Hera	Hhim	0.0066	0.004138	1.586	best	33845	33404	6671421	0.0187	0.005137	3.649	best	16594	15983	3242509
Etal	Hera	Hhim	Hcyd	0.8937	0.001277	100	-	33454	596265	6671421	0.8979	0.001005	100	-	15982	297152	3242509
Etal	Hhim	Hera	Hcyd	0.8929	0.001225	100	-	33721	596265	6671421	0.8945	0.00122	100	-	16548	297152	3242509
Etal	Hcyd	Hera	Hhim	0.004	0.004	0.993	best	33721	33454	6671421	0.0174	0.005229	3.327	best	16548	15982	3242509
Etal	Hera	Hhim	Hmel	0.8938	0.001257	100	-	33508	597482	6671421	0.8982	0.001042	100	-	15969	297736	3242509
Etal	Hhim	Hera	Hmel	0.8929	0.001206	100	-	33810	597482	6671421	0.8947	0.001206	100	-	16542	297736	3242509
Etal	Hmel	Hera	Hhim	0.0045	0.00395	1.135	best	33810	33508	6671421	0.0176	0.004945	3.563	best	16542	15969	3242509
Etal	Hera	HeraHhimHy	Hsar	0.8439	0.006103	100	-	26618	314385	6671421	0.842	0.004441	100	-	12911	150491	3242509
Etal	HeraHhimHyl	Hera	Hsar	0.8414	0.005798	100	-	27085	314385	6671421	0.8363	0.004457	100	-	13416	150491	3242509
Etal	Hsar	Hera	HeraHhimHyl	0.0087	0.004648	1.865	best	27085	26618	6671421	0.0192	0.006373	3.009	best	13416	12911	3242509
Etal	Hera	HeraHhimHy	Hdem	0.8398	0.006273	100	-	25965	298000	6671421	0.8379	0.004644	100	-	12561	142389	3242509
Etal	HeraHhimHyl	Hera	Hdem	0.8367	0.005864	100	-	26500	298000	6671421	0.8318	0.004528	100	-	13080	142389	3242509
Etal	Hdem	Hera	HeraHhimHyl	0.0102	0.004651	2.183	best	26500	25965	6671421	0.0202	0.006365	3.177	best	13080	12561	3242509
Etal	Hera	HeraHhimHy	Ldor	0.9262	0.002539	100	-	25129	655571	6671421	0.933	0.001589	100	-	11652	336261	3242509
Etal	HeraHhimHyl	Hera	Ldor	0.9253	0.002335	100	-	25439	655571	6671421	0.9305	0.001627	100	-	12103	336261	3242509
Etal	Ldor	Hera	HeraHhimHyl	0.0061	0.004581	1.333	best	25439	25129	6671421	0.019	0.007316	2.594	best	12103	11652	3242509
Etal	Hera	HeraHhimHy	Hbes	0.9261	0.002457	100	-	24734	644229	6671421	0.9283	0.001728	100	-	11927	320666	3242509
Etal	HeraHhimHyl	Hera	Hbes	0.9249	0.002349	100	-	25132	644229	6671421	0.9261	0.001801	100	-	12302	320666	3242509
Etal	Hbes	Hera	HeraHhimHyl	0.008	0.004202	1.898	best	25132	24734	6671421	0.0155	0.005889	2.626	best	12302	11927	3242509
Etal	Hera	HeraHhimHy	Hpar	0.926	0.002528	100	-	24668	641472	6671421	0.9289	0.001761	100	-	11764	318894	3242509
Etal	HeraHhimHyl	Hera	Hpar	0.9251	0.002328	100	-	24970	641472	6671421	0.9264	0.001744	100	-	12193	318894	3242509
Etal	Hpar	Hera	HeraHhimHyl	0.0061	0.005187	1.167	best	24970	24668	6671421	0.0179	0.006285	2.844	best	12193	11764	3242509
Etal	Hera	HeraHhimHy	Hnum	0.9261	0.002459	100	-	24528	639157	6671421	0.9285	0.001751	100	-	11792	318094	3242509
Etal	HeraHhimHyl	Hera	Hnum	0.9255	0.002383	100	-	24732	639157	6671421	0.9267	0.001759	100	-	12097	318094	3242509
Etal	Hnum	Hera	HeraHhimHyl	0.0041	0.004516	0.915	best	24732	24528	6671421	0.0127	0.006014	2.119	best	12097	11792	3242509
Etal	Hera	HeraHhimHy	Htim	0.9264	0.002479	100	-	24473	640150	6671421	0.9293	0.001729	100	-	11672	318590	3242509
Etal	HeraHhimHyl	Hera	Htim	0.9252	0.00229	100	-	24861	640150	6671421	0.9263	0.001802	100	-	12184	318590	3242509
Etal	Htim	Hera	HeraHhimHyl	0.0078	0.005319	1.474	best	24861	24473	6671421	0.0214	0.006508	3.296	best	12184	11672	3242509
Etal	Hera	HeraHhimHy	Hcyd	0.9262	0.002417	100	-	24495	639481	6671421	0.9291	0.001707	100	-	11704	318254	3242509
Etal	HeraHhimHyl	Hera	Hcyd	0.9257	0.002277	100	-	24687	639481	6671421	0.9267	0.001754	100	-	12111	318254	3242509
Etal	Hcyd	Hera	HeraHhimHyl	0.0039	0.005331	0.73	best	24687	24495	6671421	0.0171	0.006546	2.607	best	12111	11704	3242509
Etal	Hera	HeraHhimHy	Hmel	0.9263	0.002472	100	-	24520	640669	6671421	0.9294	0.001717	100	-	11673	318820	3242509
Etal	HeraHhimHyl	Hera	Hmel	0.9255	0.002265	100	-	24796	640669	6671421	0.9268	0.001744	100	-	12114	318820	3242509
Etal	Hmel	Hera	HeraHhimHyl	0.0056	0.00486	1.146	best	24796	24520	6671421	0.0185	0.006194	2.99	best	12114	11673	3242509
Etal	Hera	Hsar	Hdem	0.1293	0.003796	34.061	best	68706	52974	6671421	0.1322	0.005032	26.269	best	33195	25443	3242509
Etal	Hsar	Hera	Hdem	0.5173	0.003406	100	-	166505	52974	6671421	0.5331	0.0033	100	-	83544	25443	3242509
Etal	Hdem	Hera	Hsar	0.4158	0.003814	100	-	166505	68706	6671421	0.4313	0.003665	100	-	83544	33195	3242509
Etal	Hera	Hsar	Ldor	0.6656	0.003242	100	-	86082	428757	6671421	0.6965	0.002661	100	-	40760	227789	3242509
Etal	Hsar	Hera	Ldor	0.7	0.002471	100	-	75656	428757	6671421	0.7257	0.002278	100	-	36211	227789	3242509
Etal	Ldor	Hera	Hsar	0.0645	0.003005	21.448	best	75656	86082	6671421	0.0591	0.003212	18.4	best	36211	40760	3242509
Etal	Hera	Hsar	Hbes	0.6578	0.003202	100	-	86307	418035	6671421	0.6725	0.002771	100	-	41669	212828	3242509

Etal	Hsar	Hera	Hbes	0.7016	0.002661	100	-	73304	418035	6671421	0.708	0.002737	100	-	36383	212828	3242509
Etal	Hbes	Hera	Hsar	0.0815	0.003047	26.739	best	73304	86307	6671421	0.0677	0.003626	18.679	best	36383	41669	3242509
Etal	Hera	Hsar	Hpar	0.6562	0.00311	100	-	86218	415255	6671421	0.6719	0.002832	100	-	41390	210940	3242509
Etal	Hsar	Hera	Hpar	0.7025	0.002885	100	-	72573	415255	6671421	0.7073	0.002855	100	-	36170	210940	3242509
Etal	Hpar	Hera	Hsar	0.0859	0.002627	32.706	best	72573	86218	6671421	0.0673	0.003392	19.845	best	36170	41390	3242509
Etal	Hera	Hsar	Hnum	0.6548	0.003133	100	-	86168	413030	6671421	0.6712	0.002776	100	-	41326	210048	3242509
Etal	Hsar	Hera	Hnum	0.703	0.002976	100	-	72042	413030	6671421	0.7075	0.002909	100	-	35982	210048	3242509
Etal	Hnum	Hera	Hsar	0.0893	0.002674	33.392	best	72042	86168	6671421	0.0691	0.00352	19.64	best	35982	41326	3242509
Etal	Hera	Hsar	Htim	0.657	0.003209	100	-	85597	413507	6671421	0.6728	0.002873	100	-	41183	210521	3242509
Etal	Hsar	Hera	Htim	0.7022	0.002803	100	-	72348	413507	6671421	0.7082	0.002922	100	-	35959	210521	3242509
Etal	Htim	Hera	Hsar	0.0839	0.003076	27.27	best	72348	85597	6671421	0.0677	0.003593	18.846	best	35959	41183	3242509
Etal	Hera	Hsar	Hcyd	0.6568	0.003154	100	-	85501	412720	6671421	0.6726	0.0028	100	-	41119	210089	3242509
Etal	Hsar	Hera	Hcyd	0.7027	0.002721	100	-	72081	412720	6671421	0.709	0.002905	100	-	35777	210089	3242509
Etal	Hcyd	Hera	Hsar	0.0852	0.002693	31.62	best	72081	85501	6671421	0.0695	0.003559	19.52	best	35777	41119	3242509
Etal	Hera	Hsar	Hmel	0.657	0.003201	100	-	85709	414091	6671421	0.6735	0.002937	100	-	41101	210668	3242509
Etal	Hsar	Hera	Hmel	0.7023	0.002803	100	-	72426	414091	6671421	0.7089	0.002941	100	-	35892	210668	3242509
Etal	Hmel	Hera	Hsar	0.084	0.00301	27.908	best	72426	85709	6671421	0.0677	0.003654	18.518	best	35892	41101	3242509
Etal	Hera	Hdem	Ldor	0.7142	0.002578	100	-	71701	430108	6671421	0.7426	0.002073	100	-	33764	228545	3242509
Etal	Hdem	Hera	Ldor	0.7199	0.00244	100	-	70049	430108	6671421	0.7429	0.002302	100	-	33717	228545	3242509
Etal	Ldor	Hera	Hdem	0.0117	0.003028	3.849	best	70049	71701	6671421	0.0007	0.003793	0.184	best	33717	33764	3242509
Etal	Hera	Hdem	Hbes	0.708	0.00264	100	-	71662	419122	6671421	0.7214	0.002302	100	-	34551	213462	3242509
Etal	Hdem	Hera	Hbes	0.7195	0.0024	100	-	68364	419122	6671421	0.7251	0.002581	100	-	34020	213462	3242509
Etal	Hbes	Hera	Hdem	0.0236	0.00259	9.097	best	68364	71662	6671421	0.0077	0.004354	1.778	best	34020	34551	3242509
Etal	Hera	Hdem	Hpar	0.7061	0.002603	100	-	71741	416510	6671421	0.7208	0.002322	100	-	34338	211640	3242509
Etal	Hdem	Hera	Hpar	0.7197	0.002511	100	-	67880	416510	6671421	0.726	0.002644	100	-	33594	211640	3242509
Etal	Hpar	Hera	Hdem	0.0277	0.002726	10.148	best	67880	71741	6671421	0.011	0.004279	2.559	best	33594	34338	3242509
Etal	Hera	Hdem	Hnum	0.705	0.00261	100	-	71694	414288	6671421	0.7205	0.002323	100	-	34237	210711	3242509
Etal	Hdem	Hera	Hnum	0.7199	0.002698	100	-	67462	414288	6671421	0.7259	0.002648	100	-	33461	210711	3242509
Etal	Hnum	Hera	Hdem	0.0304	0.002602	11.688	best	67462	71694	6671421	0.0115	0.004399	2.606	best	33461	34237	3242509
Etal	Hera	Hdem	Htim	0.7075	0.002682	100	-	71050	414692	6671421	0.7225	0.002489	100	-	34007	211097	3242509
Etal	Hdem	Hera	Htim	0.7196	0.00259	100	-	67629	414692	6671421	0.7257	0.002676	100	-	33556	211097	3242509
Etal	Htim	Hera	Hdem	0.0247	0.002636	9.362	best	67629	71050	6671421	0.0067	0.004415	1.512	best	33556	34007	3242509
Etal	Hera	Hdem	Hcyd	0.7075	0.002683	100	-	70908	413859	6671421	0.7226	0.00241	100	-	33929	210651	3242509
Etal	Hdem	Hera	Hcyd	0.7196	0.002646	100	-	67491	413859	6671421	0.7259	0.002771	100	-	33455	210651	3242509
Etal	Hcyd	Hera	Hdem	0.0247	0.002576	9.586	best	67491	70908	6671421	0.007	0.004254	1.653	best	33455	33929	3242509
Etal	Hera	Hdem	Hmel	0.7072	0.00272	100	-	71240	415354	6671421	0.7229	0.002473	100	-	33987	211306	3242509
Etal	Hdem	Hera	Hmel	0.72	0.002666	100	-	67622	415354	6671421	0.7265	0.00273	100	-	33482	211306	3242509
Etal	Hmel	Hera	Hdem	0.0261	0.002496	10.441	best	67622	71240	6671421	0.0075	0.00411	1.82	best	33482	33987	3242509
Etal	Hera	Ldor	Hbes	0.0431	0.003848	11.199	best	132495	121548	6671421	0.1165	0.003849	30.261	best	76054	60184	3242509
Etal	Ldor	Hera	Hbes	0.3927	0.004443	88.389	-	278726	121548	6671421	0.3898	0.00387	100	-	137084	60184	3242509
Etal	Hbes	Hera	Ldor	0.3556	0.003953	89.96	-	278726	132495	6671421	0.2863	0.003406	84.064	-	137084	76054	3242509
Etal	Hera	Ldor	Hpar	0.0544	0.003958	13.734	best	132290	118652	6671421	0.1304	0.00362	36.021	best	75762	58283	3242509
Etal	Ldor	Hera	Hpar	0.4012	0.004325	92.754	-	277637	118652	6671421	0.4015	0.003666	100	-	136476	58283	3242509
Etal	Hpar	Hera	Ldor	0.3546	0.003689	96.124	-	277637	132290	6671421	0.2861	0.003405	84.016	-	136476	75762	3242509
Etal	Hera	Ldor	Hnum	0.0638	0.003821	16.704	best	131808	115995	6671421	0.1381	0.004261	32.417	best	75416	57109	3242509
Etal	Ldor	Hera	Hnum	0.4099	0.004335	94.566	-	277157	115995	6671421	0.4096	0.00404	100	-	136353	57109	3242509
Etal	Hnum	Hera	Ldor	0.3554	0.003947	90.05	-	277157	131808	6671421	0.2878	0.003456	83.271	-	136353	75416	3242509
Etal	Hera	Ldor	Htim	0.0597	0.003904	15.296	best	131032	116267	6671421	0.1335	0.003868	34.519	best	75095	57404	3242509
Etal	Ldor	Hera	Htim	0.409	0.004093	99.932	-	277176	116267	6671421	0.4073	0.00395	100	-	136293	57404	3242509
Etal	Htim	Hera	Ldor	0.358	0.003689	97.056	-	277176	131032	6671421	0.2895	0.003603	80.345	-	136293	75095	3242509
Etal	Hera	Ldor	Hcyd	0.0628	0.003927	15.996	best	130776	115320	6671421	0.1368	0.003698	36.988	best	75054	56995	3242509
Etal	Ldor	Hera	Hcyd	0.4125	0.004139	99.661	-	277227	115320	6671421	0.4102	0.003837	100	-	136270	56995	3242509
Etal	Hcyd	Hera	Ldor	0.359	0.003708	96.808	-	277227	130776	6671421	0.2897	0.003508	82.583	-	136270	75054	3242509
Etal	Hera	Ldor	Hmel	0.0577	0.004132	13.956	best	131072	116779	6671421	0.132	0.004109	32.113	best	74892	57430	3242509
Etal	Ldor	Hera	Hmel	0.4072	0.004424	92.034	-	277171	116779	6671421	0.4069	0.003974	100	-	136213	57430	3242509
Etal	Hmel	Hera	Ldor	0.3579	0.003704	96.616	-	277171	131072	6671421	0.2905	0.00354	82.064	-	136213	74892	3242509
Etal	Hera	Hbes	Hpar	0.0281	0.003411	8.252	best	49145	46454	6671421	0.0346	0.00459	7.534	best	24064	22455	3242509
Etal	Hbes	Hera	Hpar	0.8551	0.001526	100	-	594762	46454	6671421	0.8608	0.002028	100	-	300158	22455	3242509
Etal	Hpar	Hera	Hbes	0.8474	0.001626	100	-	594762	49145	6671421	0.8516	0.002021	100	-	300158	24064	3242509
Etal	Hera	Hbes	Hnum	0.055	0.003628	15.161	best	46670	41804	6671421	0.0563	0.004993	11.276	best	22861	20424	3242509
Etal	Hbes	Hera	Hnum	0.8707	0.001887	100	-	604556	41804	6671421	0.8745	0.002193	100	-	305129	20424	3242509
Etal	Hnum	Hera	Hbes	0.8567	0.002114	100	-	604556	46670	6671421	0.8606	0.002274	100	-	305129	22861	3242509
Etal	Hera	Hbes	Htim	0.0384	0.004018	9.559	best	51616	47798	6671421	0.0375	0.005008	7.496	best	25162	23341	3242509
Etal	Hbes	Hera	Htim	0.8464	0.001466	100	-	574620	47798	6671421	0.8512	0.002003	100	-	290443	23341	3242509
Etal	Htim	Hera	Hbes	0.8352	0.001949	100	-	574620	51616	6671421	0.8406	0.002094	100	-	290443	25162	3242509
Etal	Hera	Hbes	Hcyd	0.0454	0.003424	13.249	best	51958	47449	6671421	0.0451	0.004278	10.549	best	25347	23158	3242509
Etal	Hbes	Hera	Hcyd	0.8469	0.001579	100	-	572200	47449	6671421	0.8517	0.00201	100	-	289125	23158	3242509
Etal	Hcyd	Hera	Hbes	0.8335	0.001863	100	-	572200	51958	6671421	0.8388	0.002099	100	-	289125	25347	3242509
Etal	Hera	Hbes	Hmel	0.0334	0.004064	8.208	best	51811	48465	6671421	0.0329	0.00524	6.277	best	24986	23394	3242509
Etal	Hbes	Hera	Hmel	0.8446	0.001769	100	-	575053	48465	6671421	0.851	0.002119	100	-	290649	23394	3242509
Etal	Hmel	Hera	Hbes	0.8347	0.001863	100	-	575053	51811	6671421	0.8417	0.001993	100	-	290649	24986	3242509
Etal	Hera	Hpar	Hnum	0.0271	0.002662	10.184	best	41195	39020	6671421	0.0211	0.005379	3.929	best	19992	19164	3242509
Etal	Hpar	Hera	Hnum	0.8809	0.001718	100	-	615945	39020	6671421	0.8833	0.002097	100	-	309140	19164	3242509
Etal	Hnum	Hera	Hpar	0.8746	0.001807	100	-	615945	41195	6671421	0.8785	0.001958	100	-	309140	19992	3242509
Etal	Hera	Hpar	Htim	0.0133	0.003667	3.631	best	42881	41754	6671421	0.0052	0.004546	1.135	best	20617	20405	3242509
Etal	Hpar	Hera	Htim	0.8703	0.002348	100	-	602204	41754	6671421	0.8739	0.002177	100	-	303063	20405	3242509
Etal	Htim	Hera	Hpar	0.8671	0.002601	100	-	602204	42881	6671421	0.8726	0.002203	100	-	303063	20617	3242509
Etal	Hera	Hpar	Hcyd	0.021	0.003491	6.018	best	44176	42358	6671421	0.0139	0.00457	3.032	best	21186	20606	3242509
Etal	Hpar	Hera	Hcyd	0.8672	0.00247	100	-	595297	42358	6671421	0.8713	0.002338	100	-	299556	20606	3242509
Etal	Hcyd	Hera	Hpar	0.8619	0.002614	100	-	595297	44176	6671421	0.8679	0.002168	100	-	299556	21186	3242509
Etal	Hera	Hpar	Hmel	0.0078	0.004556	1.713	best	42342	41687	6671421	0.0004	0.004572	0.093	best	19972	19989	3242509
Etal	Hpar	Hera	Hmel	0.8711	0.002106	100	-	605235	41687	6671421	0.8769	0.002127	100	-	304638	19989	3242509
Etal	Hmel	Hera	Hpar	0.8693	0.002366	100	-	605235	42342	6671421	0.877	0.002094	100	-	304638	19972	3242509
Etal	Hera	Hnum	Htim	0.0118	0.003121	3.796	best	43696	44744	6671421	0.0144	0.005912	2.436	best	21077	21693	3242509
Etal	Hnum	Hera	Htim	0.8578	0.001616	100	-	584563	44744	6671421	0.863	0.001848	100	-	295053	21693	3242509
Etal	Htim	Hera	Hnum	0.8609	0.001866	100	-	584563	43696	6671421	0.8667	0.002024	100	-	295053	21077	3242509
Etal	Hera	Hnum	Hcyd	0.004	0.003184	1.259	best	44312	44669	6671421	0.0058	0.005006	1.152	best	21370	21618	3242509
Etal	Hnum	Hera	Hcyd	0.857	0.001569	100	-	580239	44669	6671421	0.8625	0.001807	100	-	292912	21618	3242509
Etal	Hcyd	Hera	Hnum	0.8581	0.001703	100	-	580239	44312	6671421	0.864	0.001891	100	-	292912	21370	3242509
Etal	Hera	Hnum	Hmel	0.0171	0.004532	3.783	best	43591	45111	6671421	0.02	0.005075	3.938	best	20730	21575	3242509
Etal	Hnum	Hera	Hmel	0.857	0.001823	100	-	585628	45111	6671421	0.864	0.001972	100	-	295666	21575	3242509
Etal	Hmel	Hera	Hnum	0.8615	0.001722	100	-	585628	43591	6671421	0.869	0.001879	100	-	295666	20730	3242509
Etal	Hera	Htim	Hcyd	0.0129	0.004768	2.715	best	27102	26411	6671421	0.0144	0.006508	2.217	best	12899	12531	3242509
Etal	Htim	Hera	Hcyd	0.9244	0.0023	100	-	671902	26411	6671421	0.9285	0.002161	100	-	338043	12531	3242509
Etal	Hcyd	Hera	Htim	0.9225	0.002457	100	-	671902	27102	6671421	0.9265	0.00208	100	-	338043	12899	3242509
Etal	Hera	Htim	Hmel	0.0081	0.005425	1.492	best	28765	29237	6671421	0.0082	0.005817	1.401	best	13936	14165	3242509
Etal	Htim	Hera	Hmel	0.9156	0.001795	100	-	663765	29237	6671421	0.9183	0.001657	100	-	332329	14165	3242509
Etal	Hmel	Hera	Htim	0.9169	0.001993	100	-	663765	28765	6671421	0.9195	0.001639	100	-	332329	13936	3242509
Etal	Hera	Hcyd	Hmel	0.02	0.004885	4.097	best	28449	29612	6671421	0.0214	0.006539	3.27	best	13655	14252	3242509
Etal	Hcyd	Hera	Hmel	0.9143	0.001701	100	-	661388	29612	6671421	0.9174	0.001582	100	-	330815	14252	3242509

Etal	Hmel	Hera	Hcyd	0.9175	0.001764	100	-	661388	28449	6671421	0.9207	0.001617	100	-	330815	13655	3242509
Etal	Hhim	HeraHhimHy	Hsar	0.8794	0.002809	100	-	21625	336970	6671421	0.8782	0.003066	100	-	10475	161457	3242509
Etal	HeraHhimHyl	Hhim	Hsar	0.8789	0.003211	100	-	21711	336970	6671421	0.8795	0.003218	100	-	10353	161457	3242509
Etal	Hsar	Hhim	HeraHhimHyl	0.002	0.005295	0.383	best	21711	21625	6671421	0.0058	0.006035	0.967	best	10353	10475	3242509
Etal	Hhim	HeraHhimHy	Hdem	0.876	0.002883	100	-	21190	320681	6671421	0.8744	0.003176	100	-	10281	153430	3242509
Etal	HeraHhimHyl	Hhim	Hdem	0.8759	0.003332	100	-	21222	320681	6671421	0.8766	0.003349	100	-	10092	153430	3242509
Etal	Hdem	Hhim	HeraHhimHyl	0.0008	0.00449	0.178	best	21222	21190	6671421	0.0092	0.00591	1.561	best	10092	10281	3242509
Etal	Hhim	HeraHhimHy	Ldor	0.9418	0.001276	100	-	20351	678633	6671421	0.9472	0.001301	100	-	9438	347704	3242509
Etal	HeraHhimHyl	Hhim	Ldor	0.9412	0.001434	100	-	20542	678633	6671421	0.9467	0.001427	100	-	9517	347704	3242509
Etal	Ldor	Hhim	HeraHhimHyl	0.0047	0.005559	0.843	best	20542	20351	6671421	0.0042	0.007251	0.582	best	9517	9438	3242509
Etal	Hhim	HeraHhimHy	Hbes	0.9412	0.00122	100	-	20222	667131	6671421	0.9435	0.001407	100	-	9655	331918	3242509
Etal	HeraHhimHyl	Hhim	Hbes	0.9416	0.001297	100	-	20075	667131	6671421	0.9442	0.001419	100	-	9525	331918	3242509
Etal	Hbes	Hhim	HeraHhimHyl	0.0036	0.003946	0.924	best	20075	20222	6671421	0.0067	0.006572	1.027	best	9525	9655	3242509
Etal	Hhim	HeraHhimHy	Hpar	0.9413	0.001194	100	-	20083	664428	6671421	0.9434	0.001393	100	-	9615	330175	3242509
Etal	HeraHhimHyl	Hhim	Hpar	0.9417	0.001354	100	-	19967	664428	6671421	0.9444	0.001414	100	-	9445	330175	3242509
Etal	Hpar	Hhim	HeraHhimHyl	0.0029	0.005068	0.569	best	19967	20083	6671421	0.0089	0.006824	1.302	best	9445	9615	3242509
Etal	Hhim	HeraHhimHy	Hnum	0.9415	0.001237	100	-	19944	662331	6671421	0.9436	0.001422	100	-	9562	329430	3242509
Etal	HeraHhimHyl	Hhim	Hnum	0.9415	0.001316	100	-	19947	662331	6671421	0.9445	0.001381	100	-	9404	329430	3242509
Etal	Hnum	Hhim	HeraHhimHyl	0.0001	0.004185	0.02	best	19947	19944	6671421	0.0083	0.007232	1.151	best	9404	9562	3242509
Etal	Hhim	HeraHhimHy	Htim	0.9416	0.001231	100	-	19937	663132	6671421	0.9438	0.001334	100	-	9537	329873	3242509
Etal	HeraHhimHyl	Hhim	Htim	0.9418	0.001288	100	-	19884	663132	6671421	0.9444	0.001382	100	-	9438	329873	3242509
Etal	Htim	Hhim	HeraHhimHyl	0.0013	0.004232	0.313	best	19884	19937	6671421	0.0052	0.006819	0.76	best	9438	9537	3242509
Etal	Hhim	HeraHhimHy	Hcyd	0.9417	0.001215	100	-	19906	662584	6671421	0.9437	0.001366	100	-	9546	329559	3242509
Etal	HeraHhimHyl	Hhim	Hcyd	0.9419	0.001331	100	-	19831	662584	6671421	0.9446	0.001417	100	-	9387	329559	3242509
Etal	Hcyd	Hhim	HeraHhimHyl	0.0019	0.004419	0.425	best	19831	19906	6671421	0.0084	0.006528	1.28	best	9387	9546	3242509
Etal	Hhim	HeraHhimHy	Hmel	0.9418	0.001176	100	-	19903	663709	6671421	0.9439	0.001386	100	-	9521	330124	3242509
Etal	HeraHhimHyl	Hhim	Hmel	0.9418	0.001327	100	-	19877	663709	6671421	0.9447	0.001394	100	-	9389	330124	3242509
Etal	Hmel	Hhim	HeraHhimHyl	0.0006	0.004062	0.157	best	19877	19903	6671421	0.0069	0.006766	1.026	best	9389	9521	3242509
Etal	Hhim	Hsar	Hdem	0.1304	0.003599	36.237	best	68700	52846	6671421	0.1338	0.004432	30.182	best	33192	25359	3242509
Etal	Hsar	Hhim	Hdem	0.517	0.00368	100	-	165996	52846	6671421	0.5312	0.003136	100	-	82833	25359	3242509
Etal	Hdem	Hhim	Hsar	0.4146	0.004075	100	-	165996	68700	6671421	0.4279	0.003611	100	-	82833	33192	3242509
Etal	Hhim	Hsar	Ldor	0.6666	0.003238	100	-	85774	428711	6671421	0.6978	0.002856	100	-	40552	227836	3242509
Etal	Hsar	Hhim	Ldor	0.7015	0.0025	100	-	75229	428711	6671421	0.7295	0.002245	100	-	35631	227836	3242509
Etal	Ldor	Hhim	Hsar	0.0655	0.002934	22.318	best	75229	85774	6671421	0.0646	0.003331	19.391	best	35631	40552	3242509
Etal	Hhim	Hsar	Hbes	0.6571	0.003078	100	-	86513	418077	6671421	0.6729	0.002816	100	-	41630	212911	3242509
Etal	Hsar	Hhim	Hbes	0.7028	0.002727	100	-	72965	418077	6671421	0.7119	0.002575	100	-	35839	212911	3242509
Etal	Hbes	Hhim	Hsar	0.085	0.002849	29.814	best	72965	86513	6671421	0.0748	0.003421	21.853	best	35839	41630	3242509
Etal	Hhim	Hsar	Hpar	0.6557	0.003035	100	-	86388	415388	6671421	0.6715	0.002815	100	-	41475	211053	3242509
Etal	Hsar	Hhim	Hpar	0.7034	0.002979	100	-	72325	415388	6671421	0.711	0.002727	100	-	35656	211053	3242509
Etal	Hpar	Hhim	Hsar	0.0886	0.00278	31.872	best	72325	86388	6671421	0.0754	0.003397	22.207	best	35656	41475	3242509
Etal	Hhim	Hsar	Hnum	0.6551	0.003102	100	-	86105	413147	6671421	0.672	0.002825	100	-	41227	210113	3242509
Etal	Hsar	Hhim	Hnum	0.704	0.002992	100	-	71778	413147	6671421	0.7115	0.002698	100	-	35420	210113	3242509
Etal	Hnum	Hhim	Hsar	0.0907	0.002529	35.874	best	71778	86105	6671421	0.0758	0.003279	23.106	best	35420	41227	3242509
Etal	Hhim	Hsar	Htim	0.6567	0.003131	100	-	85699	413549	6671421	0.6725	0.002864	100	-	41239	210593	3242509
Etal	Hsar	Hhim	Htim	0.7034	0.002895	100	-	72009	413549	6671421	0.7122	0.00274	100	-	35404	210593	3242509
Etal	Htim	Hhim	Hsar	0.0868	0.00311	27.915	best	72009	85699	6671421	0.0761	0.003444	22.104	best	35404	41239	3242509
Etal	Hhim	Hsar	Hcyd	0.6569	0.00308	100	-	85493	412826	6671421	0.6725	0.002845	100	-	41158	210189	3242509
Etal	Hsar	Hhim	Hcyd	0.7037	0.002822	100	-	71806	412826	6671421	0.7128	0.002731	100	-	35250	210189	3242509
Etal	Hcyd	Hhim	Hsar	0.087	0.002503	34.763	best	71806	85493	6671421	0.0773	0.003432	22.529	best	35250	41158	3242509
Etal	Hhim	Hsar	Hmel	0.6571	0.003098	100	-	85711	414172	6671421	0.6735	0.002933	100	-	41109	210730	3242509
Etal	Hsar	Hhim	Hmel	0.7034	0.002889	100	-	72126	414172	6671421	0.7129	0.002732	100	-	35327	210730	3242509
Etal	Hmel	Hhim	Hsar	0.0861	0.002971	28.973	best	72126	85711	6671421	0.0756	0.003513	21.536	best	35327	41109	3242509
Etal	Hhim	Hdem	Ldor	0.7156	0.002516	100	-	71318	430109	6671421	0.7443	0.002266	100	-	33511	228628	3242509
Etal	Hdem	Hhim	Ldor	0.7216	0.00251	100	-	69547	430109	6671421	0.7471	0.002186	100	-	33092	228628	3242509
Etal	Ldor	Hhim	Hdem	0.0126	0.002893	4.345	best	69547	71318	6671421	0.0063	0.003885	1.618	best	33092	33511	3242509
Etal	Hhim	Hdem	Hbes	0.7072	0.002402	100	-	71936	419354	6671421	0.7221	0.002322	100	-	34473	213587	3242509
Etal	Hdem	Hhim	Hbes	0.7206	0.002403	100	-	68093	419354	6671421	0.7293	0.002328	100	-	33437	213587	3242509
Etal	Hbes	Hhim	Hdem	0.0274	0.002366	11.603	best	68093	71936	6671421	0.0153	0.004015	3.799	best	33437	34473	3242509
Etal	Hhim	Hdem	Hpar	0.7058	0.002423	100	-	71895	416749	6671421	0.7208	0.002314	100	-	34363	211774	3242509
Etal	Hdem	Hhim	Hpar	0.7208	0.002533	100	-	67616	416749	6671421	0.7302	0.002365	100	-	33020	211774	3242509
Etal	Hpar	Hhim	Hdem	0.0307	0.00229	13.394	best	67616	71895	6671421	0.0199	0.003699	5.388	best	33020	34363	3242509
Etal	Hhim	Hdem	Hnum	0.7053	0.002469	100	-	71648	414544	6671421	0.7214	0.002331	100	-	34123	210842	3242509
Etal	Hdem	Hhim	Hnum	0.721	0.002708	100	-	67215	414544	6671421	0.7302	0.002312	100	-	32884	210842	3242509
Etal	Hnum	Hhim	Hdem	0.0319	0.00224	14.251	best	67215	71648	6671421	0.0185	0.003792	4.876	best	32884	34123	3242509
Etal	Hhim	Hdem	Htim	0.7073	0.002534	100	-	71130	414834	6671421	0.7227	0.002458	100	-	33989	211176	3242509
Etal	Hdem	Hhim	Htim	0.721	0.002658	100	-	67268	414834	6671421	0.7302	0.002398	100	-	32927	211176	3242509
Etal	Htim	Hhim	Hdem	0.0279	0.002741	10.183	best	67268	71130	6671421	0.0159	0.004009	3.959	best	32927	33989	3242509
Etal	Hhim	Hdem	Hcyd	0.7076	0.002527	100	-	70896	414083	6671421	0.7229	0.002457	100	-	33903	210767	3242509
Etal	Hdem	Hhim	Hcyd	0.7207	0.002688	100	-	67212	414083	6671421	0.7302	0.002489	100	-	32863	210767	3242509
Etal	Hcyd	Hhim	Hdem	0.0267	0.002698	9.89	best	67212	70896	6671421	0.0156	0.003918	3.975	best	32863	33903	3242509
Etal	Hhim	Hdem	Hmel	0.7073	0.002528	100	-	71249	415564	6671421	0.7233	0.002477	100	-	33943	211397	3242509
Etal	Hdem	Hhim	Hmel	0.7212	0.002713	100	-	67329	415564	6671421	0.7309	0.002432	100	-	32865	211397	3242509
Etal	Hmel	Hhim	Hdem	0.0283	0.00275	10.289	best	67329	71249	6671421	0.0161	0.003805	4.24	best	32865	33943	3242509
Etal	Hhim	Ldor	Hbes	0.0448	0.003917	11.428	best	132734	121361	6671421	0.1174	0.003964	29.608	best	76186	60183	3242509
Etal	Ldor	Hhim	Hbes	0.3929	0.004735	82.967	-	278420	121361	6671421	0.3887	0.003988	97.467	-	136711	60183	3242509
Etal	Hbes	Hhim	Ldor	0.3543	0.003859	91.829	-	278420	132734	6671421	0.2843	0.00358	79.406	-	136711	76186	3242509
Etal	Hhim	Ldor	Hpar	0.0555	0.004036	13.76	best	132461	118524	6671421	0.1318	0.003713	35.504	best	76015	58309	3242509
Etal	Ldor	Hhim	Hpar	0.4013	0.004558	88.031	-	277390	118524	6671421	0.4002	0.003721	100	-	136130	58309	3242509
Etal	Hpar	Hhim	Ldor	0.3536	0.003691	95.805	-	277390	132461	6671421	0.2834	0.003533	80.213	-	136130	76015	3242509
Etal	Hhim	Ldor	Hnum	0.0642	0.003807	16.859	best	131784	115889	6671421	0.1388	0.004481	30.967	best	75487	57089	3242509
Etal	Ldor	Hhim	Hnum	0.41	0.004555	90.011	-	276932	115889	6671421	0.4086	0.004182	97.705	-	135961	57089	3242509
Etal	Hnum	Hhim	Ldor	0.3551	0.003928	90.406	-	276932	131784	6671421	0.286	0.003619	79.027	-	135961	75487	3242509
Etal	Hhim	Ldor	Htim	0.061	0.00367	16.63	best	131160	116073	6671421	0.1351	0.00393	34.373	best	75323	57393	3242509
Etal	Ldor	Hhim	Htim	0.4092	0.00431	94.95	-	276863	116073	6671421	0.4062	0.004013	100	-	135910	57393	3242509
Etal	Htim	Hhim	Ldor	0.3571	0.00367	97.316	-	276863	131160	6671421	0.2868	0.003684	77.857	-	135910	75323	3242509
Etal	Hhim	Ldor	Hcyd	0.0635	0.003974	15.967	best	130766	115162	6671421	0.1381	0.003858	35.806	best	75191	56938	3242509
Etal	Ldor	Hhim	Hcyd	0.4126	0.004366	94.504	-	276950	115162	6671421	0.4093	0.003977	100	-	135841	56938	3242509
Etal	Hcyd	Hhim	Ldor	0.3586	0.003745	95.754	-	276950	130766	6671421	0.2874	0.003619	79.407	-	135841	75191	3242509
Etal	Hhim	Ldor	Hmel	0.0584	0.004071	14.359	best	131084	116608	6671421	0.1333	0.004198	31.753	best	75080	57417	3242509
Etal	Ldor	Hhim	Hmel	0.4073	0.004681	87.013	-	276881	116608	6671421	0.4058	0.004093	99.128	-	135828	57417	3242509
Etal	Hmel	Hhim	Ldor	0.3574	0.003722	96.03	-	276881	131084	6671421	0.288	0.003658	78.741	-	135828	75080	3242509
Etal	Hhim	Hbes	Hpar	0.0268	0.003484	7.691	best	49128	46564	6671421	0.0366	0.004412	8.297	best	24106	22403	3242509
Etal	Hbes	Hhim	Hpar	0.8547	0.001504	100	-	594327	46564	6671421	0.8609	0.002074	100	-	299601	22403	3242509
Etal	Hpar	Hhim	Hbes	0.8473	0.001647	100	-	594327	49128	6671421	0.8511	0.002027	100	-	299601	24106	3242509
Etal	Hhim	Hbes	Hnum	0.051	0.003763	13.556	best	46579	42057	6671421	0.0554	0.005169	10.71	best	22824	20429	3242509
Etal	Hbes	Hhim	Hnum	0.8699	0.001873	100	-	604264	42057	6671421	0.8743	0.002275	100	-	304629	20429	3242509
Etal	Hnum	Hhim	Hbes	0.8569	0.002131	100	-	604264	46579	6671421	0.8606	0.002293	100	-	304629	22824	3242509
Etal	Hhim	Hbes	Htim	0.0373	0.003669	10.157	best	51680	47966	6671421	0.0396	0.005037	7.871	best	25263	23336	3242509
Etal	Hbes	Hhim	Htim	0.8458	0.001564	100	-	574243	47966	6671421	0.851	0.002112	100	-	289933	23336	3242509
Etal	Htim	Hhim	Hbes	0.8349	0.001894	100	-	574243	51680	6671421	0.8397	0.002096	100	-	289933	25263	3242509

Etal	Hhim	Hbes	Hcyd	0.0425	0.003433	12.376	best	51911	47680	6671421	0.0463	0.004406	10.507	best	25423	23173	3242509
Etal	Hbes	Hhim	Hcyd	0.8461	0.00165	100	-	571886	47680	6671421	0.8514	0.00209	100	-	288635	23173	3242509
Etal	Hcyd	Hhim	Hbes	0.8336	0.00194	100	-	571886	51911	6671421	0.8381	0.002146	100	-	288635	25423	3242509
Etal	Hhim	Hbes	Hmel	0.0309	0.003469	8.903	best	51781	48678	6671421	0.0343	0.005474	6.257	best	25049	23389	3242509
Etal	Hbes	Hhim	Hmel	0.8438	0.001805	100	-	574721	48678	6671421	0.8508	0.002243	100	-	290139	23389	3242509
Etal	Hmel	Hhim	Hbes	0.8347	0.001868	100	-	574721	51781	6671421	0.8411	0.001996	100	-	290139	25049	3242509
Etal	Hhim	Hpar	Hnum	0.0244	0.002511	9.699	best	41165	39207	6671421	0.0176	0.005227	3.373	best	19946	19254	3242509
Etal	Hpar	Hhim	Hnum	0.8803	0.00167	100	-	615714	39207	6671421	0.8826	0.002168	100	-	308631	19254	3242509
Etal	Hnum	Hhim	Hpar	0.8747	0.001765	100	-	615714	41165	6671421	0.8786	0.00192	100	-	308631	19946	3242509
Etal	Hhim	Hpar	Htim	0.0136	0.003289	4.121	best	42991	41841	6671421	0.0054	0.004697	1.158	best	20694	20470	3242509
Etal	Hpar	Hhim	Htim	0.87	0.002407	100	-	601873	41841	6671421	0.8733	0.002168	100	-	302529	20470	3242509
Etal	Htim	Hhim	Hpar	0.8667	0.00256	100	-	601873	42991	6671421	0.872	0.002213	100	-	302529	20694	3242509
Etal	Hhim	Hpar	Hcyd	0.0192	0.003547	5.425	best	44147	42480	6671421	0.013	0.004464	2.923	best	21216	20669	3242509
Etal	Hpar	Hhim	Hcyd	0.8668	0.002552	100	-	595001	42480	6671421	0.8707	0.002314	100	-	299020	20669	3242509
Etal	Hcyd	Hhim	Hpar	0.8619	0.002612	100	-	595001	44147	6671421	0.8675	0.002256	100	-	299020	21216	3242509
Etal	Hhim	Hpar	Hmel	0.0064	0.004473	1.431	best	42377	41838	6671421	0.0011	0.004688	0.23	best	20010	20053	3242509
Etal	Hpar	Hhim	Hmel	0.8707	0.002158	100	-	604968	41838	6671421	0.8763	0.002159	100	-	304103	20053	3242509
Etal	Hmel	Hhim	Hpar	0.8691	0.002274	100	-	604968	42377	6671421	0.8765	0.002079	100	-	304103	20010	3242509
Etal	Hhim	Hnum	Htim	0.0091	0.002871	3.178	best	43894	44702	6671421	0.0109	0.005959	1.832	best	21199	21667	3242509
Etal	Hnum	Hhim	Htim	0.8579	0.00171	100	-	584320	44702	6671421	0.863	0.001845	100	-	294564	21667	3242509
Etal	Htim	Hhim	Hnum	0.8603	0.001714	100	-	584320	43894	6671421	0.8657	0.002027	100	-	294564	21199	3242509
Etal	Hhim	Hnum	Hcyd	0.0033	0.00355	0.92	best	44366	44657	6671421	0.0034	0.005132	0.657	best	21425	21570	3242509
Etal	Hnum	Hhim	Hcyd	0.857	0.00169	100	-	580026	44657	6671421	0.8626	0.001811	100	-	292401	21570	3242509
Etal	Hcyd	Hhim	Hnum	0.8579	0.001685	100	-	580026	44366	6671421	0.8635	0.001969	100	-	292401	21425	3242509
Etal	Hhim	Hnum	Hmel	0.016	0.004421	3.615	best	43712	45131	6671421	0.0174	0.005095	3.408	best	20802	21537	3242509
Etal	Hnum	Hhim	Hmel	0.8569	0.001859	100	-	585447	45131	6671421	0.864	0.001952	100	-	295165	21537	3242509
Etal	Hmel	Hhim	Hnum	0.8611	0.001629	100	-	585447	43712	6671421	0.8683	0.001923	100	-	295165	20802	3242509
Etal	Hhim	Htim	Hcyd	0.0097	0.004421	2.19	best	27010	26493	6671421	0.0127	0.006459	1.959	best	12892	12569	3242509
Etal	Htim	Hhim	Hcyd	0.9241	0.002295	100	-	671543	26493	6671421	0.9282	0.002125	100	-	337470	12569	3242509
Etal	Hcyd	Hhim	Htim	0.9227	0.002383	100	-	671543	27010	6671421	0.9264	0.002072	100	-	337470	12892	3242509
Etal	Hhim	Htim	Hmel	0.0105	0.005577	1.877	best	28773	29384	6671421	0.0095	0.0058	1.637	best	13934	14201	3242509
Etal	Htim	Hhim	Hmel	0.9152	0.001775	100	-	663471	29384	6671421	0.9179	0.001649	100	-	331754	14201	3242509
Etal	Hmel	Hhim	Htim	0.9169	0.001937	100	-	663471	28773	6671421	0.9194	0.001618	100	-	331754	13934	3242509
Etal	Hhim	Hcyd	Hmel	0.0194	0.004337	4.468	best	28514	29642	6671421	0.0211	0.0062	3.406	best	13675	14265	3242509
Etal	Hcyd	Hhim	Hmel	0.9142	0.001672	100	-	661151	29642	6671421	0.9172	0.001618	100	-	330262	14265	3242509
Etal	Hmel	Hhim	Hcyd	0.9173	0.001751	100	-	661151	28514	6671421	0.9205	0.001565	100	-	330262	13675	3242509
Etal	HeraHhimHyl	Hsar	Hdem	0.1299	0.003917	33.17	best	68706	52906	6671421	0.1325	0.004842	27.368	best	33183	25417	3242509
Etal	Hsar	HeraHhimHy	Hdem	0.5166	0.003789	100	-	165970	52906	6671421	0.5312	0.00325	100	-	83013	25417	3242509
Etal	Hdem	HeraHhimHy	Hsar	0.4145	0.003962	100	-	165970	68706	6671421	0.4288	0.003661	100	-	83013	33183	3242509
Etal	HeraHhimHyl	Hsar	Ldor	0.6664	0.003249	100	-	85839	428671	6671421	0.6969	0.002763	100	-	40680	227763	3242509
Etal	Hsar	HeraHhimHy	Ldor	0.7019	0.002536	100	-	75103	428671	6671421	0.7291	0.002224	100	-	35680	227763	3242509
Etal	Ldor	HeraHhimHy	Hsar	0.0667	0.002844	23.455	best	75103	85839	6671421	0.0655	0.003269	20.033	best	35680	40680	3242509
Etal	HeraHhimHyl	Hsar	Hbes	0.6582	0.003154	100	-	86164	417961	6671421	0.6733	0.002807	100	-	41558	212847	3242509
Etal	Hsar	HeraHhimHy	Hbes	0.7035	0.00279	100	-	72763	417961	6671421	0.7114	0.002626	100	-	35897	212847	3242509
Etal	Hbes	HeraHhimHy	Hsar	0.0843	0.002917	28.905	best	72763	86164	6671421	0.0731	0.003652	20.012	best	35897	41558	3242509
Etal	HeraHhimHyl	Hsar	Hpar	0.6567	0.003176	100	-	86075	415277	6671421	0.6723	0.002784	100	-	41352	210978	3242509
Etal	Hsar	HeraHhimHy	Hpar	0.7041	0.003038	100	-	72128	415277	6671421	0.7105	0.00277	100	-	35703	210978	3242509
Etal	Hpar	HeraHhimHy	Hsar	0.0882	0.003014	29.248	best	72128	86075	6671421	0.0733	0.003515	20.856	best	35703	41352	3242509
Etal	HeraHhimHyl	Hsar	Hnum	0.6558	0.003151	100	-	85864	412989	6671421	0.6724	0.002787	100	-	41150	210072	3242509
Etal	Hsar	HeraHhimHy	Hnum	0.7047	0.003076	100	-	71534	412989	6671421	0.7109	0.002772	100	-	35501	210072	3242509
Etal	Hnum	HeraHhimHy	Hsar	0.091	0.002733	33.314	best	71534	85864	6671421	0.0737	0.00349	21.117	best	35501	41150	3242509
Etal	HeraHhimHyl	Hsar	Htim	0.6575	0.003178	100	-	85435	413424	6671421	0.6728	0.002809	100	-	41184	210515	3242509
Etal	Hsar	HeraHhimHy	Htim	0.7041	0.00295	100	-	71798	413424	6671421	0.7118	0.002786	100	-	35448	210515	3242509
Etal	Htim	HeraHhimHy	Hsar	0.0867	0.003102	27.955	best	71798	85435	6671421	0.0748	0.003763	19.889	best	35448	41184	3242509
Etal	HeraHhimHyl	Hsar	Hcyd	0.6579	0.003147	100	-	85145	412639	6671421	0.6732	0.002799	100	-	41035	210103	3242509
Etal	Hsar	HeraHhimHy	Hcyd	0.7045	0.002831	100	-	71533	412639	6671421	0.7124	0.002733	100	-	35286	210103	3242509
Etal	Hcyd	HeraHhimHy	Hsar	0.0869	0.002679	32.429	best	71533	85145	6671421	0.0753	0.003583	21.021	best	35286	41035	3242509
Etal	HeraHhimHyl	Hsar	Hmel	0.6578	0.003254	100	-	85477	414050	6671421	0.674	0.002897	100	-	41020	210651	3242509
Etal	Hsar	HeraHhimHy	Hmel	0.704	0.002969	100	-	71918	414050	6671421	0.7125	0.002817	100	-	35370	210651	3242509
Etal	Hmel	HeraHhimHy	Hsar	0.0861	0.003091	27.87	best	71918	85477	6671421	0.074	0.003791	19.508	best	35370	41020	3242509
Etal	HeraHhimHyl	Hdem	Ldor	0.7151	0.002529	100	-	71456	430088	6671421	0.743	0.00219	100	-	33699	228548	3242509
Etal	Hdem	HeraHhimHy	Ldor	0.7218	0.002537	100	-	69494	430088	6671421	0.7463	0.002209	100	-	33201	228548	3242509
Etal	Ldor	HeraHhimHy	Hdem	0.0139	0.003223	4.32	best	69494	71456	6671421	0.0074	0.003804	1.957	best	33201	33699	3242509
Etal	HeraHhimHyl	Hdem	Hbes	0.7082	0.002414	100	-	71626	419223	6671421	0.7221	0.002323	100	-	34453	213508	3242509
Etal	Hdem	HeraHhimHy	Hbes	0.7211	0.002469	100	-	67930	419223	6671421	0.7284	0.002362	100	-	33547	213508	3242509
Etal	Hbes	HeraHhimHy	Hdem	0.0265	0.002648	10.002	best	67930	71626	6671421	0.0133	0.00435	3.062	best	33547	34453	3242509
Etal	HeraHhimHyl	Hdem	Hpar	0.7067	0.002557	100	-	71615	416617	6671421	0.7212	0.0023	100	-	34296	211688	3242509
Etal	Hdem	HeraHhimHy	Hpar	0.7213	0.00259	100	-	67452	416617	6671421	0.7294	0.002379	100	-	33123	211688	3242509
Etal	Hpar	HeraHhimHy	Hdem	0.0299	0.002817	10.629	best	67452	71615	6671421	0.0174	0.004032	4.315	best	33123	34296	3242509
Etal	HeraHhimHyl	Hdem	Hnum	0.7059	0.002502	100	-	71436	414361	6671421	0.7216	0.002349	100	-	34092	210780	3242509
Etal	Hdem	HeraHhimHy	Hnum	0.7216	0.002774	100	-	67000	414361	6671421	0.7292	0.002401	100	-	33011	210780	3242509
Etal	Hnum	HeraHhimHy	Hdem	0.032	0.002594	12.356	best	67000	71436	6671421	0.0161	0.004345	3.708	best	33011	34092	3242509
Etal	HeraHhimHyl	Hdem	Htim	0.7079	0.002558	100	-	70935	414724	6671421	0.7226	0.002452	100	-	34002	211099	3242509
Etal	Hdem	HeraHhimHy	Htim	0.7214	0.00272	100	-	67126	414724	6671421	0.7294	0.00243	100	-	33039	211099	3242509
Etal	Htim	HeraHhimHy	Hdem	0.0276	0.002875	9.599	best	67126	70935	6671421	0.0144	0.004331	3.317	best	33039	34002	3242509
Etal	HeraHhimHyl	Hdem	Hcyd	0.7085	0.002582	100	-	70610	413904	6671421	0.7233	0.002427	100	-	33831	210665	3242509
Etal	Hdem	HeraHhimHy	Hcyd	0.7214	0.002719	100	-	67001	413904	6671421	0.7295	0.002483	100	-	32950	210665	3242509
Etal	Hcyd	HeraHhimHy	Hdem	0.0262	0.002957	8.872	best	67001	70610	6671421	0.0132	0.004142	3.184	best	32950	33831	3242509
Etal	HeraHhimHyl	Hdem	Hmel	0.708	0.002662	100	-	71028	415401	6671421	0.7236	0.002466	100	-	33888	211285	3242509
Etal	Hdem	HeraHhimHy	Hmel	0.7218	0.002784	100	-	67134	415401	6671421	0.7302	0.002483	100	-	32942	211285	3242509
Etal	Hmel	HeraHhimHy	Hdem	0.0282	0.002904	9.707	best	67134	71028	6671421	0.0142	0.004054	3.491	best	32942	33888	3242509
Etal	HeraHhimHyl	Ldor	Hbes	0.0435	0.003772	11.522	best	132468	121433	6671421	0.1159	0.003907	29.664	best	76038	60244	3242509
Etal	Ldor	HeraHhimHy	Hbes	0.3925	0.004505	87.124	-	278301	121433	6671421	0.3882	0.003872	100	-	136693	60244	3242509
Etal	Hbes	HeraHhimHy	Ldor	0.355	0.003902	90.997	-	278301	132468	6671421	0.2851	0.00351	81.24	-	136693	76038	3242509
Etal	HeraHhimHyl	Ldor	Hpar	0.0544	0.003854	14.105	best	132198	118568	6671421	0.1301	0.003661	35.544	best	75813	58356	3242509
Etal	Ldor	HeraHhimHy	Hpar	0.4009	0.004356	92.03	-	277243	118568	6671421	0.3998	0.003674	100	-	136098	58356	3242509
Etal	Hpar	HeraHhimHy	Ldor	0.3543	0.003805	93.114	-	277243	132198	6671421	0.2845	0.00346	82.233	-	136098	75813	3242509
Etal	HeraHhimHyl	Ldor	Hnum	0.0635	0.003708	17.12	best	131579	115872	6671421	0.1371	0.004362	31.426	best	75319	57158	3242509
Etal	Ldor	HeraHhimHy	Hnum	0.4097	0.004393	93.278	-	276724	115872	6671421	0.408	0.004098	99.58	-	135951	57158	3242509
Etal	Hnum	HeraHhimHy	Ldor	0.3555	0.00398	89.329	-	276724	131579	6671421	0.287	0.003485	82.353	-	135951	75319	3242509
Etal	HeraHhimHyl	Ldor	Htim	0.0601	0.003608	16.652	best	130971	116128	6671421	0.1339	0.003853	34.74	best	75188	57436	3242509
Etal	Ldor	HeraHhimHy	Htim	0.4088	0.004169	98.062	-	276727	116128	6671421	0.4058	0.003946	100	-	135874	57436	3242509
Etal	Htim	HeraHhimHy	Ldor	0.3575	0.003757	95.149	-	276727	130971	6671421	0.2875	0.003633	79.138	-	135874	75188	3242509
Etal	HeraHhimHyl	Ldor	Hcyd	0.0624	0.003837	16.271	best	130513	115175	6671421	0.1364	0.003771	36.178	best	75038	57023	3242509
Etal	Ldor	HeraHhimHy	Hcyd	0.4123	0.004193	98.345	-	276772	115175	6671421	0.4087	0.003902	100	-	135847	57023	3242509
Etal	Hcyd	HeraHhimHy	Ldor	0.3591	0.003845	93.391	-	276772	130513	6671421	0.2884	0.003573	80.7	-	135847	75038	3242509
Etal	HeraHhimHyl	Ldor	Hmel	0.0576	0.003917	14.705	best	130922	116663	6671421	0.1319	0.004092	32.218	best	74907	57455	3242509
Etal	Ldor	HeraHhimHy	Hmel	0.4069	0.004487	90.694	-	276745	116663	6671421	0.4054	0.004013	100	-	135787	57455	3242509
Etal	Hmel	HeraHhimHy	Ldor	0.3577	0.003768	94.942	-	276745	130922	6671421	0.289	0.003603	80.192	-	135787	74907	3242509
Etal	HeraHhimHyl	Hbes	Hpar	0.0271	0.003359	8.081	best	49101	46506	6671421	0.0357	0.004535	7.873	best	24116	22453	3242509

Etal	Hbes	HeraHhimHyl	Hpar	0.8549	0.001435	100	-	594416	46506	6671421	0.8607	0.002074	100	-	299781	22453	3242509
Etal	Hpar	HeraHhimHyl	Hbes	0.8474	0.001596	100	-	594416	49101	6671421	0.8511	0.001964	100	-	299781	24116	3242509
Etal	HeraHhimHyl	Hbes	Hnum	0.0529	0.004093	12.915	best	46527	41855	6671421	0.0548	0.00508	10.789	best	22775	20408	3242509
Etal	Hbes	HeraHhimHyl	Hnum	0.8705	0.001877	100	-	604209	41855	6671421	0.8745	0.002278	100	-	304738	20408	3242509
Etal	Hnum	HeraHhimHyl	Hbes	0.857	0.002142	100	-	604209	46527	6671421	0.8609	0.002253	100	-	304738	22775	3242509
Etal	HeraHhimHyl	Hbes	Htim	0.0383	0.004002	9.567	best	51628	47820	6671421	0.0403	0.005018	8.032	best	25267	23309	3242509
Etal	Hbes	HeraHhimHyl	Htim	0.8463	0.001484	100	-	574244	47820	6671421	0.8512	0.00208	100	-	290036	23309	3242509
Etal	Htim	HeraHhimHyl	Hbes	0.835	0.001865	100	-	574244	51628	6671421	0.8397	0.002101	100	-	290036	25267	3242509
Etal	HeraHhimHyl	Hbes	Hcyd	0.0433	0.003765	11.496	best	51861	47558	6671421	0.0457	0.004501	10.154	best	25408	23187	3242509
Etal	Hbes	HeraHhimHyl	Hcyd	0.8465	0.001586	100	-	571911	47558	6671421	0.8514	0.002092	100	-	288779	23187	3242509
Etal	Hcyd	HeraHhimHyl	Hbes	0.8337	0.001918	100	-	571911	51861	6671421	0.8383	0.002121	100	-	288779	25408	3242509
Etal	HeraHhimHyl	Hbes	Hmel	0.0321	0.003992	8.048	best	51771	48547	6671421	0.0342	0.005328	6.422	best	25044	23386	3242509
Etal	Hbes	HeraHhimHyl	Hmel	0.8442	0.001743	100	-	574737	48547	6671421	0.8509	0.002222	100	-	290266	23386	3242509
Etal	Hmel	HeraHhimHyl	Hbes	0.8347	0.001823	100	-	574737	51771	6671421	0.8412	0.001938	100	-	290266	25044	3242509
Etal	HeraHhimHyl	Hpar	Hnum	0.0259	0.002633	9.829	best	41159	39082	6671421	0.018	0.005109	3.515	best	19934	19230	3242509
Etal	Hpar	HeraHhimHyl	Hnum	0.8806	0.001669	100	-	615705	39082	6671421	0.8828	0.002132	100	-	308777	19230	3242509
Etal	Hnum	HeraHhimHyl	Hpar	0.8747	0.001779	100	-	615705	41159	6671421	0.8787	0.001909	100	-	308777	19934	3242509
Etal	HeraHhimHyl	Hpar	Htim	0.0143	0.003375	4.24	best	42976	41763	6671421	0.0072	0.004571	1.568	best	20717	20422	3242509
Etal	Hpar	HeraHhimHyl	Htim	0.8703	0.002403	100	-	601911	41763	6671421	0.8736	0.002145	100	-	302651	20422	3242509
Etal	Htim	HeraHhimHyl	Hpar	0.8667	0.002554	100	-	601911	42976	6671421	0.8719	0.002219	100	-	302651	20717	3242509
Etal	HeraHhimHyl	Hpar	Hcyd	0.0197	0.003465	5.695	best	44128	42420	6671421	0.0133	0.004451	2.992	best	21206	20648	3242509
Etal	Hpar	HeraHhimHyl	Hcyd	0.8669	0.002524	100	-	595057	42420	6671421	0.8709	0.002308	100	-	299169	20648	3242509
Etal	Hcyd	HeraHhimHyl	Hpar	0.862	0.002636	100	-	595057	44128	6671421	0.8676	0.002243	100	-	299169	21206	3242509
Etal	HeraHhimHyl	Hpar	Hmel	0.0075	0.004214	1.775	best	42377	41748	6671421	0.0001	0.00457	0.028	best	20011	20016	3242509
Etal	Hpar	HeraHhimHyl	Hmel	0.8709	0.002114	100	-	604994	41748	6671421	0.8766	0.002114	100	-	304236	20016	3242509
Etal	Hmel	HeraHhimHyl	Hpar	0.8691	0.0023	100	-	604994	42377	6671421	0.8766	0.00204	100	-	304236	20011	3242509
Etal	HeraHhimHyl	Hnum	Htim	0.0098	0.002968	3.292	best	43778	44642	6671421	0.0096	0.005938	1.609	best	21187	21596	3242509
Etal	Hnum	HeraHhimHyl	Htim	0.858	0.001701	100	-	584257	44642	6671421	0.8634	0.001816	100	-	294651	21596	3242509
Etal	Htim	HeraHhimHyl	Hnum	0.8606	0.001775	100	-	584257	43778	6671421	0.8658	0.002077	100	-	294651	21187	3242509
Etal	HeraHhimHyl	Hnum	Hcyd	0.0042	0.00363	1.144	best	44208	44577	6671421	0.0034	0.005115	0.664	best	21397	21543	3242509
Etal	Hnum	HeraHhimHyl	Hcyd	0.8573	0.001638	100	-	579943	44577	6671421	0.8628	0.001776	100	-	292532	21543	3242509
Etal	Hcyd	HeraHhimHyl	Hnum	0.8584	0.001746	100	-	579943	44208	6671421	0.8637	0.001991	100	-	292532	21397	3242509
Etal	HeraHhimHyl	Hnum	Hmel	0.0164	0.004515	3.622	best	43575	45023	6671421	0.0168	0.005196	3.231	best	20772	21481	3242509
Etal	Hnum	HeraHhimHyl	Hmel	0.8572	0.001833	100	-	585336	45023	6671421	0.8644	0.001966	100	-	295267	21481	3242509
Etal	Hmel	HeraHhimHyl	Hnum	0.8614	0.001669	100	-	585336	43575	6671421	0.8686	0.001907	100	-	295267	20772	3242509
Etal	HeraHhimHyl	Htim	Hcyd	0.0093	0.004385	2.116	best	26984	26489	6671421	0.0103	0.006191	1.66	best	12874	12611	3242509
Etal	Htim	HeraHhimHyl	Hcyd	0.9241	0.002314	100	-	671592	26489	6671421	0.928	0.002158	100	-	337611	12611	3242509
Etal	Hcyd	HeraHhimHyl	Htim	0.9228	0.002428	100	-	671592	26984	6671421	0.9266	0.002063	100	-	337611	12874	3242509
Etal	HeraHhimHyl	Htim	Hmel	0.01	0.005513	1.816	best	28753	29337	6671421	0.0107	0.006171	1.728	best	13929	14229	3242509
Etal	Htim	HeraHhimHyl	Hmel	0.9153	0.001771	100	-	663477	29337	6671421	0.9178	0.001715	100	-	331881	14229	3242509
Etal	Hmel	HeraHhimHyl	Htim	0.9169	0.001967	100	-	663477	28753	6671421	0.9195	0.00162	100	-	331881	13929	3242509
Etal	HeraHhimHyl	Hcyd	Hmel	0.0186	0.004587	4.048	best	28483	29562	6671421	0.0202	0.006175	3.266	best	13675	14238	3242509
Etal	Hcyd	HeraHhimHyl	Hmel	0.9144	0.001666	100	-	661146	29562	6671421	0.9174	0.001624	100	-	330394	14238	3242509
Etal	Hmel	HeraHhimHyl	Hcyd	0.9174	0.001755	100	-	661146	28483	6671421	0.9205	0.001577	100	-	330394	13675	3242509
Etal	Hsar	Hdem	Ldor	0.8139	0.001275	100	-	53356	519988	6671421	0.8331	0.001178	100	-	25010	274689	3242509
Etal	Hdem	Hsar	Ldor	0.7866	0.001944	100	-	62130	519988	6671421	0.806	0.001674	100	-	29512	274689	3242509
Etal	Ldor	Hsar	Hdem	0.076	0.003338	22.761	best	62130	53356	6671421	0.0826	0.004469	18.478	best	29512	25010	3242509
Etal	Hsar	Hdem	Hbes	0.8161	0.001458	100	-	51649	509911	6671421	0.824	0.001408	100	-	25052	259598	3242509
Etal	Hdem	Hsar	Hbes	0.7852	0.001859	100	-	61354	509911	6671421	0.794	0.001793	100	-	29807	259598	3242509
Etal	Hbes	Hsar	Hdem	0.0859	0.003959	21.691	best	61354	51649	6671421	0.0867	0.004873	17.789	best	29807	25052	3242509
Etal	Hsar	Hdem	Hpar	0.817	0.001442	100	-	51107	507320	6671421	0.8236	0.001417	100	-	24933	257804	3242509
Etal	Hdem	Hsar	Hpar	0.7857	0.001834	100	-	60891	507320	6671421	0.7952	0.001869	100	-	29409	257804	3242509
Etal	Hpar	Hsar	Hdem	0.0874	0.003586	24.363	best	60891	51107	6671421	0.0824	0.004855	16.968	best	29409	24933	3242509
Etal	Hsar	Hdem	Hnum	0.8172	0.001595	100	-	50825	505344	6671421	0.824	0.001412	100	-	24798	256965	3242509
Etal	Hdem	Hsar	Hnum	0.7855	0.00203	100	-	60719	505344	6671421	0.7949	0.001919	100	-	29366	256965	3242509
Etal	Hnum	Hsar	Hdem	0.0887	0.003913	22.67	best	60719	50825	6671421	0.0843	0.00463	18.218	best	29366	24798	3242509
Etal	Hsar	Hdem	Htim	0.8168	0.001519	100	-	50981	505671	6671421	0.8249	0.001452	100	-	24701	257364	3242509
Etal	Hdem	Hsar	Htim	0.7853	0.001959	100	-	60809	505671	6671421	0.7945	0.001748	100	-	29474	257364	3242509
Etal	Htim	Hsar	Hdem	0.0879	0.004027	21.829	best	60809	50981	6671421	0.0881	0.004239	20.786	best	29474	24701	3242509
Etal	Hsar	Hdem	Hcyd	0.8176	0.001495	100	-	50670	504840	6671421	0.8256	0.001432	100	-	24550	256963	3242509
Etal	Hdem	Hsar	Hcyd	0.7854	0.001928	100	-	60673	504840	6671421	0.7946	0.001816	100	-	29418	256963	3242509
Etal	Hcyd	Hsar	Hdem	0.0898	0.003731	24.079	best	60673	50670	6671421	0.0902	0.004249	21.228	best	29418	24550	3242509
Etal	Hsar	Hdem	Hmel	0.817	0.001569	100	-	50995	506191	6671421	0.8253	0.001486	100	-	24652	257529	3242509
Etal	Hdem	Hsar	Hmel	0.786	0.001958	100	-	60660	506191	6671421	0.7954	0.001795	100	-	29356	257529	3242509
Etal	Hmel	Hsar	Hdem	0.0866	0.004013	21.57	best	60660	50995	6671421	0.0871	0.004193	20.775	best	29356	24652	3242509
Etal	Hsar	Ldor	Hbes	0.0329	0.003556	9.246	best	131471	123101	6671421	0.1098	0.003748	29.309	best	76452	61319	3242509
Etal	Ldor	Hsar	Hbes	0.405	0.004207	96.279	-	290705	123101	6671421	0.3991	0.003694	100	-	142768	61319	3242509
Etal	Hbes	Hsar	Ldor	0.3772	0.003863	97.634	-	290705	131471	6671421	0.3025	0.003555	85.086	-	142768	76452	3242509
Etal	Hsar	Ldor	Hpar	0.0415	0.003586	11.578	best	130709	120290	6671421	0.1239	0.00357	34.703	best	76248	59440	3242509
Etal	Ldor	Hsar	Hpar	0.4132	0.004024	100	-	289701	120290	6671421	0.4104	0.003445	100	-	142182	59440	3242509
Etal	Hpar	Hsar	Ldor	0.3782	0.003769	100	-	289701	130709	6671421	0.3019	0.003441	87.714	-	142182	76248	3242509
Etal	Hsar	Ldor	Hnum	0.0489	0.003645	13.409	best	129970	117857	6671421	0.1307	0.004235	30.862	best	75756	58244	3242509
Etal	Ldor	Hsar	Hnum	0.4213	0.004139	100	-	289445	117857	6671421	0.4184	0.003903	100	-	142037	58244	3242509
Etal	Hnum	Hsar	Ldor	0.3802	0.003943	96.444	-	289445	129970	6671421	0.3043	0.003456	88.055	-	142037	75756	3242509
Etal	Hsar	Ldor	Htim	0.0482	0.003383	14.251	best	129838	117896	6671421	0.1268	0.003712	34.156	best	75607	58591	3242509
Etal	Ldor	Hsar	Htim	0.4209	0.003851	100	-	289231	117896	6671421	0.4159	0.003646	100	-	142029	58591	3242509
Etal	Htim	Hsar	Ldor	0.3804	0.00374	100	-	289231	129838	6671421	0.3052	0.00365	83.61	-	142029	75607	3242509
Etal	Hsar	Ldor	Hcyd	0.0506	0.003347	15.122	best	129368	116906	6671421	0.1293	0.003594	35.977	best	75395	58129	3242509
Etal	Ldor	Hsar	Hcyd	0.4243	0.003926	100	-	289239	116906	6671421	0.419	0.003641	100	-	141953	58129	3242509
Etal	Hcyd	Hsar	Ldor	0.3819	0.003844	99.349	-	289239	129368	6671421	0.3062	0.003575	85.66	-	141953	75395	3242509
Etal	Hsar	Ldor	Hmel	0.0461	0.003671	12.551	best	129808	118372	6671421	0.1254	0.003964	31.641	best	75382	58580	3242509
Etal	Ldor	Hsar	Hmel	0.4191	0.004248	98.662	-	289190	118372	6671421	0.4156	0.003805	100	-	141912	58580	3242509
Etal	Hmel	Hsar	Ldor	0.3804	0.003745	100	-	289190	129808	6671421	0.3062	0.003681	83.175	-	141912	75382	3242509
Etal	Hsar	Hbes	Hpar	0.0213	0.003693	5.757	best	49229	47180	6671421	0.0354	0.004776	7.418	best	24478	22803	3242509
Etal	Hbes	Hsar	Hpar	0.8561	0.001406	100	-	608491	47180	6671421	0.8612	0.001962	100	-	305792	22803	3242509
Etal	Hpar	Hsar	Hbes	0.8503	0.001672	100	-	608491	49229	6671421	0.8518	0.002045	100	-	305792	24478	3242509
Etal	Hsar	Hbes	Hnum	0.042	0.004606	9.113	best	46470	42727	6671421	0.0542	0.004745	11.416	best	23151	20772	3242509
Etal	Hbes	Hsar	Hnum	0.8708	0.001771	100	-	618482	42727	6671421	0.8747	0.002132	100	-	310763	20772	3242509
Etal	Hnum	Hsar	Hbes	0.8603	0.002129	100	-	618482	46470	6671421	0.8614	0.002264	100	-	310763	23151	3242509
Etal	Hsar	Hbes	Htim	0.0354	0.003906	9.064	best	52227	48655	6671421	0.0382	0.004797	7.957	best	25605	23722	3242509
Etal	Hbes	Hsar	Htim	0.8473	0.001467	100	-	588480	48655	6671421	0.8517	0.002036	100	-	296110	23722	3242509
Etal	Htim	Hsar	Hbes	0.837	0.001768	100	-	588480	52227	6671421	0.8408	0.001977	100	-	296110	25605	3242509
Etal	Hsar	Hbes	Hcyd	0.0407	0.003785	10.749	best	52331	48239	6671421	0.0433	0.004661	9.282	best	25716	23583	3242509
Etal	Hbes	Hsar	Hcyd	0.8479	0.001575	100	-	585993	48239	6671421	0.8519	0.002099	100	-	294836	23583	3242509
Etal	Hcyd	Hsar	Hbes	0.836	0.001814	100	-	585993	52331	6671421	0.8396	0.002039	100	-	294836	25716	3242509
Etal	Hsar	Hbes	Hmel	0.0302	0.003689	8.184	best	52305	49239	6671421	0.0339	0.005254	6.461	best	25412	23743	3242509
Etal	Hbes	Hsar	Hmel	0.8457	0.00165	100	-	588830	49239	6671421	0.8516	0.0021	100	-	296284	23743	3242509
Etal	Hmel	Hsar	Hbes	0.8368	0.001787	100	-	588830	52305	6671421	0.842	0.002025	100	-	296284	25412	3242509
Etal	Hsar	Hpar	Hnum	0.021	0.003699	5.67	best	41223	39529	6671421	0.0176	0.005179	3.405	best	20297	19593	3242509
Etal	Hpar	Hsar	Hnum	0.8819	0.001746	100	-	630099	39529	6671421	0.8828	0.002097	100	-	314789	19593	3242509

Etal	Hnum	Hsar	Hpar	0.8772	0.001917	100	-	630099	41223	6671421	0.8789	0.002004	100	-	314789	20297	3242509
Etal	Hsar	Hpar	Htim	0.0178	0.003261	5.453	best	43579	42056	6671421	0.005	0.004603	1.08	best	20995	20787	3242509
Etal	Hpar	Hsar	Htim	0.8722	0.002261	100	-	616151	42056	6671421	0.8738	0.002176	100	-	308665	20787	3242509
Etal	Htim	Hsar	Hpar	0.8679	0.002414	100	-	616151	43579	6671421	0.8726	0.002179	100	-	308665	20995	3242509
Etal	Hsar	Hpar	Hcyd	0.0234	0.003683	6.357	best	44648	42605	6671421	0.0108	0.00442	2.434	best	21471	21013	3242509
Etal	Hpar	Hsar	Hcyd	0.8693	0.002328	100	-	609189	42605	6671421	0.8712	0.002352	100	-	305183	21013	3242509
Etal	Hcyd	Hsar	Hpar	0.8635	0.002487	100	-	609189	44648	6671421	0.8686	0.00215	100	-	305183	21471	3242509
Etal	Hsar	Hpar	Hmel	0.012	0.004144	2.892	best	42972	41955	6671421	0.0002	0.004609	0.033	best	20382	20388	3242509
Etal	Hpar	Hsar	Hmel	0.8731	0.00201	100	-	619148	41955	6671421	0.8767	0.002106	100	-	310257	20388	3242509
Etal	Hmel	Hsar	Hpar	0.8702	0.002217	100	-	619148	42972	6671421	0.8767	0.002094	100	-	310257	20382	3242509
Etal	Hsar	Hnum	Htim	0.0019	0.002883	0.665	best	44549	44720	6671421	0.0114	0.005519	2.067	best	21493	21989	3242509
Etal	Hnum	Hsar	Htim	0.861	0.001748	100	-	598665	44720	6671421	0.8637	0.00188	100	-	300693	21989	3242509
Etal	Htim	Hsar	Hnum	0.8615	0.001653	100	-	598665	44549	6671421	0.8666	0.001826	100	-	300693	21493	3242509
Etal	Hsar	Hnum	Hcyd	0.0039	0.003618	1.076	best	44983	44634	6671421	0.0056	0.004845	1.165	best	21680	21926	3242509
Etal	Hnum	Hsar	Hcyd	0.8603	0.00171	100	-	594330	44634	6671421	0.8632	0.001888	100	-	298564	21926	3242509
Etal	Hcyd	Hsar	Hnum	0.8593	0.001552	100	-	594330	44983	6671421	0.8646	0.001797	100	-	298564	21680	3242509
Etal	Hsar	Hnum	Hmel	0.0076	0.004426	1.709	best	44474	45151	6671421	0.0165	0.004581	3.601	best	21172	21882	3242509
Etal	Hnum	Hsar	Hmel	0.86	0.001992	100	-	599794	45151	6671421	0.8646	0.001945	100	-	301317	21882	3242509
Etal	Hmel	Hsar	Hnum	0.8619	0.001675	100	-	599794	44474	6671421	0.8687	0.001877	100	-	301317	21172	3242509
Etal	Hsar	Htim	Hcyd	0.0096	0.004391	2.193	best	27343	26823	6671421	0.0096	0.005799	1.653	best	13114	12864	3242509
Etal	Htim	Hsar	Hcyd	0.9247	0.00228	100	-	685563	26823	6671421	0.9278	0.002133	100	-	343600	12864	3242509
Etal	Hcyd	Hsar	Htim	0.9233	0.002412	100	-	685563	27343	6671421	0.9265	0.002021	100	-	343600	13114	3242509
Etal	Hsar	Htim	Hmel	0.0085	0.005028	1.699	best	29256	29762	6671421	0.0075	0.005421	1.381	best	14201	14415	3242509
Etal	Htim	Hsar	Hmel	0.9159	0.001646	100	-	677539	29762	6671421	0.9182	0.00158	100	-	337803	14415	3242509
Etal	Hmel	Hsar	Htim	0.9172	0.00181	100	-	677539	29256	6671421	0.9193	0.001552	100	-	337803	14201	3242509
Etal	Hsar	Hcyd	Hmel	0.0174	0.004526	3.853	best	28889	29915	6671421	0.0163	0.005846	2.788	best	14002	14466	3242509
Etal	Hcyd	Hsar	Hmel	0.9152	0.001582	100	-	675111	29915	6671421	0.9175	0.001548	100	-	336371	14466	3242509
Etal	Hmel	Hsar	Hcyd	0.9179	0.001603	100	-	675111	28889	6671421	0.9201	0.001581	100	-	336371	14002	3242509
Etal	Hdem	Ldor	Hbes	0.0375	0.003308	11.328	best	128748	119447	6671421	0.1139	0.00379	30.054	best	75233	59847	3242509
Etal	Ldor	Hdem	Hbes	0.3994	0.004532	88.132	-	278277	119447	6671421	0.3913	0.003915	99.964	-	136794	59847	3242509
Etal	Hbes	Hdem	Ldor	0.3674	0.004011	91.589	-	278277	128748	6671421	0.2904	0.003815	76.1	-	136794	75233	3242509
Etal	Hdem	Ldor	Hpar	0.0467	0.003421	13.642	best	128171	116742	6671421	0.1263	0.003671	34.397	best	74854	58072	3242509
Etal	Ldor	Hdem	Hpar	0.4076	0.004252	95.87	-	277379	116742	6671421	0.4025	0.003651	100	-	136312	58072	3242509
Etal	Hpar	Hdem	Ldor	0.3679	0.003832	96.018	-	277379	128171	6671421	0.2911	0.003811	76.367	-	136312	74854	3242509
Etal	Hdem	Ldor	Hnum	0.0547	0.003321	16.475	best	127567	114334	6671421	0.1338	0.004321	30.967	best	74476	56898	3242509
Etal	Ldor	Hdem	Hnum	0.4159	0.00429	96.957	-	277148	114334	6671421	0.4107	0.004036	100	-	136189	56898	3242509
Etal	Hnum	Hdem	Ldor	0.3696	0.003989	92.647	-	277148	127567	6671421	0.293	0.003808	76.936	-	136189	74476	3242509
Etal	Hdem	Ldor	Htim	0.0538	0.003175	16.943	best	127303	114307	6671421	0.1313	0.003773	34.808	best	74460	57173	3242509
Etal	Ldor	Hdem	Htim	0.4156	0.004015	100	-	276868	114307	6671421	0.4084	0.003868	100	-	136109	57173	3242509
Etal	Htim	Hdem	Ldor	0.3701	0.003777	97.967	-	276868	127303	6671421	0.2928	0.003957	74	-	136109	74460	3242509
Etal	Hdem	Ldor	Hcyd	0.0569	0.003172	17.952	best	127056	113365	6671421	0.1346	0.003733	36.046	best	74336	56704	3242509
Etal	Ldor	Hdem	Hcyd	0.4191	0.004098	100	-	276924	113365	6671421	0.4116	0.00387	100	-	136026	56704	3242509
Etal	Hcyd	Hdem	Ldor	0.371	0.00387	95.863	-	276924	127056	6671421	0.2933	0.003841	76.346	-	136026	74336	3242509
Etal	Hdem	Ldor	Hmel	0.0509	0.003605	14.124	best	127222	114895	6671421	0.1294	0.00404	32.033	best	74202	57198	3242509
Etal	Ldor	Hdem	Hmel	0.4136	0.004477	92.384	-	276939	114895	6671421	0.408	0.003937	100	-	136028	57198	3242509
Etal	Hmel	Hdem	Ldor	0.3705	0.00382	96.983	-	276939	127222	6671421	0.2941	0.003893	75.538	-	136028	74202	3242509
Etal	Hdem	Hbes	Hpar	0.0227	0.003013	7.528	best	47978	45850	6671421	0.0304	0.00522	5.817	best	23682	22286	3242509
Etal	Hbes	Hdem	Hpar	0.8575	0.001403	100	-	597456	45850	6671421	0.8619	0.002032	100	-	300520	22286	3242509
Etal	Hpar	Hdem	Hbes	0.8513	0.001634	100	-	597456	47978	6671421	0.8539	0.002039	100	-	300520	23682	3242509
Etal	Hdem	Hbes	Hnum	0.0453	0.004227	10.715	best	45384	41452	6671421	0.0511	0.0052	9.829	best	22541	20349	3242509
Etal	Hbes	Hdem	Hnum	0.8723	0.001822	100	-	607502	41452	6671421	0.8752	0.002183	100	-	305585	20349	3242509
Etal	Hnum	Hdem	Hbes	0.861	0.002247	100	-	607502	45384	6671421	0.8626	0.002364	100	-	305585	22541	3242509
Etal	Hdem	Hbes	Htim	0.0377	0.003912	9.636	best	50857	47162	6671421	0.0395	0.005204	7.581	best	25040	23139	3242509
Etal	Hbes	Hdem	Htim	0.849	0.001522	100	-	577282	47162	6671421	0.8526	0.002061	100	-	290772	23139	3242509
Etal	Htim	Hdem	Hbes	0.8381	0.002007	100	-	577282	50857	6671421	0.8414	0.002086	100	-	290772	25040	3242509
Etal	Hdem	Hbes	Hcyd	0.0448	0.003524	12.726	best	51141	46751	6671421	0.0466	0.004755	9.808	best	25203	22957	3242509
Etal	Hbes	Hdem	Hcyd	0.8496	0.001656	100	-	574800	46751	6671421	0.853	0.002093	100	-	289455	22957	3242509
Etal	Hcyd	Hdem	Hbes	0.8366	0.00199	100	-	574800	51141	6671421	0.8398	0.002099	100	-	289455	25203	3242509
Etal	Hdem	Hbes	Hmel	0.0307	0.003983	7.701	best	50826	47800	6671421	0.0338	0.005363	6.294	best	24774	23156	3242509
Etal	Hbes	Hdem	Hmel	0.8472	0.001754	100	-	577686	47800	6671421	0.8526	0.002091	100	-	290942	23156	3242509
Etal	Hmel	Hdem	Hbes	0.8383	0.001944	100	-	577686	50826	6671421	0.8431	0.002055	100	-	290942	24774	3242509
Etal	Hdem	Hpar	Hnum	0.0229	0.003621	6.328	best	40268	38464	6671421	0.0205	0.005093	4.03	best	19782	18986	3242509
Etal	Hpar	Hdem	Hnum	0.883	0.0016	100	-	619250	38464	6671421	0.8845	0.002023	100	-	309706	18986	3242509
Etal	Hnum	Hdem	Hpar	0.8779	0.001832	100	-	619250	40268	6671421	0.8799	0.00197	100	-	309706	19782	3242509
Etal	Hdem	Hpar	Htim	0.0188	0.00336	5.586	best	42522	40955	6671421	0.0124	0.004965	2.5	best	20593	20088	3242509
Etal	Hpar	Hdem	Htim	0.8733	0.002329	100	-	605266	40955	6671421	0.8759	0.002218	100	-	303490	20088	3242509
Etal	Htim	Hdem	Hpar	0.8687	0.002566	100	-	605266	42522	6671421	0.8729	0.00224	100	-	303490	20593	3242509
Etal	Hdem	Hpar	Hcyd	0.0266	0.003372	7.886	best	43655	41393	6671421	0.0206	0.004577	4.494	best	21073	20223	3242509
Etal	Hpar	Hdem	Hcyd	0.8706	0.002436	100	-	598193	41393	6671421	0.8737	0.002389	100	-	299917	20223	3242509
Etal	Hcyd	Hdem	Hpar	0.864	0.002579	100	-	598193	43655	6671421	0.8687	0.002231	100	-	299917	21073	3242509
Etal	Hdem	Hpar	Hmel	0.0109	0.0045	2.415	best	41781	40883	6671421	0.0056	0.004643	1.209	best	19910	19688	3242509
Etal	Hpar	Hdem	Hmel	0.8741	0.002113	100	-	608292	40883	6671421	0.8788	0.002104	100	-	305081	19688	3242509
Etal	Hmel	Hdem	Hpar	0.8715	0.002286	100	-	608292	41781	6671421	0.8775	0.002161	100	-	305081	19910	3242509
Etal	Hdem	Hnum	Htim	0.0027	0.003346	0.815	best	43399	43636	6671421	0.0069	0.005931	1.155	best	21088	21379	3242509
Etal	Hnum	Hdem	Htim	0.8618	0.001691	100	-	587687	43636	6671421	0.8651	0.001874	100	-	295515	21379	3242509
Etal	Htim	Hdem	Hnum	0.8625	0.001723	100	-	587687	43399	6671421	0.8668	0.001909	100	-	295515	21088	3242509
Etal	Hdem	Hnum	Hcyd	0.0052	0.003803	1.376	best	43962	43504	6671421	0.0013	0.005146	0.246	best	21334	21280	3242509
Etal	Hnum	Hdem	Hcyd	0.8612	0.001717	100	-	583306	43504	6671421	0.8647	0.001903	100	-	293350	21280	3242509
Etal	Hcyd	Hdem	Hnum	0.8598	0.001647	100	-	583306	43962	6671421	0.8644	0.001844	100	-	293350	21334	3242509
Etal	Hdem	Hnum	Hmel	0.0104	0.005254	1.979	best	43143	44049	6671421	0.0137	0.004623	2.959	best	20703	21277	3242509
Etal	Hnum	Hdem	Hmel	0.8608	0.001925	100	-	588798	44049	6671421	0.8659	0.001893	100	-	296144	21277	3242509
Etal	Hmel	Hdem	Hnum	0.8635	0.001709	100	-	588798	43143	6671421	0.8693	0.00183	100	-	296144	20703	3242509
Etal	Hdem	Htim	Hcyd	0.0132	0.003998	3.29	best	26784	26089	6671421	0.0136	0.006158	2.205	best	12840	12495	3242509
Etal	Htim	Hdem	Hcyd	0.9256	0.002311	100	-	675001	26089	6671421	0.9288	0.002126	100	-	338458	12495	3242509
Etal	Hcyd	Hdem	Htim	0.9237	0.002359	100	-	675001	26784	6671421	0.9269	0.00202	100	-	338458	12840	3242509
Etal	Hdem	Htim	Hmel	0.0116	0.005839	1.985	best	28459	29128	6671421	0.0101	0.005955	1.7	best	13839	14122	3242509
Etal	Htim	Hdem	Hmel	0.9163	0.001745	100	-	667077	29128	6671421	0.9186	0.001664	100	-	332737	14122	3242509
Etal	Hmel	Hdem	Htim	0.9182	0.001843	100	-	667077	28459	6671421	0.9202	0.001615	100	-	332737	13839	3242509
Etal	Hdem	Hcyd	Hmel	0.0238	0.005444	4.366	best	28000	29364	6671421	0.0226	0.006212	3.64	best	13565	14193	3242509
Etal	Hcyd	Hdem	Hmel	0.9154	0.001657	100	-	664557	29364	6671421	0.9178	0.001529	100	-	331230	14193	3242509
Etal	Hmel	Hdem	Hcyd	0.9192	0.00167	100	-	664557	28000	6671421	0.9213	0.001597	100	-	331230	13565	3242509
Etal	Ldor	Hbes	Hpar	0.0175	0.003468	5.058	best	52407	50600	6671421	0.0263	0.004465	5.899	best	25193	23900	3242509
Etal	Hbes	Ldor	Hpar	0.7989	0.001773	100	-	452677	50600	6671421	0.8193	0.002685	100	-	240573	23900	3242509
Etal	Hpar	Ldor	Hbes	0.7925	0.002139	100	-	452677	52407	6671421	0.8104	0.002591	100	-	240573	25193	3242509
Etal	Ldor	Hbes	Hnum	0.0418	0.00526	7.944	best	49650	45666	6671421	0.0517	0.005272	9.808	best	23836	21492	3242509
Etal	Hbes	Ldor	Hnum	0.8202	0.003133	100	-	462187	45666	6671421	0.8388	0.002905	100	-	245167	21492	3242509
Etal	Hnum	Ldor	Hbes	0.806	0.003593	100	-	462187	49650	6671421	0.8228	0.003087	100	-	245167	23836	3242509
Etal	Ldor	Hbes	Htim	0.0349	0.004195	8.309	best	55385	51654	6671421	0.039	0.004866	8.006	best	26524	24535	3242509
Etal	Hbes	Ldor	Htim	0.7865	0.002078	100	-	432245	51654	6671421	0.8077	0.002681	100	-	230607	24535	3242509
Etal	Htim	Ldor	Hbes	0.7729	0.002828	100	-	432245	55385	6671421	0.7937	0.00261	100	-	230607	26524	3242509

Etal	Ldor	Hbes	Hcyd	0.0442	0.003894	11.342	best	55903	51174	6671421	0.0466	0.004331	10.765	best	26659	24284	3242509
Etal	Hbes	Ldor	Hcyd	0.7872	0.002097	100	-	429694	51174	6671421	0.8084	0.002567	100	-	229221	24284	3242509
Etal	Hcyd	Ldor	Hbes	0.7698	0.00295	100	-	429694	55903	6671421	0.7916	0.002784	100	-	229221	26659	3242509
Etal	Ldor	Hbes	Hmel	0.0298	0.003685	8.097	best	55457	52243	6671421	0.0369	0.00483	7.643	best	26445	24562	3242509
Etal	Hbes	Ldor	Hmel	0.7845	0.002083	100	-	432600	52243	6671421	0.8076	0.002626	100	-	230787	24562	3242509
Etal	Hmel	Ldor	Hbes	0.7728	0.002726	100	-	432600	55457	6671421	0.7944	0.002653	100	-	230787	26445	3242509
Etal	Ldor	Hpar	Hnum	0.0253	0.004029	6.277	best	44106	41929	6671421	0.0255	0.005123	4.987	best	21088	20037	3242509
Etal	Hpar	Ldor	Hnum	0.8373	0.002106	100	-	473507	41929	6671421	0.8512	0.002595	100	-	249299	20037	3242509
Etal	Hnum	Ldor	Hpar	0.8296	0.002327	100	-	473507	44106	6671421	0.844	0.002676	100	-	249299	21088	3242509
Etal	Ldor	Hpar	Htim	0.0212	0.003471	6.102	best	46405	44481	6671421	0.0161	0.005355	3.011	best	21943	21247	3242509
Etal	Hpar	Ldor	Htim	0.8236	0.003527	100	-	459584	44481	6671421	0.8393	0.002816	100	-	243191	21247	3242509
Etal	Htim	Ldor	Hpar	0.8166	0.003975	100	-	459584	46405	6671421	0.8345	0.002917	100	-	243191	21943	3242509
Etal	Ldor	Hpar	Hcyd	0.0315	0.003573	8.817	best	47857	44935	6671421	0.0246	0.004767	5.166	best	22513	21431	3242509
Etal	Hpar	Ldor	Hcyd	0.8194	0.003682	100	-	452527	44935	6671421	0.8359	0.002952	100	-	239667	21431	3242509
Etal	Hcyd	Ldor	Hpar	0.8088	0.004196	100	-	452527	47857	6671421	0.8283	0.003107	100	-	239667	22513	3242509
Etal	Ldor	Hpar	Hmel	0.0156	0.004001	3.901	best	45806	44399	6671421	0.0139	0.004978	2.798	best	21505	20915	3242509
Etal	Hpar	Ldor	Hmel	0.8249	0.003085	100	-	462600	44399	6671421	0.8426	0.00265	100	-	244850	20915	3242509
Etal	Hmel	Ldor	Hpar	0.8199	0.003623	100	-	462600	45806	6671421	0.8386	0.00291	100	-	244850	21505	3242509
Etal	Ldor	Hnum	Htim	0.0027	0.002888	0.918	best	47464	47717	6671421	0.0079	0.005456	1.449	best	22268	22623	3242509
Etal	Hnum	Ldor	Htim	0.8052	0.002467	100	-	442187	47717	6671421	0.8244	0.0025	100	-	235046	22623	3242509
Etal	Htim	Ldor	Hnum	0.8062	0.002435	100	-	442187	47464	6671421	0.8269	0.002419	100	-	235046	22268	3242509
Etal	Ldor	Hnum	Hcyd	0.0078	0.00339	2.302	best	48121	47376	6671421	0.0007	0.005004	0.139	best	22484	22453	3242509
Etal	Hnum	Ldor	Hcyd	0.8046	0.002466	100	-	437597	47376	6671421	0.8241	0.002402	100	-	232810	22453	3242509
Etal	Hcyd	Ldor	Hnum	0.8019	0.002278	100	-	437597	48121	6671421	0.8239	0.002462	100	-	232810	22484	3242509
Etal	Ldor	Hnum	Hmel	0.0081	0.003469	2.327	best	47369	48139	6671421	0.0103	0.005248	1.968	best	22085	22546	3242509
Etal	Hnum	Ldor	Hmel	0.8041	0.00259	100	-	443307	48139	6671421	0.8254	0.002588	100	-	235700	22546	3242509
Etal	Hmel	Ldor	Hnum	0.8069	0.002211	100	-	443307	47369	6671421	0.8287	0.002459	100	-	235700	22085	3242509
Etal	Ldor	Htim	Hcyd	0.0174	0.004179	4.152	best	29300	28302	6671421	0.0145	0.00703	2.056	best	13548	13162	3242509
Etal	Htim	Ldor	Hcyd	0.8982	0.003397	100	-	527649	28302	6671421	0.9095	0.002685	100	-	277476	13162	3242509
Etal	Hcyd	Ldor	Htim	0.8948	0.003677	100	-	527649	29300	6671421	0.9069	0.002846	100	-	277476	13548	3242509
Etal	Ldor	Htim	Hmel	0.0082	0.004338	1.897	best	31053	31570	6671421	0.0036	0.006023	0.592	best	14704	14810	3242509
Etal	Htim	Ldor	Hmel	0.8856	0.002781	100	-	519954	31570	6671421	0.8967	0.002086	100	-	271776	14810	3242509
Etal	Hmel	Ldor	Htim	0.8873	0.002977	100	-	519954	31053	6671421	0.8974	0.002337	100	-	271776	14704	3242509
Etal	Ldor	Hcyd	Hmel	0.0242	0.004706	5.146	best	30517	32032	6671421	0.0168	0.006435	2.607	best	14410	14902	3242509
Etal	Hcyd	Ldor	Hmel	0.8834	0.002628	100	-	517357	32032	6671421	0.8955	0.002206	100	-	270249	14902	3242509
Etal	Hmel	Ldor	Hcyd	0.8886	0.002675	100	-	517357	30517	6671421	0.8988	0.002263	100	-	270249	14410	3242509
Etal	Hbes	Hpar	Hnum	0.1197	0.024587	4.868	-	67839	53395	6671421	0.1163	0.01639	7.095	-	33684	26682	3242509
Etal	Hpar	Hbes	Hnum	0.2268	0.006471	35.05	-	84703	53395	6671421	0.2065	0.006302	32.766	-	40564	26682	3242509
Etal	Hnum	Hbes	Hpar	0.1103	0.029543	3.734	best	84703	67839	6671421	0.0925	0.019814	4.669	best	40564	33684	3242509
Etal	Hbes	Hpar	Htim	0.164	0.006418	25.556	-	54755	76241	6671421	0.1653	0.008619	19.182	-	26765	37366	3242509
Etal	Hpar	Hbes	Htim	0.0889	0.018414	4.825	best	91074	76241	6671421	0.0808	0.01485	5.442	best	43930	37366	3242509
Etal	Htim	Hbes	Hpar	0.2493	0.019098	13.054	-	91074	54755	6671421	0.2429	0.012237	19.851	-	43930	26765	3242509
Etal	Hbes	Hpar	Hcyd	0.1744	0.006798	25.65	-	55771	79328	6671421	0.1773	0.008656	20.485	-	27232	38968	3242509
Etal	Hpar	Hbes	Hcyd	0.0444	0.021191	2.093	best	86650	79328	6671421	0.0354	0.015961	2.219	best	41824	38968	3242509
Etal	Hcyd	Hbes	Hpar	0.2171	0.021438	10.128	-	86650	55771	6671421	0.2114	0.012908	16.38	-	41824	27232	3242509
Etal	Hbes	Hpar	Hmel	0.1678	0.006523	25.729	-	53839	75559	6671421	0.1672	0.008554	19.551	-	26014	36462	3242509
Etal	Hpar	Hbes	Hmel	0.1063	0.017004	6.25	best	93490	75559	6671421	0.1051	0.014234	7.381	best	45017	36462	3242509
Etal	Hmel	Hbes	Hpar	0.2694	0.018289	14.729	-	93490	53839	6671421	0.2676	0.012415	21.558	-	45017	26014	3242509
Etal	Hbes	Hnum	Htim	0.2503	0.02047	12.228	-	53914	89844	6671421	0.2496	0.014866	16.79	-	26486	44089	3242509
Etal	Hnum	Hbes	Htim	0.1121	0.024404	4.592	best	71777	89844	6671421	0.1125	0.016906	6.654	best	35181	44089	3242509
Etal	Htim	Hbes	Hnum	0.1422	0.004851	29.312	-	71777	53914	6671421	0.141	0.005797	24.328	-	35181	26486	3242509
Etal	Hbes	Hnum	Hcyd	0.26	0.01963	13.245	-	54172	92173	6671421	0.2616	0.014109	18.542	-	26465	45203	3242509
Etal	Hnum	Hbes	Hcyd	0.138	0.02242	6.154	best	69857	92173	6671421	0.1383	0.015605	8.86	best	34229	45203	3242509
Etal	Hcyd	Hbes	Hnum	0.1265	0.003912	32.333	-	69857	54172	6671421	0.1279	0.00535	23.913	-	34229	26465	3242509
Etal	Hbes	Hnum	Hmel	0.2525	0.020693	12.2	-	53663	89827	6671421	0.2513	0.015119	16.624	-	26022	43472	3242509
Etal	Hnum	Hbes	Hmel	0.1073	0.025249	4.251	best	72458	89827	6671421	0.104	0.017825	5.833	best	35295	43472	3242509
Etal	Hmel	Hbes	Hnum	0.1491	0.004743	31.432	-	72458	53663	6671421	0.1513	0.005374	28.146	-	35295	26022	3242509
Etal	Hbes	Htim	Hcyd	0.0271	0.004699	5.774	best	37145	39216	6671421	0.0314	0.006406	4.899	best	17540	18675	3242509
Etal	Htim	Hbes	Hcyd	0.6099	0.01764	34.572	-	161703	39216	6671421	0.6173	0.012293	50.218	-	78906	18675	3242509
Etal	Hcyd	Hbes	Htim	0.6266	0.016893	37.092	-	161703	37145	6671421	0.6364	0.011473	55.466	-	78906	17540	3242509
Etal	Hbes	Htim	Hmel	0.0028	0.004998	0.56	best	41097	41331	6671421	0.0038	0.006002	0.636	best	20234	20081	3242509
Etal	Htim	Hbes	Hmel	0.5745	0.012515	45.9	-	152855	41331	6671421	0.5684	0.008905	63.833	-	72964	20081	3242509
Etal	Hmel	Hbes	Htim	0.5764	0.013231	43.562	-	152855	41097	6671421	0.5659	0.009549	59.26	-	72964	20234	3242509
Etal	Hbes	Hcyd	Hmel	0.0222	0.006025	3.69	best	42353	40516	6671421	0.0319	0.006972	4.581	best	20838	19550	3242509
Etal	Hcyd	Hbes	Hmel	0.5793	0.011021	52.565	-	152050	40516	6671421	0.5745	0.008332	68.954	-	72335	19550	3242509
Etal	Hmel	Hbes	Hcyd	0.5644	0.013018	43.354	-	152050	42353	6671421	0.5528	0.009769	56.586	-	72335	20838	3242509
Etal	Hpar	Hnum	Htim	0.103	0.02748	3.747	best	71480	87955	6671421	0.0957	0.019936	4.798	best	34539	41857	3242509
Etal	Hnum	Hpar	Htim	0.2478	0.005544	44.697	-	53024	87955	6671421	0.2325	0.008481	27.409	-	26069	41857	3242509
Etal	Htim	Hpar	Hnum	0.1488	0.02756	5.401	-	53024	71480	6671421	0.14	0.017324	8.082	-	26069	34539	3242509
Etal	Hpar	Hnum	Hcyd	0.1486	0.030243	4.915	-	68488	92474	6671421	0.1432	0.021035	6.807	-	32959	43985	3242509
Etal	Hnum	Hpar	Hcyd	0.2688	0.006037	44.529	-	53294	92474	6671421	0.2547	0.008446	30.155	-	26131	43985	3242509
Etal	Hcyd	Hpar	Hnum	0.1255	0.029823	4.208	best	53294	68488	6671421	0.1159	0.01806	6.415	best	26131	32959	3242509
Etal	Hpar	Hnum	Hmel	0.0831	0.026515	3.134	best	73431	86808	6671421	0.07	0.019526	3.583	best	35329	40656	3242509
Etal	Hnum	Hpar	Hmel	0.2456	0.006466	37.985	-	52575	86808	6671421	0.2273	0.008628	26.342	-	25599	40656	3242509
Etal	Hmel	Hpar	Hnum	0.1661	0.027363	6.071	-	52575	73431	6671421	0.16	0.017634	9.071	-	25599	35329	3242509
Etal	Hpar	Htim	Hcyd	0.0888	0.005828	15.233	best	38607	46118	6671421	0.0929	0.005634	16.483	best	18120	21828	3242509
Etal	Htim	Hpar	Hcyd	0.4829	0.017191	28.09	-	132286	46118	6671421	0.4966	0.01393	35.649	-	64894	21828	3242509
Etal	Hcyd	Hpar	Htim	0.5481	0.013308	41.188	-	132286	38607	6671421	0.5635	0.011908	47.317	-	64894	18120	3242509
Etal	Hpar	Htim	Hmel	0.0332	0.007686	4.314	best	48280	45182	6671421	0.044	0.009404	4.677	best	23631	21640	3242509
Etal	Htim	Hpar	Hmel	0.4542	0.008982	50.568	-	120387	45182	6671421	0.4522	0.0095	47.597	-	57358	21640	3242509
Etal	Hmel	Hpar	Htim	0.4275	0.008605	49.677	-	120387	48280	6671421	0.4165	0.010214	40.774	-	57358	23631	3242509
Etal	Hpar	Hcyd	Hmel	0.1141	0.008345	13.67	best	51848	41239	6671421	0.1263	0.008994	14.047	best	25412	19713	3242509
Etal	Hcyd	Hpar	Hmel	0.4944	0.006018	82.16	-	121894	41239	6671421	0.4921	0.008119	60.613	-	57906	19713	3242509
Etal	Hmel	Hpar	Hcyd	0.4031	0.009396	42.905	-	121894	51848	6671421	0.39	0.010837	35.989	-	57906	25412	3242509
Etal	Hnum	Htim	Hcyd	0.0536	0.00476	11.263	best	37568	41817	6671421	0.0549	0.005287	10.384	best	17805	19871	3242509
Etal	Htim	Hnum	Hcyd	0.5561	0.022411	24.812	-	146441	41817	6671421	0.5647	0.015542	36.337	-	71407	19871	3242509
Etal	Hcyd	Hnum	Htim	0.592	0.019558	30.269	-	146441	37568	6671421	0.601	0.013494	44.537	-	71407	17805	3242509
Etal	Hnum	Htim	Hmel	0.0082	0.005542	1.475	best	43439	42741	6671421	0.0175	0.006772	2.589	best	21265	20534	3242509
Etal	Htim	Hnum	Hmel	0.5231	0.016128	32.432	-	136402	42741	6671421	0.5184	0.011288	45.926	-	64722	20534	3242509
Etal	Hmel	Hnum	Htim	0.5172	0.017775	29.095	-	136402	43439	6671421	0.5055	0.012579	40.186	-	64722	21265	3242509
Etal	Hnum	Hcyd	Hmel	0.0577	0.006688	8.623	best	45466	40519	6671421	0.0671	0.007669	8.747	best	22269	19472	3242509
Etal	Hcyd	Hnum	Hmel	0.5421	0.01307	41.473	-	136368	40519	6671421	0.5363	0.009419	56.934	-	64493	19472	3242509
Etal	Hmel	Hnum	Hcyd	0.5001	0.017488	28.597	-	136368	45466	6671421	0.4868	0.012615	38.587	-	64493	22269	3242509
Etal	Htim	Hcyd	Hmel	0.0935	0.019581	4.775	-	53065	64028	6671421	0.129	0.017391	7.419	-	24786	32134	3242509
Etal	Hcyd	Htim	Hmel	0.1129	0.024939	4.529	-	51004	64028	6671421	0.154	0.019209	8.016	-	23553	32134	3242509
Etal	Hmel	Htim	Hcyd	0.0196	0.009656	2.032	best	51004	53065	6671421	0.0255	0.009121	2.79	best	23553	24786	3242509

C	Intro Rate
1	0.1
2	0.2
3	0.3
4	0.4
5	0.5
6	0.6
7	0.7
8	0.8
9	0.9
10	-

Table S12 Branch length test tree simulation parameters

650 coalescent trees for a population of size 1E6 were generated for 10 replicates of every combination of the values of C and introgression probabilities listed above.

Table S13: QuIBL results

triplet	outgroup	C1	C2	topology ILS proportion	topology non-ILS proportion	numTrees	BIC ILS+Introgression	BIC ILS only	dBIC	total non-ILS
Hdem_HeraRef_Hhim	HeraRef	0	2.057531	0.793465	0.206535	71	-361.505298	-370.068824	8.563526	0.002618569
Hdem_HeraRef_Hhim	Hhim	0	15.227301	0.983312	0.016688	61	-294.136955	-284.724582	-9.412373	0.00018178
Hdem_HeraRef_Hhim	Hdem	0	1.125482	0.010098	0.989902	5469	-29597.94544	-25645.6843	-3952.261131	0.966745364
HeraRef_Hhim_Hsar	HeraRef	0	1.87269	0.643545	0.356455	78	-413.101013	-420.635075	7.534062	0.004964909
HeraRef_Hhim_Hsar	Hhim	0	14.418657	0.982132	0.017868	57	-257.665278	-251.163442	-6.501836	0.000181871
HeraRef_Hhim_Hsar	Hsar	0	1.125737	0.010423	0.989577	5466	-29590.5868	-25647.1986	-3943.388221	0.965897836
HeraRef_Hhim_Hhsa	HeraRef	0	0.925975	0.613002	0.386998	99	-524.283413	-532.33038	8.046967	0.006841572
HeraRef_Hhim_Hhsa	Hhim	0	10.600214	0.975165	0.024835	91	-458.014902	-446.75402	-11.260882	0.000403569
HeraRef_Hhim_Hhsa	Hhsa	0	1.059925	0.009218	0.990782	5411	-32520.3515	-28848.8324	-3671.51913	0.957343108
HeraRef_Hhim_Htel	HeraRef	0	2.477635	0.762397	0.237603	80	-423.580761	-431.460546	7.879785	0.003394329
HeraRef_Hhim_Htel	Hhim	0	8.40641	0.957962	0.042038	68	-323.848983	-317.012627	-6.836356	0.000510461
HeraRef_Hhim_Htel	Htel	0	1.10061	0.007925	0.992075	5453	-30696.52225	-26824.997	-3871.525274	0.966033031
Hdem_HeraRef_Hsar	HeraRef	0	0.789898	0.031609	0.968391	5181	-32382.32376	-30086.4459	-2295.877874	0.895934602
Hdem_HeraRef_Hsar	Hdem	0	4.94368	0.949868	0.050132	220	-1257.595307	-1257.73713	0.141827	0.001969471
Hdem_HeraRef_Hsar	Hsar	0	3.909883	0.951471	0.048529	199	-1134.873815	-1144.51409	9.640273	0.001724513
Hdem_HeraRef_Hhsa	HeraRef	0	0.459958	0.189623	0.810377	1308	-8823.137161	-8620.84017	-202.296992	0.189280914
Hdem_HeraRef_Hhsa	Hdem	0	0.504114	0.09214	0.90786	3884	-25362.25088	-24456.4777	-905.773168	0.629665757
Hdem_HeraRef_Hhsa	Hhsa	0	0.254643	0.77184	0.22816	409	-2597.708981	-2611.22678	13.517799	0.016663829
Hdem_HeraRef_Htel	HeraRef	0	0.359318	0.197908	0.802092	1746	-12345.2966	-12113.8402	-231.456445	0.250080827
Hdem_HeraRef_Htel	Hdem	0	0.443302	0.136761	0.863239	2816	-19898.97183	-19384.3412	-514.630632	0.434085897
Hdem_HeraRef_Htel	Htel	0	0.487047	0.278998	0.721002	1039	-7396.028943	-7289.86701	-106.161934	0.133771621
HeraRef_Hhsa_Hsar	HeraRef	0	0.468472	0.195945	0.804055	1304	-8840.500303	-8639.38476	-201.115544	0.18722995
HeraRef_Hhsa_Hsar	Hsar	0	0.515912	0.093607	0.906393	3879	-25401.63856	-24494.598	-907.040515	0.627839008
HeraRef_Hhsa_Hsar	Hhsa	0	0.261912	0.702549	0.297451	418	-2690.742075	-2702.51712	11.775048	0.022202593
HeraRef_Hsar_Htel	HeraRef	0	0.350743	0.207251	0.792749	1741	-12244.25297	-12025.0904	-219.162545	0.246460002
HeraRef_Hsar_Htel	Hsar	0	0.450188	0.139836	0.860164	2823	-20045.16677	-19522.3369	-522.829914	0.433614816
HeraRef_Hsar_Htel	Htel	0	0.466968	0.23126	0.76874	1037	-7385.346024	-7258.93623	-126.40979	0.142354175
HeraRef_Hhsa_Htel	HeraRef	0	0.643171	0.059855	0.940145	2252	-15606.37346	-14906.64	-699.733488	0.378072596
HeraRef_Hhsa_Htel	Hhsa	0	0.319433	0.49473	0.50527	546	-3516.346509	-3508.04387	-8.30264	0.049263825
HeraRef_Hhsa_Htel	Htel	0	0.563221	0.073115	0.926885	2803	-18771.0552	-18007.0465	-764.00872	0.463939046
Hdem_Hhim_Hsar	Hhim	0	0.779486	0.03104	0.96896	5186	-32380.66898	-30094.3696	-2286.299341	0.897326171
Hdem_Hhim_Hsar	Hdem	0	5.222097	0.951884	0.048116	211	-1196.043605	-1192.12261	-3.920993	0.001812942
Hdem_Hhim_Hsar	Hsar	0	3.895007	0.953575	0.046425	203	-1157.629236	-1167.60083	9.971596	0.001682906
Hdem_Hhim_Hhsa	Hhim	0	0.456133	0.180636	0.819364	1312	-8846.481866	-8637.2574	-209.224464	0.19196528
Hdem_Hhim_Hhsa	Hdem	0	0.50376	0.080657	0.919343	3874	-25345.41414	-24406.934	-938.480151	0.635988354
Hdem_Hhim_Hhsa	Hhsa	0	0.257622	0.738655	0.261345	415	-2663.923935	-2676.66086	12.736922	0.019367531
Hdem_Hhim_Htel	Hhim	0	0.36801	0.235066	0.764934	1758	-12379.498	-12176.2094	-203.288565	0.240134638
Hdem_Hhim_Htel	Hdem	0	0.443385	0.116065	0.883935	2804	-19853.56392	-19306.4731	-547.090809	0.442598882
Hdem_Hhim_Htel	Htel	0	0.484657	0.271341	0.728659	1039	-7394.195951	-7285.25548	-108.940473	0.135192268
Hhim_Hhsa_Hsar	Hhim	0	0.456081	0.172768	0.827232	1301	-8795.495182	-8583.19927	-212.295914	0.19218372
Hhim_Hhsa_Hsar	Hsar	0	0.514892	0.082006	0.917994	3872	-25400.03989	-24459.6468	-940.393073	0.63472728
Hhim_Hhsa_Hsar	Hhsa	0	0.289956	0.712546	0.287454	428	-2795.830827	-2808.99046	13.159631	0.021969699
Hhim_Hsar_Htel	Hhim	0	0.342549	0.211073	0.788927	1744	-12205.23495	-11991.7364	-213.498556	0.245694409
Hhim_Hsar_Htel	Hsar	0	0.449463	0.124215	0.875785	2816	-20020.48942	-19472.8728	-547.616667	0.440394743
Hhim_Hsar_Htel	Htel	0	0.481915	0.261653	0.738347	1041	-7409.311041	-7295.31707	-113.993968	0.137253433
Hhim_Hhsa_Htel	Hhim	0	0.636701	0.065522	0.934478	2257	-15592.59829	-14912.6958	-679.902535	0.376628008
Hhim_Hhsa_Htel	Hhsa	0	0.308069	0.456403	0.543597	546	-3546.425361	-3532.38628	-14.039083	0.053000708
Hhim_Hhsa_Htel	Htel	0	0.555889	0.059001	0.940999	2798	-18781.74554	-17983.4117	-798.33379	0.470163429
Hdem_Hhsa_Hsar	Hdem	0	0.395254	0.865194	0.134806	249	-1448.460406	-1462.508	14.047589	0.005994053
Hdem_Hhsa_Hsar	Hsar	0	0.523523	0.817126	0.182874	259	-1557.644272	-1571.58832	13.944047	0.008457923
Hdem_Hhsa_Hsar	Hhsa	0	0.798602	0.037758	0.962242	5092	-32711.07474	-30546.4139	-2164.660869	0.874952904
Hdem_Hsar_Htel	Hdem	0	5.167494	0.953091	0.046909	220	-1226.673099	-1222.77547	-3.897628	0.001842854
Hdem_Hsar_Htel	Hsar	0	0.406189	0.857314	0.142686	213	-1218.517329	-1234.26056	15.74323	0.005427164
Hdem_Hsar_Htel	Htel	0	0.82382	0.030906	0.969094	5167	-33218.78113	-30839.2075	-2379.573656	0.894162268
Hdem_Hhsa_Htel	Hdem	0	0.670144	0.295311	0.704689	3259	-21402.17834	-20939.4945	-462.683837	0.410103831
Hdem_Hhsa_Htel	Hhsa	0	0.308819	0.360583	0.639417	1066	-7338.899598	-7275.55391	-63.345685	0.121717593
Hdem_Hhsa_Htel	Htel	0	0.498155	0.158744	0.841256	1276	-8843.001179	-8620.02517	-222.976008	0.191686189
Hhsa_Hsar_Htel	Hsar	0	0.991904	0.544019	0.455981	3255	-21207.36039	-20978.4174	-228.942978	0.265038956
Hhsa_Hsar_Htel	Hhsa	0	0.298721	0.365553	0.634447	1069	-7337.194619	-7275.52445	-61.670169	0.121111401
Hhsa_Hsar_Htel	Htel	0	0.525667	0.180016	0.819984	1277	-8888.16268	-8671.74486	-216.4178162	0.186985637

triplet: The three-taxon subset considered. Species abbreviations separated by underscores. **Outgroup:** Species inferred to be the outgroup in the triplet gene tree topology tested.
Cx: Inferred species tree branch length for (1) the ILS case and (2) the non-ILS case. The ILS case is forced to be 0, as all lineages must be in the same population.
Topology proportions: Inferred mixture proportion for the ILS and non-ILS distributions. These values sum to 1.
numTrees: Frequency of the topology in the sample. **BICx:** Raw BIC values for each model **dBIC:** difference in BIC value between the models. dBIC < -10 implies that the ILS+introgression model is a better fit for the data.
total non-ILS: topology non-ILS proportion * (numTrees/total trees in sample). This value represents the genome-wide introgression fraction

Table S14: Topology to chromosome size correlation. This table shows correlations for the relationship of percent of windows within a chromosome showing a particular topology to chromosome total size. Formula for each linear model is lm(percent topology ~ Chromosome Length)

Topology	r^2	p	slope	intercept
Tree 1	0.883	0	-0.0328905	0.89383691
Tree 2	0.726	0	0.01694918	-0.0731941
Tree 3	0.584	1.00E-04	0.01592566	-0.1597327
Tree 4	0.197	0.0286	-0.0035893	0.14176093
Tree 5	0.854	0	0.0056696	-0.0523581
Tree 6	0.712	0	-0.0029986	0.08772379
Tree 7	0.195	0.0294	0.00129813	0.01784327
Tree 8	0.248	0.0148	0.00187587	-7.13E-05